

Doctoral Dissertation

博士論文

Spatially resolved microspectroscopy of flavin-based
magnetosensitive photochemistry

(フラビンに基づく磁気感受性光化学の空間分解顕微分光)

ルイス マーティン アンテル

Lewis Martyn Antill

*Dedicated to the memory of my little sister and grandparents,
Eternally in my heart wherever I may be*

A thesis submitted for the degree of Doctor of Philosophy

Graduate School of Arts and Sciences

The University of Tokyo

Japan

2018

Dissertation Supervisor:

Jonathan R. Woodward, Associate Professor, The University of Tokyo

Dissertation Committee (in alphabetical order):

Kiminori Maeda, Associate Professor, Saitama University

Fumitaka Mafune, Professor, The University of Tokyo

Motoyuki Matsuo, Professor, The University of Tokyo

Taro Toyota, Associate Professor, The University of Tokyo

Dissertation Abstract

論文の内容の要旨

Spatially resolved microspectroscopy of flavin-based magnetosensitive photochemistry

(フラビンに基づく磁気感受性光化学の空間分解顕微分光)

ルイス マーティン アンテル

Lewis Martyn Antill

An important scientific question derives from epidemiological studies that show a weak correlation between the development of cancer and teratological effects and exposure to 50-60 Hz extremely low frequency (ELF) magnetic fields (MFs). In 2002, IARC classified ELF MF as a 2B carcinogen based on studies of the association between exposure to ELF MFs and childhood leukaemia. Due to the lack of experimental laboratory evidence and plausible mechanisms, ELF MFs are classed as 2B or "*possibly carcinogenic to humans*". The radical pair mechanism (RPM) is considered to be the most plausible mechanism for explaining the biological effects of ELF MFs, if they do indeed exist.

Evolution has given numerous species of animals the ability to perceive magnetic fields, known as magnetoreception. The extent to which a magnetic field influences an animal and the degree of magnetic sensing varies between species. In the simplest case, a species can detect only the presence of the geomagnetic field ($\sim 50 \mu\text{T}$). At a more sophisticated level, the magnetic information is used as an inclination compass, which is the case in migratory birds. While this higher-level phenomenon has been known for almost half a century, the primary biophysical sensory mechanism behind this astonishing ability remains poorly understood.

To date, research related to animal magnetoreception has been conducted in a wide range of scientific areas, from observational and experimental biology to quantum physics. The results from these different scientific pursuits have established the following key findings: 1. Migratory birds cannot use their magnetic compass at night. 2. During the day, the magnetic compass appears to be wavelength dependent (between ~ 400 and ~ 565 nm). The proposed

magnetoreceptor is the protein cryptochrome, with a flavin adenine dinucleotide (FAD) chromophore. 3. Radiofrequency radiation appears to be able to disrupt the compass sensing ability. There is currently one hypothesis that can in principle, explain these observations, the chemical (RPM) magnetoreception hypothesis.

To fully understand the biological and chemical processes involved in animal magnetoreception, one needs to make observations at the cellular level. This requires spatially resolved spectroscopic investigations of magnetic field effects on biological reactions in living cells. The aim of the work described in this thesis was to develop a spatially resolved microspectroscope to allow the study of magnetosensitive photochemistry of flavins not only in solution, but also in biomimetic and cellular environments. The primary objective was to unravel the mechanisms of the photochemical reactions involved in cryptochromes and ultimately, develop key connections between the fields of spin chemistry and behavioural biology.

The work described in this thesis can be broken down into 4 main sections, each of which proceeds logically from the former. First is the optimisation, testing, and enhancement of the microspectroscope itself, along with an evaluation of its utility in studying spatially localised RP reactions (Chapter 2). Next is the exploitation of the instrument to study basic model chemical RP reactions, exploiting its high sensitivity and the low sample volume capabilities (Chapter 3). The third main objective of this work was to develop spatially localised RP reaction systems that mimic critical features of biology (Chapter 4). The final section of the thesis describes the first attempts to use the microspectroscope to study RP reactions and their magnetosensitivity in actual biological samples (Chapter 5).

The technique utilises a pump-probe methodology where one laser (pump) generates RPs in a photochemical reaction and one (probe) monitors the transient RPs by their optical absorption. Two kinds of measurement are possible: transient optical absorption detection (TOAD) imaging and magnetic intensity modulation (MIM) imaging. The former technique allows the photochemical reactions taking place in flavin-based systems to be monitored inside a tiny sample volume region (<4 fL) with a beam waist of ca. 240 nm. This allows selective photoexcitation of molecules within individual organelles inside cells (for example the nucleus) and any RPs produced can be monitored. Furthermore, any magnetic field response to the photochemistry within these regions can then also be recorded. In the latter MIM technique, direct detection of magnetic field sensitive photochemistry, which is used as the signal to create the image of a sample, only allows regions that contain magnetosensitive photochemical processes to materialise in the image.

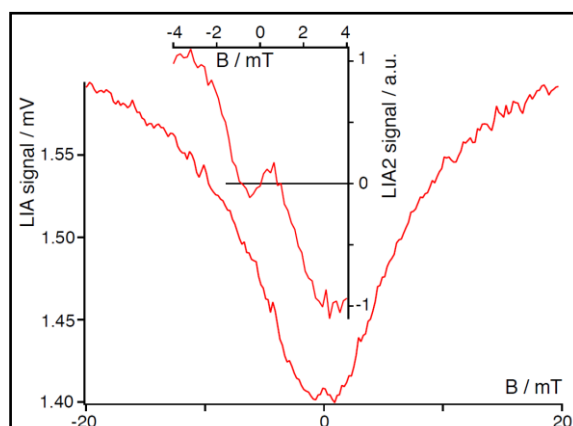


Figure 1: Single (main) and double modulation (inset) MARY spectra for the intramolecular photochemical reaction of FAD, revealing and confirming the presence of a LFE.

The starting point for this work was the successful construction of the microspectroscope and so, work began with its comprehensive testing and optimisation. To demonstrate the capabilities of the instrument, a model chemical system, believed to be responsible for the magnetosensitivity of cryptochromes, was used. Flavin adenine dinucleotide (FAD) is a blue-light absorbing molecule which undergoes intramolecular electron transfer to form a RP, which is magnetic field sensitive. TOAD and MIM images of $\sim 2.5 \mu\text{m}$ polymer beads surrounded by a sea of FAD in acidic solution were recorded. TOAD images are created

with the signal from green light absorbing flavin semiquinone radicals which are created by blue light photoexcitation, therefore a greater RP concentration gives rise to a brighter pixel. For MIM images, the signal used to create the images is proportional to the magnetic sensitivity of the photo-generated FAD RPs, which means that greater magnetic sensitivity gives rise to brighter pixels. For both TOAD and MIM imaging, a low field effect (LFE) on the photochemistry of FAD was resolved for the first time (see Figure 1). This observation is an important step forward in addressing the potential role of FAD in biological magnetoreception.

At present, studies have only examined the MFE on FAD at pH values of < 3.6 , where the adenine moiety is protonated and FAD assumes an ‘open’ conformation. The reasoning behind this was that at higher pH it is believed that the adenine moiety is not protonated and that FAD adopts a ‘closed’ conformation, in which rapid electron transfer between the flavin and adenine moieties results in a considerable decline in fluorescence quantum yield and terminates RP formation. Exploiting the high sensitivity of our instrument, we studied reaction kinetics and MF dependence at pH values up to pH 8 and captured the time-resolved transient absorption signal with and without magnetic fields at each pH value. Furthermore, by measuring MARY spectra at each pH value, the pH dependence of the $B_{1/2}$ value for FAD was recorded. Measurements clearly demonstrate that at physiological pH and higher, FAD is capable of producing RPs that are magnetosensitive. The observed magnitude of the MFE under these conditions ($\sim 2\%$, corresponding to $\Delta\Delta A \sim 2 \times 10^{-7}$) exemplifies the sensitivity of the instrument and its potential capability for observing MFEs in living tissues and cells.

Immobilisation of flavins is desirable to simulate the orientationally structured protein environment of cryptochrome. Our approach was to study the photochemistry and magnetosensitivity of flavins in different biomimetic systems, which included small and giant unilamellar vesicles. DOPC giant unilamellar vesicles (GUVs) were synthesised, using the water-in-oil centrifugation method, with various flavins-based systems, such as flavin mononucleotide (FMN) and hen egg-white lysozyme (HEWL), encapsulated within them (see Figure 2). Such systems are a means of mimicking cellular environments and exist on length scales which could be readily observed using our microspectroscope.

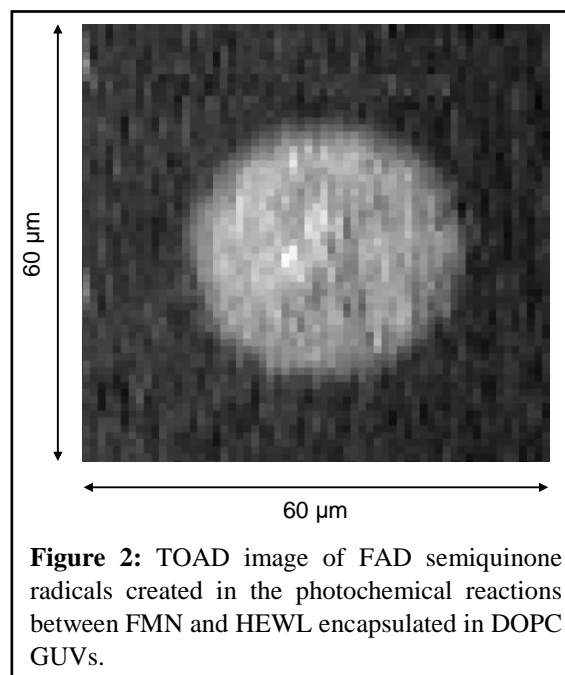


Figure 2: TOAD image of FAD semiquinone radicals created in the photochemical reactions between FMN and HEWL encapsulated in DOPC GUVs.

One of the key longer-term goals of this work was to enable direct spectroscopic measurements of RPs in real biological systems both ‘*in vitro*’ purified protein samples, and ‘*in vivo*’ by imaging photochemical RP reactions localised in living cells. Experiments on isolated *D. melanogaster* cryptochrome protein (*DmCry*) were conducted under pseudo-continuous illumination, similar to the continuous exposure to light that animals navigating in the geomagnetic field experience, rather than the series of short nanosecond pulses typical in photochemical kinetic measurements. No MFE was observed at room temperature, which is consistent with previous research, however, a clear reproducible light induced reaction cycle was observed where previous studies have suggested that substantial time must pass after photoexcitation before the sample returns to its initial state. Initial ‘*in vivo*’ experiments were conducted on buccal mucosa squamous epithelial cells. The ‘cheek’ cells were incubated with FAD, which exhibited a TOAD image of flavin semiquinone radicals within the cell. However, for unaltered ‘cheek’ cells no TOAD image was resolved. Human cervical carcinoma (HeLa) cells are known to exhibit auto-fluorescence due to the presence of FAD. We have developed this as a model system to investigate the magnetosensitivity of FAD photochemistry at the cellular level.

This work demonstrated for the first time the techniques of TOAD microscopy, which allows direct imaging of photochemically generated radicals, and MIM microscopy, which can selectively image regions containing magnetically sensitive RPs. Both techniques possess sub-micron spatial resolution, high sensitivity, and high information content due to the ability to resolve spatial, kinetic, and magnetic information on flavin-based photoreactions in a wide range of reaction environments, from isotropic solutions to living cells.

Acknowledgements

I would like to say thank you to my supervisor Prof. Jonathan R. Woodward for introducing the fascinating world of spin chemistry and letting me explore the wonders of biological magnetoreception. He has been a fantastic mentor and friend. Always being there to support any of my academic or personal needs, for which I am eternally grateful.

I thank Dr. Joshua. P. Beardmore for constructing a beautiful microspectroscope, which has given me many rewards over the past three and half years.

Thanks to Noboru and Masaya for being great lab mates (after two and half years alone), which has led to many fruitful discussions and great social gatherings.

A tremendous thank you to the Ministry of Education, Culture, Sports, Science and Technology: MEXT-Japan for financially supporting my PhD studies.

Thank you to Profs. S. Murata and S. Takizawa at The University of Tokyo for SUV sample preparation, and Mr. Yuta Sato for preliminary experiments regarding the SUV preparation.

Thank you to Prof. T. Toyota at The University of Tokyo for instructing me on GUV synthesis and collaborative work.

Thank you to Prof. N. Scrutton and Dr. A. Jones at The University of Manchester (A. J. now at the National Physical Laboratory) for supplying *DmCry* samples.

Thank you to Profs. R. Matsuda and M. Omi at The University of Tokyo for advice and instruction on cell culturing techniques.

Thank you to Mr. N. Ashta for preliminary work on starch films.

Thank you to Imai-san and co-workers, and Iizuka-san and co-workers for help with all the administrative procedures.

Fellow GPES members, thank you for warm welcomes and fun times.

Thank you to Emma for being a terrific mansion-mate and great friend.

Mau and the `guys`, thanks for the great izakaya/karaoke sessions and day trips.

I am forever in debt to my parents for all the love and support they have given me over the years. I could not have done it without you.

Thank you to my family for the love and support over the years.

My family in S. Korea have provided much love and support for which I am forever grateful.

My wife Kyoung-Ok, you have been there always. You have given me so much love, support, and encouragement.

I could not have done it without you. Thank you for everything.

Table of Contents

Abstract	iv
Acknowledgements	viii
1 Introduction	12
1.1 Biological Magnetoreception	13
1.1.1 The Geomagnetic Field	14
1.1.2 A Magnetic Compass Sense	16
1.1.3 Mechanisms for Magnetic Field Sensing	17
1.2 Radical Pair Mechanism	25
1.2.1 Introduction	25
1.2.2 Radical Pair Formation	26
1.2.3 Spin-State Mixing	28
1.2.5 Radical Pairs in Magnetic Fields	31
1.3 Cryptochromes	36
1.3.1 Introduction	36
1.3.2 Structure of Cryptochromes	37
1.3.3 Magnetosensitive Photochemistry of Cryptochromes	39
1.4 Flavins	41
1.4.1 Introduction	41
1.4.2 Properties of Flavins	42
1.4.3 Magnetosensitive Photochemistry of Flavins	43
1.5 A Microscopic Approach	47
2 Instrumental	60
2.1 Measurement Sensitivity	61
2.2 Spatially Resolved Measurements	79
3 Flavins in Solution	88
3.1 Intramolecular Flavin Photochemistry	89
4 Immobilised Flavins	101
4.1 Small Unilamellar Vesicles	102
4.2 Giant Unilamellar Vesicles	118
5 Flavins in Biological Environments	128

5.1 <i>D. melanogaster</i> Cryptochrome	129
5.2 Flavins in Cellular Environments	138
5.2.1 Buccal Mucosa Squamous Epithelial Cells	138
5.2.2 Human Cervical Carcinoma Cells	140
6 Conclusion	144
A Publications and Related Information	147
B Supporting Information	150
B.1 Chapter 3.1	150
B.2 Chapter 4.1	152

Introduction

An important scientific question arises from epidemiological studies that show a weak correlation between the development of cancer and teratological effects and exposure to 50/60 Hz extremely low frequency magnetic fields (ELF-MFs). An initial 23-year study published in 1979 by Wertheimer and Leeper¹ examined 344 children aged 0-18 years. They found that the homes of children (living in the Denver area, Colorado, USA) who developed cancer were found more often near overhead electric cables carrying high currents, with an almost 3-fold likelihood of developing leukaemia. Subsequent studies followed (for example, refs. 2-4) and in 2002, the International Agency for Research on Cancer (IARC) classified ELF-MFs as a 2B carcinogen based on the numerous studies of the association between exposure to ELF-MFs and childhood leukaemia.⁵ Due to the lack of experimental laboratory evidence and plausible mechanisms, ELF-MFs are classed as 2B or “*possibly carcinogenic to humans*”. The radical pair mechanism (RPM, Chapter 1.2) is considered to be the most plausible mechanism, with a cryptochrome blue-light photoreceptor molecule (Chapter 1.3), for explaining the biological effects of ELF-MFs, if they do indeed exist.^{6,7}

Furthermore, cryptochromes have other mechanistic roles in nature. Evolution has given numerous species of flora and fauna the ability to perceive MFs. This phenomenon is known as magnetoreception (Chapter 1.1).⁸ The extent to which a magnetic field influences a plant or animal and the degree of magnetic sensing varies between species, examples includes, the entrainment of circadian rhythms in fruit flies (*D. Melanogaster*),^{9,10} and light-dependent regulation of growth and development in plants,^{11,12} These mechanisms function with cryptochrome photoreceptors. In 2000,¹³ cryptochromes were also proposed as the magnetoreceptor molecule to allow the ability of migratory birds to sense the direction of the Earth’s MF (~50 μ T) for navigational purposes. This navigational compass molecule is proposed to involve a MF sensitive flavin-tryptophan radical pair, which has received great

attention over the past 18 years.¹⁴ Given the known (photo)chemical and physical properties of cryptochromes,⁷ they are considered the most likely candidate biological magnetoreceptor molecule.

To date, studies on flavin-based chemical systems (Chapter 1.4) and in vitro proteins conducted by spin chemists have been performed with spectroscopic techniques, such as flash photolysis transient absorption and fluorescence spectroscopy.¹⁵⁻²⁰ In contrast, biologists have made observations on animal behaviour²¹ and also connected magnetic sensing to particular organs and genes.²² To fully understand the biological and chemical processes, one needs to make observations at the cellular level. This requires spatially resolved spectroscopic investigations of magnetic field effects on biological reactions in living cells. To this end, this thesis aimed to develop a spatially resolved microspectroscopic technique (Chapter 2) to allow the study of magnetosensitive photochemistry of flavins, not only in solution (Chapter 3), but also in biomimetic (Chapter 4) and cellular environments (Chapter 5). Next, an introduction to magnetoreception and a discussion of the proposed mechanisms and evidence to support these hypotheses is included.

1.1 BIOLOGICAL MAGNETORECEPTION

The ability to perceive magnetic fields, known as Magnetoreception, is a fascinating sixth sense found in plants and a diverse range of animals from worms and insects to migratory species such as birds and turtles. The idea that animals use the Earth's magnetic field for orientation purposes is a longstanding one. During the middle of the 19th century, Russian zoologist Alexander von Middendorff suggested that insects and birds might use the geomagnetic field for navigation,²³ and Charles Darwin thought of the idea of manipulating the orientation behaviour of bees by attaching small permanent magnets to them.²⁴ The first experimental evidence arrived in the 1960s when Wiltschko and Merkel demonstrated that the directional orientation of European Robins (*Erithacus rubecula*) was disrupted by the presence of a magnetic field comparable to that of the Earth.²⁵ After initial skepticism, the evidence supporting magnetoreception in birds²⁶ and many other species of bacteria,²⁷ nematodes,²⁸ chordates,²⁹ fish,³⁰ molluscs,³¹ arthropods,³² amphibians,³³ and mammals³⁴ has grown substantially over the past 50 years. Locating magnetoreceptors (a biological assembly that can transduce the magnitude and/or orientation of a local magnetic field to the organism's nervous system) is extremely difficult. Several factors account for this difficulty, one major issue is that magnetic fields pass freely through biological tissue meaning that the magnetoreceptor can, in principle, be located at any location in an organism's body. Another issue is concerned with the fact that there is not any palpable organ or structure committed to magnetoreception,³⁵ they might be miniscule or dispersed throughout a large area of tissue, or a set of chemical reactions might be

responsible for the transduction process.¹³ Furthermore, as humans we cannot intuitively think of where a magnetoreceptor may be located because a) we lack magnetoreception³⁶ or b) we are not aware of our magnetic field sensing ability.³⁷ The body of evidence that has accumulated over the past 50 years has mainly come from behavioural experiments and theoretical approaches. Over this period, there have been numerous proposed mechanisms of biological magnetoreception,^{38,39} however, at present there are three candidate magnetoreceptor hypotheses. They are the electromagnetic induction, biogenic magnetite, and magnetosensitive biochemical reaction hypotheses, which will all be explained in turn. To fully understand magnetoreception, we must first consider the types of information we can gather from the geomagnetic field, and ultimately, which types of information do plants and animals utilise.

1.1.1 The Geomagnetic Field

The Earth's magnetic field is a dipole field, like a bar magnet. The field is generated by a self-nourishing geodynamo, where the Earth's core's fluid motion moves electrically conducting iron across an existing magnetic field.⁴⁰ The magnetic field lines leave the Earth from the southern hemisphere, enter space, and then re-enter in the northern hemisphere (Fig. 1.2). Consequently, the magnetic field lines point upward in the southern hemisphere and downward in the northern hemisphere. The geomagnetic field intensity is minimal close to the magnetic equator ($\sim 22 \mu\text{T}$), where field lines are parallel to the surface of the Earth (inclination angle 0°) and rises to a maximum at the magnetic poles ($\sim 67 \mu\text{T}$), with field lines perpendicular to the Earth's surface (inclination angle 90°). Fig. 1.1 and 1.2 illustrate the intensity and inclination of the geomagnetic field, respectively. The magnetic poles do not match the geographic poles (distinguished by the rotational axis of the Earth), in fact the geomagnetic field is a non-static or wandering entity.⁴¹ The poles wander several tenths of a degree annually, known as secular variation, and the total intensity of the geomagnetic field has declined by approximately 10% since 1900.

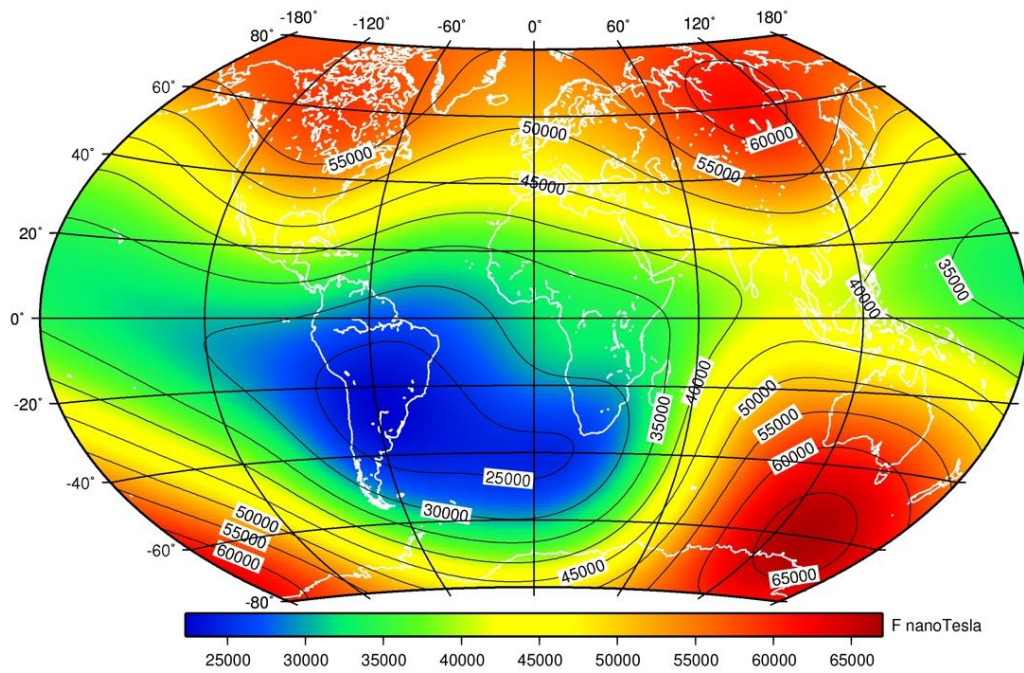


Figure 1.1. Map of total intensity of the geomagnetic field (2015, British Geological Survey⁴²). The magnetic field intensity ranges from 22,000 nT to 67,000 nT (0.22 G to 0.67 G).

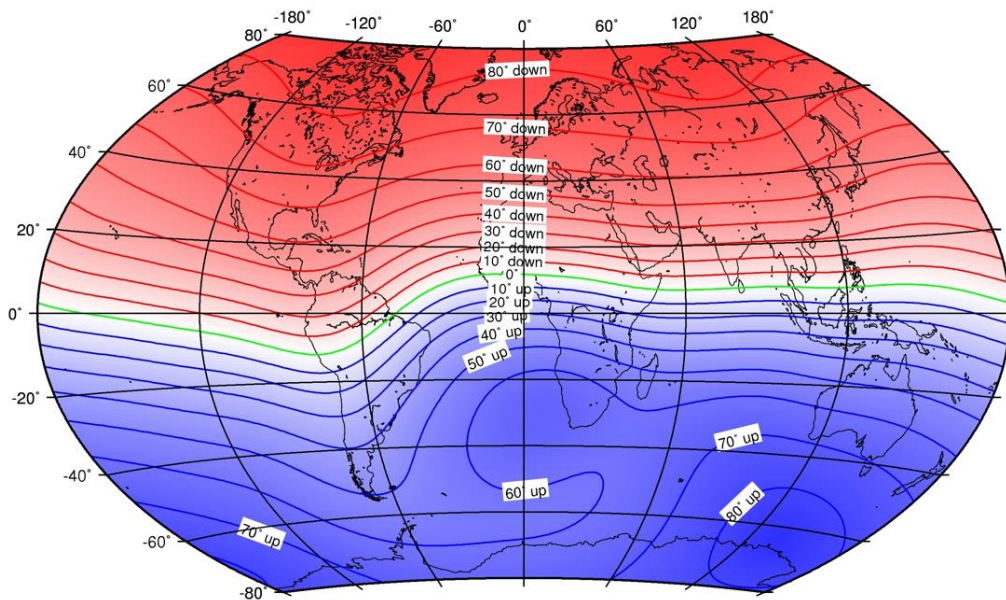


Figure 1.2. Map of the geomagnetic field inclination (magnetic field vector angle in degrees, up or down from the horizontal (2015, British Geological Survey⁴²). The green and black lines at 0° represent the magnetic and geographic equators, respectively.

1.1.2 A Magnetic Compass Sense

Animals can potentially obtain information from the geomagnetic field in the forms of 1) a polarity compass, a simple compass, which allows an animal to head north or south while maintaining a continual heading, and 2) an inclination compass, a simple global positioning system (GPS), which permits an animal to determine their position relative to their desired destination. They can utilise both the inclination and intensity of the geomagnetic field to achieve this GPS ability. The simple compass ability exists in many species, including insects, molluscs, crustaceans, and in all five classes of vertebrate.³⁹ The GPS ability has been found in a few species, including sea turtles,⁴³ salamanders,⁴⁴ lobsters,⁴⁵ and birds.⁴⁶

The avian magnetic compass is insensitive to the polarity of the geomagnetic field, rather they sense only the axis of the field and therefore rely on the magnetic field inclination to navigate. This inclination compass is used to distinguish which side of the magnetic axis steers toward the closer magnetic pole (polewards) or toward the magnetic equator (equatorwards). For polewards steering, the magnetic axis will be on the side where the magnetic field lines meet the horizon, and for equatorwards steering, the magnetic axis will be on the side where the MF lines and horizon diverge. These cases stay true in both northern and southern hemispheres (Fig. 1.3).²⁴

Determining the form of compass an animal possesses (polarity or inclination) is commonly done with magnetic coils surrounding the test subject. For creatures of the avian variety, the subject is placed in an Emlen funnel⁴⁷ (an inverted cone shaped bird cage) and the vertical component of the encompassing magnetic field is inverted. This inversion reverses the inclination of the field, with the polarity unchanged. If the bird is endowed with an inclination compass it will reverse its orientation direction even though the polarity of the field is untouched. For animals possessing a polarity compass, an inversion of the vertical field will have no effect on the animal, therefore it will remain facing in the same direction.⁴⁸⁻⁵⁰

The following chapter will introduce the three biological magnetoreception hypotheses.

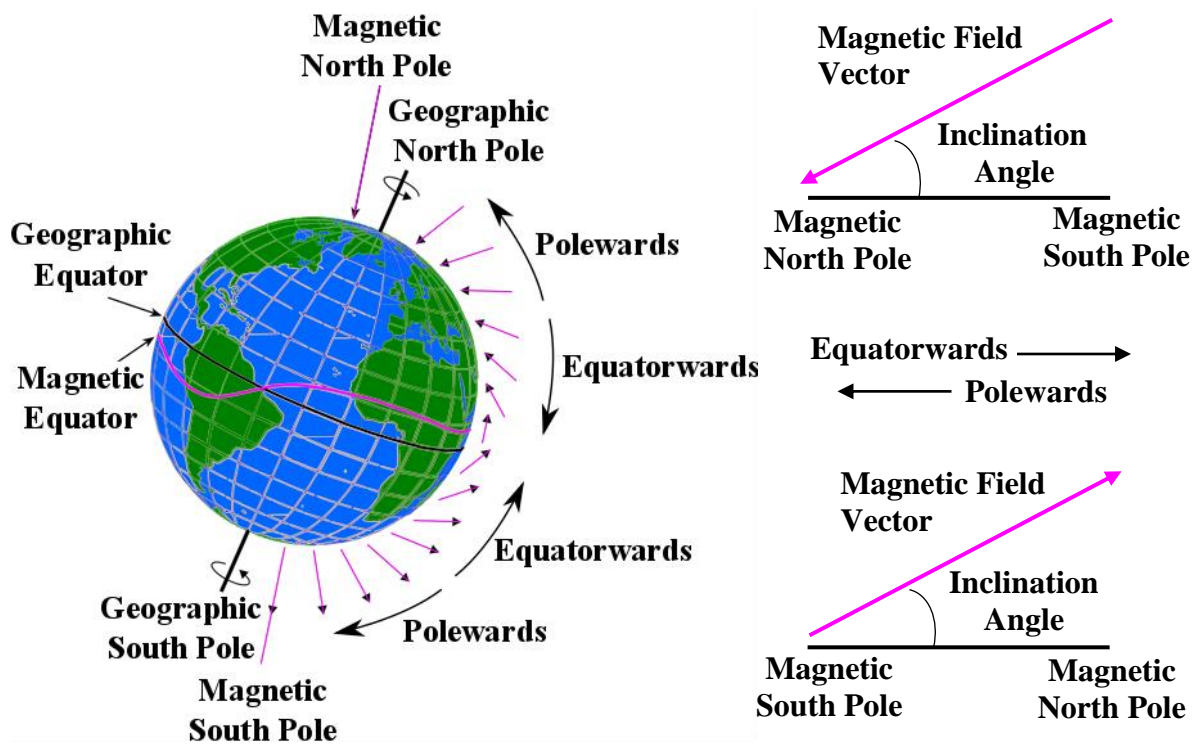


Figure 1.3. Key geomagnetic and geographic locations (left) and description of the avian inclination compass (right). Left: The length of the pink arrows near the surface of the Earth indicate field intensity, angle of inclination is indicated by the steepness of the pink arrows with respect to the Earth, and direction is indicated by the arrowhead of the pink arrows. Right: The inclination compass does not perceive the polarity of the magnetic field vector but is sensitive to the alignment and sign of inclination. Therefore, birds do not discriminate between north and south, but between equatorwards and polewards. Based on ref. 24.

1.1.3 Mechanisms for Magnetic Field Sensing

In this section, three main magnetoreceptor hypotheses will be introduced. The first hypothesis involves an anatomical structure that enables electromagnetic transduction, this mechanism is considered the prime candidate for magnetoreception in elasmobranchs (sharks, rays, skates, and sawfish). Secondly, a hypothesis predicts that magnetic fields are perceived by a mechanical magnetite-based magnetoreceptor, which has been proposed to be utilized by bacteria, amphibians, reptiles, and birds. Finally, the light-sensitive chemical-based mechanism, involves the phenomenon of the radical pair mechanism and blue-light receptor proteins, cryptochromes. This hypothesis is proposed as a mechanism used by plants, amphibians, arthropods, chordates, and birds. Only a brief description of the first two mechanisms will be given. The third mechanism will be described in more detail as it is the focus of this thesis.

Electromagnetic Induction

The Lorentz force is movement of a charged particle in a magnetic field, which creates a force. The Lorentz force causes charged particles to migrate to opposite ends of a conducting bar when moving through a magnetic field (not parallel to the field lines), which generates a voltage. If the bar is immersed in a conductive medium stationary to the magnetic field, an electric circuit is formed and some current flows. In 1832, Michael Faraday remarked that ocean currents ought to produce electric fields as they move through the geomagnetic field.⁵¹ Elasmobranchs possess several hundred long canals that consist of resistive walls and are filled with highly conductive jelly, which act as electric wires. The ampullae of Lorenzini, a collection of extremely sensitive cells, are located at the end of these wires and detect any slight changes in voltage of the induced current. The surrounding ocean acts as the stationary conducting medium. A typical shark or ray moving horizontally through the ocean at a speed of 1 ms^{-1} could, theoretically, produce a voltage gradient at the ampullae of Lorenzini of $25 \text{ } \mu\text{Vm}^{-1}$. This estimate is above the proposed ampullae detection threshold of $2 \text{ } \mu\text{Vm}^{-1}$.⁵² Electromagnetic induction is only considered to be relevant to aquatic species, as they are surrounded by a conductive medium, and because elasmobranchs are the only known species to contain extreme electrical sensitivity.⁵³⁻⁵⁵

Evidence to support electromagnetic induction has not yet been observed directly, although elasmobranchs do have an electrosensory system that is sensitive enough to allow detection of fields generated by their prey and presumably the geomagnetic field.^{53,56} Several studies seem to contradict this proposed mechanism,^{39,56,57} however more investigation is required to determine whether electromagnetic induction gives the magnetoreception ability to elasmobranchs, or another mechanism is involved.

Magnetite-Based Magnetoreception

The orientational movement along geomagnetic field lines is found in a diverse conglomeration of algae and bacteria.⁵⁸ These organisms exploit the biomineralisation of magnetite (Fe_3O_4) and greigite (Fe_3S_4) and, since their discovery, have been found in numerous species including birds, salmon, honey bees, and sea turtles.⁵⁷ Magnetite is a crystalline form of iron oxide, which can exist as $\sim 50 \text{ nm}$ single-domain particles, similar to those found in magnetotactic bacteria, and are permanently magnetised particles that can rotate into alignment with a magnetic field comparable to that of the Earth.⁵⁹⁻⁶¹ In some species, the magnetite crystals are smaller ($\sim 20 \text{ nm}$) and are proposed to be superparamagnetic, but they do not possess a permanent magnetic moment and therefore, cannot rotate into alignment with the geomagnetic field.⁵⁸ External MFs induce magnetic moments in the superparamagnetic particles, which can cause adjacent particles to attract or repel. The movements could be

detected by mechanoreceptors or by ion channels opening, forming the foundation for a magnetic field intensity or directional sensory mechanism.^{62,63}

Magnetic particles can only be considered as a magnetosensory mechanism if they are discovered at precise and unswerving locations within the body and if they are connected to the nervous system.⁶⁴⁻⁶⁶ They were proposed to be located in the upper beak (specifically the dendrites (sensory nerve endings) at three bilateral locations) of the avian species and operate as a magnetoreceptor.^{67,68} This hypothesis was largely discredited in 2012, when the proposed magnetosensitive neurons found in the beaks of pigeons were found to be macrophages, which are found throughout the pigeon's body, not at a specific location and therefore, cannot play a role as a magnetoreceptor.⁶⁹

Nevertheless, there is one nerve located in the upper beak of birds that is not involved in olfaction, which is the ophthalmic branch of the trigeminal nerve (V1) and is believed to be involved in magnetoreception. Supporting evidence has shown compelling effects in the removal of the ability of birds to detect induced magnetic field changes when V1 was severed, and also reduction of neural responses to induced fields in the specific hindbrain structures after either the induced MF is removed or V1 is ablated (surgically cut).^{70,71} V1 is thought to transmit positional magnetic information to the brain, but is unlikely to afford compass information as intact trigeminal nerves are neither essential or adequate for magnetic compass orientation.^{72,73} Further studies are required to determine the true nature of the involvement of V1 in animal magnetoreception.

Chemical Magnetoreception

The chemical magnetoreception hypothesis involves radical pairs, which are magnetically sensitive chemical intermediates formed inside cryptochrome proteins after photoexcitation. In 1978, a photoinduced radical pair magnetic compass sense in migratory birds and other animals was first proposed.⁷⁴ Schulten's proposal focusses on the radical pair mechanism (RPM, see Chapter 1.2), which provides an explanation of how magnetic fields can alter the rate and yield of chemical reactions.⁷⁵ This visionary proposal was largely ignored for reasons which include the following, no biological receptor molecule was put forward, the magnetite hypothesis was largely accepted by the scientific community, and during this period of time, the RPM was in its infancy and a minority of scientists were aware of / believed the RPM. In the early 1990s, there were key developments that supported this hypothesis. Firstly, behavioural studies suggested that the magnetic compass sense of newts⁷⁶ and birds⁷⁷ is light dependent, supporting a photochemical magnetoreceptor. Secondly, the radical pair mechanism matured into a bona fide field of science, exhibiting a plethora of experimental, and theoretical quantitative explanations, evidence to show that magnetic fields have an effect on radical pair reactions.⁷⁸ Finally, a new blue-light

photoreceptor protein, the cryptochrome, was discovered.¹¹ In 2000, Ritz *et al.*, reintroduced the 1978 hypothesis with a biologist accessible explanation and with a specific biomolecule, the cryptochrome, in which appropriate radical pairs could be formed.¹³ To this day, cryptochrome is the only candidate radical pair magnetoreceptor molecule.^{14,79,80}

Since the year 2000, there has been a tremendous scientific endeavor to support this chemical magnetoreception hypothesis. The evidence gathered from this quest can be categorized into several key observations, the following timeline was adapted, updated and corrected, from Wang *et al.*, 2015:⁸¹

1) Evidence to support the hypothesis that avian magnetoreception requires light, cryptochrome, and a visual system

a. Neurology

1984 – Neurophysiological responses dependent on the presence of light and a naturally intact retina.⁸² Magnetic field responses were recorded in two areas of the bird's optic system, the tectum opticum (superior colliculus) and the nucleus of the basal optic root (nBOR).⁸³

2004 – Cryptochrome found to be located in the ganglion cells of migratory birds, which display high activity under migratory navigation.⁸⁴ An area of the brain considered to be associated with visual signal reception, called Cluster N, was activated under magnetic field orientation, suggesting the visual system could be used for transduction.^{70,85,86}

b. Ethology

1993 – The orientation of the avian species, European Robin (*Erithacus rubecula*), Australian Silveryeye (*Zosterops lateralis*), Garden Warbler (*Sylvia borin*), and Carrier Pigeon (*Columba livia*), operated normally under blue (450 nm) and green (550 nm) light irradiation. However, they were disorientated under yellow (590 nm) and red (635-645 nm) light.⁸⁷⁻⁹⁴

2002 – Covering a bird's right eye disabled their navigation ability.⁹¹ Suggesting that the magnetic compass ability involves the eye and light.^{91,95}

2009 – Magnetic field effects were recorded on the circadian rhythm of *Drosophila melanogaster*, conversely, fruit flies with Cry mutants could no longer sense the magnetic field.⁹⁶

c. Biophysics and Biochemistry

1993 – Cryptochromes are blue-light sensing photoreceptors which are found in plants, animals, and humans. They absorb light in the same wavelength range as that to which the avian species orientate themselves in a magnetic field.^{97,98}

d. Cell Biology

2004 – Cryptochromes were discovered in the retina of several migratory birds, including European Robins, Garden Warblers, and Chickens (*Gallus gallus domesticus*).^{99,100}

2011 – Immunochemical studies on Cry1 identified its location in the retina of robins and chickens, where it is situated at the discs in the outer segment of the UV/violet cones.¹⁰¹ Further supporting the RPM.

2013 – Cry1a was activated under all wavelengths where birds were able to use their magnetic compass: UV, blue, turquoise, and green.¹⁰²

2016 – Activated Cry1b was found to be expressed in the ganglion cells of the retina in European Robins and Garden Warblers during their respective migratory seasons.¹⁰³

2018 – Cry4 was discovered in double cones and long-wavelength single cones in birds. Cry4 was upregulated during the migratory season in night-migratory European Robins and Zebra Finches (*Taeniopygia guttata*). A homology model of ErCry4 (European Robin Cryptochrome 4) predicts strong FAD binding. Cry4 was also found to be expressed at constant levels over time, compared to daily variations in Cry1 and Cry2. At present, Cry4 is the most likely candidate magnetoreceptor of the chemical magnetoreception hypothesis.^{104,105}

Evidence to support the radical pair mechanism is the primary magnetic sensory process

2) Resonance frequency effects

a. Spin Chemistry

1997 – S-T mixing could be affected by resonance effects in the MHz range of an oscillating magnetic field.¹⁰⁶⁻¹¹¹

b. Ethology

2004 – The magnetic field orientation behaviour of migratory birds seemed to be disorientated by an externally applied MHz oscillating magnetic field.^{109,112}

3) Reaction rates and yields of FAD photochemistry in cryptochromes

a. Quantum Chemistry (theoretical)

1996 – Radical pair reaction can be influenced by a low magnetic field.^{113,114}

2007 – MFEs on cryptochrome FAD were studied in various species.¹¹⁵⁻¹¹⁷

2009 – Theoretical calculations indicated the cryptochromes could produce a 10% increase in signal activity for magnetic fields of 500 μ T, through the RPM.^{118,119}

2012 – FAD semiquinone radical absorption between 550-630 nm increased by $\sim 0.2 \times 10^{-4}$ for a 355 nm 5 mJ pulse under an external magnetic field.¹²⁰

b. Botany

2007 – *Arabidopsis thaliana* (Mouse-Ear Cress or Thale Cress) hypocotyl length was enhanced by 5% in a 500 μ T field compared to that in a 50 μ T field.¹²¹ Giving further evidence to support the cryptochrome magnetoreception hypothesis, even though the plant growth under external magnetic field analyses are highly inconsistent.¹²²

c. Biophysics and Biochemistry

2008 – MFEs on the photoreduction reaction in photolyase expressed in *E. coli*. The yield of the photoreaction altered in a 40 mT applied magnetic field.¹¹⁶

2012 – The dynamics and reaction yield of FAD-Trp radical pairs in *in vitro* AtCry (*A. thaliana* cryptochrome) and EcPL (*E. coli* photolyase) were affected by the presence of applied weak magnetic fields as low as 0.7 mT.¹⁹

2017 – MFE on *in vitro* animal cryptochrome DmCry (*D. melanogaster* cryptochrome) photochemistry was smaller than of that observed for AtCry and EcPL. The kinetics have been interpreted as involving the newly proposed tryptophan tetrad.^{20,123}

4) FAD radical intermediates have multiple states and lifetimes

a. Quantum Chemistry (theoretical)

1998 – RPM states that for a magnetic field on the order of the geomagnetic field to have a noticeable effect of S-T mixing, the lifetime of both radical pair and spin-correlation should be longer than $\sim 1 \mu$ s.^{124,125}

b. Spin Chemistry

2002 – EPR spectroscopy has verified the excited states of numerous FAD cofactors. CPD (cyclobutene pyrimidine dimer) photolyase photochemistry can undergo intersystem crossing

to produce an excited triplet state. Whereas, only singlet state products are observed in *Xenopus laevis* (6-4) photolyase, EcPL, AtCry, and DmCry.^{19,20,126,127}

c. Biophysics and Biochemistry

2003 – Under blue-light irradiation, radical pairs can be produced in cryptochromes.¹²⁸

2009 – Using EPR, NMR, and transient absorption techniques, flavin radical pairs, under blue light irradiation, have been shown to be long-lived in various cryptochromes. Flavin radicals (FADH•) in gwCry (Garden Warbler cryptochrome) and AtCry displayed a lifetime of 14 ms and a half-life of 5 ms, respectively, and tryptophanyl radicals (Trp•) have a half-life of 1 ms in AtCry and a 4 ms lifetime in gwCry.^{127,129,130} Furthermore, time-resolved EPR has also suggested that the spin-correlation time could be as long as 10 μs.¹¹⁹

5) Anisotropic radical pair photochemistry

a. Quantum Chemistry (theoretical)

2003 – Theoretical work showed that FAD-Trp radical pair anisotropic product yields could be tuned by minute variations in the hyperfine tensors of the nuclear spins of the two radicals in a 50 μT magnetic field.¹²⁵

b. Synthetic Chemistry

2008 – A chemical model magnetic compass in the form of the triad carotenoid-porphyrin-fullerene (CPF) produced photoinduced electron transfer radical pairs whose RP lifetime was altered by the application of an Earth strength magnetic field (~40 μT). Also, this model was also able to sense the direction of a stronger magnetic field.¹⁶ Provides proof that a chemical magnetoreceptor is physically possible.

c. Ethology

2010 – Numerous migratory birds prefer to fly in low light conditions, where ambient light intensity is relatively low.¹³¹

Figure 1.4 summarises the current model of chemical magnetoreception based of the evidence above. This evidence supports that both the RPM and cryptochrome magnetoreceptor are involved, however, there is still no direct evidence to prove this chemical magnetoreception hypothesis. Many open questions still exist⁷⁹, questions like, can RF disorientation in migratory birds be independently reproduced under double-blind conditions? Can

MFES be detected on *in vitro* migratory bird cryptochrome proteins? Which regions of the brain are involved beyond Cluster N in magnetic compass processing pathways? Do cryptochrome-containing cells in the retina alter their membrane potential in response to changes in geomagnetic-strength magnetic fields? An excellent review by Hore and Mouritsen makes two suggestions to answer these questions, 1) A “killer experiment” is required to establish that cryptochrome is the magnetoreceptor *in vivo*. 2) To fully understand this important enduring biological problem, a pure multidisciplinary approach involving chemistry, mathematical modeling, quantum physics, computer simulation, biochemistry, and behavioural, neuro-, and molecular biology is required.¹⁴

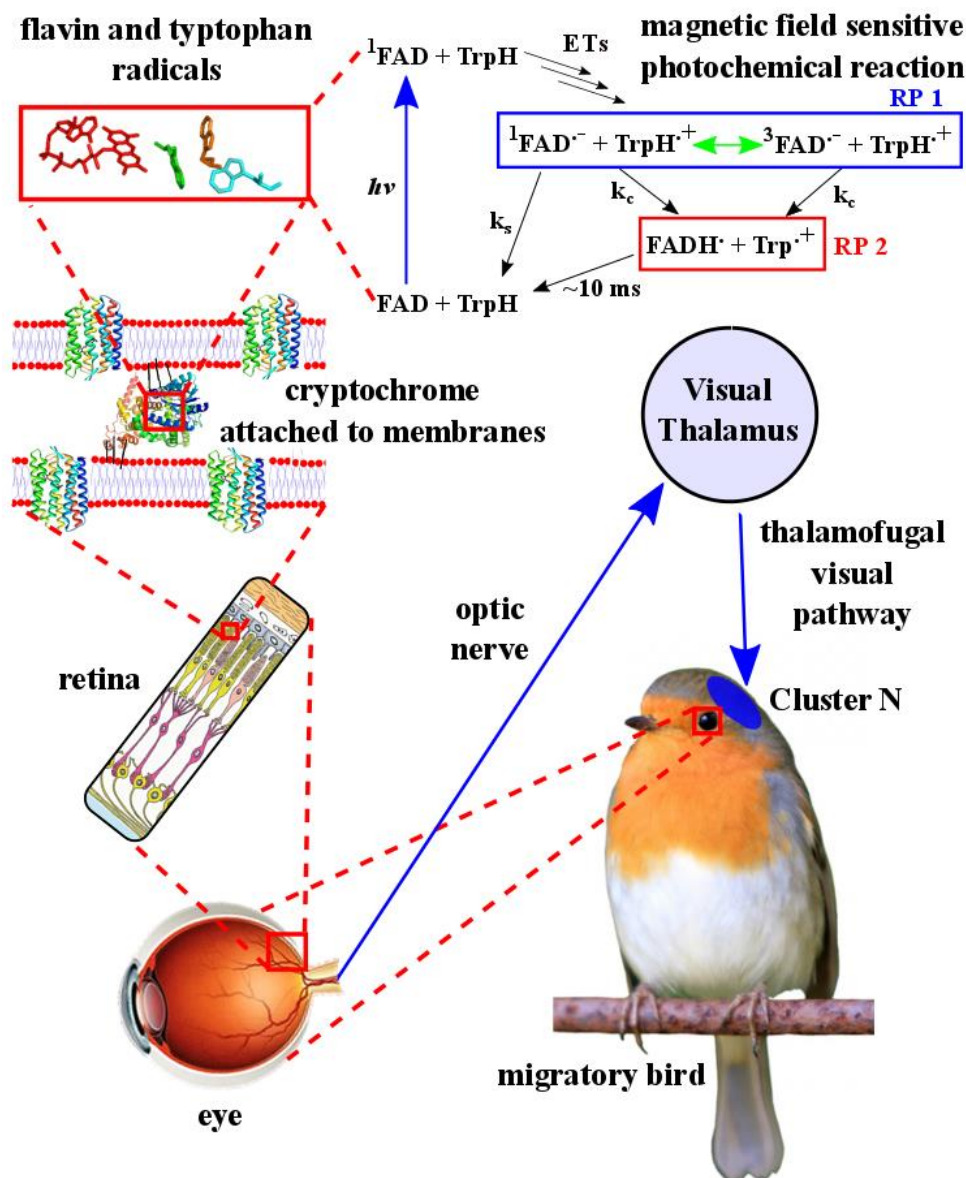


Figure 1.4. Summary of the proposed light-dependent chemical magnetic compass sense in migratory birds.

Based on ref. 79.

1.2 RADICAL PAIR MECHANISM

1.2.1 Introduction

The previous chapter introduced the chemical hypothesis for magnetoreception, we will now take a step back and look at the theoretical aspects of the radical pair mechanism. In the year 1900, Gomberg discovered free radicals (a species with an unpaired electron) in the form of the triphenylmethyl radical formed from the reaction between triphenylmethyl bromide and silver.¹³² The role of free radicals as solution phase reaction intermediates was first hypothesised by Hey and Waters in 1937.¹³³ In 1944, the Russian scientist Zavoisky made the discovery of electron paramagnetic resonance (EPR), which revolutionised science by providing a spectroscopic method for studying unpaired electrons.^{134,135} The interaction of a pair of radicals, from here on known as a radical pair (RP), was first observed as anomalous line intensities in EPR spectroscopy by Fessenden and Schule in 1963,¹³⁶ and in 1967, Bargon, Fischer, and Johnsen¹³⁷ and independently Ward and Lawler¹³⁸ observed similar anomalies in nuclear magnetic resonance (NMR) spectroscopy. These phenomena are known as chemically induced dynamic electron polarisation (CIDEP) and chemically induced dynamic nuclear polarisation (CIDNP), respectively. In 1969, new theory was postulated to explain these anomalous intensities by Closs¹³⁹ and independently by Kaptein and Oosterhoff,¹⁴⁰ this theory is the radical pair mechanism (RPM).

Around this time, most scientists believed that magnetic fields (<2 T) could not affect chemical or biochemical reactions, this was due to the lack of reproducibility or theoretical clarification. Peter Atkins famously wrote a review article on magnetic field effects, stating that “The study of the effect of magnetic fields on chemical reactions has long been a romping ground for charlatans”.¹⁴¹ The main argument given by the nonbelievers was supported by the comparison of magnetic energies of molecules and thermal energies in chemical reactions. Zeeman splitting (vide infra) of electron spin states at 2 T is ~ 2 cm⁻¹, and for a proton the splitting for the nuclear spin states is 1,000 times smaller at ~ 0.002 cm⁻¹. This is considerably less than thermal energy at room temperature ~ 200 cm⁻¹ and typical activation energies of ~ 3000 cm⁻¹ for chemical reactions. Therefore, from a thermodynamic viewpoint, magnetic field effects on chemical reactions were considered unfeasible unless gigantic magnetic fields were employed.¹⁴²

Since the 1970's, there has been considerable advances in the theoretical framework and many methods and experiments have been developed and is now known as the field of ‘Spin Chemistry’.^{75,143} This field extends from chemical systems encompassing the solid and liquid state, to both biological systems and material science, with the application of magnetic field strengths ranging from very weak fields of tens of microtesla (comparable to the

geomagnetic field) up to tens of tesla. Scientists of this area of research encompassing chemistry, physics, biology, and material science meet (approximately) biennially at the *International Symposium on Spin and Magnetic Field Effects in Chemistry and Related Phenomena* or ‘*Spin Chemistry Meeting*’, which was first held in Tomakomai, Japan, 1991.

1.2.2 Radical Pair Formation

Spin-correlated radical pairs (RPs) are key to the magnetic field sensitivity of chemical reactions. Formation of paramagnetic free radicals can occur in numerous ways, most commonly through hydrogen atom abstraction of, homolytic fission of, and electron transfer in diamagnetic species (Fig. 1.5). It can be clearly seen that free radicals must always be formed in pairs (radical pairs), this is significant because a RP is the reaction intermediate which exists prior to the free radical stage of the reaction. Also, in each reaction case, the spin multiplicity (singlet or triplet) of the RP is indicated, the significance of this is discussed below. RPs can also be formed in the random encounter of free radicals, where recombination of the radical species is dependent on their relative spin states. When the radicals come together with antiparallel spins, bond formation can occur (singlet born). If the spins are parallel then no reaction can occur as it is forbidden by the Pauli exclusion principle (which states that two or more fermions (particles with half-integer spin, i.e. an electron) cannot occupy the same quantum state in a given quantum system), in this instance the radicals will tend to drift apart (triplet born) (Fig. 1.5).¹⁴⁴

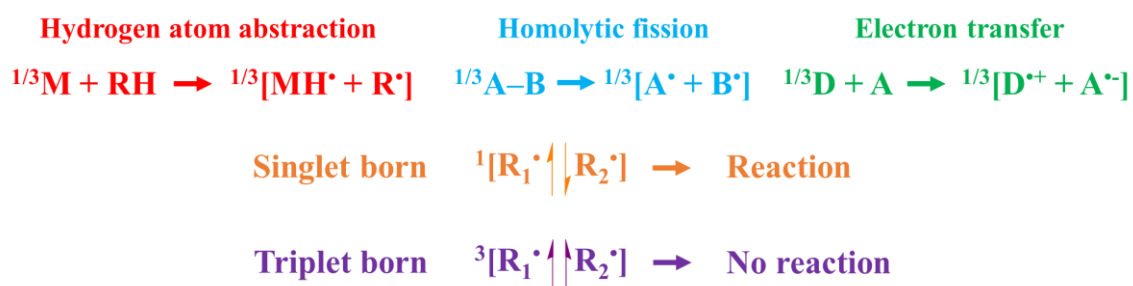


Figure 1.5. General scheme of common radical pair formation methods and radical pair recombination fates depending on the spin state of the radicals.

For a triplet born RP to react, some process must transpire to change one of the radical spin states. For intersystem crossing to befall the radicals diffuse sufficiently apart to a distance where the singlet and triplet energy is dwarfed by the interactions that cause spin-state interconversion (or spin-state mixing). Figure 1.6 shows how the singlet and triplet energies vary with interrational separation (r), with the energy difference between the singlet and triplet states given by $2J(r)$ (the electron exchange interaction),

$$J(r) = J_0 e^{-r/r_J} \quad (1.1)$$

At equilibrium bond lengths (2-3 Å, $J = \text{v. large}$) $J(r)$ dominates any local magnetic field, however, as the radical separates (>5 Å, $J = \text{small}$) the exchange interaction rapidly decreases, and spin-state mixing can now occur. When the radicals have sufficiently separated the following can arise, 1) spin-state mixing occurs and the radicals can diffuse back together, 2) spin-state mixing occurs and the radicals can diffuse back together and recombine (geminate product), and 3) the radicals completely diffuse apart (>10 Å, $J = 0$) to produce F-pairs and free radicals and can undergo other reactions.

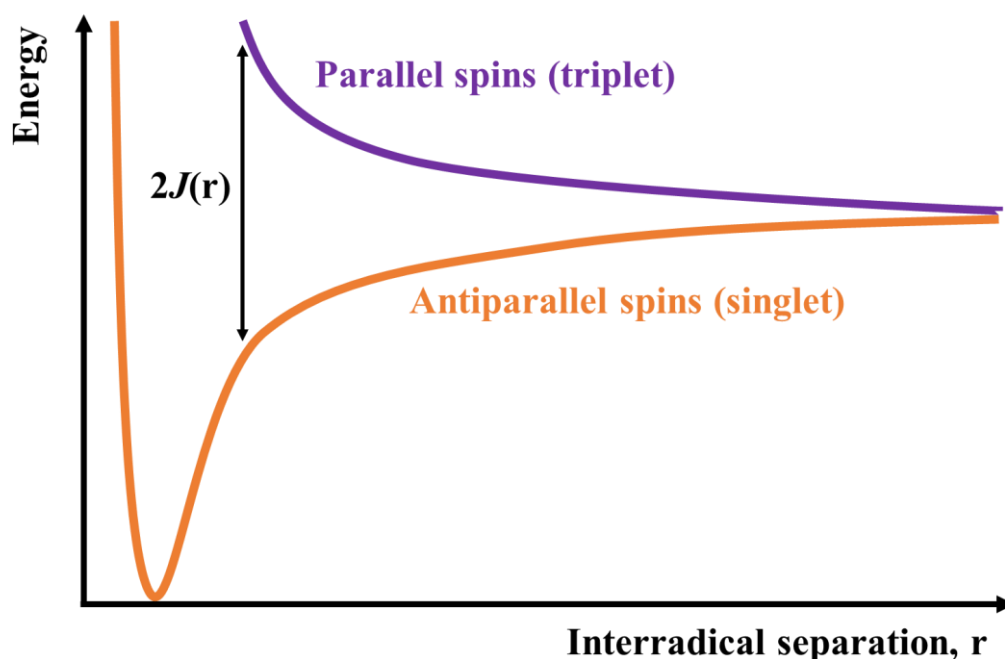


Figure 1.6. Energy dependence of singlet and triplet states with interrational separation. $J(r)$ is the electron exchange interaction.

Diffusive reencounter of radicals in solution can occur through the phenomenon known as the cage effect.¹⁴⁵ In solution, radicals must displace the solvent molecules to escape the 'solvent cage' to separate from one another. The solvent cage temporarily traps the solute radicals, which affords the radical pair to separate and collide numerous times before they escape from the cage. During the time they are trapped, the magnitude of the electron exchange interaction can alter significantly and therefore spin-state mixing can occur allowing situations 1 and 2 described above.¹⁴⁴ In solution, typically after photoexcitation, the rate of intersystem crossing (ISC) is generally faster than radical pair formation, which is due to the unbound tumbling motion of the radical species. This generally leads to a triplet born radical pair. Conversely, in a protein environment where the molecule is bound, and cannot move freely, the rate of ISC is slower than RP formation, therefore, singlet born RPs are normally formed. The processes in solution are illustrated in Fig. 1.7.

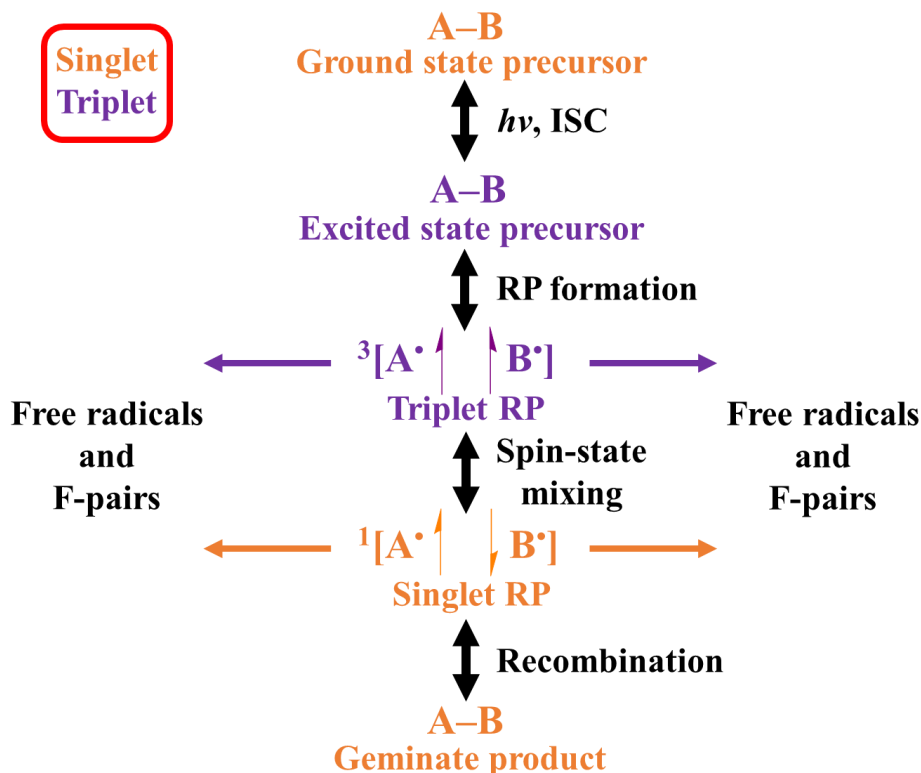


Figure 1.7. A scheme of the various fates of triplet born radical pairs in solution.¹⁴⁴

1.2.3 Spin-State Mixing

The previous section discussed how radical pairs are formed and introduced spin-state mixing. A discussion of the three processes which can cause spin-state mixing will commence, they can be classified as 1) coherent spin-state mixing, 2) incoherent spin-state mixing, and 3) chemical relaxation.

Coherent Spin-State Mixing

Free radicals possess magnetic moments which produce two different Zeeman energies when subjected to an external magnetic field, they are denoted α (higher in energy) and β (lower in energy). When two radicals form a radical pair their situation is rather different. Singlet RPs have an overall spin angular momentum of zero ($S = 0$), therefore they possess no magnetic moment and are consequently unmoved by an applied external magnetic field. However, a triplet radical pair possesses a spin quantum number of one ($S = 1$), which means there are three triplets states that are degenerate in zero field. Through the Zeeman effect, when a magnetic field is applied the triplet state degeneracies are removed to give the T_0 , T_{+1} , and T_{-1} states. The spin-state terms for the four coupled states are written as follows,

$$|S\rangle = 2^{-\frac{1}{2}} (\alpha_1\beta_2 - \beta_1\alpha_2) \quad (1.2)$$

$$|T_0\rangle = 2^{-\frac{1}{2}} (\alpha_1\beta_2 + \beta_1\alpha_2) \quad (1.3)$$

$$|T_{+1}\rangle = (\alpha_1\alpha_2) \quad (1.4)$$

$$|T_{-1}\rangle = (\beta_1\beta_2) \quad (1.5)$$

All the states of the triplet are magnetic, however, only the T_{+1} and T_{-1} have magnetic moments in the direction of the applied field (z-axis), with the T_0 state having a magnetic moment in the xy-plane in energy and is therefore unaffected by the external magnetic field. Figure 1.8 displays the differences in energy of the four spin states with the application of an external magnetic field, through the Zeeman effect. The S and T_0 states remain unchanged as the field increases, only separated by $2J(r)$, whereas the $T_{\pm 1}$ states are separated in energy and become decoupled from the S and T_0 states as the magnetic field strength increases.

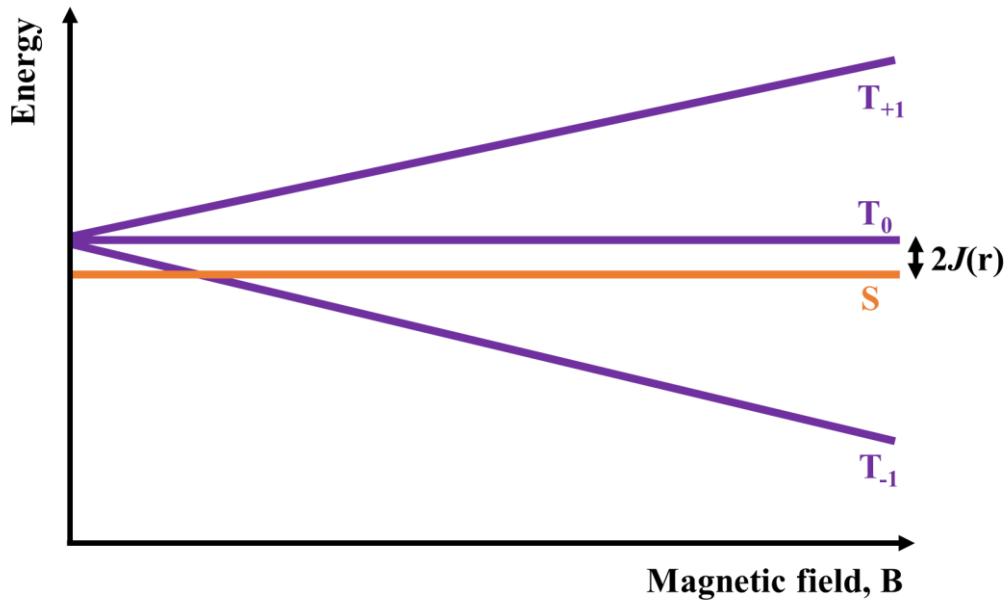


Figure 1.8. Energy variation of the singlet and triplet states in the presence of an applied external magnetic field through the Zeeman effect.

Representing the S and T spin-states in a vector model allows visualisation of their precession about the applied magnetic field direction (z-axis) at the Larmor frequency (Fig. 1.9). The electron spin Larmor frequency depends upon the g-value (for a free electron $g_e = 2.0023$) and the local magnetic field, B_L , which is the combination of the hyperfine coupling to magnetic nuclei and the field created by the external magnetic field. The Larmor frequency (ω) is given by,

$$\omega = \frac{g\mu_B B_L}{\hbar} \quad (1.6)$$

Where μ_B is the Bohr Magnetron and \hbar is the reduced Planck's constant. If the electrons possess different g-values or local magnetic fields, then the S and T_0 states possess different Larmor frequencies and can therefore interconvert.

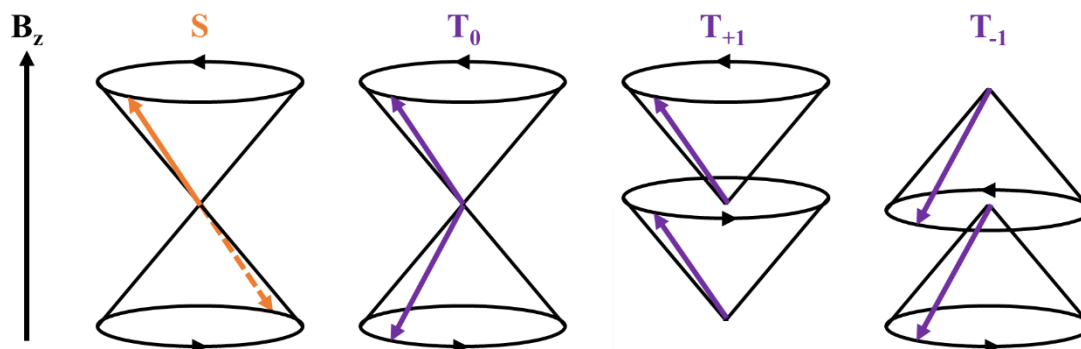


Figure 1.9. A vector representation of the singlet and triplet coupled states of a radical pair in the presence of an external magnetic field.¹⁴⁶

Two coherent spin-state mixing processes arise from equation 1.6, the Δg mechanism and the hyperfine coupling mechanism. The Δg mechanism is dependent on differences in the g-values of the radical pair, which only shows a significant impact at much higher magnetic field strengths than of interest to the work described in this thesis and will not be discussed further. The hyperfine coupling mechanism (HFCM) operates by differences in B_L , which involves the external magnetic field and the hyperfine couplings of the electron spins to magnetic nuclei. Coupling to magnetic nuclei means that even if the radicals are identical, they can still experience different local magnetic fields. This is the principal mechanism by which S- T_0 mixing occurs. In a zero magnetic field, a RP can undergo spin-state mixing or S-T mixing between all 4 spin states, the rate at which this occurs depends on the strengths of the hyperfine coupling constants (HFCs, typically 1-10 mT in organic radicals) in the radicals and operates through the HFCM.

Incoherent Spin-State Mixing

Coherent processes take place in the RPs, we will now consider processes which arise from the tumbling motion of RPs. Spin-lattice and spin-spin relaxation arise from radicals experiencing varying local magnetic fields due to their motion, which consequently induces an electron spin flip. This causes S- $T_{\pm 1}$ transitions and affects S- T_0 state mixing by spin-dephasing. The relaxation times (T_1 and T_2 , respectively) in solution are normally on the order of microseconds, and therefore much slower than coherent processes and RP diffusion. Therefore, in isotropic solution relaxation effects are negligible, however in viscous or restricted locales (i.e. micelles or vesicles), the lifetime of the radical pair can be increased somewhat, and relaxation effects become manifest.

Chemical Relaxation

Some chemical reactions can occur where the character of the radical remains unchanged, however, they are responsible for relaxation processes. There are other chemical relaxation processes, but only one will be discussed here. Degenerate electron exchange (DEE) or ‘electron hopping’ involves the transfer of an electron between a donor or acceptor and its uncharged form. This process is a common occurrence in radical ion pairs, for example between the tryptophanyl radical cation (Trp^{•+}) and the tryptophan molecule (Trp) and can narrow the width of magnetically affected reaction yield (MARY) spectra (vide infra) as the rate of DEE increases.^{147,148}

1.2.4 Radical Pairs in Magnetic Fields

The previous chapters introduced the intraradical (coherent processes), interrational (incoherent processes), and external (Zeeman effect) interactions a RP can experience. It is customary practice to describe RP reactions with a spin Hamiltonian, which is reduced to only contain spin-dependent terms. The spin Hamiltonian, containing the three interactions, can be written as,

$$\hat{H}_{RP} = \hat{H}_{inter} + \hat{H}_{intra} + \hat{H}_{ext} \quad (1.7)$$

The spin state of a radical can be explained by the spin operator,

$$\hat{\mathbf{S}} = \hat{S}_x \mathbf{i} + \hat{S}_y \mathbf{j} + \hat{S}_z \mathbf{k} \quad (1.8)$$

Where \mathbf{i} , \mathbf{j} , and \mathbf{k} are the unit vectors along the x, y, and z axes. The Hamiltonian for interrational interactions contains the term for the electron exchange interaction,

$$\hat{H}_{exchange} = -J(r)\left(\frac{1}{2} + 2\mathbf{S}_1 \cdot \mathbf{S}_2\right) \quad (1.9)$$

The Hamiltonian term for interrational interactions also contains the electron dipolar interaction term, which explains the interaction between the magnetic dipoles of the electrons in the two radicals. The interrational distance (r) in which this can influence spin-state mixing is much larger than the exchange interaction and is usually not taken into consideration when dealing with RPs in isotropic solution.

The intraradical term for the spin Hamiltonian explains the hyperfine coupling mechanism (hyperfine interaction),

$$\hat{H}_{hfi} = a_i \hat{\mathbf{S}} \cdot \hat{\mathbf{I}}_i \quad (1.10)$$

a_i is the isotropic hyperfine coupling constant (HFC) for the interaction between the electron (S) and nuclear (I_i) spins. A RP possesses two sets of electron-nuclear interactions and therefore one must contain two terms in the Hamiltonian to give,

$$\hat{H}_{intra} = \sum_i a_i \hat{\mathbf{S}}_1 \cdot \hat{\mathbf{I}}_{1i} + \sum_k a_k \hat{\mathbf{S}}_2 \cdot \hat{\mathbf{I}}_{2k} \quad (1.11)$$

Therefore, the spin Hamiltonian for a RP in zero field can be represented as,

$$\hat{H}_{RP, B=0} = -J(r) \left(\frac{1}{2} + 2\mathbf{S}_1 \cdot \mathbf{S}_2 \right) + \sum_i a_i \hat{\mathbf{S}}_1 \cdot \hat{\mathbf{I}}_{1i} + \sum_k a_k \hat{\mathbf{S}}_2 \cdot \hat{\mathbf{I}}_{2k} \quad (1.12)$$

When a RP is subjected to an external magnetic field, we must include the Zeeman interaction term (as described above), which is given by,

$$\hat{H}_{Zeeman} = g\mu_B \hat{\mathbf{S}} \cdot \mathbf{B} = g\mu_B S_z B \quad (1.13)$$

Where g is the g -value of the radical and μ_B is the Bohr Magnetron. The full spin Hamiltonian for a RP can now be written as,

$$\hat{H}_{RP} = -J(r) \left(\frac{1}{2} + 2\mathbf{S}_1 \cdot \mathbf{S}_2 \right) + \sum_i a_i \hat{\mathbf{S}}_1 \cdot \hat{\mathbf{I}}_{1i} + \sum_k a_k \hat{\mathbf{S}}_2 \cdot \hat{\mathbf{I}}_{2k} + \mu_B B (g_1 S_{1z} + g_2 S_{2z}) \quad (1.14)$$

We will now consider how the rate and yield of chemical reactions are affected by varying magnetic field magnitudes relevant to this thesis. Typically, the radical product yield changes with the application of an external magnetic field. This is experimentally measured with a magnetically affect reaction yield (MARY) curve. For “normal” magnetic field regimes (hyperfine coupling mechanism), magnetic field range ~ 10 mT, a magnetic field effect (MFE) is observed when the applied MF is larger than the HFCs of the respective RP.¹⁴⁹ This mechanism operates through the Zeeman interaction, where the rate of S-T mixing (spin-state mixing, S = singlet, T = triplet) decreases by the energetic separation of the $T_{\pm 1}$ states from the S and T_0 states. The MARY curve saturates when S- $T_{\pm 1}$ mixing halts (Fig. 1.10). A method of analysing the magnetic field dependence is to compare the $B_{1/2}$ values for the reaction. The $B_{1/2}$ corresponds to the field value where the MFE is half of the saturation value, which can be compared to the theoretical averaged HFCs (a) in the RP, which are calculated by,

$$\tilde{a}_r = \sqrt{\frac{4}{3} \sum_i a_{ik}^2 I_{ik} (I_{ik} + 1)} \quad (1.15)$$

The $B_{1/2}$ can then be calculated using the Weller equation,¹⁵⁰

$$B_{1/2} = \sqrt{3} \frac{\tilde{a}_1^2 + \tilde{a}_2^2}{\tilde{a}_1 + \tilde{a}_2} \quad (1.16)$$

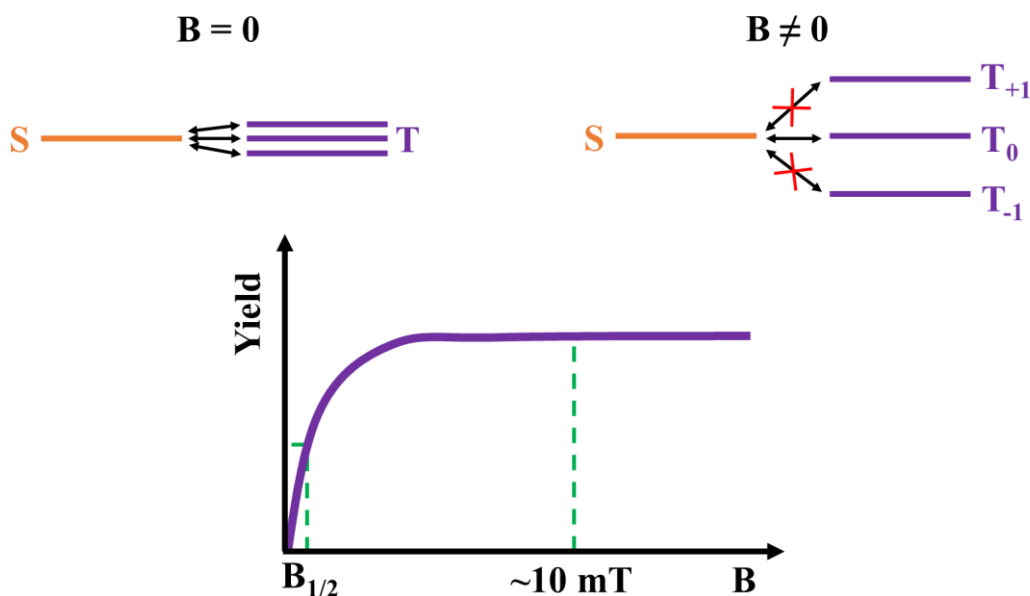


Figure 1.10. Hyperfine Coupling Mechanism. Schematic of the conversions between singlet and triplet states in the absence and presence of an applied magnetic field (top). A typical MARY curve for a triplet born RP with a triplet product yield. Key features are shown, the $B_{1/2}$ is the value of the field at which the reaction yield is half the saturation value (bottom).¹⁴³

The %MFE is regularly plotted to show the percentage change in radical yield, which looks like the MARY curve in Fig. 1.10. The %MFE is calculated using the following,

$$\%MFE = \frac{\text{yield}(B \neq 0) - \text{yield}(B = 0)}{\text{yield}(B = 0)} \quad (1.17)$$

Another process exists, the level crossing mechanism (LCM) when the exchange interaction (J) is not zero. The LCM operates through the Zeeman interaction as in the case of the HFCM. However, a level crossing between S and T_{-1} (or T_{+1}) states can occur when RP members move slowly enough to allow a jump from one state to another, where the states overlap. At this level crossing position, S and T_{-1} (or T_{+1}) mixing is enhanced and an increase (decrease) in spin-state mixing efficiency is observed as a decrease (or increase) in yield in the MARY curve (Fig. 1.11). This mechanism is usually observed in RPs in viscous solvents and fixed RPs/diradicals, where the time spent at the level crossing region is much longer than in isotropic solution.

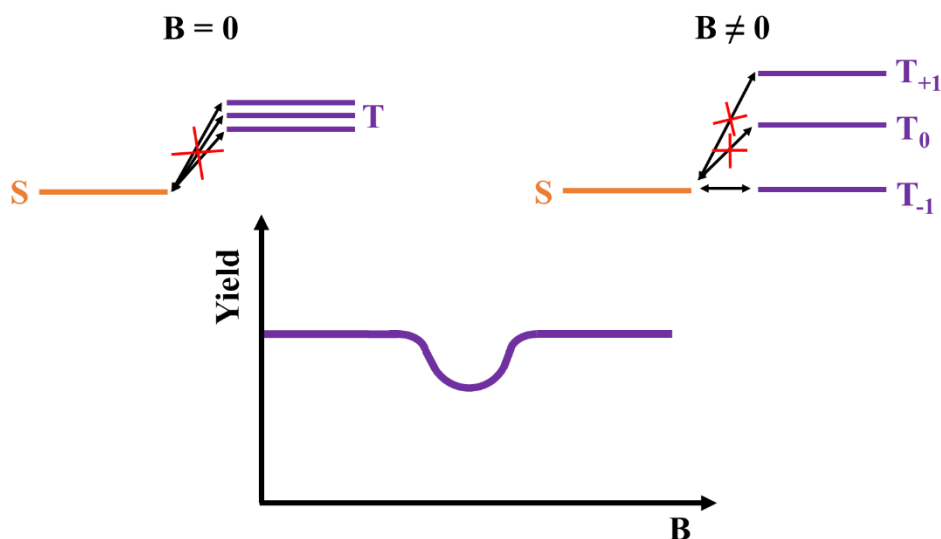


Figure 1.11. Level Crossing Mechanism. Schematic of the conversions between singlet and triplet states in the absence and presence of an applied magnetic field (top). A typical MARY curve for a triplet born RP with a triplet product yield.¹⁴³

The final mechanism of interest is observed in the low magnetic field region and is known as the low field effect (LFE). This mechanism is of extreme importance to the chemical magnetoreception hypothesis and ELF MF effects as the field range is in the same region as the geomagnetic field. When the spin Hamiltonian ($B = 0$) is solved for a one-proton RP (possessing two electrons and one nucleus) eight eigenstates are produced. Many of the eight eigenstates are degenerate and coherent spin-state mixing cannot occur. This suggests that the efficiency of S-T mixing is not at its full theoretical capacity. However, when a low magnetic field is applied (~ 0.1 mT) many of the eigenstate degeneracies are removed and increases the rate of S-T mixing. This will continue to happen until the field strength becomes high enough that the Zeeman effect dominates and the efficiency of S-T mixing decreases (Fig. 1.12).

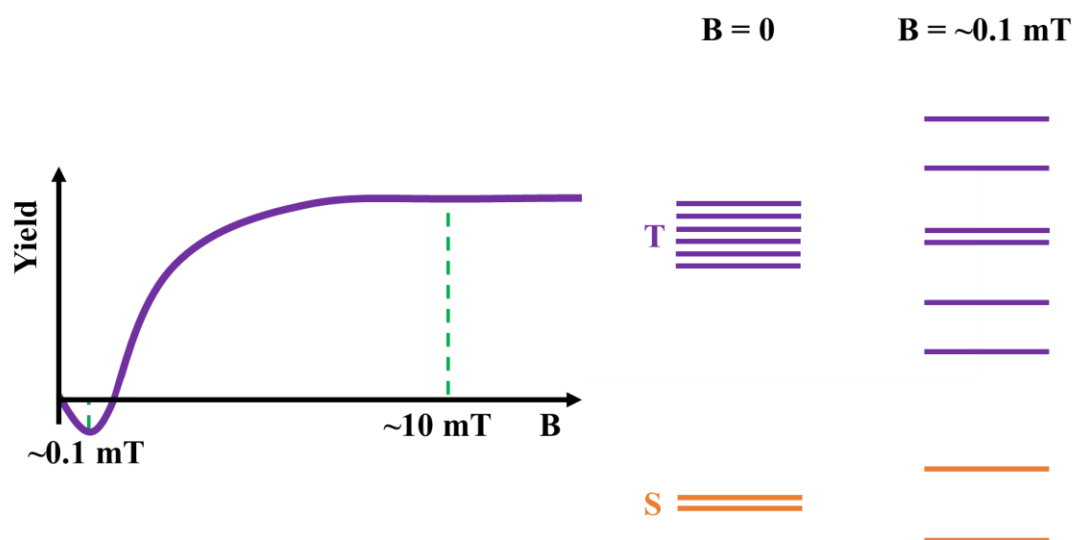


Figure 1.12. Low Field Effect. A typical MARY curve for a triplet born RP with a triplet product yield, showing the LFE at the low field region and an MFE (HFCM) at higher magnetic field strengths (left). A schematic of the removal of several eigenstate degeneracies with an applied low magnetic field, which enhances the efficiency of S-T mixing and is responsible for the decrease in triplet yield in the MARY curve (right).¹⁴³

All the above MARY spectra are characteristic of triplet born RPs with a triplet product yield. The following describes the effect of magnetic fields on the product yield for varying initial RP and product spin states,

Singlet born RP and singlet product yield: LFE = reduced yield, HFCM = increased yield, LCM = reduced yield

Singlet born RP and triplet product yield: LFE = increased yield, HFCM = reduced yield, LCM = increased yield

Triplet born RP and triplet product yield: LFE = reduced yield, HFCM = increased yield, LCM = reduced yield

Triplet born RP and singlet product yield: LFE = increased yield, HFCM = reduced yield, LCM = increased yield

RPs in flavin photochemistry in both solution and cryptochrome are typically formed by electron transfer reactions (after photoexcitation). For flavins in solution, ISC occurs to give rise to a triplet born radical pair, however, ISC does not occur in protein environments and consequently a singlet RP is born. The following chapter will introduce cryptochromes and discuss the mechanisms behind their proposed role as a magnetoreceptor.

1.3 CRYPTOCHROMES

1.3.1 Introduction

During the late 19th century many botanists, including Darwin, became aware of the acute effect of blue light on the growth, phototropic movement, and development of plants.¹⁵¹ For a prolonged period of time, the identity of the blue light photoreceptor remained elusive, which inspired some botanists to use the term cryptochrome for this enigmatic photoreceptor.¹⁵² There are now at least four classes of blue light photoreceptors (flavoproteins) that have been discovered.¹⁵³ Cryptochromes (Crys) are part of the archaic photolyase/cryptochrome superfamily (which contains two classes of flavoproteins), which also includes the (6-4) pyrimidine-pyrimidone adduct [(6-4) photoproduct] photolyases and the cyclobutene pyrimidine dimer (CPD) photolyases, which are found in all three kingdoms of life.¹⁵⁴ Photolyases are found in almost all species of eukaryotes and prokaryotes and are the enzymes that exploit light for repairing UV-damaged DNA.¹⁵² Cryptochromes are less diverse, existing in many animals, higher plants, and some other eukaryotes and prokaryotes and are responsible for controlling plant growth and development, and the entrainment of circadian rhythms in plants and animals.^{154,155}

Since the first Cry (HY4) gene was discovered,¹¹ later named *AtCry1* (*Arabidopsis*),¹⁵⁶ Crys have been found by homology in numerous species.¹⁵⁴ Cryptochromes can be further categorised into three sub-families, animal cryptochromes, plant cryptochromes, and Cry-DASH proteins, Cry-DASH is so named to highlight their relationship with Crys found in *Drosophila*, *Arabidopsis*, *Synechocystis* (cyanobacteria), and *Homo sapiens*.^{157,158} Animal and plant Crys are the product of two different evolutionary paths from their ancestral roots (photolyase), they both do not possess DNA repair ability, and mainly function as signaling molecules.¹⁵⁴ However, Cry-DASH Crys are a hybrid of photolyase and Cry, as they retain DNA repair activity. Recent research has shown that Cry-DASH can repair single-stranded DNA (ssDNA) with a high specificity for CPD in ssDNA and have consequently been reclassified as ssDNA photolyases.^{81,159} Animal Crys can be classified into two sub-categories, light-sensitive (Type I) and light-insensitive (Type II).¹⁶⁰ Type I mainly act as photoreceptors for entraining circadian rhythms in *D. melanogaster* (*DmCry*) and *D. plexippus* (*DpCry1*),¹⁶¹ whereas Type II act as light-independent transcription repressors of the circadian clock in mice (*mCry1* and *mCry2*), humans (*HsCry1*) and monarch butterflies (*DpCry2*).¹⁶²⁻¹⁶⁵ Plant Crys do not fall into the animal classification system as they are both light sensitive and responsible for blue light growth and entrainment of circadian rhythms.¹⁶⁶

1.3.2 Structure of Cryptochromes

The structure of cryptochromes and photolyases are similar, they are single domain proteins with a conserved photolyase homology region (PHR) domain comprising mainly α -helices, with a single area of β -sheets located near the N-terminus (amino-terminal) of the photoreceptor. FAD is buried within the PHR domain, and for DNA photolyases, the isoalloxazine ring (see Chapter 1.4) of FAD is involved in electron transport processes between the neighboring DNA-binding pocket and damaged DNA.^{128,167,168} The PHR domain of Crys also contains an additional chromophore in the form of 5,10-methenyltetrahydrofolate (MTHF or pterin).^{156,169,170} In the case of photolyases, the second chromophore can be either pterin or deazaflavin.^{169,170} The additional C-terminal (carboxy-terminal) domain found in cryptochromes is generally less conserved than the PHR region.¹⁷¹ The size can vary between Crys, being longer in most plant Crys than animal Crys. However, Cry-DASH proteins do not possess this domain.¹⁷² The C-terminal is involved in the functions of cryptochromes in the cell and in interactions with protein binding partners (Fig. 1.13).¹⁷³

There are two structural features important for the photochemistry of both Crys and photolyases, they are the FAD cofactor and the chain of three (*AtCry* and *EcPL*)¹⁹ or four (*DmCry*)²⁰ conserved tryptophan residues (Trp_A, Trp_B, Trp_C, and Trp_D representing proximal, medial, and terminal Trp(s) with respect to the FAD moiety), which connect the FAD cofactor with the protein surface. This Trp triad/tetrad is believed to form an electron transport (ET) chain from Trp_C, or Trp_D, to the isoalloxazine ring of FAD. Their average spacing of ~ 5 Å is ideal for stepwise ultrafast ET (~ 30 ps for *EcPL*).¹⁷⁴ These Trp triads/tetrads are believed to be involved in forming magnetic field sensitive radical pairs, and are therefore, central to the chemical magnetoreception hypothesis.¹⁴ An additional conserved residue near the N5 position (~ 3.5 Å) of the isoalloxazine ring of FAD plays a key role in the function of Crys and photolyases.⁸⁰ For most Crys and photolyases the residue is asparagine (Asn), however, in insect cryptochromes the residue is replaced by a cysteine (Cys) amino acid and in plant Crys it is substituted by aspartic acid (Asp). In plants Crys, Asp acts as a proton donor in photoactivation. Due to the low pK_a (~ 3.9) of the acid it can donate a proton to FAD to form FADH \cdot through the Trp ET chain.¹⁷⁵ Conversely, for Cys and Asn proton transfer (PT) cannot usually occur. This is due to the larger pK_a of Cys at ~ 8.3 and consequently FAD \cdot^- is found in insect Cry photoactivation.⁸¹ However, for Crys possessing the conserved Asn residue the case is less clear. Some Crys can undergo PT and others cannot, even though the pK_a of Asn is as high as 17. It is believed that the proton donor is likely a trapped water molecule with a highly acidic proton, with Asn contributing to the formation of FADH \cdot^- by stabilising the molecule via hydrogen bonding between the Asn and isoalloxazine residues.¹³⁰

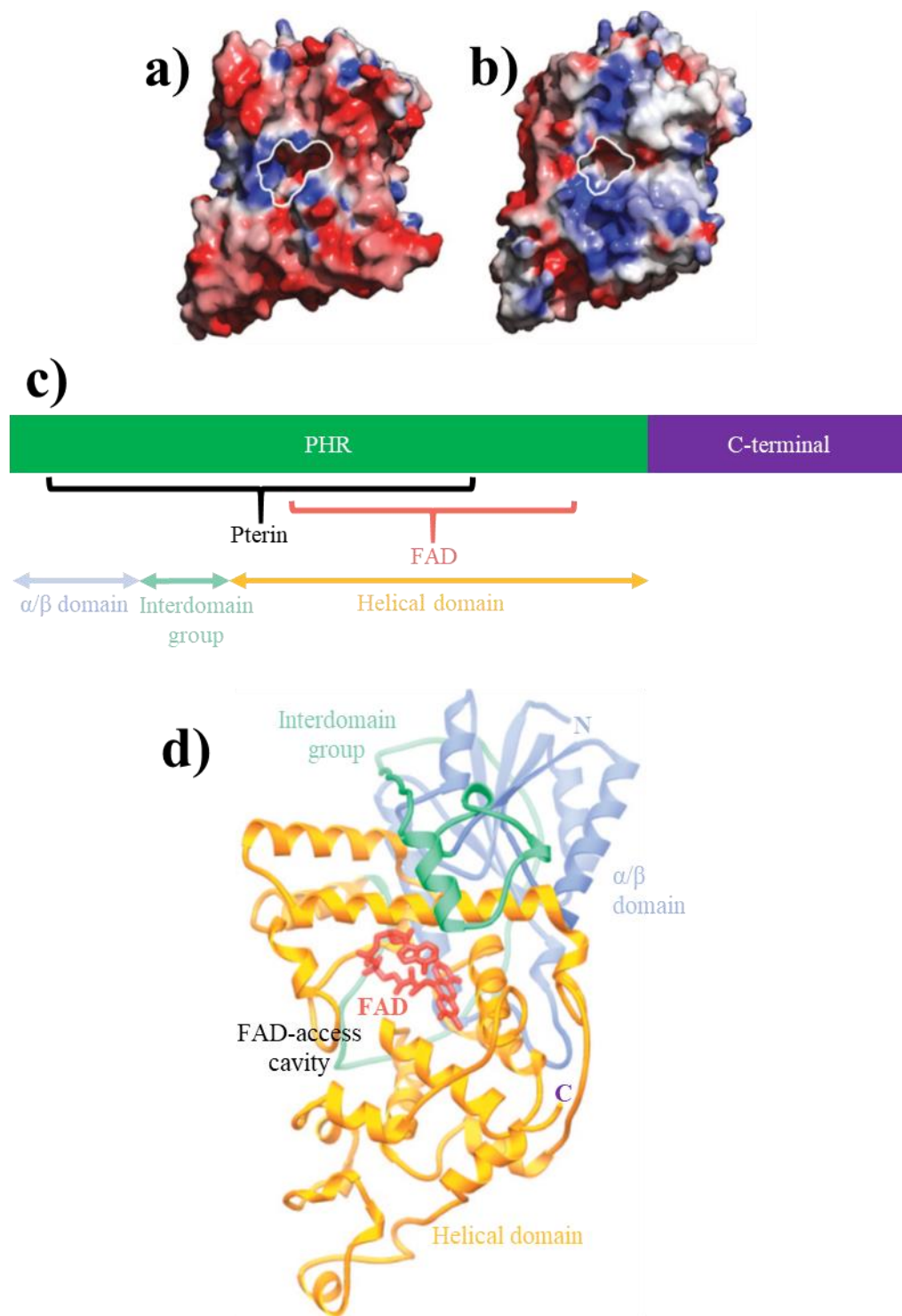


Figure 1.13. Cryptochrome structure. A structural comparison of the PHR domains of a) *Arabidopsis* cryptochrome (*AtCry1*) and b) *E. coli* DNA photolyase (*EcPL*). White boundaries represent the FAD-access cavities and red and blue represent regions of negative and positive electrostatic potential, respectively. c) A pictorial representation of an archetypal cryptochrome/photolyase superfamily protein. PHR region areas are shown in d). d) Overall fold of the Cry-DASH protein (*Synechosystis* sp. PCC6803 Cry). Based on ref. 159.

1.3.3 Magnetosensitive Photochemistry of Cryptochromes

The photochemistry of cryptochromes/photolyases is initiated by blue light photoexcitation of FAD to produce the singlet excited state (^1FAD) flavin, which is followed by stepwise ET along the Trp triad/tetrad producing the flavosemiquinone radical, $\text{FAD}^{\cdot-}$ or $\text{FADH}^{\cdot-}$ (as discussed above), and terminal Trp radical, forming a singlet born RP. Unlike flavins in solution (which form a triplet born RP, see Chapter 1.4), the RPs in Cry/PL are singlet born due to the close locale of the proximal Trp to FAD meaning that the singlet excited state flavin is quenched prior to intersystem crossing of the respective singlet excited state.¹⁷³ Figure 1.14 displays the absorption spectra for different flavin species in cryptochromes and photolyases. The absorption spectra of all species are characteristic of the equivalent flavin species in solution, however there is a distinct difference between the two (Fig. 1.18). Vibronic structure is displayed in the protein absorption spectra, this is due to the flavin being bound within the protein.¹⁷⁶ In solution, the flavin is tumbling freely and therefore vibronic structure is not observed. This spectroscopic marker is one way to identify bound or free flavin species within a sample, which is expanded on in Chapter 4.

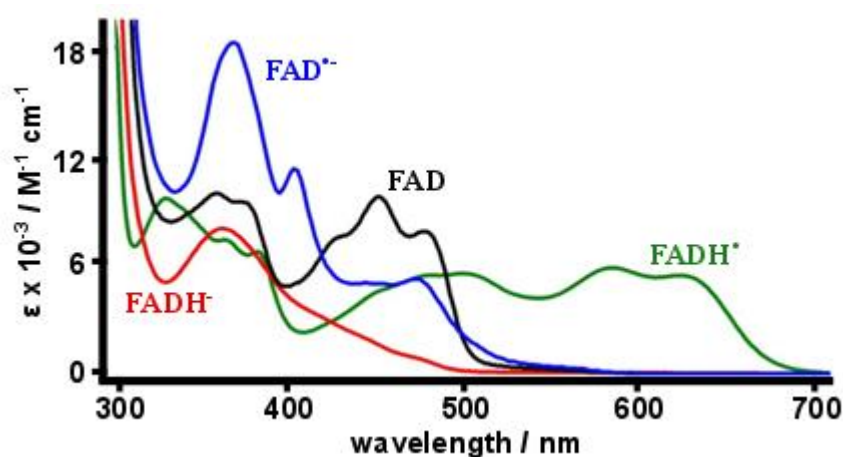


Figure 1.14. Absorption spectra for different redox of cryptochrome/photolyase. Data from mosquito (*Anopheles gambiae*) cryptochrome (AgCry1) = FAD and $\text{FAD}^{\cdot-}$, data from *E. coli* photolyase (EcPL) = $\text{FADH}^{\cdot-}$ and $\text{FADH}^{\cdot+}$. Based on ref. 177.

At present, MFEs have only been measured on three members of the Cry/PL superfamily of proteins, *EcPL*, *AtCry1*, and *DmCry*.^{19,20} In all cases, the measurements were conducted by transient absorption (TA) using purified (*in vitro*) proteins in 50-60% glycerol at 265-277 K. The similarities between the three proteins are, 1) a singlet born [$\text{FAD}^{\cdot-} + \text{TrpH}^{\cdot+}$] radical pair is initially formed, b) MFEs are observed on the long-lived FAD and Trp radical yields, which are consistent with the RPM, and c) changes in the protonation state of one or more of

the initial radicals ensures a quantifiable MFE. Differences between the three proteins are, a) the MFEs (at 510 nm and 22 mT) were ~-2%, ~-7%, and ~-20% for *DmCry*, *EcPL*, and *AtCry1*, respectively, b) the $\text{TrpH}^{\bullet+}$ to TrpH^{\bullet} step is slower in *DmCry* (~36 μs) than in *EcPL* (~2 μs) in 50% glycerol, c) an additional fast (~3 μs) component is examined in *DmCry*, d) for *DmCry* there is no measurable recovery of FAD (ground state) during the first 70 μs , where more than 50% recovery is observed in both *EcPL* and *AtCry1*.²⁰

The stark difference between *DmCry* and the other two proteins, *EcPL* and *AtCry1*, is explained by the existence of a fourth Trp residue in *DmCry*, which acts as the terminal Trp electron donor. The proposed photochemical reaction schemes are summarised in Fig. 1.15, which highlight the key mechanistic assumptions for the findings for *DmCry*, a) the ET from $\text{Trp}_\text{D}\text{H}^{\bullet+}$ to $\text{Trp}_\text{C}\text{H}^{\bullet+}$ occurs in ~3 μs , b) back electron transfer (BET) in both RP1_C and RP1_D is much slower than RP1_C to RP1_D and RP1_D to RP2_D , respectively, which also accounts for the small MFE, c) in all 3 proteins, the RP1_C is the only radical pair which produces MFEs. RP1_D and RP2_D are both too prolonged for spin-selective recombination to compete effectively with spin relaxation,^{20,178-180} and d) $\text{Trp}_\text{D}\text{H}^{\bullet+}$ and $\text{Trp}_\text{C}\text{H}^{\bullet+}$ have slight differences in their absorption spectra and/or molar extinction coefficients caused by variances in local distributions of the charged/polar species and/or discrepancies in the solvent accessibilities at the two radicals.^{20,179,181} Due to the limited availability of Cry samples and difficult purification processes, and the need for more sensitive spectroscopic techniques, no MFEs have been measured on avian Crys or in magnetic fields as weak as the geomagnetic field.

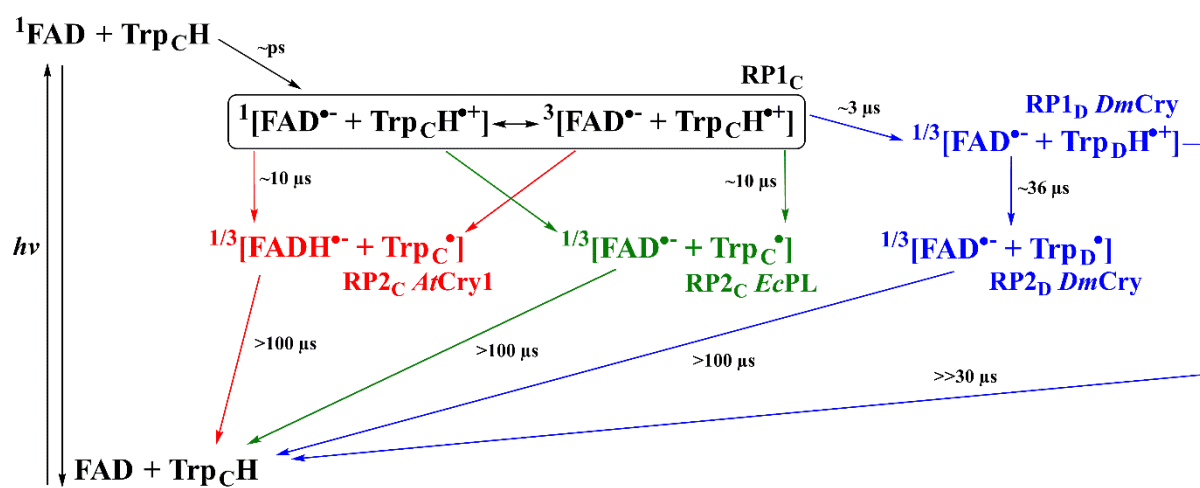


Figure 1.15. Proposed photochemical reaction schemes for *AtCry1*, *EcPL*, and *DmCry*. The black arrows and species are common to all species; the red, green, and blue features refer to *AtCry1*, *EcPL*, and *DmCry*, respectively. The double-headed arrow represents the coherent, magnetic field dependent spin-state mixing of the singlet and triplet states of RP1_C . Based on refs. 19 and 20.

1.4 FLAVINS

1.4.1 Introduction

The first partial purification of a flavin (lactochrome from cow's milk) was reported as early as 1879 by Blyth.¹⁸² The first pure flavin was not identified until 1933, when Kuhn *et al.*, isolated the vitamin riboflavin (RF, the flavin previously known as lactochrome) from whey.¹⁸³ The chemical structure of yellow pigment with bright greenish fluorescence was deduced from analysis of its chemical reactivity and elemental analysis, with confirmation when first lumiflavin and then RF were synthesised in 1934 and 1935, respectively.^{184,185} Old source descriptive names such as lactoflavin and ovoflavin were discarded. The name of riboflavin was decided, which was derived from the ribityl side chain and the yellow (latin: *flavus* meaning yellow) colour of the isoalloxazine conjugated ring system. In 1932, Warburg and Christian isolated an 'old yellow protein' from yeast and found that the product of photodegradation was identical to that of the photodegradation of RF. That compound was lumiflavin (LF).¹⁸⁶ Shortly after, Theorell made a landmark discovery, by showing the role of RF as a cofactor in enzyme catalysis and also in revealing a flavin similar to RF, but having a phosphate residue in ester linkage at the terminal hydroxyl group of the ribityl chain, this compound is flavin mononucleotide (FMN).¹⁸⁷ In a few following years, Warburg and Christian revealed enzyme activity in another protein on mixing of the apoprotein (a protein which together with a prosthetic group form a biochemical molecule, e.g. an enzyme) and isolated flavin.¹⁸⁸ This flavin was not RF or FMN, but a new flavin formed from the condensation of FMN and AMP (adenine monophosphate), the structure was finally proved by total synthesis by Todd in 1954 and is known as flavin adenine dinucleotide (FAD).¹⁸⁹ Although RF (vitamin B₂) occurs free in milk, eggs, urine, whey, and the retina, flavins inside living cells are generally in the forms of FAD and FMN (Fig. 1.16).¹⁹⁰ These two nucleotide forms of flavin have been identified to be the prosthetic groups (a tightly bound molecule (not composed of amino acids) required for the biological function of some proteins) of numerous flavoproteins,¹⁹¹ which include, entrainment of circadian rhythms (regulation of biological clocks) by cryptochrome (2017 Nobel Prize in Physiology or Medicine),¹⁵³ DNA repair by DNA photolyase (2015 Nobel Prize in Chemistry),¹⁵² and the focus of this thesis, the proposed role for cryptochrome in biological magnetoreception.¹⁴

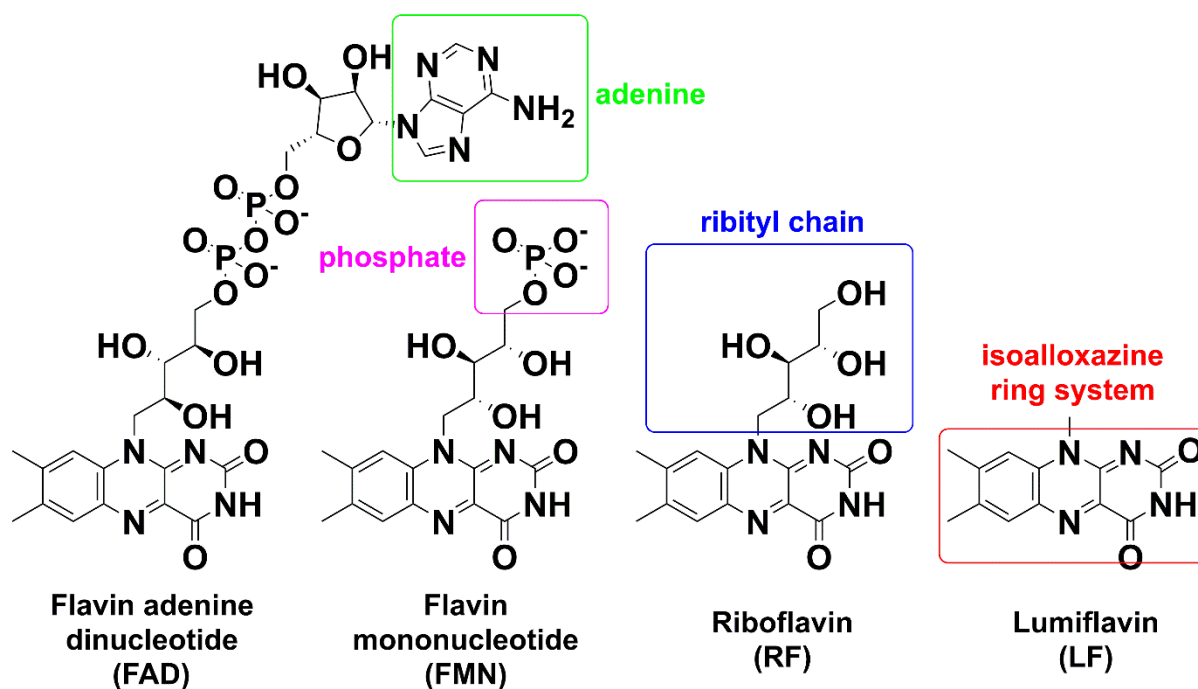


Figure 1.16. Chemical structures of key flavins. Notable features are highlighted.

1.4.2 Properties of Flavins

The chemical versatility of flavins is the reason they are involved in a wide variety of biological processes. They can exist in three different redox states: oxidized (quinone), one-electron reduced (semiquinone), and two-electron reduced (hydroquinone) (Fig. 1.17). Therefore, flavins can potentially undergo electron transfer, proton transfer, and hydride ion transfer, making them extremely versatile regarding types of reactions and substrate modifications. In solution, the equilibrium between different flavin species is pH dependent (Fig. 1.17). The neutral oxidized flavin exists between pH 1-9. Above pH 10, the N3 position is deprotonated to form the anionic flavin and additionally below pH 1 the N1 position is protonated to form the cationic moiety. Reduction of the quinone produces the semiquinone. Around pH 2 the protonation at the N5 position gives rise to the cationic semiquinone, and above pH 8 the anion is formed. Upon further reduction the hydroquinone is neutral between pH 0 and 6.7.

The hydrophilicity of flavins increases from RF to FMN to FAD. All three are miscible in water, however, there is another flavin, riboflavin tetrabutyrate (RFTB, see Chapter 4) which is immiscible in water and can be in hydrophobic environments. The isoalloxazine moiety is hydrophobic in nature, however the ribityl chains are more hydrophilic.¹⁹² The importance of the hydrophilicity of flavins is expanded on in Chapter 4. It can be seen from Fig. 1.16 that FAD possesses an adenine moiety, this allows FAD to undergo intramolecular radical pair formation (vide infra).

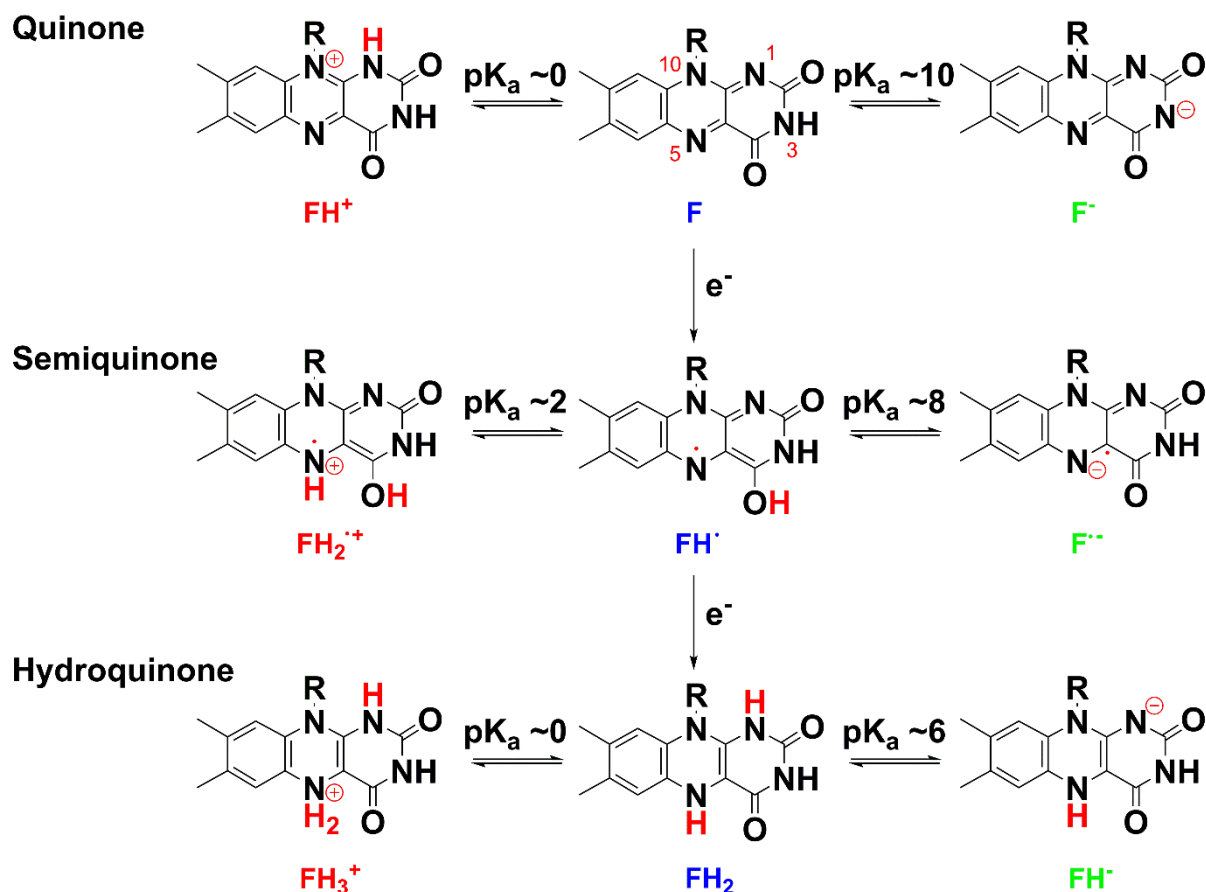


Figure 1.17. Redox and acid-base equilibria of flavins. Cationic, neutral, and anionic flavins are named in red, blue, and green, respectively. Positions of protonation and deprotonation are indicated in red.¹⁷⁶

1.4.3 Magnetosensitive Photochemistry of Flavins

The absorption spectra of flavins are influenced by the redox potential of the isoalloxazine ring system and pH (Fig. 1.18).¹⁹³ The ribityl derivatives of FAD, FMN, RF, and RFTB have almost no influence on the absorption spectra because in the same redox and acid-base forms the spectra are similar.¹⁹⁴ All the aforementioned flavins exhibit characteristic ground state absorption bands centred at 450 nm ($S_0 \rightarrow S_1$, $\pi \rightarrow \pi^*$) and 370 nm ($S_0 \rightarrow S_2$, $\pi \rightarrow \pi^*$), with similar molar extinction coefficients at $\sim 12,000$ and $\sim 11,000 \text{ M}^{-1} \text{ cm}^{-1}$, respectively. Flavin fluorescence ($\lambda_{\text{max}} \sim 530 \text{ nm}$) appears predominately in the neutral form, the anionic form is weakly fluorescent, and fluorescence from the cationic form is fundamentally non-existent.^{194,195} The fluorescence lifetime and quantum yield for FAD ($\tau = 2.27 \text{ ns}$, $\Phi = 0.04$, respectively, $\text{pH} < 3.6$) is considerably smaller than other flavins ($\tau \sim 5.09 \text{ ns}$, $\Phi \sim 0.25$, respectively), which is mainly due to the addition of the adenine moiety in the FAD molecule, which exists in open and closed conformations.^{193,196,197} FAD can undergo intramolecular electron transfer from the adenine moiety of FAD to the isoalloxazine ring.¹⁷³ At low pH (< 3.6) the adenine group of FAD is protonated (F-AH_2^+) and adopts the open conformer, while at higher pH the molecule is neutral (F-AH) and adopts the closed

conformer. In the neutral state, there is a proclivity for π -stacking between the adenine and isoalloxazine moieties, which leads to rapid electron transfer (ET) in the photoexcited singlet state and rapid internal conversion (IC), thus reducing the fluorescence lifetime and quantum yield (Fig. 1.1).^{193,196,197} Stob *et al.*,¹⁹⁸ conducted a CIDNP study on the pH dependence of FAD and found radical pair formation between pH 1.5 and 4.0. They argued that the ground state conformation of FAD, above pH 3.6, halts RP formation due to the strong (interradical) exchange interaction caused by the close proximity of the flavin and adenine moieties in the closed conformation.

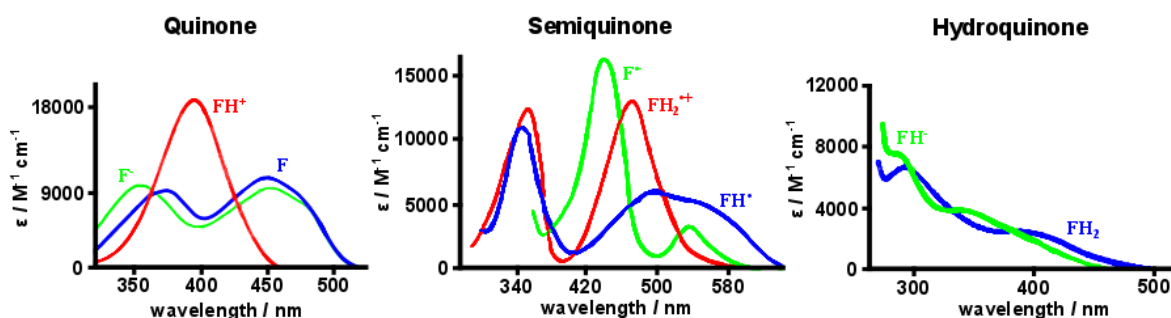


Figure 1.18. Absorption spectra of flavins in various oxidation and protonation states. Cationic, neutral, and anionic flavins are represented in red, blue, and green, respectively. Based on refs. 195, 199-201.

At low pH (<3.6), the situation is rather different. The open conformation can undergo rapid intersystem crossing to the triplet state on the timescale of a few nanoseconds.²⁰² Intramolecular ET creates a spin-correlated radical pair (SCRPs), formed in the triplet state $^3[\text{FH}\cdot - \text{AH}\cdot^+]$, where FH and AH represent the flavin and adenine moieties, respectively (Fig. 1.19). MFE studies on FAD photochemistry, using transient absorption (TA) spectroscopy, revealed that pH affects the radical pair dynamics. The time dependence and magnitude of the MFEs were explained by an equilibrium between the protonated triplet state ($\lambda_{\text{max}} \sim 680$ nm, $\tau = 0.7$ μs at pH 2.3) and the radical pair ($\lambda \sim 500$ -580 nm, assigned to the neutral semiquinone radical $\text{FADH}\cdot$), which is pH dependent.¹⁵ Both CIDNP and MFE studies on FAD suggest that no magnetic field sensitivity at neutral and physiological pH should exist. Elaboration of these observations is found in Chapter 3.1.

For other flavins such as FMN, RF, and RFTB no intramolecular ET is possible, however, they are susceptible to intermolecular ET from an external electron donor (Fig. 1.19b). Again, photoexcitation leads to formation of the singlet excited state, which rapidly internally converts to the excited triplet state. The singlet state is short-lived due to competing radiative (i.e. fluorescence) and non-radiative (i.e. internal conversion) processes and ISC. The triplet state is relatively long-lived and can undergo intermolecular ET from donor species, such as tryptophan, indole and other reducing species. Subsequently, a triplet born radical pair is produced to give $^3[\text{F}\cdot^- + \text{D}\cdot^+]$, see Fig. 1.19b. Through coherent S-T mixing, evolution of the singlet state from the triplet born radical pair is possible.

An external MF can energetically separate the T_{\pm} states from the S and T_0 states and consequently hinders the hyperfine driven S-T mixing. As only singlet states are reactive, recombination occurs solely from the singlet state, and therefore an increasing magnetic field will increase the concentration of the radical species and reduces the ground state population. As the radicals are not fixed together, as in FAD, the radicals can drift apart by diffusion. Recombination and S-T mixing are competing with diffusion, and the geminate radical pairs will separate leading to the formation of free radicals or F-pairs that can undergo spin state unselective reactions (Fig. 1.19b).¹⁷³

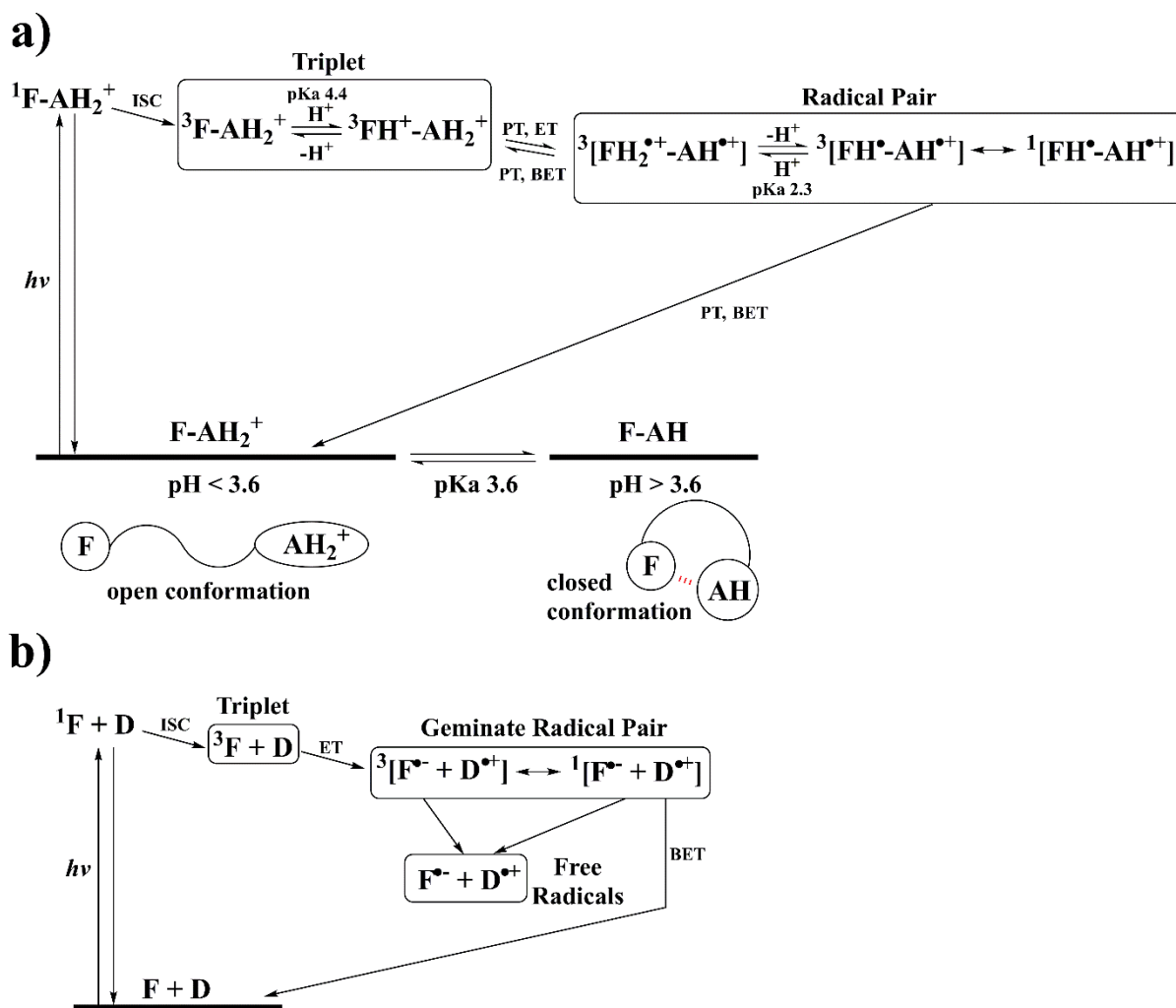


Figure 1.19. Proposed reaction schemes for flavin photochemistry. a) pH dependence of intramolecular radical pair formation for FAD below pH 3.6.¹⁵ b) Reaction scheme for intermolecular radical pair formation between flavin (F) and an electron donor (D).¹⁷³

Immobilising flavins provides an environment that simulates a more biologically pertinent one, which is desirable for understanding flavin-based RP systems in the cryptochrome protein. There have been numerous publications on MFEs on flavin-based systems in spatially localised environments, such as micelles and in the presence of

proteins.^{192,203,204} The author will highlight key observations that are relevant to the work discussed in Chapter 4, for a more comprehensive review the author recommends the reader to peruse Evans *et al.*, 2013.¹⁷³

Studies on the interaction with flavins and the hen egg-white lysozyme (HEWL) protein have been conducted with photo-CIDNP²⁰⁵ and MFE (by TA²⁰⁴ and cavity ring-down (CRD)²⁰⁶ spectroscopies) studies. Photo-CIDNP studied RF and HEWL, and elucidated intermolecular radical pair formation between RF and the Trp-62 and Trp-123 residues in the native state of HEWL.²⁰⁵ Thereafter, TA studies on RF-HEWL RPs observed an increased radical yield of 7% (indicating triplet born RP) in a 250 mT static magnetic field, however, a MFE of 13% was observed for a FMN-HEWL RP.²⁰⁴ The MF enhanced radical yield in the FMN-HEWL RP was attributed to the Coulombic interaction between the negatively charged phosphate group of FMN ($pK_a = 0.7$) and the positively charged HEWL (isoelectric point, $pI = 11.4$). This was confirmed by increasing the ionic strength of the FMN-HEWL solution, which induced charge screening and reduced the MFE to the 7% seen in the uncharged RF-HEWL system. Additionally, the MFE for a FMN-Trp RP in isotropic solution was considerably lower at 2%, which is ascribed to the faster diffusion for the free Trp amino acid compared with the HEWL protein, which leads to lower reencounter probability of the free radicals for the FMN-Trp isotropic system.²⁰⁴

This concludes the overview of the current understanding of biological magnetoreception and the associated theoretical background. We will now move on to discuss the motivation and objectives of this thesis.

1.5 A MICROSCOPIC APPROACH

At present, studies on flavin-based chemical systems and *in vitro* proteins conducted by spin chemists have been performed with spectroscopic techniques, such as flash photolysis transient absorption and fluorescence spectroscopy. Conversely, biologists have made observations on animal behavior and connected magnetic sensing to organs and genes. To fully understand the biological and chemical processes involved in animal magnetoreception, one needs to make observations at the cellular level. This requires spatially resolved spectroscopic investigations of magnetic field effects on biological reactions in living cells. Therefore, the aim of the work described in this thesis was to develop a spatially resolved microspectroscope to allow the study of magnetosensitive photochemistry of flavins not only in solution, but also in biomimetic and cellular environments. The primary objective was to unravel the mechanisms of the photochemical reactions involved in cryptochromes and ultimately, develop key connections between the fields of spin chemistry and biology (Fig. 1.20). We aim to build a bridge between the two fields by achieving the following:

- 1) Observe flavins inside living cells.
- 2) Particularly within the organelles of cells.
- 3) Finally, detect small magnetic field induced changes within these organelles.

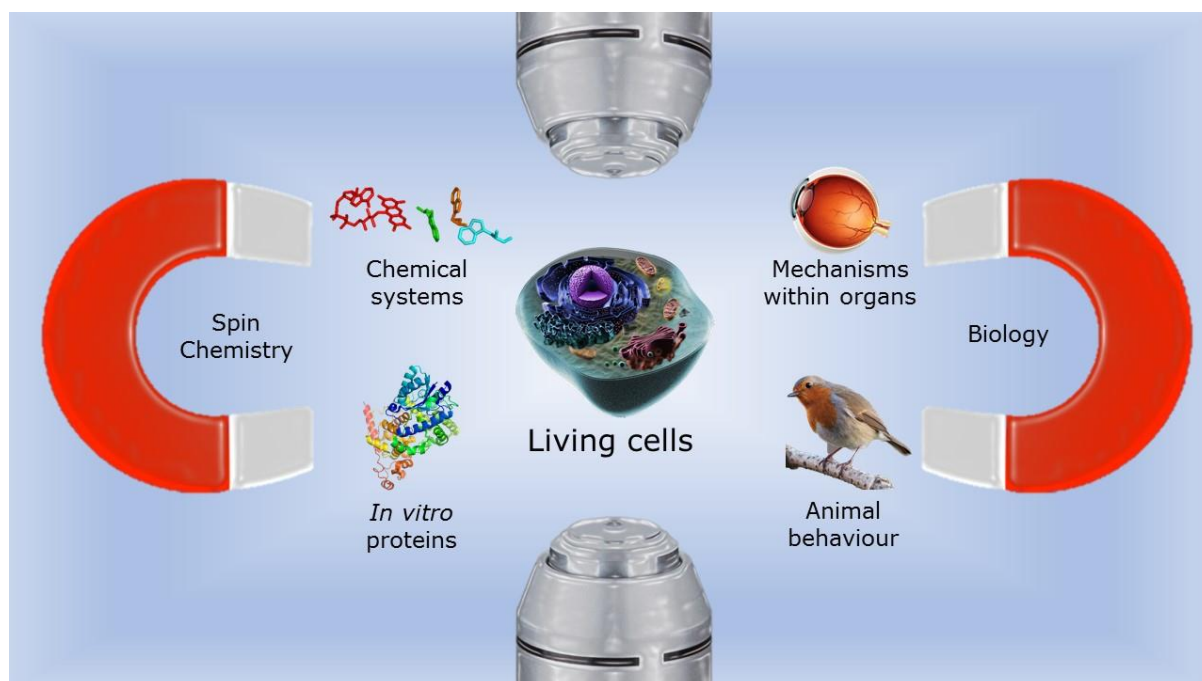


Figure 1.20. Schematic of the aim of the work described in this thesis.

Details of the microscope design and utility are described in the following Chapter.

References

- [1] N. Wertheimer and E. Leeper, *Am. J. Epidemiol.* **1979**, 109, 273.
- [2] S. Greenland, A. R. Sheppard, W. T. Kaune, C. Poole, and M. A. Kelsh, *Epidemiology* **2000**, 11, 624.
- [3] S. Ahlbom, N. Day, M. Feychting, E. Roman, J. Skinner, J. Dockerty, M. Linet, M. McBride, J. Michaelis, J. H. Olsen, T. Tynes, and P. K. Verkasalof, *Brit. J. Cancer* **2000**, 85, 692.
- [4] Advisory Group on Non-Ionising Radiation (AGNIR) ELF Electromagnetic Fields and the Risk of Cancer. *Report of an Advisory Group on Non-Ionising Radiation. Documents of the NRPB*, Vol. 12, National Radiology Protection Board, Chilton, Oxon, UK, **2001**.
- [5] International Agency for Research on Cancer, Static and Extremely Low-Frequency (ELF) Electric and Magnetic Fields. *IARC Monographs on the Evaluation of Carcinogenic Risks to Humans*, vol. 80, IARC, Lyon, **2002**.
- [6] P. L. Bounds, and N. Kuster, *Biophys J.* **2015**, 108, 562a.
- [7] a) I. Lagroye, Y. Percherancier, J. Juutilainen, F. Poullietier De Gannes, and B. Veyret, *Prog. Biophys. Molec. Biol.* **2011**, 107, 369–373. b) J. Juutilainen, M. Herrala, J. Luukkonen, J. Naarala, P. J. Hore, *Proc. R. Soc. B*, **2018**, 285, 20180590.
- [8] R. Wiltschko, W. Wiltschko, Magnetoreception. In: López-Larrea C. (eds) *Sensing in Nature. Advances in Experimental Medicine and Biology*, vol 739. Springer, New York, NY, **2012**.
- [9] P. Emery, W. Venus So, M. Kaneko, J. C. Hall, M. Rosbash, *Cell*, **1998**, 95, 669.
- [10] R. Stanewsky, M. Kaneko, P. Emery, B. Beretta, K. Wager-Smith, S. A. Kay, M. Rosbash, and J. C. Hall, *Cell*, **1998**, 95, 681.
- [11] M. Ahmad and A. R. Cashmore, *Nature* **1993**, 366, 162.
- [12] M. Koornneef, E. Rolff, C. J. P. Spruit, *Z. Pflanzenphysiol.* **1980**, 100, 147.
- [13] T. Ritz, S. Adem, and K. Schulten, *Biophys. J.* **2000**, 78, 707.
- [14] P. J. Hore and H. Mouritsen, *Annu. Rev. Biophys.* **2016**, 45, 299.
- [15] M. Murakami, K. Maeda, and T. Arai, *J. Phys. Chem. A*, **2005**, 109, 5793.

- [16] K. Maeda, K. B. Henbest, F. Cintolesi, I. Kuprov, C. T. Rodgers, P. A. Liddell, D. Gust, C. R. Timmel, and P. J. Hore. *Nature*, **2008**, 453, 387.
- [17] E. W. Evans, J. Li, J. G. Storey, K. Maeda, K. B. Henbest, P. J. Hore, S. R. Mackenzie, and C. R. Timmel, *Phys. Chem. Chem. Phys.*, **2015**, 17, 18456.
- [18] C. A. Dodson, C. J. Wedge, M. Murakami, K. Maeda, M. I. Wallace, and P. J. Hore, *Chem. Commun.*, **2015**, 51, 8023.
- [19] K. Maeda, A. J. Robinson, K. B. Henbest, H. J. Hogben, T. Biskup, M. Ahmad, E. Schleicher, S. Weber, C. R. Timmel, and P. J. Hore, *Proc. Natl. Acad. Sci. U. S. A.* **2012**, 109, 4774.
- [20] D. M. W. Sheppard, J. Li, K. B. Henbest, S. R. T. Neil, K. Maeda, J. Storey, E. Schleicher, T. Biskup, R. Rodriguez, S. Weber, P. J. Hore, C. R. Timmel, and S. R. Mackenzie, *Scientific Reports*, **2017**, 7, 42228.
- [21] R. Wiltchko, K. Stapput, P. Thalau, and W. Wiltchko, *J. R. Soc. Interface*, **2010**, 7, S163.
- [22] R. Marley, C. N. G. Giachello, N. S. Scrutton, R. A. Baines, and A. R. Jones, *Sci. Rep.*, **2014**, 4, 5799.
- [23] A. von Middendorf, *Mem. Acad. Sci. St. Petersburg*, **1855**, 8, 1.
- [24] M. E. Deutschlander and R. Muheim, Magnetic Orientation in Migratory Songbirds. In: *Breed M.D. and Moore J., (eds.) Encyclopedia of Animal Behavior*, volume 2, pp. 314-323 Oxford: Academic Press, **2010**.
- [25] W. Wiltchko, F. W. Merkel, *Verh. der Dtsch. Zoolog. Ges.*, **1966**, 59, 362.
- [26] W. Wiltchko, R. Wiltchko, and T. Ritz, *Procedia Chem.*, **2011**, 3, 276.
- [27] R. Blakemore, *Science*, **1975**, 190, 377.
- [28] A. Vidal-Gadea, K. Ward, C. Beron, N. Ghorashian, S. Gokce, J. Russell, N. Truong, A. Parikh, O. Gadea, A. Ben-Yakar, and J. Pierce-Shimomura, *eLife*, **2015**, 4, e07493.
- [29] K. J. Lohmann, *J. Exp. Biol.*, **1991**, 155, 37.
- [30] T. P. Quinn, R. T. Merrill, E. L. Brannon, *J. Exp. Biol.*, **1981**, 217, 137.
- [31] K. J. Lohmann, A. O. Willows, and R. B. Pinter, *J. Exp. Biol.*, **1991**, 161, 1.
- [32] S. M. Reppert, P. A. Guerra, and C. Merlin, *Annu. Rev. Entomol.*, **2016**, 61, 25.

- [33] J. B. Phillips, *Science*, **1986**, 233, 765.
- [34] P. Němec, J. Altmann, S. Marhold, H. Burda, and H. H. A. Oelschläger, *Science*, **2001**, 294, 366.
- [35] J. L. Kirschvink, *Trends Neurosci.*, **1982**, 5, 160.
- [36] J. L. Gould and K. P. Able, *Science*, **1981**, 212, 1061.
- [37] R. R. Baker, *Human Navigation and Magnetoreception*, Manchester University Press, UK, **1989**.
- [38] K. J. Lohmann and S. Johnsen, *Trends Neurosci.*, **2000**, 23, 153.
- [39] R. Wiltschko and W. Wiltschko, *Magnetic Orientation in Animals*, Springer, Berlin, Germany, **1995**.
- [40] J. Bloxham and D. Gubbins, *Sci. Am.*, **1989**, 261, 68.
- [41] D. Skiles, *Magnetite Biomineralization and Magnetoreception in Organisms: a New Biomagnetism*, chapter The geomagnetic field: its nature, history, and biological relevance. New York, London: Plenum Press, 43, **1985**.
- [42] <http://www.geomag.bgs.ac.uk/education/earthmag.html>
- [43] K. J. Lohmann and C. M. F. Lohmann, *Nature*, **1996**, 380, 59.
- [44] J. H. Fischer, M. J. Freake, S. C. Borland, and J. B. Phillips, *Anim. Behav.*, **2001**, 62, 1.
- [45] L. C. Boles and K. J. Lohmann, *Nature*, **2003**, 421, 60.
- [46] P. Semm and R. C. Beason, *Brain Res. Bull.*, **1990**, 25, 735.
- [47] S. T. Emlen and J. T. Emlen Jr., *Auk*, **1966**, 83(3), 361.
- [48] W. Wiltschko and R. Wiltschko, *Naturwissenschaften*, **2002**, 89, 445.
- [49] W. Wiltschko and R. Wiltschko, *Science*, **1972**, 176, 62.
- [50] S. Akesson, J. Morin, R. Muheim, and U. Ottosson, *Proc. R. Soc. Lond. B. (Biol. Sci.)*, **2001**, 268, 1907.
- [51] M. Faraday, *Phil. Trans. R. Soc. Lond.*, **1832**, 122, 125.
- [52] S. Johnsen and K. J. Lohmann, *Physics Today*, **2008**, 61, 3, 29.
- [53] A. J. Kalmijn, *J. Exp. Biol.*, **1971**, 5, 371.

- [54] A. J. Kalmijn, *Science*, **1982**, 218, 916.
- [55] C. G. Meyer, K. N. Holland, Y. P. Papastamatiou, *J. R. Soc. Interface*, **2005**, 2, 129.
- [56] A. J. Kalmijn, in *Sensory Biology of Aquatic Animals* (eds Atema, J., Fay, R. R., Popper, A. N. & Tavalga, W. N.) 151–186, Springer, Berlin, Germany, **1988**.
- [57] J. L. Kirschvink, *Bioelectromagnetics*, **1989**, 10, 239.
- [58] D. A. Bazylinski, and R. B. Frankel, *Nature Rev. Microbiol.*, **2004**, 2, 217.
- [59] J. L. Kirschvink and J. L. Gould, *Biosystems*, **1981**, 13, 181.
- [60] I. A. Solov'yov and W. Greiner, *Eur. Phys. J. D*, **2009**, 51, 161.
- [61] J. L. Kirschvink, M. M. Walker, and C. E. Diebel, *Curr. Opin. Neurobiol.*, **2001**, 11, 462.
- [62] I. A. Solov'yov and W. Greiner, *Biophys. J.*, **2007**, 93, 1493.
- [63] M. M. Walker, T. E. Dennis, and J. L. Kirschvink, *Curr. Opin. Neurobiol.*, **2002**, 12, 735.
- [64] M. Winklhofer and J. L. Kirschvink, *J. R. Soc. Interface*, **2010**, 7, S273.
- [65] A. F. Davila, G. Fleissner, M. Winklhofer, and N. Petersen, *Phys. Chem. Earth*, **2003**, 28, 647.
- [66] H. Mouritsen, *Nature*, **2012**, 484, 320.
- [67] G. Fleissner, E. Holtkamp-Rotzler, M. Hanzlik, M. Winklhofer, G. Fleissner, N. Petersen, and W. Wiltshko, *J. Comp. Neurol.*, **2003**, 458, 350.
- [68] G. Falkenberg, G. Fleissner, K. Schuchardt, M. Kuehbach, P. Thalau, H. Mouritsen, D. Heyers, G. Wellenreuther, and G. Fleissner, *PLOS ONE*, **2010**, 5, e9231.
- [69] C. D. Treiber, M. C. Salzer, J. Riegler, N. Edelman, C. Sugar, M. Breuss, P. Pichler, H. Cadiou, M. Saunders, M. Lythgoe, J. Shaw, and D. A. Keays, *Nature*, **2012**, 484, 367.
- [70] D. Heyers, M. Manns, H. Luksch, O. Güntürkün, and H. Mouritsen, *PLoS ONE* **2007**, 9, e937.
- [71] N. Lefeldt, D. Heyers, N. L. Schneider, S. Engels, D. Elbers, and H. Mouritsen, *J. R. Soc. Interface*, **2014**, 11, 20140777.
- [72] R. C. Beason and P. Semm, *J. Exp. Biol.*, **1996**, 199, 1241.

- [73] M. Zapka, D. Heyers, C. M. Hein, S. Engels, N. L. Schneider, J. Hans, S. Weiler, D. Dreyer, D. Kishkinev, J. M. Wild, and M. Mouritsen, *Nature*, **2009**, 461, 1274.
- [74] K. Schulten, C. E. Swenberg, and A. Weller, *Z. Phys. Chem. N. F.*, **1978**, 111, 1.
- [75] U. E. Steiner, and T. Ulrich, *Chem. Rev.*, **1989**, 89, 51.
- [76] J. B. Phillips and S. C. Borland, *Nature* **1992**, 359, 142.
- [77] W. Wiltschko, U. Munro, H. Ford, and R. Wiltschko, *Nature* **1993**, 364, 525.
- [78] M. Liedvogel and H. Mouritsen, *J. R. Soc. Interface*, **2010**, 7, S147.
- [79] H. Mouritsen and P. J. Hore, *Curr. Opin. Neurobiol.*, **2012**, 22, 343.
- [80] C. A. Dodson, P. J. Hore, and M. I. Wallace, *Trends Biochem. Sci.*, **2013**, 38, 435.
- [81] J. Wang, X. Du, W. Pan, X. Wang, and W. Wu, *J. Photochem. Photobiol. C*, **2015**, 22, 84.
- [82] P. Semm, D. Nohr, C. Demaine, and W. Wiltschko, *J. Comp. Physiol. A*, **1984**, 155, 283.
- [83] P. Semm and C. Demaine, *J. Comp. Physiol. A*, **1986**, 159, 619.
- [84] H. Mouritsen, U. Janssen-bienhold, M. Liedvogel, G. Feenders, J. Stalleicken, P. Dirks, and R. Weiler, *Proc. Natl. Acad. Sci. U. S. A.*, **2004**, 101, 14294.
- [85] M. Liedvogel, G. Feenders, K. Wada, N.F. Troje, and E.D. Jarvis, *Eur. J. Neurosci.*, **2007**, 25, 1166.
- [86] H. Mouritsen, G. Feenders, M. Liedvogel, K. Wada, and E.D. Jarvis, *Proc. Natl. Acad. Sci. U. S. A.* **2005**, 102, 8339.
- [87] W. Wiltschko and R. Wiltschko, *Naturwissenschaften*, **2002**, 89, 445.
- [88] U. Munro, J.A. Munro, J.B. Philips, and W. Wiltschko, *Aust. J. Zool.*, **1997**, 45, 189.
- [89] W. Wiltschko and R. Wiltschko, *J. Comp. Physiol. A* **1999**, 184, 295.
- [90] W. Wiltschko and R. Wiltschko, *Naturwissenschaften*, **2000**, 87, 36.
- [91] W. Wiltschko, J. Traudt, O. Güntürkün, H. Prior, and R. Wiltschko, *Nature* **2002**, 419, 467.
- [92] W. Wiltschko and R. Wiltschko, *J. Exp. Biol.*, **2001**, 204, 3295.

- [93] R. Wiltschko, M. Gesson, and W. Wiltschko, *Naturwissenschaften* **2001**, 88, 387.
- [94] W. Wiltschko and R. Wiltschko, *J. Comp. Physiol. A Neuroethol. Sens. Neural.Behav. Physiol.*, **1995**, 177, 363.
- [95] P. Semm and C. Demaine, *J. Comp. Physiol. A* **1986**, 159, 619.
- [96] T. Yoshii, M. Ahmad, and C. Helfrich-Forster, *PLoS Biol.*, **2009**, 7, e1000086.
- [97] C. Lin and T. Todo, *Genome Biol.*, **2005**, 6, 220.
- [98] R. Banerjee and A. Batschauer, *Planta* **2005**, 220, 498.
- [99] A. Möller, S. Sagasser, W. Wiltschko, and B. Schierwater, *Naturwissenschaften*, **2004**, 99, 585.
- [100] H. Mouritsen, U. Janssen-bienhold, M. Liedvogel, G. Feenders, J. Stalleicken, P. Dirks, and R. Weiler, *Proc. Natl. Acad. Sci. U. S. A.*, **2004**, 101, 14294.
- [101] C. Nießner, S. Denzau, J. C. Gross, L. Peichl, H.-J. Bischof, G. Fleissner, W. Wiltschko, and R. Wiltschko, *PLoS ONE*, **2011**, 6(5), e20091.
- [102] C. Nießner, S. Denzau, K. Stapput, M. Ahmad, L. Peichl, W. Wiltschko, and R. Wiltschko, *J. R. Soc. Interface*, **2013**, 10(88), 20130638.
- [103] C. Nießner, J. C. Gross, S. Denzau, L. Peichl, G. Fleissner, W. Wiltschko, and R. Wiltschko, *PLoS ONE*, **2016**, 11(3), e0150377.
- [104] A. Pinzon-Rodriguez, S. Bensch, and R. Muheim, *J. R. Soc. Interface*, **2018**, 15, 20180058.
- [105] A. Günther, A. Einwich, E. Sjulstok, R. Feederle, P. Bolte, K.-W. Koch, I. A. Solov'yov, and H. Mouritsen, *Current Biology*, **2018**, 28(2), 211.
- [106] J. R. Woodward, R. J. Jackson, C. R. Timmel, P. J. Hore, and K. A. McLauchlan, *Chem. Phys. Lett.*, **1997**, 272, 376.
- [107] C. T. Rodgers and P. J. Hore, *Proc. Natl. Acad. Sci. U. S. A.* **2009**, 106, 353.
- [108] J. R. Woodward, C. R. Timmel, K. A. McLauchlan, and P. J. Hore, *Phys. Rev. Lett.*, **2001**, 87, 077602.
- [109] T. Ritz, P. Thalau, J. B. Phillips, R. Wiltschko, and W. Wiltschko, *Nature* **2004**, 429, 177.

- [110] K. B. Henbest, P. Kukura, C. T. Rodgers, P. J. Hore, and C. R. Timmel, *J. Am. Chem. Soc.*, **2004**, 126, 8102.
- [111] C. T. Rodgers, K. B. Henbest, P. Kukura, C. R. Timmel, and P. J. Hore, *J. Phys. Chem. A* **2005**, 109, 5035.
- [112] T. Ritz, R. Wiltchko, P. J. Hore, C. T. Rodgers, K. Stapput, P. Thalau, C. R. Timmel, and W. Wiltchko, *Biophys. J.*, **2009**, 96, 3451.
- [113] C. Eichwald and J. Walleczek, *Biophys. J.*, **1996**, 71, 623.
- [114] C. R. Timmel and K. B. Henbest, *Philos. Trans. R. Soc. Lond. A* **2004**, 362, 2573.
- [115] I. A. Solov'yov, D. E. Chandler, and K. Schulten, *Biophys. J.*, **2007**, 92, 2711.
- [116] K. B. Henbest, K. Maeda, P. J. Hore, M. Joshi, A. Bacher, R. Bittl, S. Weber, C. R. Timmel, E. Schleicher, *Proc. Natl. Acad. Sci. U. S. A.* **2008**, 105, 14395.
- [117] I. A. Solov'yov, D. E. Chandler, K. Schulten, *Plant Signal. Behav.*, **2008**, 3, 676.
- [118] I. A. Solov'yov and K. Schulten, *Biophys. J.*, **2009**, 96, 4804.
- [119] T. Biskup, E. Schleicher, A. Okafuji, G. Link, K. Hitomi, E. D. Getzoff, and S. Weber, *Angew. Chem. Int. Ed.*, **2009**, 48, 404.
- [120] I. A. Solov'yov and K. Schulten, *J. Phys. Chem. B* **2012**, 116, 1089.
- [121] M. Ahmad, P. Galland, T. Ritz, R. Wiltchko, and W. Wiltchko, *Planta*, **2007**, 225, 615.
- [122] S. R. Harris, K. B. Henbest, K. Maeda, J. R. Pannell, C. R. Timmel, P. J. Hore, and H. Okamoto, *J. R. Soc. Interface* **2009**, 6, 1193.
- [123] D. Nohr, S. Franz, R. Rodriguez, B. Paulus, L.-O. Essen, S. Weber, and E. Schleicher, *Biophys. J.*, **2016**, 111(2), 301.
- [124] C. R. Timmel, U. Till, and B. Brocklehurst, *Mol. Phys.*, **1998**, 95, 71.
- [125] F. Cintolesi, T. Ritz, C. W. M. Kay, C. R. Timmel, and P. J. Hore, *Chem. Phys.*, **2003**, 294, 385.
- [126] S. Weber, *Biochim. Biophys. Acta*, **2005**, 1707, 1.

- [127] S. Weber, C. W. M. Kay, H. Mögling, K. Möbius, K. Hitomi, and T. Todo, *Proc. Natl. Acad. Sci. U. S. A.* **2002**, 99, 1319.
- [128] A. Sancar, *Chem. Rev.*, **2003**, 103, 2203.
- [129] M. Liedvogel, K. Maeda, K. Henbest, E. Schleicher, T. Simon, C.R. Timmel, P.J.Hore, and H. Mouritsen, *PLoS ONE*, **2007**, 2, 1.
- [130] N. Hoang, E. Schleicher, S. Kacprzak, J.-P. Bouly, M. Picot, W. Wu, A. Berndt, E. Wolf, R. Bittl, and M. Ahmad, *PLoS Biol.*, **2008**, 6, 1559.
- [131] I. A. Solov'yov, H. Mouritsen, and K. Schulten, *Biophys. J.*, **2010**, 99, 40.
- [132] M. Gomberg, *J. Am. Chem. Soc.*, **1900**, 22 (11), 757.
- [133] D. H. Hey and W. A. Waters, *Chem. Rev.*, **1937**, 21 (1), 169.
- [134] E. Zavoisky, *Fizicheskii Zhurnal.*, **1945**, 9, 211.
- [135] E. Zavoisky, Paramagnetic Absorption in Perpendicular and Parallel Fields for Salts, Solutions and Metals, *PhD thesis*, **1944**.
- [136] R. W. Fessenden and R. H. Schuler, *J. Chem Phys.*, **1963**, 39, 2147.
- [137] J. Bargon, H. Fischer, and U. Johnsen, *Z. Naturforsch.*, A, **1967**, 22, 1551.
- [138] H. R. Ward and R. R. Lawler, *J. Am. Chem. Soc.*, **1967**, 89, 5518.
- [139] G. L. Closs, *J. Am. Chem. Soc.*, **1969**, 91, 4552.
- [140] R. Kaptein and L. J. Oosterhoff, *Chem. Phys. Lett.*, **1969**, 4, 195, 214.
- [141] P. W. Atkins, *Chem. in Britain*, **1976**, 12, 214.
- [142] H. Hayashi, *Introduction to Dynamic Spin Chemistry: Magnetic Field Effects on Chemical and Biological Reactions*, World Scientific, **2004**.
- [143] S. Nagakura, H. Hayashi, and T. Azumi, *Dynamic Spin Chemistry: Magnetic Controls and Spin Dynamics of Chemical Reactions*, Kodansha/Wiley, Tokyo/New York, **1998**.

- [144] J. R. Woodward, *Magnetic Field Effects on Radicals Pairs in Homogeneous Solution, Carbon-Centered Free Radicals and Radical Cations*, John Wiley & Sons, Inc., **2010**.
- [145] J. Franck and E. Rabinowitsch, *Trans. Faraday Soc.*, **1934**, 30, 120.
- [146] N. J. Turro and B. Krautler, *In Diradicals*, W. T. Borden New York: Wiley, **1982**, 259.
- [147] S. Batchelor, C. Kay, K. Mclauchlan, and I. Shkrob, *J. Phys. Chem.*, **1993**, 97, 13250.
- [148] M. Justinek, G. Grampp, and S. Landgraf, *Phys. Chem. Chem. Phys.*, **2002**, 4, 5550.
- [149] J. R. Woodward, *Radical Pairs in Solution, Progress in Reaction Kinetics and Mechanism*, Vol. 27, 165-207, **2002**.
- [150] A. Weller, F. Nolting and H. Staerk, *Chem. Phys. Lett*, **1983**, 96, 24-27.
- [151] C. Darwin, *The power of movement in plants*. Da Capo, Press, New York, **1881**.
- [152] J. Gressel, *Photochem. Photobiol.*, **1977**, 30, 749.
- [153] N. Oztürk, S. H. Song, S. Ozgür, C. P. Selby, L. Morrison, C. Partch, D. Zhong, and A. Sancar, *Cold Spring Harb. Symp. Quant. Biol.*, **2007**, 72, 119.
- [154] I. Chaves, R. Pokorny, M. Byrdin, N. Hoang, T. Ritz, K. Brettel, L.-O. Essen, G. T. J. van der Horst, A. Batschauer, and M. Ahmad, *Annu. Rev. Plant Biol.*, **2011**, 62, 335.
- [155] A. Sancar, Mechanisms of DNA Repair by Photolyase and Excision Nuclease (Nobel Lecture). *Angew. Chem., Int. Ed.*, **2016**, 55, 8502.
- [156] C. Lin, D. E. Robertson, M. Ahmad, A. A. Raibekas, M. S. Jorns, P. L. Dutton, and A. R. Cashmore, *Science*, **1995**, 269, 968.
- [157] "Michael Rosbash - Nobel Lecture: The Circadian Clock, Transcriptional Feedback and the Regulation of Gene Expression". *Nobelprize.org*. Nobel Media AB 2014. Web. 19 May **2018**.
http://www.nobelprize.org/nobel_prizes/medicine/laureates/2017/rosbash-lecture.html
- [158] R. Brudler, K. Hitomi, H. Daiyasu, H. Toh, K.-I. Kucho, M. Ishiura, M. Kanehisa, V.A. Roberts, T. Todo, J.A. Tainer, and E.D. Getzoff, *Mol. Cell*, **2003**, 11, 59.
- [159] C. Lin and T. Todo, *Genome Biol.*, **2005**, 6, 220.

- [160] P. Zirak, A. Penzkofer, J. Moldt, R. Pokorny, A. Batschauer, and L.O. Essen, *J. Photochem. Photobiol. B*, **2009**, 97, 94.
- [161] Q. Yuan, D. Metterville, A. D. Briscoe, and S. M. Reppert, *Mol. Biol. Evol.*, **2007**, 24, 948.
- [162] A. Sancar, *Annu. Rev. Biochem.*, **2000**, 69, 31.
- [163] A. Sancar, *J. Biol. Chem.*, **2004**, 279, 34079.
- [164] H. Zhu, I. Sauman, Q. Yuan, A. Casselman, M. Emery-Le, P. Emery, and S. M. Reppert, *PLoS Biol.*, **2008**, 6, e4.
- [165] G. T. J. van der Horst, M. Muijtjens, K. Kobayashi, R. Takano, S.-I. Kanno, M. Takao, J. de Wit, A. Verkerk, A. P. M. Eker, D. van Leenen, R. Buijs, D. Bootsma, J. H. J. Hoeijmakers, and A. Yasui, *Nature*, **1999**, 398, 627.
- [166] C. Kami, S. Lorrain, P. Hornitschek, and C. Fankhauser, *Curr. Top. Dev. Biol.*, **2010**, 91, 29.
- [167] Z. Liu, C. Tan, X. Guo, Y.-T. Kao, J. Li, L. Wang, A. Sancar, and D. Zhong, *Proc. Natl Acad. Sci. USA*, **2011**, 108, 14831.
- [168] K. Brettel and M. Byrdin, *Curr. Opin. Struct. Biol.*, **2010**, 20, 693.
- [169] D. S. Hsu, X. Zhao, S. Zhao, A. Kazantsev, R. P. Wang, T. Todo, Y. F. Wei, and A. Sancar, *Biochemistry*, **1996**, 35, 13871.
- [170] K. Malhotra, S. T. Kim, A. Batschauer, L. Dawut, and A. Sancar, *Biochemistry*, **1995**, 34, 6892.
- [171] C. Lin and D. Shalitin, *Annu. Rev. Plant Biol.*, **2003**, 54, 469.
- [172] T. Todo, *Mutat. Res.*, **1999**, 434, 89.
- [173] E. W. Evans, C. A. Dodson, K. Maeda, T. Biskup, C. J. Wedge, and C. R. Timmel, *Interface Focus*, **2013**, 3, 20130037.
- [174] A. Lukacs, A. P. M. Eker, M. Byrdin, K. Brettel, and M. H. Vos, *J. Am. Chem. Soc.*, **2008**, 130, 14394.
- [175] A. Berndt, T. Kottke, H. Breitkreuz, R. Dvorsky, S. Hennig, M. Alexander, and E. Wolf, *J. Biol. Chem.*, **2007**, 282, 13011.

- [176] S. Weber and E. Schleicher, *Flavins and Flavoproteins: Methods and Protocols*; Methods in Molecular Biology. Springer, New York, **2014**.
- [177] B. Liu, H. Liu, D. Zhong, and C. Lin, *Curr. Opin. Plant Biol.*, **2010**, 13, 578.
- [178] B. Paulus, C. Bajzath, F. Melin, L. Heidinger, V. Kromm, C. Herkersdorf, U. Benz, L. Mann, P. Stehle, P. Hellwig, S. Weber, and E. Schleicher, *FEBS. J.*, **2015**, 282, 3175.
- [179] P. Müller, J. Yamamoto, R. Martin, S. Iwai, and K. Brettel, *Chem. Commun.*, **2015**, 51, 15502.
- [180] D. R. Kattnig, I. A. Solov'yov, and P. J. Hore, *Phys. Chem. Chem. Phys.*, **2016**, 18, 12443.
- [181] C. Bernini, T. Andruniów, M. Olivucci, R. Pogni, R. Basosi, and A. Sinicropi, *J. Am. Chem. Soc.*, **2013**, 135, 4822.
- [182] A. Wynter Blyth, *J. Chem. Soc. Trans.*, **1879**, 35, 530.
- [183] R. Kuhn, P. György, and T. Wagner-Jauregg, *Ber.*, **1933**, 66, 576.
- [184] R. Kuhn, K. Reinemund, and F. Weygand, *Ber.*, **1934**, 67, 1460.
- [185] P. Karrer, K. Schopp, and F. Benz, *Helvetica Chim. Acta*, **1935**, 18, 426.
- [186] O. Warburg and W. Christian, *Naturwissenschaften* **1932**, 20, 688.
- [187] H. Theorell, *Biochem. Z.*, **1935**, 275, 344.
- [188] O. Warburg and W. Christian, *Biochem. Z.*, **1938**, 298, 150.
- [189] S. M. H. Christie, G. W. Kenner, and A. R. Todd, *J. Chem. Soc.*, **1954**, 46-52.
- [190] T. Wagner-Jauregg, in W. H. Sebrell and R. S. Harris (Eds.), *Riboflavin, The Vitamins*, Vol. III, Academic Press, New York, **1954**.
- [191] P. F. Heelis, *Chem. Soc. Rev.*, **1982**, 11, 15.
- [192] M. Horiuchi, K. Maeda, and T. Arai, *Appl. Magn. Reson.*, **2003**, 23, 309.
- [193] A. Sengupta, R. V. Khade, and P. Hazra, *J. Photochem. Photobiol. A*, **2011**, 221, 105.
- [194] M. Sun, T. A. Moore, and P. S. Song, *J. Am. Chem. Soc.*, **1972**, 94, 1730.
- [195] P. Drössler, W. Holzer, A. Penzkofer, and P. Hegemann, *Chem. Phys.*, **2002**, 282, 429.

- [196] S. D. M. Islam, T. Susdorf, A. Penzkofer, and P. Hegemann, *Chem. Phys.*, **2003**, 295, 137.
- [197] R. Y. Stanley and A. W. MacPharlane IV, *J. Phys. Chem. A*, **2000**, 104, 6899.
- [198] S. Stob, J. Kemmink, and R. Kaptein, *J. Am. Chem. Soc.*, **1989**, 111, 7036.
- [199] E. J. Land and A. J. Swallow, *Biochemistry*, **1969**, 8, 2117.
- [200] Y. Kao, C. Saxena, T. He, L. Guo, L. Wang, A. Zhu, and D. Zhong, *J. Am. Chem. Soc.*, **2008**, 130, 13132.
- [201] J. Brazard, A. Usman, F. Lacombat, C. Ley, M. M. Martin, and P. Plaza, *J. Phys. Chem. A*, **2011**, 115, 3251.
- [202] E. Silva and A. M. Edwards, *Flavins: photochemistry and photobiology*. Cambridge, UK: RSC Publishing, **2006**.
- [203] M. Horiuchi, K. Maeda, and T. Arai, *Chem. Phys. Lett.*, **2004**, 394, 344.
- [204] T. Miura, K. Maeda, and T. Arai, *J. Phys. Chem. B*, **2003**, 107, 6474.
- [205] P. J. Hore and R. Kaptein, *Biochemistry*, **1983**, 22, 1906.
- [206] K. Maeda, S. R. T. Neil, K. B. Henbest, S. Weber, E. Schleicher, P. J. Hore, S. R. Mackenzie, and C. R. Timmel, *J. Am. Chem. Soc.*, **2011**, 133, 17807.

CHAPTER 2

Instrumental

This chapter discusses the design of the instrument and demonstration of its capabilities with basic model chemical radical pair reactions in solution and in the solid-state. The instrument was designed by Prof. Jonathan R. Woodward and Dr. Joshua P. Beardmore. Construction was completed by Dr. Joshua P. Beardmore before the author joined the Woodward Group. The author optimised, tested, and enhanced the instrument, also evaluating its utility by studying spatially localised radical pair reactions. All experimental data were recorded by the author. Additionally, the stage scanning algorithm was written by the author. The three-colour approach was designed by the author and Prof. Woodward, and constructed, optimised, and evaluated by the author.

The work in this chapter has been published in the following peer-reviewed journals:

L. M. Antill, J. P. Beardmore, and J. R. Woodward, Time-resolved optical absorption microspectroscopy of magnetic field sensitive flavin photochemistry, *Review of Scientific Instruments*, 89, 023707, February **2018**

J. P. Beardmore, L. M. Antill, and J. R. Woodward, Optical Absorption and Magnetic Field Effect Based Imaging of Transient Radicals, *Angewandte Chemie International Edition*, 54, 8494-8497, June **2015**

J. P. Beardmore, L. M. Antill, and J. R. Woodward, Optical Absorption and Magnetic Field Effect Based Imaging of Transient Radicals, *Angewandte Chemie*, 127, 8614-8617, **2015**.

Chapters 2.1 and 2.2 are reformatted versions of Antill *et al.*, and Beardmore *et al.*, respectively.

2.1 MEASUREMENT SENSITIVITY

Abstract

The photochemical reactions of blue-light receptor proteins have received much attention due to their very important biological functions. In addition, there is also growing evidence that the one particular class of such proteins, the cryptochromes, may be associated with not only a biological photo-response but also a magneto-response, which may be responsible for the mechanism by which many animals can respond to the weak geomagnetic field. Therefore, there is an important scientific question over whether it is possible to directly observe such photochemical processes, and indeed the effects of weak magnetic fields thereon, taking place both in purified protein samples *in vitro* and in actual biochemical cells and tissues. For the former samples, the key lies in being able to make sensitive spectroscopic measurements on very small volumes of samples at potentially low protein concentrations, while the latter requires, in addition, spatially resolved measurements on length scales smaller than typical cellular components, i.e., sub-micron resolution. In this work, we discuss a two- and three-color confocal pump-probe microscopic approach to this question which satisfies these requirements and is thus useful for experimental measurements in both cases.

Introduction

Recent experiments on magnetically sensitive animals including birds,¹ fruit flies,² and monarch butterflies³ have provided increasing amounts of circumstantial evidence that the class of blue-light receptor proteins called the cryptochromes may be involved in the process of detecting the geomagnetic field. It is proposed that spin correlated radical pairs (RPs) generated by photoinduced electron transfer from a protein residue (likely tryptophan) to a bound flavin adenine dinucleotide (FAD) cofactor molecule show magnetic field dependent kinetics via the radical pair mechanism (RPM) and that under the correct conditions, low field effects (LFEs) in this reaction might lead to the ability to detect magnetic fields as weak as that of the Earth (30-50 μ T).^{4,5} Maeda and co-workers⁶ first demonstrated that cryptochrome purified from *Arabidopsis thaliana* exhibited magnetic field sensitive photochemistry when excited with nanosecond pulses of blue light *in vitro*, while a model radical pair system has demonstrated a measurable difference in photochemical kinetics in zero and Earth strength magnetic field.⁷

We describe in this paper, an instrument which aims to address two key experimental challenges in studying the magnetic field sensitivity of cryptochrome photochemistry:

1. Measurement sensitivity. The study of cryptochrome photochemistry requires the production of purified, cofactor bound samples of cryptochrome proteins from a variety of different species. For unravelling mechanistic aspects of the magnetoresponse, site-directed mutagenesis is extremely useful as it allows the modification of the structure in the region of the cofactor binding pocket and thus in the electron transfer, or other photochemical reaction processes, that can take place therein. Such experiments typically only produce small volumes (tens to thousands, in ideal cases, of microliters) of protein samples, typically at concentrations of tens or hundreds of micromoles per litre. This means that spectrometers capable of making sensitive time-resolved spectroscopic measurements on such samples are invaluable.

2. Spatially resolved measurements. Beyond the need to study the magnetic sensitivity of the photoreactions of isolated cryptochromes is the need to make corresponding measurements in cells and tissues, not least to address the question of anisotropic magnetic field responses, i.e., the ability to sense the direction of external magnetic fields.

The preliminary results obtained using our instrument were recently published elsewhere (Chapter 2.2).⁸ In this paper, we provide details on our instrumental and experimental approach, demonstrating our technique's capabilities for use with biological samples and describe a methodology which allows the instrument to be used to make measurements on small volumes of samples in which the photochemical processes are non-cyclic, i.e., in which photoexcitation is destructive to the sample.

Experimental

Reaction systems

As a proxy for investigations on cryptochromes, we base our measurements on the photochemistry of the key cryptochrome cofactor, FAD, and observe photoinduced electron transfer reactions of this molecule in isolation, in which the intramolecular electron transfer can take place from the adenine moiety to the flavin moiety to generate a separated biradical at low pH. Such a system represents the lower limit of sensitivity for observing the corresponding photochemistry in cryptochromes as the latter benefits from an optimal spatial arrangement of FAD and donor residues within the binding pocket. The efficiency of the electron transfer is substantially increased as evidenced by the fact that in the studies to date, RPs generated in cryptochrome (and the structurally similar photolyase protein from *E. coli*) are born in the singlet state, from the short-lived FAD excited singlet state, while FAD photochemistry in solution produces triplet born RPs, as the electron transfer is not fast enough to compete with intersystem crossing (ISC) in the excited FAD (Fig. 2.1). In the case of FAD alone at low pH, there appears

to be an equilibrium established between the protonated triplet state of FAD and the radical pair and so the total concentration of triplet state FAD and semiquinone radical combined are likely similar to the concentration of the protonated semiquinone radical produced in cryptochromes.

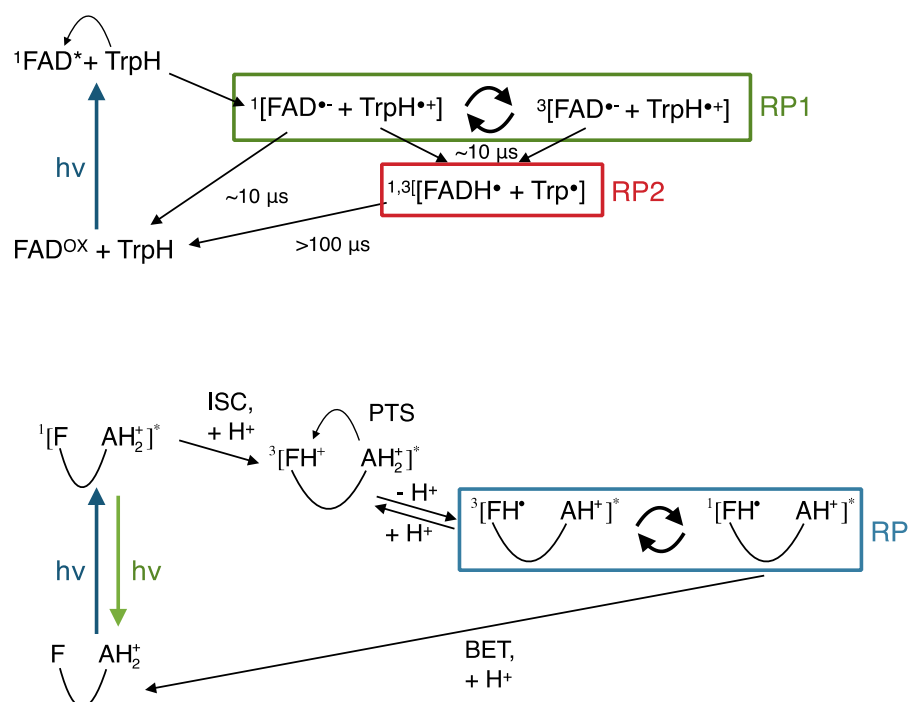


Figure. 2.1. Reaction scheme overviewing the spin selective photochemical reactions of FAD, (a) bound within *A. thaliana* cryptochromes (AtCry, based on Ref. 6) and (b) in acid solution. For AtCry, after photoexcitation, an electron is transferred along a chain of tryptophan (Trp) residues generating RP1 which undergoes spin selective back electron transfer (BET). RP1 is magnetically sensitive, and RP2 is long lived and magnetically insensitive. For FAD in acidic solution, (b), the electron transfer takes place to flavin (F) from adenine (A) in the excited protonated triplet state [PTS, generated by intersystem crossing (ISC) from and protonation of the excited singlet state of protonated FAD] which generates a triplet born diradical which can undergo spin-selective BET.

Our apparatus uses a blue laser to photoexcite the FAD molecule and then a (typically) green laser to probe the RP by detecting the one electron reduced semiquinone form of FAD produced by the electron transfer and the protonated triplet state of the flavin from which it is formed. Thus, the basic spectroscopic approach is the classic transient optical absorption spectroscopy, as used in the majority of studies of cryptochrome photochemistry to date.

For animals in the wild, blue-light irradiation conditions are quite different from the short (ns), intense laser pulses employed in flash photolysis measurements, being continuous wave and of considerably lower intensity. Therefore, it is important to be able to study the photochemistry under both sets of irradiation conditions. Our

instrument allows measurements to be made in both irradiation regimes. Indeed, it has been recently demonstrated⁹ that under appropriate reaction conditions, continuous blue-light irradiation of flavins can lead to chemical amplification of observed magnetic field effects (MFEs), which may be important in understanding the biological response.

Instrumental details

A schematic of the experimental arrangement is shown in Fig. 2.2. The pump and probe beams are provided by a pair of solid-state lasers [Coherent CUBE 449 nm (pump) and Coherent Sapphire 532 nm (probe)]. The output of the 532 nm laser is first beam split using a variable polarizing beam splitter before being combined with the output of the 449 nm laser using a dichroic mirror. The combined beams are then launched into a single mode optical fiber which conducts the laser light to the microscope apparatus. The single mode optical fiber ensures optimal spatial overlap and clean Gaussian beam profiles of the two laser beams used.

The microscope, shown in Fig. 2.3, is similar to an instrument used to image single molecules.^{10,11} It is constructed in a transmission confocal arrangement and utilizes the absorption (and/or scattering) of photons, at an appropriate wavelength, for imaging purposes.

The major components of the apparatus consist of a piezoelectric sample translation stage (PI nano[®] P-545), two super apochromat objective lenses (Olympus UPlanSApo20 \times), and a number of micrometer adjusted translation stages (Thorlabs). The use of the apochromatic lenses minimizes the relative displacement of the focal beam waists of the two wavelengths used to within 150 nm, well within the Rayleigh lengths of the two beams. The beam waists are approximately 240 nm and 285 nm for the 449 nm and 532 nm beams, respectively. The microscope is assembled on a vibrationally isolated optical bench (Herz DT-8060M-D) to eliminate any potential external sources of spurious signals.

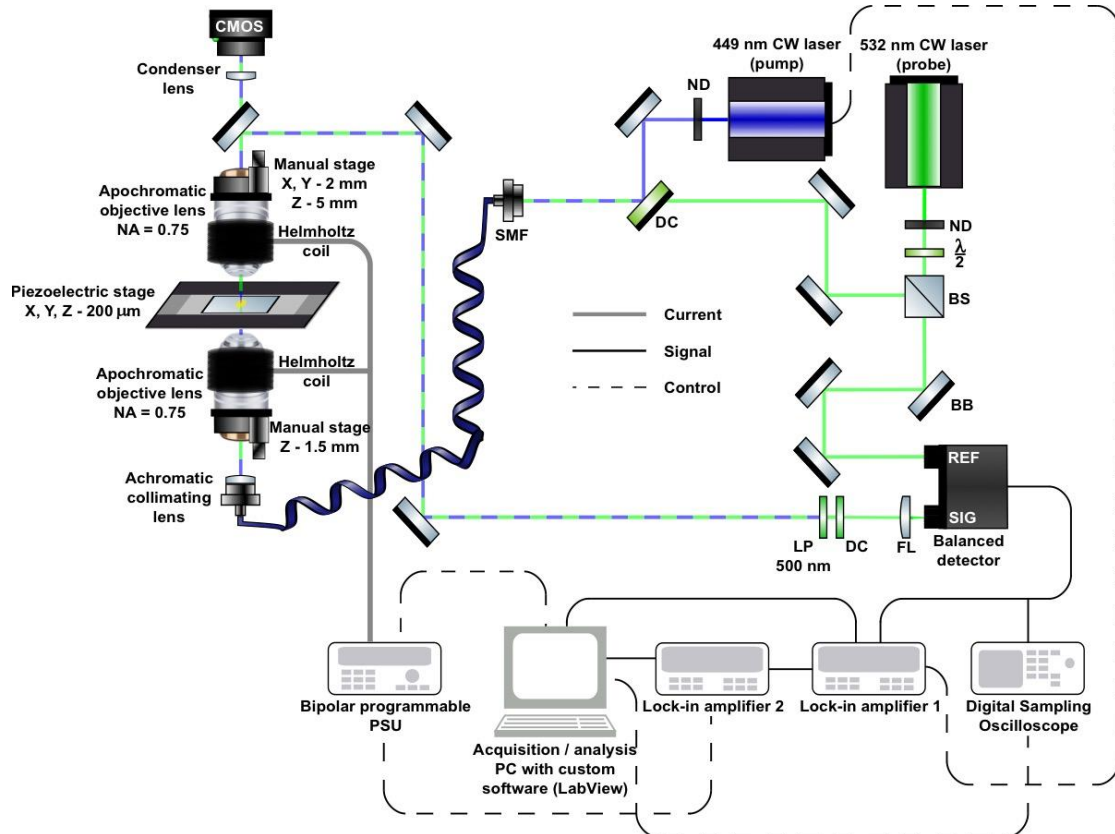


Figure 2.2. Basic layout of the microscope. SMF = single mode fiber, DC = dichroic mirror, ND = neutral density filter, $\lambda/2$ = half-wave plate polarizer, BS = beam splitter, BB = broadband dielectric mirror, LP = longpass filter, FL = focusing lens, PSU = power supply unit.

The optical axis of the microscope is defined by a 95 mm optical rail. This is mounted to an x- and y-axis translation stage which enables 12.5 mm of travel across the sample. The microscope optics are mounted within a 30 mm cage system (Thorlabs) to allow accurate axial alignment and structural rigidity. The optical fiber from the laser system is introduced under the sample stage and is collimated at the optimal beam diameter for the objective lenses chosen. The lower objective lens is mounted on a z-axis translation stage enabling the lens to sample distance to be adjusted with high precision. The upper objective can be adjusted along all three (x-, y-, and z-) axes and allows the pair of lenses to be accurately aligned into the confocal arrangement.

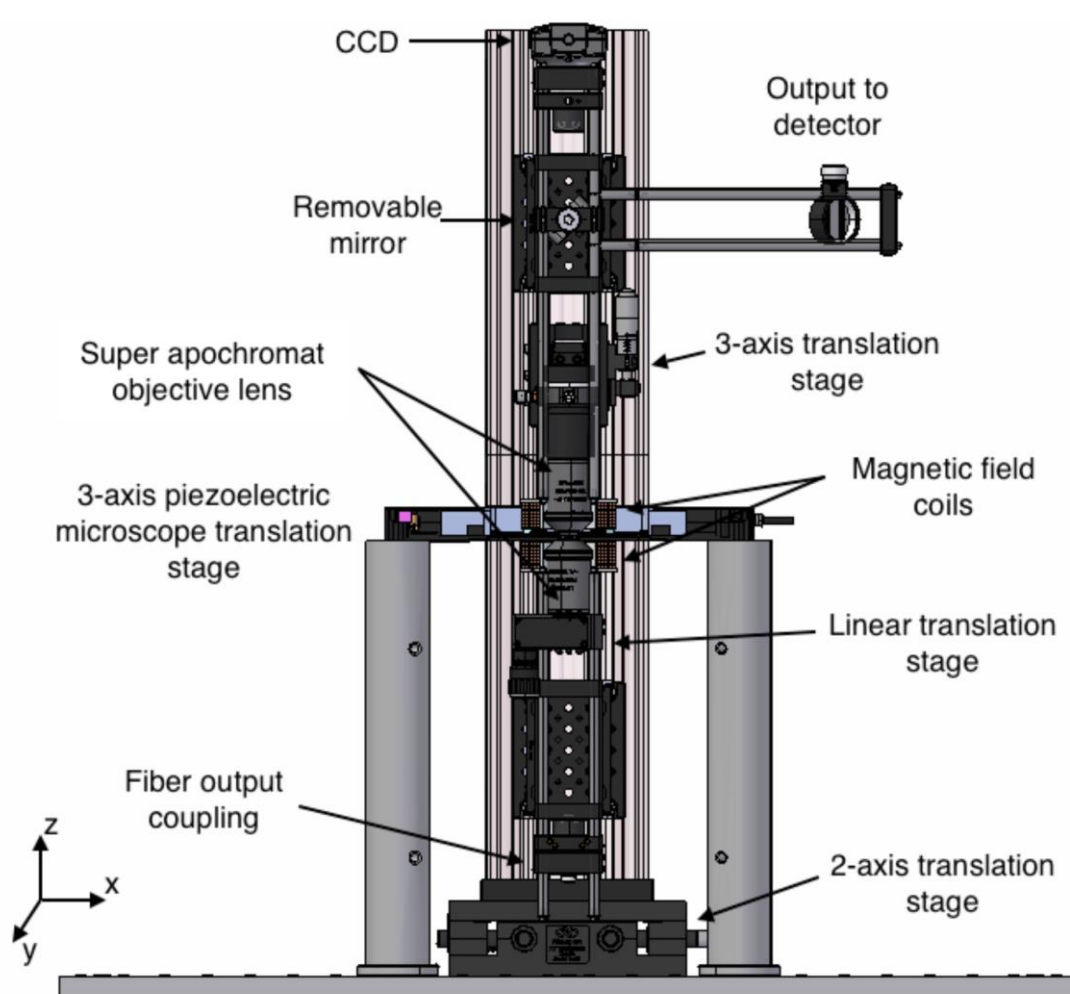


Figure 2.3. Side-on-view of the main microscope unit, indicating the relative locations of the sample, objective lenses, magnetic field coils, and translation stages.

The output of the upper objective can be directed onto a CCD camera (Thorlabs DCC1645C-HQ), for alignment purposes, or reflected onto the input of either an auto-balanced photodetector (Nirvana, New Focus) or a fast-balanced photodetector when short transients are to be measured (Thorlabs PDB460A-AC). The reference for the balanced detection is provided by the split output of the 532 nm laser. Using this method, we are able to reduce the fluctuations in laser intensity by >50 dB. The output of the (auto-)balanced photodetector is then passed into a lock-in amplifier (LIA, Stanford Research Systems SR830 DSP) which enables the sensitive detection of small modulated signals in real time or alternatively to a digital sampling oscilloscope (DSO, Tektronix TDS7104 DPO) for direct observation of kinetic signals.

Magnetic fields are applied by a custom-built pair of coils, configured in the Helmholtz arrangement, and are powered using a computer controlled bi-polar power supply (Kikusui PBX 20-20). The coils are aligned to apply a magnetic field which is co-axial to the optical axis. The maximum DC magnetic field strength applied to the

sample is approximately 45 mT although for typical measurements a maximum field strength of 20 mT is employed to ensure no problems with heating are encountered.

Initial alignment of the upper objective lens is performed whilst the lower objective is removed. This also allows regions of interest in the sample to be imaged using the CCD camera. Once centred on a region of interest, the lower objective is installed and the confocal arrangement is established using the 532 nm probe light. While this means that the arrangement is not truly confocal for the pump light, imaging and detection are only carried out using the probe light in this work. The arrangement is easily modified if detection of the pump light is to be performed. The output from the upper objective lens is then directed onto the detector through several long-pass filters (ensuring that no probe light reaches the detector) and enables the laser shot noise limited detection of the modulated absorption signal. In addition, if the probe beam is disabled, the experimental arrangement allows the direct confocal measurement of fluorescence from the sample, which can be useful for studying reaction systems in which the fluorescence allows monitoring of a spin-selective reaction.

Imaging Methods

We have already introduced new terms to describe the two different operational modes of the microscope: transient optical absorption detection (TOAD) and magnetic intensity modulation (MIM) imaging (Chapter 2.2).⁸ We provide details on the instrumental aspects of these techniques below.

TOAD (transient optical absorption detection)

The basic principle behind the TOAD measurement is to measure the change induced in the probe light reaching the detector by modulation of the pump light. There are primarily two approaches—one for measuring the effect of a short pump pulse (Fig. 2.4a) and one for measuring the effect of a slower square wave modulation of the pump light (Fig. 2.4b). The latter allows the equilibrium state of a cyclic photochemical reaction to be reached and MFEs thereon to be measured, while the former is a classic flash-photolysis approach, measuring the decay of transient species generated in the laser flash. Slow pump-light modulation utilizes a transistor-transistor logic (TTL) output of the lock-in amplifier to switch the output from the 449 nm laser. The laser is capable of being modulated at frequencies up to 150 MHz, though in this case is limited to around 102 kHz due to the bandwidth of the detector. For measuring equilibrium reaction kinetics in flavin reactions, actual modulation frequencies employed are typically 1 kHz or below. For flash photolysis measurements, the laser can also be modulated using a pulse generator (Stanford Research Systems DG535), which allows the pulse length to be adjusted down to about 300 ns, limited by the laser diode driver circuitry. All data presented here were measured with this

arrangement; however, in recent experiments, we have been able to reduce the pulse width to a minimum of around 50 ns by using a short pulse laser driver (PicoLAS LDP-V 10-70). This enables experiments to be performed under conditions similar to those used in conventional flash photolysis apparatus, allowing time-resolved optical absorption kinetic curves to be recorded from the photodetector. Using blue laser diodes with a CW output of up to 6 W, effective flash photolysis measurements can be made by focusing the beam to the diffraction limit, despite the relatively low single pulse energy (0.6 μ J). In actual experiments, much lower laser powers are used. For cyclic flavin photoreactions, repetition rates of up to 10 kHz provide rapid data acquisition while still providing sufficient sampling time to record complete kinetic transients and for the full reaction cycle to complete. In cryptochrome samples, slower repetition rates are likely to be necessary, a simple adjustment, due to the fact that our pump beam modulation is achieved by simple switching of a CW laser, meaning that modulation frequencies of <1 Hz are readily obtained.

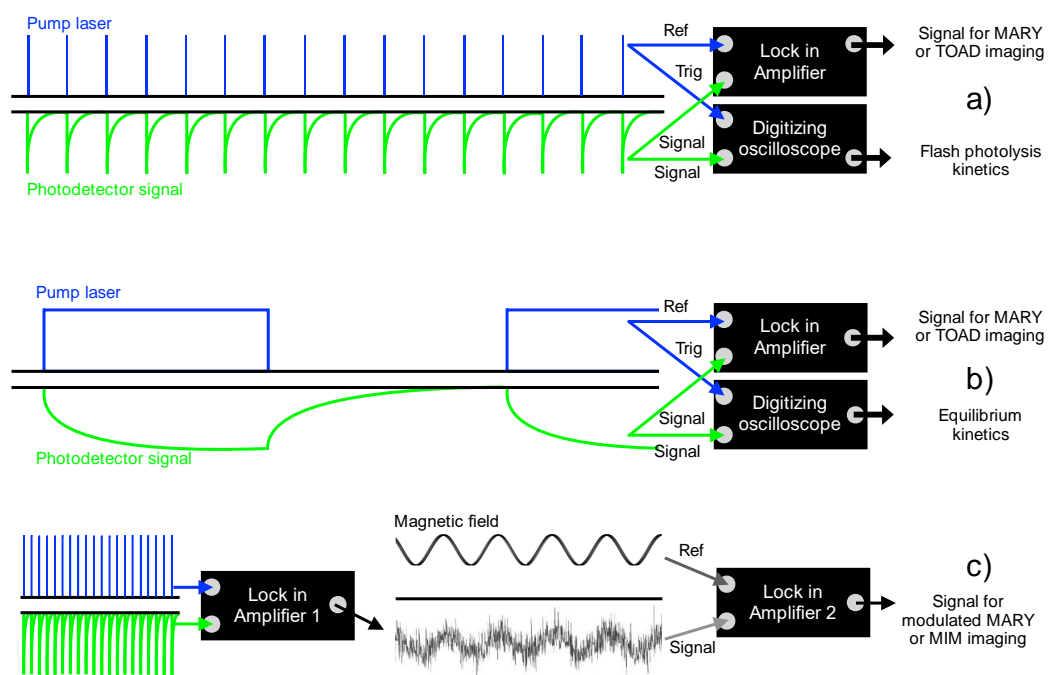


Figure 2.4. Graphical representations summarizing the imaging methodologies. (a) TOAD imaging approach for the flash photolysis mode and (b) for slower square wave modulation. (c) The methodology for MIM imaging and modulated MARY.

In the TOAD configuration, there are a number of different measurements that can be made. By fixing the position of the sample, direct flash photolysis or slow modulation kinetic traces can be captured by the DSO and such kinetics can be observed in the presence or absence of a magnetic field of selectable intensity. For the short pulse experiments, use of a fast photodetector allows direct measurement of the time dependence of the probe light following pump light excitation, giving direct kinetic information about the radical decay processes.

Both slow modulation and short pulse experiments can exploit lock-in detection at the modulation/pulse repetition frequency to provide a signal directly related to the amount of probe light absorbance, which is of great utility in imaging. To record a TOAD image, the focused beams are rastered across the region of the sample of interest using the x- and y-axes of the piezo-stage which allows single steps down to 1 nm in all three dimensions. The output of the lock-in amplifier is converted to a relative absorbance and plotted against the x- and y-coordinates to generate the image. This means that a TOAD image effectively plots the signal that is proportional to the concentration of the probe beam absorbing transient species (in these measurements, the signal comes from both the FAD triplet state and the semiquinone radical, which are in rapid equilibrium). Slices through different layers of the sample can be obtained by controlling the z-axis of the stage.

Under either modulation scheme, by stepping a DC magnetic field from negative to positive magnetic field strengths and by recording the lock-in detected signal at each field point, a curve indicating the magnetically affected reaction yield (MARY) can be quickly obtained. It is also possible to record the averaged kinetic trace at a given field position using the DSO and thus obtain a two-dimensional data set that comprises the variation of the absorption signal with time and magnetic field. Data extracted from this set can be used to plot the time dependence of the MARY spectrum.

MIM (magnetic intensity modulation)

As an alternative to modulating the pump light, it is possible to use constant pump light irradiation and instead modulate the applied magnetic field (magnetic intensity modulation— MIM). The magnetic field is still stepped through multiple DC magnetic field strengths but also has a small AC magnetic field component. This is achieved using a sine-wave output of the lock-in amplifier and an external input into the bi-polar power supply. The amplitude and frequency of this input can be used to alter the sensitivity, and signal strength, of this technique. Larger modulation depths provide stronger signals but at the expense of removing sharp features, for example, the LFE. Very large magnetic field modulations can affect the stability of the microscope, and as such modulations in this study are limited to less than 1 mT_{pk-pk}. The magnetic field is modulated at frequencies ≤ 5 kHz.

This method results in data which are the first derivative (with respect to magnetic field strength) of those obtained using the TOAD method. This is a classic magnetic field modulation MARY experiment.

In practice, a much more effective approach, and the one actually used for all MIM measurements, is a combination of both previous techniques in a double modulation measurement (Fig. 2.4c). A second lock-in amplifier (NF Electronic Instruments LI-570A) is required for this measurement. The pump laser is pulsed at >1

kHz (typically 10 kHz) using short (typically 300 ns) pulses from the delay generator. The phase sensitive detected absorption signal is then output directly from the first lock-in amplifier into the second. The second amplifier's internal signal generator is used to modulate the magnetic field, typically at around 100 Hz (which allows the use of appropriate time constants based on the averaging cycle of the first lock-in), and allows the detection of the component of the signal from the first lock-in amplifier that varies at this frequency. This AC magnetic field is combined with a static DC field, which can be varied to obtain the first derivative MARY spectrum, as mentioned previously, or which can be tuned to the value which provides maximum signal to use for magnetic sensitive imaging. Monitoring the output of the second lock-in amplifier as the laser beams are scanned over the sample allows the direct recording of a magnetic intensity modulation (MIM) image. In such an image, the signal is only non-zero when there is a non-zero modulated absorption signal due to the effect of the pump laser, and there is a subsequent lower frequency modulation of that signal by the oscillating magnetic field. This approach results in substantially improved signal-to-noise ratios over that of the single field modulation approach. The main reason is that the primary optical signal is much more sensitive to vibrations and other fluctuations at frequencies in the range of hertz to hundreds of hertz. The first high frequency light modulation then acts as a filter to remove such fluctuations before using the lower frequency range for field modulation. This approach can, in principle, be used to image regions of biological cells and tissues to search for regions in which magnetically sensitive photochemistry is occurring. It is expected that experiments, which are currently underway, on the imaging of cultured cells and retinal tissue may allow identification of cells and cell components where such processes are occurring.

Materials

The samples used in this work consist of flavin adenine dinucleotide (FAD) in a disodium phosphate/citric acid buffer solution, which allows the pH to be controlled over a wide range (pH 2.2–pH 8.0). In some experiments, tryptophan was added as an external electron donor. All chemicals were used as supplied (Sigma-Aldrich). The concentrations used in each experiment are detailed in the text.

The solution is placed between two standard cover glasses, and the sample thickness can be set using an appropriate spacer. In the investigations discussed here, the sample thickness is set either using 100 μm glass beads (Sigma-Aldrich) or 2.5 μm polymer particles (Spherotech).

Results and Discussion

In our previous paper,⁸ we demonstrated the imaging capability and spatial resolution of the microscope (Chapter 2.2). Here we focus on the kinetic and MARY data that can be readily obtained from very small samples, even at low concentrations. Figure 2.5 shows a typical set of data that can be obtained from the standard TOAD configuration, for a 200 μM sample of FAD in pH 2.3 disodium phosphate/citric acid buffer in the presence of 1.5 mM tryptophan. The sample was a 5 μL spot of solution sandwiched between two glass cover slides at a separation of 100 μm (achieved using glass spheres of this diameter as spacers). The operating repetition rate of photoexcitation is 10 kHz which, in principle, allows a decay curve obtained from averaging 10 000 shots to be recorded each second [in practice, acquisition is slower due to the retriggering rate of the DPO (Tektronix TDS7104 DPO)]. The kinetic curve in Fig. 2.5a is the result of averaging 30 such decay curves. Figure 2.5b shows the MARY curve obtained under the same conditions using lock-in detection with a 300 ms time constant and sweeping the magnetic field from positive to negative. The curve is an average of 4 individual MARY curves, each with an acquisition time of approximately 1 min.

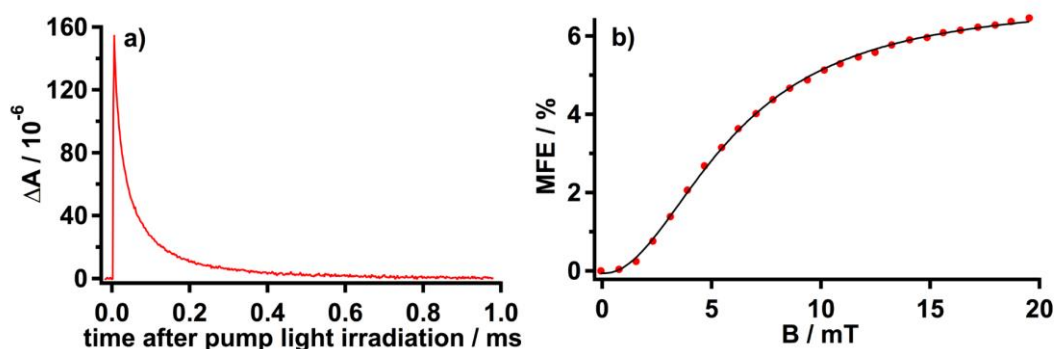


Figure 2.5. (a) Time dependence of the 532 nm absorption signal (ΔA); (b) MARY spectrum for FAD (200 μM) and Trp (1.5 mM) at pH 2.3; the $B_{1/2}$ value is 6.0 ± 0.7 mT.

Studies to date have only examined the magnetic field effect on FAD at pH values less than about 3.6.¹² It is believed that at higher pH the adenine moiety is not protonated and that FAD molecules adopt a closed configuration, in which the rapid (forward and backward) electron transfer between flavin and adenine moieties results in substantially diminished fluorescence quantum yield and halts RP formation. Due to the high sensitivity of our microspectroscope, we were able to study the reaction kinetics and field dependence at pH values up to pH 8.0 and resolve not only the time-resolved optical absorption signals but also effects of a magnetic field thereon. In addition, by measuring the MARY curves at each pH value, we were able to measure the pH dependence of the $B_{1/2}$ value (magnetic field strength at half the saturation value of the MFE, commonly used to characterize MFEs arising due to the hyperfine mechanism) for FAD (200 μM) (Fig. 2.6) (a full analysis will appear in a future

publication (Chapter 3.1). These measurements demonstrate clearly that at physiological pH and higher, FAD is actually capable of producing radical pairs that are magnetic field sensitive. In addition, the drop in both the size of the absorption signal and the magnitude of the MFE demonstrates the sensitivity of the instrument and its potential utility for MFE measurements in cellular and tissue samples.

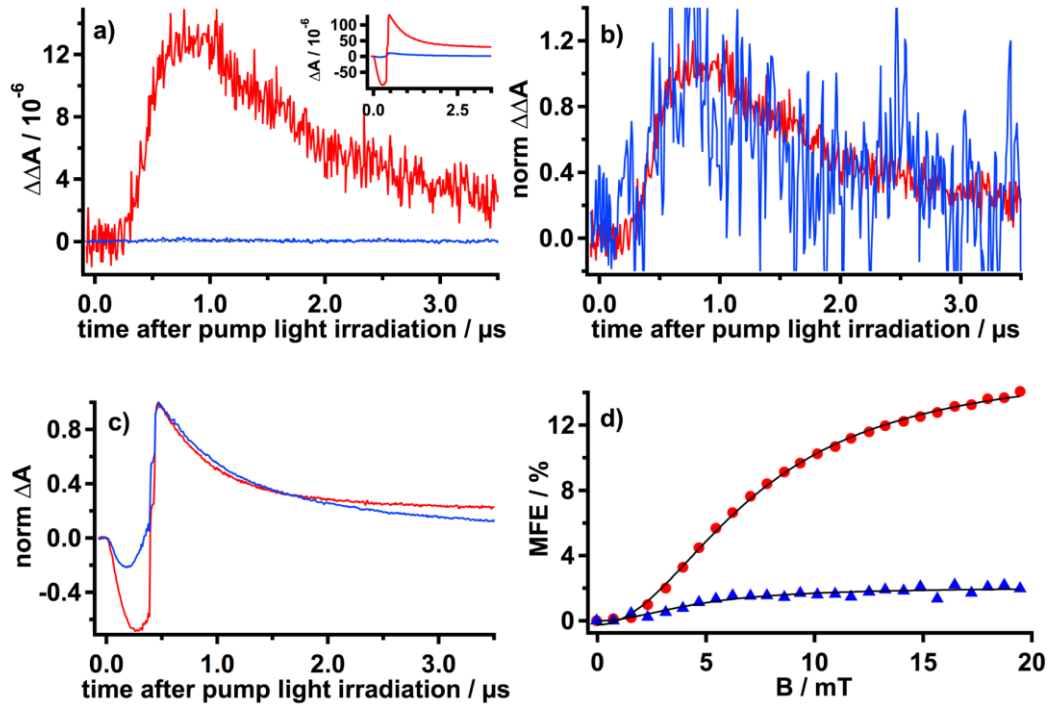


Figure 2.6. pH dependence of FAD (200 μM) (pH 2.3 = red and pH 8.0 = blue). (a) $\Delta\Delta A$ [$\Delta\Delta A = \Delta A(B = 20 \text{ mT}) - \Delta A(B = 0 \text{ mT})$] of $\sim 12 \times 10^{-6}$ and $\sim 2 \times 10^{-7}$ for pH 2.3 and pH 8.0, respectively, and inset ΔA (x-axis has the same time scale as main), (b) normalized $\Delta\Delta A$ [$\Delta\Delta A = \Delta A(B = 20 \text{ mT}) - \Delta A(B = 0 \text{ mT})$], (c) normalized ΔA , (d) MARY curve pH 2.3 (red dots) and pH 8.0 (blue triangles); the $B_{1/2}$ values are 7.3 ± 1.0 mT and 4.6 ± 2.4 mT, respectively.

Finally, to demonstrate that our instrument can resolve very small field induced changes, rather than relatively large changes on weak absorption signals, we made measurements of riboflavin (RF) in water [Fig. 2.7a]. The primary photo-chemistry of RF in water is not field sensitive, as there is no appropriate electron donor to quench the photoexcited RF triplet state. However, it has been demonstrated that the reaction of two excited RF triplets can produce a pair of RF radical ions,¹³



where



which forms a radical pair with another semiquinone radical,¹⁴



The time-resolved optical absorption measurement on this signal is dominated by the RF photoexcited triplet state, but a very small magnetic field effect (of about 0.2%) is observed and can be readily resolved as a clear MARY curve by our instrument [Fig. 2.7b].

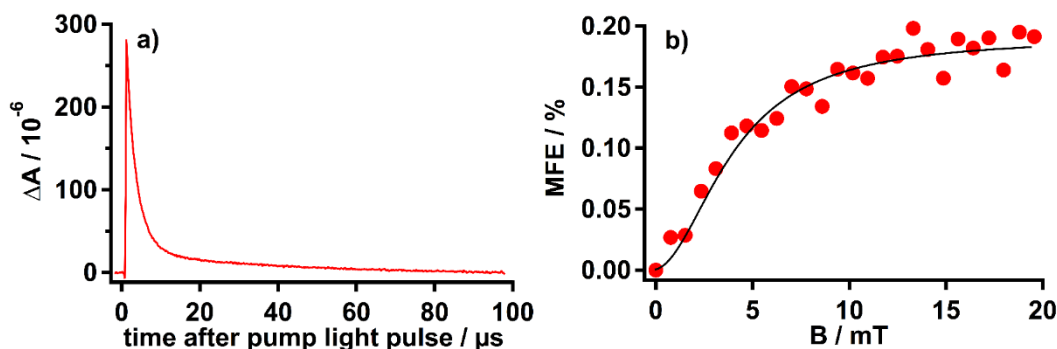


Figure 2.7. Riboflavin in water. (a) Time dependence of the 532 nm absorption signal and (b) MARY spectrum for a pair of riboflavin radical ions in water; the $B_{1/2}$ value is 4.1 ± 1.8 mT.

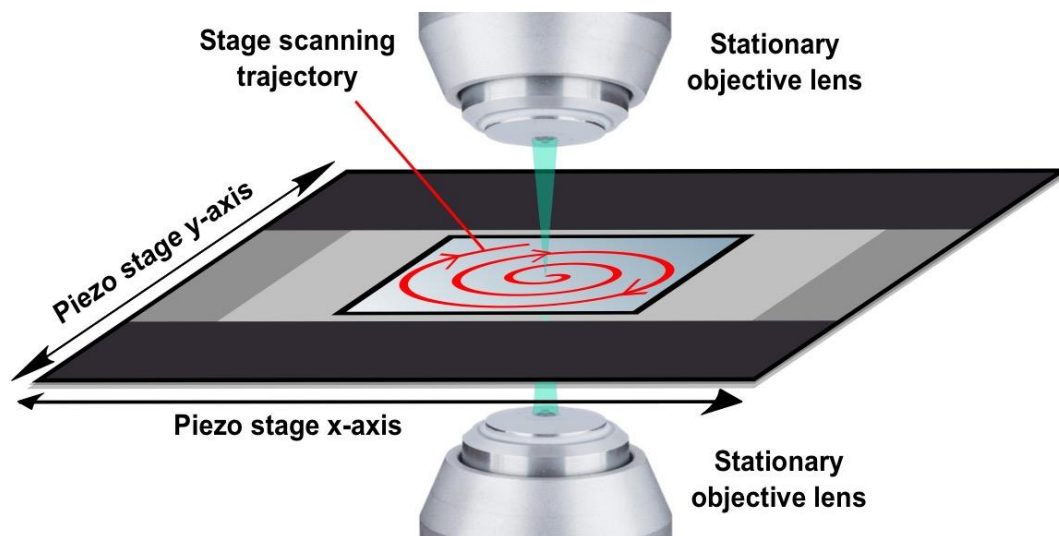


Figure 2.8. Schematic of the spiral stage scanning principle.

The use of our instrument as a microspectroscope for MFE studies can be potentially extended to a wide-range of RP generating photochemical reactions. The primary limitation is that most photochemical processes that generate magnetically sensitive RPs are non-cyclic, i.e., the photochemical precursor is not regenerated in the reaction. Therefore, in instruments employed to date to study such reactions, the sample is usually refreshed using a flow system. To address this restriction and allow our instrument to make measurements on non-cyclic photoreactions, we have developed a sample rastering approach. For example, to record a MARY spectrum or a kinetic curve,

after acquisition begins, the sample is moved using the piezoelectric stage such that a fresh sample is continuously introduced. To optimize this process, the piezo-stage operates in a manner that allows the sample to move outwards from the center in a spiral at a definable rate such that the sample is continuously replenished and the maximum sampling can be achieved for the minimum area of sample scanned (Fig. 2.8).

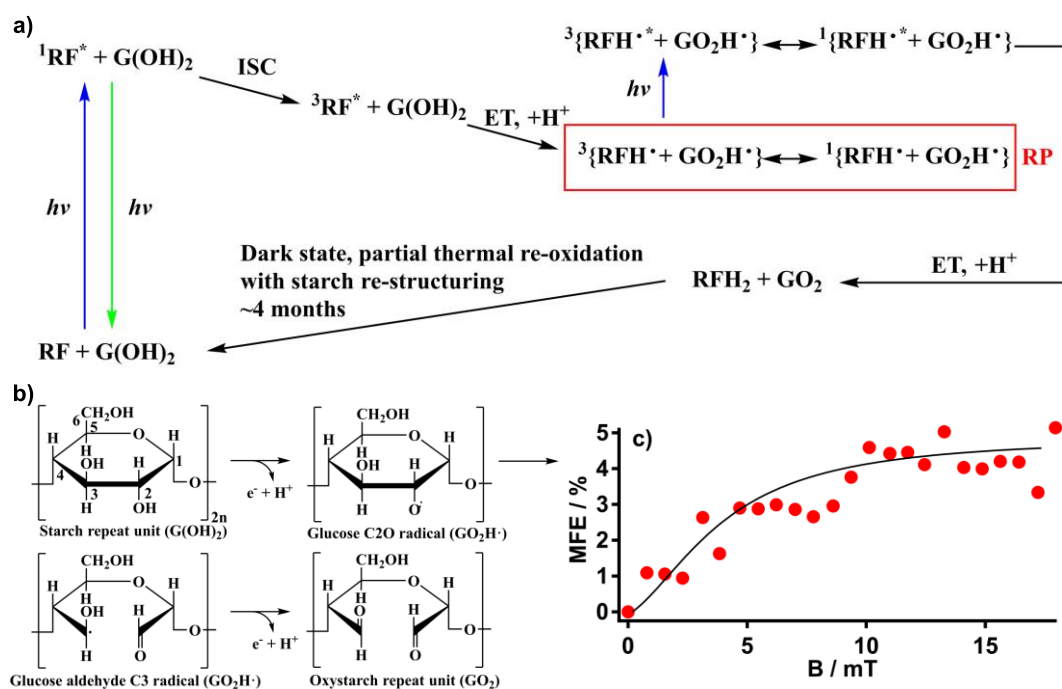


Figure 2.9. (a) Photochemical reaction scheme for riboflavin and the glucose repeat unit of the starch thin film, (b) oxidation scheme of the glucose repeat unit of starch to the di-aldehyde glucose repeat unit of oxystarch (based on Ref. 15), (c) MARY spectrum displaying the magnetic field effect on the photochemical reaction between the riboflavin semiquinone and the oxidized glucose radicals; the $B_{1/2}$ value is 4.6 ± 2.7 mT.

To demonstrate the utility of this technique, along with an additional advantage of being able to do sample replenishment for solid-state samples, we measured the MARY curve for a sample of riboflavin dissolved in a solid starch film. It has been previously shown that flavins embedded in a starch matrix can undergo a photochemical reaction involving glucose repeat units of the starch film (Ref. 15 and the references therein). The photoexcited fully oxidized riboflavin quinone undergoes intersystem crossing (ISC), electron transfer (ET), and proton transfer (PT) to produce a triplet born riboflavin semiquinone and glucose C2O radical pair [Fig. 2.9b]. Surprisingly there is no evidence of exchange coupling in the MARY spectrum, which would be anticipated for a fixed RP with a small separation between the pair members. The simplest explanation is that both flavin molecules and semiquinone flavin radicals are mobile within the porous starch matrix such that radical pairs can undergo diffusive recombination, and therefore features due to level crossing are not observed. Upon further

photoexcitation, subsequent ET and PT produce a fully reduced riboflavin hydroquinone and the photochemically degraded starch repeat unit, oxystarch. In the dark state, partial thermal re-oxidation (with starch restructuring) of the hydroquinone to the quinone ground-state is possible by the oxidizing action of the di-aldehyde groups of oxystarch; this process takes ~4 months [Fig. 2.9a]. Due to the long ground-state and starch repeat unit recovery time, our spiral scanning algorithm was able to replenish the sample, producing a MARY spectrum for the photochemical reaction between riboflavin and glucose repeat unit [Fig. 2.9c].

Three-color approach—two probes and one pump

The photochemistry of different flavin and tryptophan species has specific absorption wavelengths, which are discernible in transient absorption spectroscopic techniques. It is therefore valuable to utilize multiple wavelengths in a spectroscopic analysis, to develop a more concrete understanding of the photochemistry taking place in the chosen sample. This led us to develop a two-probe technique specific to the proposed magnetosensitive photochemistry of cryptochromes.^{6,16} The technique comprises three laser beams (each separated by 1.5 mm), 449 nm (pump), 532 nm (probe), and 635 nm (probe, Thorlabs CPS635S), directly entering the objective lenses without fiber-coupling and with no beam expansion for back aperture filling. The pump beam passes through the center of the objective lenses, with a probe beam 1.5 mm on either side of the pump beam [Fig. 2.10a]. This technique allows us to record simultaneous MARY spectra and kinetic information at 532 nm and 635 nm using two (auto-) balanced detectors (Fig. 2.10) or alternatively by selectively steering the output and reference beams of either wavelength into the detector. This scheme can be extended to multiple different probe wavelengths due to the wide range of diode laser wavelengths available in the visible region. In our instrument, the primary limitation of two probe beam colors comes from the amount of available space on our optical bench.

The kinetic data for FAD (200 μ M, pH 2.3) in Fig. 2.10 illustrate that the 532 nm decay curve exhibits the presence of a long-lived species that is not observed in the 635 nm decay curve. This long-lived species is assigned to an intermediate generated from a bimolecular reaction at acidic pH,^{12,17} which also increases in lifetime with increasing laser power. At 635 nm, only a short-lived signal is observed, attributed to signals from both the RP (minor) and T-T absorption of the cation $^3\text{FH}^+$ (major).^{12,18} The MARY spectra for the two wavelengths display a difference of 3%. The lower MFE of 12% at 532 nm can be attributed to the long-lived species [which is not magnetic field (MF) sensitive] observed at this wavelength, as the %MFE is calculated using the absolute detector signal from the LIA as an external MF is swept from -20 to +20 mT. The 532 nm MARY spectra and kinetic curves are comparable for the separated and fiber-coupled beam experiments. An MFE of 12% for both

experiments is observed, and the decay curves are identical [Fig. 2.10e] except for the early time fluorescence component, which is substantially reduced in the separated beam arrangement. This is due to the use of irises in the paths of the separated probe beams which means that the majority of the fluorescence signal does not reach the detector—unlike in the original arrangement. Alternatively, the arrangement can be used to capture the absorption signal at one wavelength using one detector and only fluorescence using the other. These two features are both substantial advantages of this arrangement. Essentially no fluorescence is observed for the 635 nm decay curve due to the weaker fluorescence signal at this wavelength. The signal-to-noise ratio is much poorer in the separated beam arrangement for conventional samples, where photoreaction takes place at all sample depths, but the vertical spatial resolution is increased as the beams only overlap in the beam waist region. In the combined beams arrangement, there is beam overlap across the entire width of the sample, leading to a substantially stronger signal. This may be an advantage for purely spectroscopic measurements while the separated beam arrangement should show comparable signal-to-noise ratios in true sub-micron scale measurements but with an inherent resolution reduction in all three dimensions due to the (possibly) non-Gaussian beams and lack of back aperture filling. In future work, the pump laser will be replaced by the new 6 W diode laser with a rapid current switching circuit, which will limit the pulse width to 50 ns or less and allow better discrimination of the absorption kinetics.

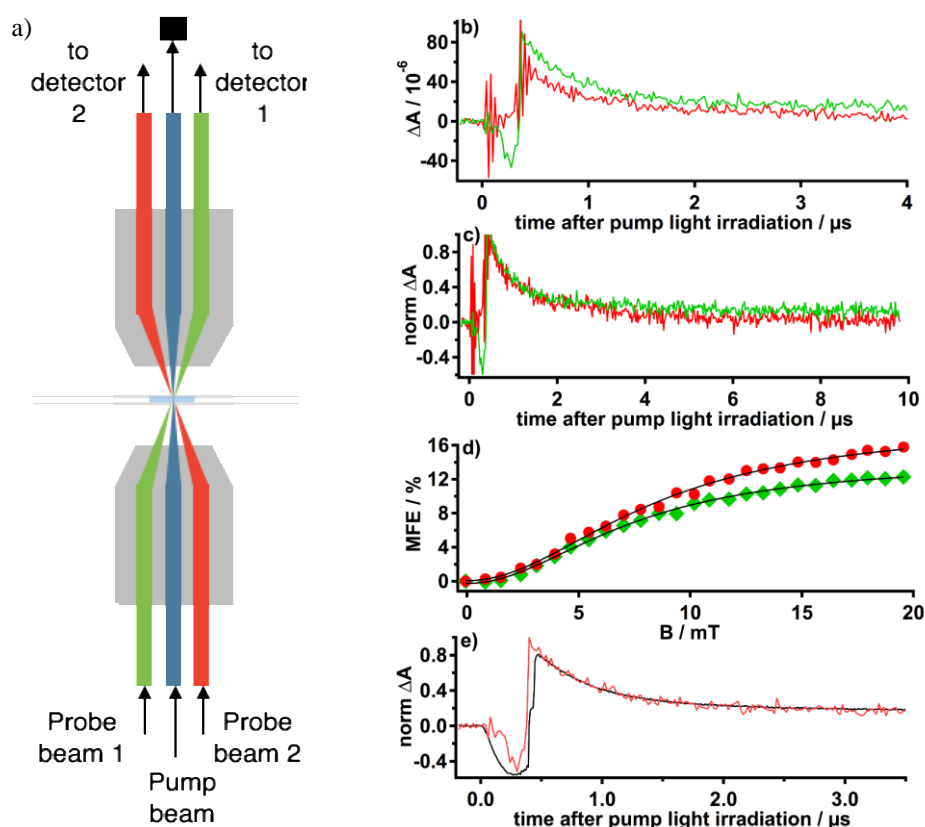


Figure 2.10. Three-color approach. (a) Schematic of the separated beams experimental design. [(b)–(e)] Wavelength dependence on the kinetics and MFE for FAD (200 μM) at pH 2.3 [532 nm (green curve) and 635 nm (red curve)]. (b) ΔA for 532 nm and 635 nm, (c) normalized ΔA for 532 nm and 635 nm, (d) MARY curve at 635 nm (red dots) and 532 nm (green diamonds), $B_{1/2}$ values are 8.4 ± 2.0 mT and 7.5 ± 1.6 mT, respectively, (e) normalized ΔA at 532 nm for fiber-coupled probe beam (black curve) and separated non-fiber-coupled probe beam (red curve).

Summary and Conclusions

In this paper, we described the confocal magnetic field based microspectroscopic techniques of TOAD and MIM and demonstrated the excellent sensitivity of our instrumental arrangement by observing, for the first time, MFEs on the photochemistry of FAD at around biological pH ($\Delta\Delta A \sim 2 \times 10^{-7}$) and on the photochemistry of riboflavin (vitamin B2) in water ($\Delta\Delta A \sim 6 \times 10^{-7}$). The ability to work with non-cyclic reactions, using a spiral scanning approach, was confirmed through the observation of a MFE on the non-cyclic reaction between riboflavin and a thin film starch matrix at neutral pH. The possibility of recording two probe wavelengths simultaneously was demonstrated in acidic FAD solution, and this arrangement is freely extendable to a much larger number of wavelengths, where sources, detectors, and bench space allow. The ability to make magnetic field measurements

on photochemistry both in a spatially resolved manner and with high sensitivity in small volume, low concentration samples makes this a powerful tool in the armoury of a spin chemist. The instrument is already proving useful in measuring flavin photochemistry in micron scale reactors, and measurements are underway to try to observe flavin photochemistry within living cells.

2.2 SPATIALLY RESOLVED MEASUREMENTS

Abstract

Short-lived radicals generated in the photoexcitation of flavin adenine dinucleotide (FAD) in aqueous solution at low pH are detected with high sensitivity and spatial resolution using a newly developed transient optical absorption detection (TOAD) imaging microscope. Radicals can be studied under both flash photolysis and continuous irradiation conditions, providing a means of directly probing potential biological magnetoreception within sub-cellular structures. Direct spatial imaging of magnetic field effects (MFEs) by magnetic intensity modulation (MIM) imaging is demonstrated along with transfer and inversion of the magnetic field sensitivity of the flavin semiquinone radical concentration to that of the ground state of the flavin under strongly pumped reaction cycling conditions. A low field effect (LFE) on the flavin semiquinone – adenine radical pair is resolved for the first time, with important implications for biological magnetoreception through the radical pair mechanism.

Introduction

Short-lived radical intermediates are common in a wide range of thermal and photochemical enzyme catalyzed chemical reactions. To date, however, there do not exist microscopic methods for their direct observation. Furthermore spin-correlated radical pairs (RPs) have been extensively studied for the last four decades.¹⁹⁻²¹ In recent years they have returned to the spotlight, primarily due to their proposed role in animal magnetoreception,²² their importance in solid-state devices involving electron–hole recombination²³ and renewed interest in quantum information related phenomena in the physics community. Surprisingly, with few exceptions,²⁴ the study of RPs in a spatially resolved manner has been largely ignored. In recent years, a range of sophisticated fluorescence-based microscopy methods have been developed and have received much attention.²⁵ However, fluorescence is not an ideal method for the study of photochemically generated radicals or RPs. Photochemically generated free radicals in general do not fluoresce. Furthermore, although there are many examples of the use of fluorescence detection to study RP dynamics,¹⁹⁻²¹ such measurements are typically only possible in spin-selective reactions from singlet RPs to fluorescing exciplexes. In particular, to study RPs proposed in biological magnetoreception, an alternative approach is desirable. In functioning cryptochrome photochemistry, electron transfer to the photoexcited singlet state of FAD (from a neighboring tryptophan residue) is sufficiently rapid to make fluorescence signals extremely weak. In addition, fluorescence only tracks ground state FAD molecules, whose concentration is not magnetic field-sensitive in flash photolysis experiments. In general, transient absorption spectroscopy is the best optical spectroscopic method for studying transient radicals and RPs.

Here, we demonstrate for the first time a new imaging microscope (TOAD) that can observe photochemically generated radicals and RPs with high sensitivity and sub-micrometer spatial resolution, paving the way for the direct measurement of, for example, flavin photochemistry in cells and tissues, and localized polaron pairs in solid-state devices.

The TOAD/MIM microscope is described only briefly here. Full technical details will be published elsewhere. The optical arrangement is based on an instrument for detecting single molecules,^{10,11} and employs a transmission confocal arrangement. Two solid-state lasers act as pump and probe. The output of the 532 nm (probe) laser, used for imaging detection, is beam-split before being combined with the output of the 450 nm (pump) laser. The combined beams enter the microscope objective through a single mode optical fiber. The major microscope components comprise a piezo-electric sample translation stage, two apochromatic objective lenses, optical filters/dichroic mirrors and micrometer adjusted translation stages. The microscope is assembled on a vibrationally isolated optical bench to eliminate spurious signals from vibrations, particularly at the audio frequencies used for signal modulation. The output of the upper objective can be directed onto an imaging camera for alignment purposes, or onto the input of an auto-balanced photo-detector. The reference for the balanced detection is provided by the split output of the probe laser. Using this method, it is possible to reduce fluctuations in laser intensity by >50 dB and the signal becomes shot noise limited. The output of the photodetector is applied to the input of a lock-in amplifier, allowing the sensitive detection of very small changes to the probe beam intensity.

Pump light modulation imaging

The basic imaging technique (TOAD) employs pump laser modulation and monitoring of the induced modulation in the probe beam whilst the lasers are scanned in up to three dimensions over the sample. In the simplest arrangement, square wave modulation is applied to the 450 nm pump laser at an audio frequency. This allows long timescale reaction cycling in flavin photoreactions to be probed directly when the light-on cycle is long enough to allow ground state FAD and RP concentrations to reach equilibrium. The equilibrium position can then be controlled with the pump laser power.

The microscope objectives employed allow high laser intensities to be produced at the focal point of the microscope, corresponding to FAD photoexcitation rate constants of up to ca. 10^8 s^{-1} . Under these conditions, continuous pumping of the sample is capable of significant FAD ground state (GS) photobleaching. By applying short (ca. 300 ns) TTL pulses to the modulation input of the pump laser, the experiment can be operated in flash photolysis mode, and high modulation frequencies (1–100 kHz) can be employed when reaction kinetics are

sufficiently fast. Under such conditions, time-resolved optical absorption kinetic curves can be digitized from the photodetector or the signal from the lock-in can be used for imaging or MARY (magnetically affected reaction yield) curve acquisition.

A custom-built Helmholtz coil pair aligned to apply a DC + AC magnetic field co-axial to the optical axis is driven by a 4-pole power supply. The direct effect of the magnetic field on the decay kinetics or modulated signal can be recorded or alternatively, a double modulation scheme can be employed.

Pump light magnetic field double modulation measurements

For flash photolysis type irradiation, the output of the lock-in can be applied to a second lock-in amplifier, referenced to a sine wave modulation signal (frequency to ~ 1 kHz), used to drive an AC magnetic field at the sample. Monitoring the output of this second lock-in as the laser beams are scanned over the sample, allows the direct recording of a magnetic intensity modulation (MIM) image when the AC magnetic field is combined with a static DC field (tuned to observe the maximum signal). A simple demonstration of this technique is provided here, but its true potential will be fully unlocked in future studies.

MFEs on the RP generated by the photoexcitation of FAD at low pH have previously been reported.^[12,26] Electron transfer takes place from the adenine to the flavin moiety generating a separated biradical. Low pH is necessary to stop the two moieties stacking, which facilitates rapid forward and backward electron transfer.^[12] Unusually this system appears to involve an equilibrium between RP and protonated FAD triplet state (PTS). Both transient species absorb light at 532 nm with almost equal extinction coefficients. Typical RP / PTS lifetimes under these conditions are a few microseconds.

Figure 2.11a shows an image of a ~ 2.5 μm microbead surrounded by 200 μM FAD in pH 2.3 buffer in flash photolysis mode. The sample thickness is bead limited (i.e. < 3 μm) and the lasers irradiate a sample volume of < 4 femtolitres (fL) with a beam waist of ~ 240 nm. The signal used for imaging is a direct measure of RP concentration and is reduced to near zero in the region of the bead as no photochemistry can occur in this region. Figure 2.11b shows the time decay following photoexcitation and the subtracted curves recorded in the presence and absence of a 20 mT magnetic field (inset), at a single pixel position away from the microbead. The black line is a numerical simulation employing the kinetic model and parameters described in reference ^[12]. Such kinetic curves can be obtained at any sample location (the sample stage can access submicron horizontal spatial regions) and so could be used to target particular sub-cellular structures to observe flavin photochemistry therein. Figure 2.11c shows a MARY curve recorded again at a single point within the sample. Only 8 minutes was required to record a MARY

spectrum at this S/N level. The vertical scale of the MARY curve is the percentage change in the output of the lock-in signal as the field is scanned.

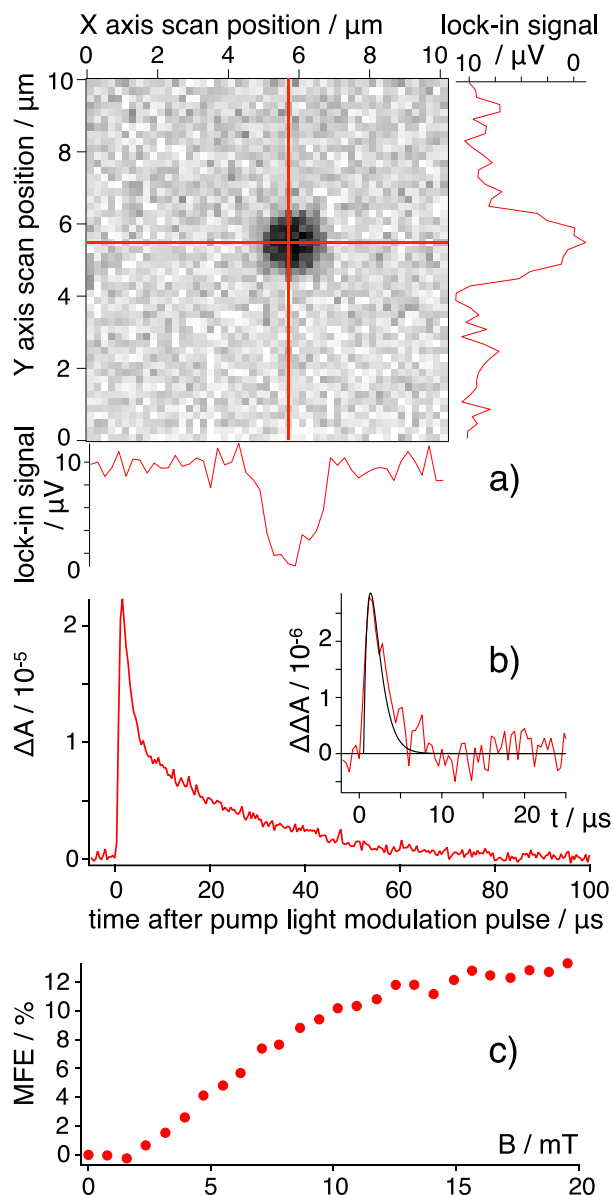


Figure 2.11. a) Pump light modulation image of FAD semiquinone radicals in the presence of a 2.5 μm microbead generated from 200 μM FAD. Horizontal and vertical slices are shown. b) 532 nm absorption kinetics recorded at a single location. The inset shows subtracted field on / off curves with a simulation based on ref 12. c) Pump Light Modulation MARY curve recorded at the same location. The sample (1 μL) was $<3 \mu\text{m}$ thick.

Figure 2.12a shows a double modulation image for a slightly larger microbead, this time in 1 mM FAD in pH 2.3 buffer. This is an example of the MIM technique – a non-zero signal is only observed if the probe beam light is absorbed by a magnetically sensitive species. The inset of Figure 2.12b shows a typical double modulation-MARY signal obtained at any point in the image. The characteristic first derivative MFE signal is observed. For the image, the DC component of the applied field was matched to the peak of this MARY signal. Figure 2.12b shows the compatibility between the single and double modulation techniques. The integrated double modulation MARY signal (line) overlaps perfectly the MARY curve from Figure 2.11c (dots).

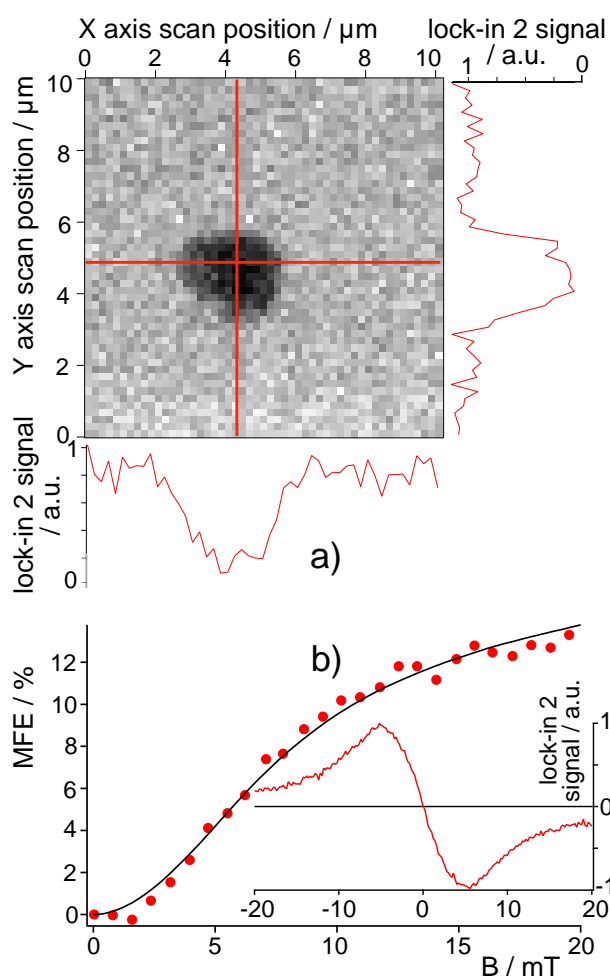


Figure 2.12. a) Double modulation image of 2.9 μm microbead. b) Inset shows the double modulation MARY curve at a single pixel position. The main curve shows the inset signal integrated and overlaid on the MARY curve from Figure 2.11c (dots).

By acquiring single (Figure 2.13, main) and double (Figure 2.13, inset) modulation MARY curves at a greater magnetic field resolution (and a suitably small MF modulation depth of 0.35 mT peak-to-peak in the double modulation case) it was possible to successfully resolve and confirm a LFE. Although this reaction has been carefully studied by conventional^[12,26] and high sensitivity cavity enhanced techniques^[27], this LFE has not

previously been resolved. This reveals the high sensitivity of this approach, which detected the feature using a sample volume of only 5 μL and a 2nd lock-in time constant of only 300 ms. If flavin-based RPs are responsible for biological magnetoreception, then the LFE represents the most likely mechanism by which fields as small as the geomagnetic field (30-50 μT) might deliver a chemical response.

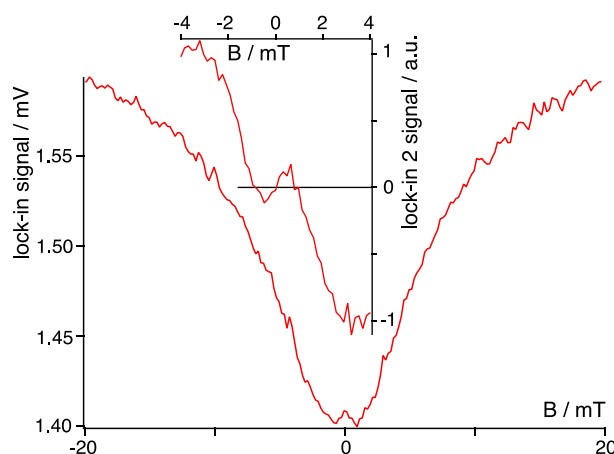


Figure 2.13. Single (main) and double modulation (inset) MARY curves revealing and confirming the presence of a LFE (5 μL sample with 100 μm glass beads).

For animals navigating in the geomagnetic field, exposure to light is continuous rather than the series of short nanosecond pulses typical in photochemical kinetic measurements. Our approach allows the observation of MFEs on the equilibrium established between RPs and FAD GS molecules by the use of square wave pump light modulation at variable modulation frequencies and laser powers. For CW irradiation at low pump powers, MFEs are observed in agreement with the effects seen in flash photolysis measurements. As the pump light power is raised the equilibrium shifts towards the RP / PTS state (Figure 2.14a and equation, Figure 2.14c) and the size of the MFE gradually diminishes. Figure 2.14b demonstrates the effect of increasing the length of the pump laser pulse width from 300 ns to 2000 ns. As the pulse length increases, the complete reaction cycle can occur during the irradiation period, establishing the GS – RP / PTS equilibrium and pushing it in the direction of the RP / PTS due to the intensity of the laser beam. Thus, the MARY curves saturate at increasingly low MFE values.

Concomitant with the reduction of the MFE in the RP, the concentration of FAD GS becomes limited by spin-selective back electron transfer from the singlet RP and should thus exhibit an MFE in the opposite sense to that observed in the RP (i.e. a magnetic field should reduce the fluorescence intensity). In order to monitor the concentration of FAD GS, the probe light was removed and the microscope configured to detect the fluorescence signal from excited singlet state FAD. Figure 2.14c shows the MARY curve obtained for a square wave pump light modulation measurement with the pump intensity tuned such that the FAD fluorescence is weak enough to

reveal the MFE on the FAD GS / excited singlet state, but still sufficiently large to be measurable. The inverted MFE on fluorescence is clearly observed. Thus, the field sensitivity of FAD derived triplet born RPs can exhibit a positive or negative MFE depending on which state is observed and the intensity of the irradiation light.

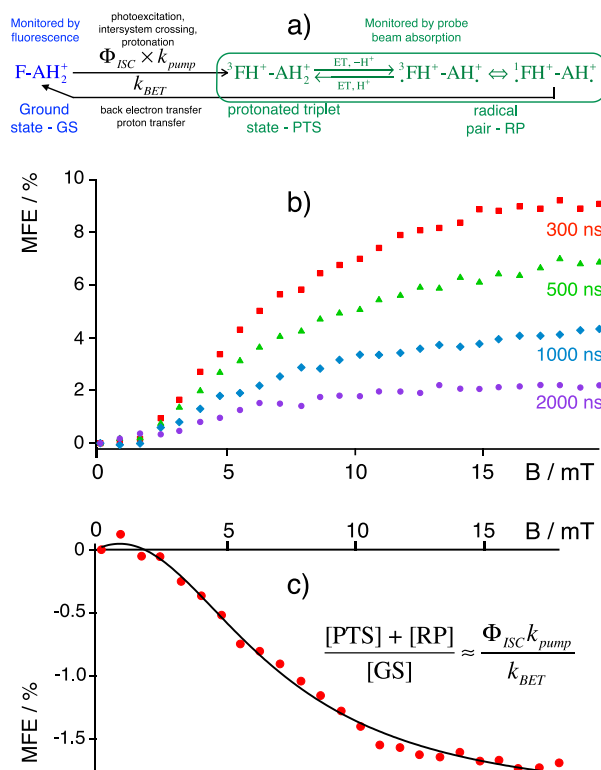


Figure 2.14. a) Simplified reaction scheme for FAD photoexcitation at pH 2.3. b) Reduction of the MFE on RP / PTS concentration with increasing pump light pulse length. c) Singlet excited state FAD fluorescence detected MARY curve under high power CW pump light modulation, revealing an inverse MFE on the FAD GS concentration.

We have demonstrated for the first time the techniques of TOAD microscopy, which allows direct imaging of photochemically generated radicals, and MIM microscopy, which can selectively image regions containing magnetically sensitive RPs. The techniques have both submicron spatial resolution and high sensitivity, as demonstrated by the ability to rapidly record images and MARY curves by irradiating a 200 μ M FAD sample of less than 4 fL. This means that even when spatial resolution is unnecessary, the instrument can be employed as a high sensitivity spectroscope that can operate on (for example precious biological) samples of less than 1 μ L, and by scanning the total sample area allow progressive photoexcitation of unirradiated sample, analogous to sample flow in a conventional cuvette. In addition, a LFE on FAD photochemistry was resolved for the first time, and the shift of MFE from RP to FAD GS under cycling conditions was also clearly observed. These features are both important for the understanding of magnetoreception in cryptochromes. TOAD and MIM measurements on both

plant and animal cells and tissues, and MFE measurements on pure cryptochrome protein in solution are currently underway.

Experimental Section

FAD was purchased from Wako and used as received. pH 2.3 buffer solution was made by combining citric acid and disodium hydrogen phosphate solutions (Wako) in distilled water (Wako).^[28] Thin samples were produced by adding polymer microbeads (diameter 2.5-2.9 μm , Spherotech Inc.) to the sample solution and sandwiching 1 μL of this solution between glass cover slips (0.13-0.16 mm, Marienfeld). For thicker samples, the polymer beads were replaced with 100 μm glass beads (Toshin Riko) and the volume of solution increased to 5 μL .

References

- [1] W. Wiltschko, R. Wiltschko, and T. Ritz, *Procedia Chem.* **2011**, 3, 276.
- [2] R. J. Gegear, A. Casselman, S. Waddell, and S. M. Reppert, *Nature* **2008**, 454, 1014.
- [3] S. M. Reppert, P. A. Guerra, and C. Merlin, *Annu. Rev. Entomol.* **2016**, 61, 25.
- [4] T. Ritz, S. Adem, and K. Schulten, *Biophys. J.* **2000**, 78, 707.
- [5] P. J. Hore and H. Mouritsen, *Annu. Rev. Biophys.* **2016**, 45, 299.
- [6] K. Maeda, A. J. Robinson, K. B. Henbest, H. J. Hogben, T. Biskup, M. Ahmad, E. Schleicher, S. Weber, C. R. Timmel, and P. J. Hore, *Proc. Natl. Acad. Sci. U. S. A.* **2012**, 109, 4774.
- [7] K. Maeda, K. B. Henbest, F. Cintolesi, I. Kuprov, C. T. Rodgers, P. A. Liddell, D. Gust, C. R. Timmel, and P. J. Hore, *Nature* **2008**, 453, 387.
- [8] J. P. Beardmore, L. M. Antill, and J. R. Woodward, *Angew. Chem., Int. Ed.* **2015**, 54, 8494.
- [9] D. R. Kattnig, E. W. Evans, V. De'jean, C. A. Dodson, M. I. Wallace, S. R. Mackenzie, C. R. Timmel, and P. J. Hore, *Nat. Chem.* **2016**, 8, 384.
- [10] P. Kukura, M. Celebrano, A. Renn, V. Sandoghdar, *J. Phys. Chem. Lett.* **2010**, 1, 3323-3327.
- [11] M. Celebrano, P. Kukura, A. Renn, V. Sandoghdar, *Nat. Photonics* **2011**, 5, 95-98.
- [12] M. Murakami, K. Maeda, T. Arai, *J. Phys. Chem. A*, **2005**, 109, 5793-5800.

- [13] T. B. Melø, M. A. Ionescu, G. W. Haggquist, and K. Razi Naqvi, *Spectrochim. Acta, Part A* **1999**, 55, 2299.
- [14] V. Massey and G. Palmer, *Biochemistry* **1966**, 5, 3181.
- [15] A. Penzkofer, *Int. J. Mol. Sci.* **2012**, 13, 9157.
- [16] D. M. W. Sheppard, J. Li, K. B. Henbest, S. R. T. Neil, K. Maeda, J. Storey, E. Schleicher, T. Biskup, R. Rodriguez, S. Weber, P. J. Hore, C. R. Timmel, and S. R. Mackenzie, *Sci. Rep.* **2017**, 7, 42228.
- [17] M. S. Grodowski, B. Veyret, and K. Weiss, *Photochem. Photobiol.* **1977**, 26, 341.
- [18] M. Sakai and H. Takahashi, *J. Mol. Struct.* **1996**, 379, 9.
- [19] U. E. Steiner, T. Ulrich, *Chem. Rev.* **1989**, 89, 51-147.
- [20] J. R. Woodward, *Prog. React. Kinet. Mech.* **2002**, 27, 165-207.
- [21] C. T. Rodgers, *Pure Appl. Chem.* **2009**, 81, 19-43.
- [22] H. Mouritsen, P. J. Hore, *Curr. Opin. Neurobiol.* **2012**, 22, 343-352.
- [23] E. Ehrenfreund, Z. V. Vardeny, in *Organic Spintronics*, CRC Press: Florida, USA. **2010**, pp. 217-255.
- [24] H. Lee, N. Yang, A. E. Cohen, *Nano Lett.* **2011**, 11, 5367-5372.
- [25] C. A. Combs, *Curr. Protoc. Neurosci.* **2001**, 2.1.1-2.1.14.
- [26] M. Murakami, K. Maeda, T. Arai, *Chem. Phys. Lett.* **2002**, 362, 123 -129.
- [27] S. R. T. Neil, J. Li, D. M. W. Sheppard, J. Storey, K. Maeda, K. B. Henbest, P. J. Hore, C. R. Timmel, S. R. Mackenzie, *J. Phys. Chem. B*, **2014**, 118, 4177-4184.
- [28] T. C. McIlvaine, *J. Biol. Chem.* **1921**, 49, 183-186.

Flavins in Solution

This chapter discusses the pH dependence of flavin adenine dinucleotide magnetic field sensitivity between the pH range 2-8.

The work in this chapter has been published in the following peer-reviewed journal:

L. M. Antill and J. R. Woodward, Flavin adenine dinucleotide photochemistry is magnetic field sensitive at physiological pH, *The Journal of Physical Chemistry Letters*, 9, 2691-2696, **2018**

Chapter 3.1 is a reformatted version of the above publication. The corresponding supporting information is found in Appendix B.1.

3.1 MAGNETOSENSITIVE INTRAMOLECULAR FLAVIN PHOTOCHEMISTRY

Abstract

We present time-resolved optical absorption and magnetic field effect data on the photochemistry following blue light excitation of flavin adenine dinucleotide (FAD) in aqueous solution in the pH range 2.3 to 8.0. Effects of closed form conformations of FAD in ground, excited singlet, and radical pair states exhibit significant influence on the observed kinetics and magnetic field dependence and remarkably, magnetic field effects are observed even at physiological pH where the FAD radical pairs are only 75% less magnetic field sensitive than at pH 2.3.

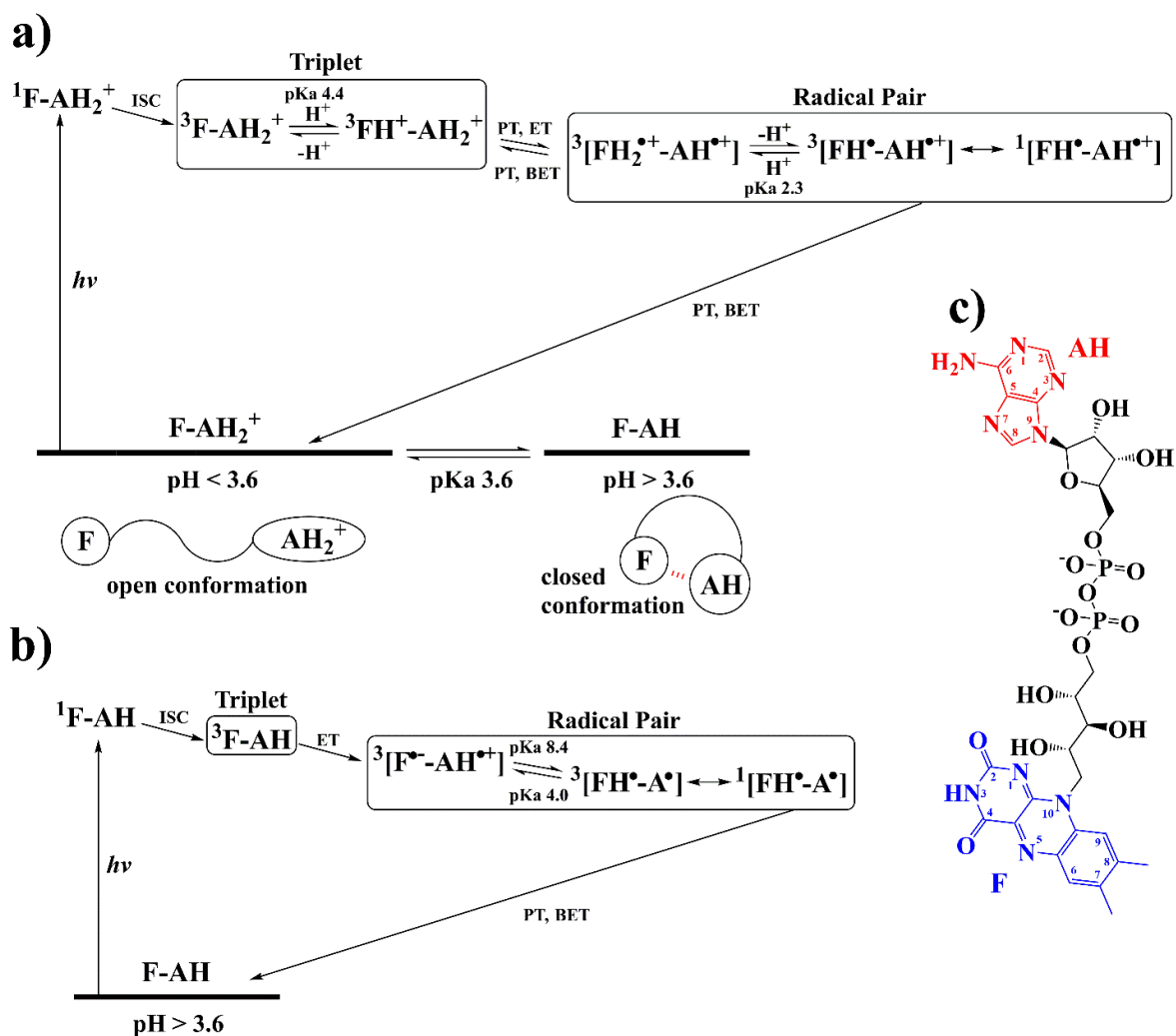
Introduction

Flavins are found throughout nature and participate in a wide range of biochemical reactions as coenzymes and photoreceptors.¹ They are broadly distributed as both free cellular flavins,² and bound in flavoproteins, mainly in the forms of FAD and flavin mononucleotide (FMN). Mechanisms involving UV-/blue-light absorbing flavoproteins include DNA repair by DNA photolyase³ and the entrainment of circadian rhythms by cryptochrome,⁴ both of which utilize a FAD chromophore. A growing body of evidence suggests that cryptochromes might have a role in the ability of flora and fauna to sense the geomagnetic field.^{5,6} This chemical magnetoreception hypothesis operates through spin correlated radical pairs (RPs) generated by a photoinduced electron transfer from a nearby protein residue to a bound FAD cofactor molecule. The process by which these cryptochrome RPs respond to an external magnetic field (MF) is via the radical pair mechanism (RPM), and low field effects (LFEs, the name given to the effect of very weak magnetic fields on RP reactions due to the unlocking of zero quantum coherences) may allow plants and animals to detect fields as weak as the geomagnetic field ($\sim 30\text{--}50\text{ }\mu\text{T}$).⁷ Furthermore, epidemiological studies suggest a weak correlation between the development of cancer and teratological effects and exposure to 50/60 Hz extremely low frequency- (ELF) MFs.^{8–11} The cryptochrome RPM hypothesis is considered a plausible mechanism for explaining the biological effects of ELF-MFs.^{12,13}

In isolation, the key cryptochrome cofactor, FAD, has also been shown, on blue light excitation in aqueous solution, to generate RPs through intramolecular electron transfer from the adenine to the isoalloxazine moiety, which undergo spin-selective recombination, yielding both chemically induced dynamic nuclear polarization¹⁴ (CIDNP) and magnetic field effects^{15,16} (MFEs). The original CIDNP studies showed the strong dependence of the CIDNP signal on pH and argued that the primary pH dependence was due to the conformation of ground state

FAD. At low pH (<3.6), the adenine group of FAD is protonated ($F-AH_2^+$) while at higher pH the molecule is neutral ($F-AH$). In the neutral form, there is a tendency for π -stacking between the flavin and adenine moieties, which leads to rapid electron transfer in the photoexcited singlet state and rapid internal conversion. This has been confirmed in numerous fluorescence-based and other measurements,^{17–22} which have determined that in neutral FAD, the majority of the molecules are in stacked conformations at any given time. The CIDNP study also proposed that, at high pH (>3.6), the excited triplet state and RP are both electrically neutral and that the RP formed under such conditions produces no CIDNP due to stacking analogous to that in the ground state, which in this case leads to a very large exchange interaction and thus the removal of any coherent spin effects. This explanation suggests that FAD should demonstrate no magnetic field sensitivity at neutral and physiological pH. Subsequently, MFE studies of FAD photochemistry revealed that the photochemistry at low pH (<3.6) is more complex than the CIDNP study suggested. While the CIDNP study allocated all the pH dependence to differences in the ground state FAD conformations, the MFE study clearly revealed that pH affects the radical pair dynamics. In order to explain the time dependence and magnitude of the MFEs, Murakami *et al.*,¹⁵ argued that the pH dependence at low pH is due to an equilibrium between the protonated FAD triplet state and the radical pair, and that this process is pH dependent. They proposed a kinetic model that can be used to explain the MFEs at low pH. Their model quantitatively explains the difference in time-resolved optical absorption (TROA) signals in the presence and absence of a magnetic field. The magnitude of such signals is also dependent on the ground state equilibrium, but this is not included in their model. It seems likely that the true picture involves both the ground state and excited state pH dependences. Scheme 3.1 shows the proposed reaction schemes for the pH dependence of FAD photochemistry at pH < 3.6 (based on the MFE studies) and at pH > 3.6 (based on the CIDNP study).

Perhaps because the TROA signal and the magnitude and time scale of the observed MFE are reduced rapidly on increasing the pH from 2 to 3.6, and the absence of any CIDNP signal above pH 6, no previous studies have attempted to look at MFEs at higher pH values. Our recently developed microspectroscope has proven capable of studying TROA of FAD photochemistry with very high sensitivity.^{23,24} Here we describe the magnetic field dependence at pH values up to 8, for the first time.



Scheme 3.1. Proposed reactions schemes for pH dependence of FAD photochemistry. a) Below pH 3.6, based on Murakami *et al.*,¹⁵ and b) above pH 3.6, based on Stob *et al.*.¹⁴ c) Structure of flavin adenine dinucleotide. F = flavin, A = adenine, $h\nu$ = light, PT = proton transfer, ET = electron transfer, BET = back electron transfer, ISC = intersystem crossing. The pK_a of the neutral flavin semiquinone radical is 8.4.

Results and Discussion

Figure 3.1 shows the TROA signal obtained after the 449 nm photoexcitation of FAD in phosphate/citrate buffers over the pH range from 2.3 to 8.0. Changes are observable in both the absolute size of the absorption signal and the time dependence of the signal. The decay curves display two components, corresponding to a long-lived and a short-lived species. The former is assigned to an intermediate generated from a bimolecular reaction, which also increases in lifetime with increasing laser power.^{15,25} Its rate coefficient is independent of pH and the magnitude of its contribution to the total signal decreases with pH. For measurements conducted at 635 nm, this long-lived species is not observed, and it will be discussed no further here.^{15,24,26} The short-lived species is attributed to signals arising from both the RP and T-T absorption of the excited FAD triplet state.^{15,26} The signal decays

monoexponentially as the RP is formed directly from the triplet state and decays to the ground state by spin-selective back electron transfer from the singlet RP. Direct decay of the triplet state happens during the blind time of our spectrometer due to the intense fluorescence during irradiation.

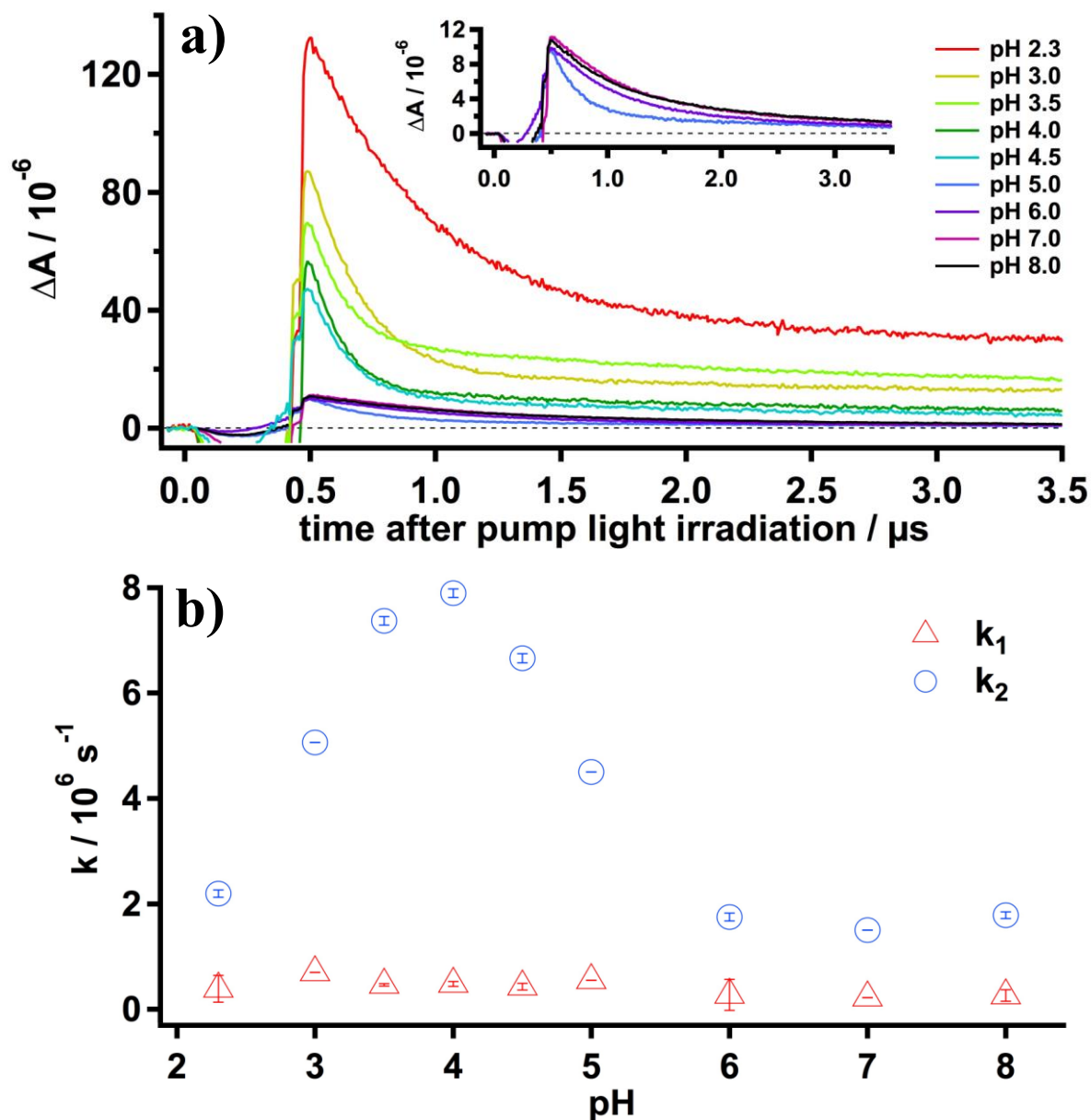


Figure 3.1. FAD ΔA spectra and rate coefficients. a) Time-resolved optical absorption signals recorded at 532 nm following 449 nm laser excitation of a solution of 200 μM FAD from pH 2.3-8.0. b) Rate coefficients obtained from a biexponential fit to the decay curves (a) for each pH value. Error bars represent one standard deviation (1σ) in the fitting.

Of particular note is that the size of the total absorption signal decreases rapidly with an increase in pH for pH values less than 5.0. The signal at pH 8.0 is roughly a factor of 12 smaller than that at pH 2.3. In contrast, existing fluorescence studies observe a decrease in the size of the fluorescence signal over the same pH range, but the

decrease in signal size is much less (a factor of approximately 5). In the pH range 2.3–8.0, fluorescence signals have been explained in terms of the equilibrium between the protonated (PGS) and neutral (at the adenine moiety, $pK_a = 3.6$ (N1 position), NGS) ground state forms of FAD. In the NGS, the FAD exists primarily (around 80%) in the closed form, which undergoes very rapid internal conversion from the excited singlet state (lifetime ~ 10 ps), while the open form has a much longer fluorescence lifetime (~ 3 ns) and dominates the fluorescence signal.¹⁷ However, Sengupta *et al.*, have identified that above pH 3.0, some “open” conformations of the FAD are not fully open but have a flavin-adenine separation such that they can become closed (and rapidly quenched) during the lifetime of the excited singlet state, exhibiting a reduced fluorescence lifetime (2.2 ns vs 4.0 ns). Thus, the partially open conformations are returned to the ground state more rapidly than the fully open ones. While the effect on the total fluorescence signal is very small, the more rapid removal of the singlet excited state is in direct competition with intersystem crossing. This leads to a more significant effect on the concentration of the triplet state and might account for the difference in the magnitude of the decrease in the fluorescence and TROA signals. Due to our relatively long laser excitation pulse and early time domination of the photodetector signal with strong fluorescence (see Appendix for more information), the spectrometer is blind for the first 700 ns, during which decay of the triplet and RP signals can take place, which may also lead to small differences compared to the fluorescence studies.

Figure 3.1b shows the rate coefficients obtained from a biexponential fit to the TROA signals. The rate coefficient of the slow component remains constant across the pH range, while the lifetime of the component associated with the triplet state/RP intermediate increases rapidly until pH 4 and then falls again until it stabilizes at pH values of 6 and above. As the pH increases up to 4.0, the rate coefficient increases 4-fold, which implies that the triplet or RP states are being removed more rapidly. This is entirely consistent with the findings of Murakami *et al.*,¹⁵ because the triplet/RP lifetime decreases as the back reaction from RP to triplet state becomes unavailable as the RP protonation is switched off in this pH range. Murakami *et al.*,¹⁵ also suggest that in this pH range, stacking can occur in the RP. At this pH, the majority of triplet states and RPs are protonated, and so this seems unlikely, but this process almost certainly takes place at higher pH. This forms part of our rationalization of the decrease in the decay rate constant above pH 4.0.

As the pH increases, the proportion of triplet states generated from the PGS decreases and the proportion from the NGS increases. Triplets from the NGS are also generated in the neutral state. It has been shown that at pH 4.0 the excited triplet state of the flavin moiety can be protonated within about 80 ns.²⁶ Therefore, the key species observed around this pH will be the protonated triplet state (PTS, $pK_a = 4.4$ (N5 position on the flavin)),²⁶ which

subsequently generates the RP ($\text{FH}^- - \text{AH}^+$). As the pH increases between pH 4.0 and 6.0, protonation of the triplet state becomes inefficient and a transition from the PTS to the neutral triplet state (NTS) occurs. The NTS gives rise to a neutral RP, which is likely to exist primarily in a closed form conformation. Both Stob *et al.*,¹⁴ and Murakami *et al.*,¹⁵ have argued that formation of the closed form conformation of the RP would lead to a very large electron exchange interaction, which would serve to halt coherent spin-state mixing. As the RP is triplet born and return to the ground state can only occur through the singlet RP, the interruption of coherent spin-state mixing will lead to a reduction in the rate of return to the ground state from the RP. This is the reason for the reduction of the observed rate constant between pH 4.0 and 6.0. This argument is also based on the observed MFE dependence, which we discuss next.

We now examine the effect of an applied magnetic field on the observed kinetics to provide further mechanistic insights. Application of a magnetic field can alter the degree and efficiency of mixing between the triplet and singlet states (ST mixing) of the photochemically generated RP. At a field of 20 mT, the Zeeman effect leads to the energetic separation of the triplet sublevels of the RP, leading to a reduction in spin-state mixing and thus a reduction in the rate of disappearance of the signal at 532 nm. The effect of a 20 mT magnetic field on the TROA signal following blue light excitation of FAD is presented in Figure 3.2 for the pH range 2.3 to 8.0. These signals correspond to the following:

$$\Delta\Delta A(B = 20 \text{ mT}) = \Delta A(B = 20 \text{ mT}) - \Delta A(B = 0 \text{ mT}) \quad (1)$$

$\Delta\Delta A$ for FAD is strongly pH dependent. High sensitivity measurements were necessary to record MFEs for all pH values up to pH 8.0 (measurements were not undertaken at higher pH values). $\Delta\Delta A$ values decreased from $\sim 1.2 \times 10^{-5}$ at pH 2.3 to $\sim 2 \times 10^{-7}$ at pH 8.0. The 60-fold decrease in this signal size is a convolution of the reduction of the overall size of the absorption signal, as seen in Figure 3.1, with the reduction of the size of the magnetic field effect itself. This is further clarified by plotting the corresponding MARY (Magnetically Affected Reaction Yield) curves at each pH value (Figure 3.3). Here the vertical axis is the percentage MFE obtained by

dividing $\Delta\Delta A$ by $\Delta A(B = 0 \text{ mT})$ and integrating across the entire time window (experimentally this is achieved by the use of phase sensitive detection).^{23,24}

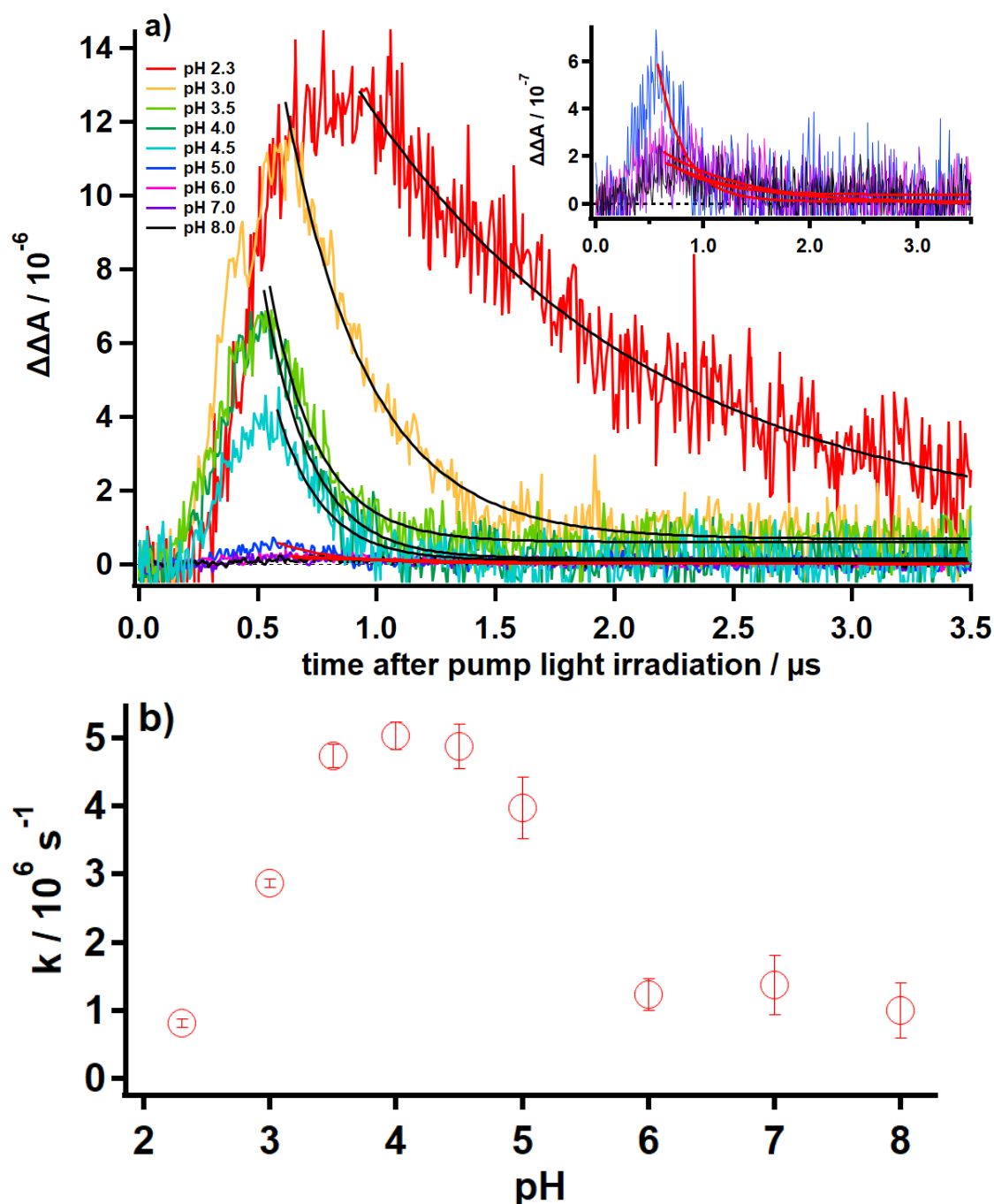


Figure 3.2. FAD $\Delta\Delta A$ spectra and rate coefficients. a) pH dependence of the MFE decay curves ($\Delta\Delta A$) at 532 nm. The inset displays the pH range 5.0-8.0 (x-axis has the same time scale as main). MFEs were measured in a 20 mT field. b) Rate coefficients obtained from an exponential fit to the decay curves (a) for each pH value. Error bars represent one standard deviation (1σ) in the fitting. Rate coefficients for the rise portion of the curves was similar for all $\Delta\Delta A$ spectra, $k \sim 3 \times 10^6 \text{ s}^{-1}$.

The $\Delta\Delta A$ signals show a consistent rise time, while a single exponential fit to the decay of the $\Delta\Delta A$ signals (Figure 3.2b) reproduces the behaviour observed in the TROA signals and can be rationalized as described above. Figure 3.3 shows the change in the MFE and the $B_{1/2}$ value (extracted from the MARY curve) with pH. Unlike the sharply decreasing TROA signal, the MFE decreases quite smoothly from $\sim 12\%$ (at pH 2.3) to $\sim 2\%$ (at pH 8.0). The $B_{1/2}$ values also decrease from 7.3 ± 1.0 mT (at pH 2.3) to 4.6 ± 2.6 mT (at pH 8.0). The $B_{1/2}$ value decreases with pH until around pH 4, after which it remains constant. These changes indicate variations in the underlying photochemistry with increasing pH. The decrease in the observed MFE between pH 2.3 and 3.5 has already been explained¹⁵ as corresponding to RP protonation ($pK_a = 2.3$, Scheme 3.1). At low pH, the doubly protonated triplet state (DPTS) and the RP are believed to be similar in energy and an equilibrium exists between them, allowing for the MFE on the RP to be transferred to the triplet state. Thus, both transient species exhibit magnetic field dependence.

As the pH increases, this equilibrium is gradually removed, and the signal from the triplet state no longer exhibits magnetic field dependence, leading to a reduction of the observed MFE magnitude of around one-half over this pH range (the extinction coefficients of RP and triplet state are approximately equal at our probe wavelength). A new observation is that the $B_{1/2}$ value also decreases over this pH range. The estimated $B_{1/2}$ value for a flavin-adenine RP based on the Weller formula²⁷ was determined to be 2.6 mT using literature hyperfine couplings.²⁸ Thus, for all pH values, the observed $B_{1/2}$ value is greater. For high pH values, it falls to around 4.5. The reason for the higher value is likely due to electron spin relaxation in the long-lived RP. A likely possibility is modulation of the electron exchange and dipolar couplings as the two ends of the chain move around. At lower pH, as the equilibrium between the RP and triplet state prolongs their total lifetime, electron spin relaxation increases, leading to a larger observed $B_{1/2}$ value. As the equilibrium is removed with increasing pH (as the RP can no longer be protonated), the $B_{1/2}$ value also decreases. Above pH 3.5, the $B_{1/2}$ value remains essentially constant, indicating that no such RP/triplet state equilibrium exists at higher pH.

We also observe that (unlike the $B_{1/2}$ value) the MFE continues to decrease at higher pH and that the decrease, while less steep than at low pH, takes place over a range that corresponds well with the pK_a of triplet state protonation discussed earlier (see Appendix). As the pH increases, there is a change from PTS to NTS as we described above to explain the decrease in the decay rate constant for the TROA signals. The NTS generates neutral RPs which can, when they adopt closed form configurations, experience a very large electron exchange interaction. Besides decreasing the decay rate constant, this has the effect of removing any MFE as the electron exchange interaction energetically dwarfs the Zeeman interaction, which leads to the observed MFE. Thus, at pH

values above 4.4, the neutral RP replaces the protonated RP. Our experimental data shows a reduction of the MFE value at pH 8.0 to around 25% of its value around pH 4.0, suggesting that around 25% of neutral RPs adopt an open conformation, capable of coherent S-T state mixing, while the remaining 75% are closed and show no MFE due to the halting of coherent S-T state mixing by the very large electron exchange interaction. The fitting to the MFE pH dependence in Figure 3.3b is composed by scaling a signal by a 50% reduction corresponding to a pKa value of 2.3 (representing the removal of the back reaction from RP to DPTS) and a 75% reduction corresponding to a pKa value of 4.4 (removal of NTS protonation).

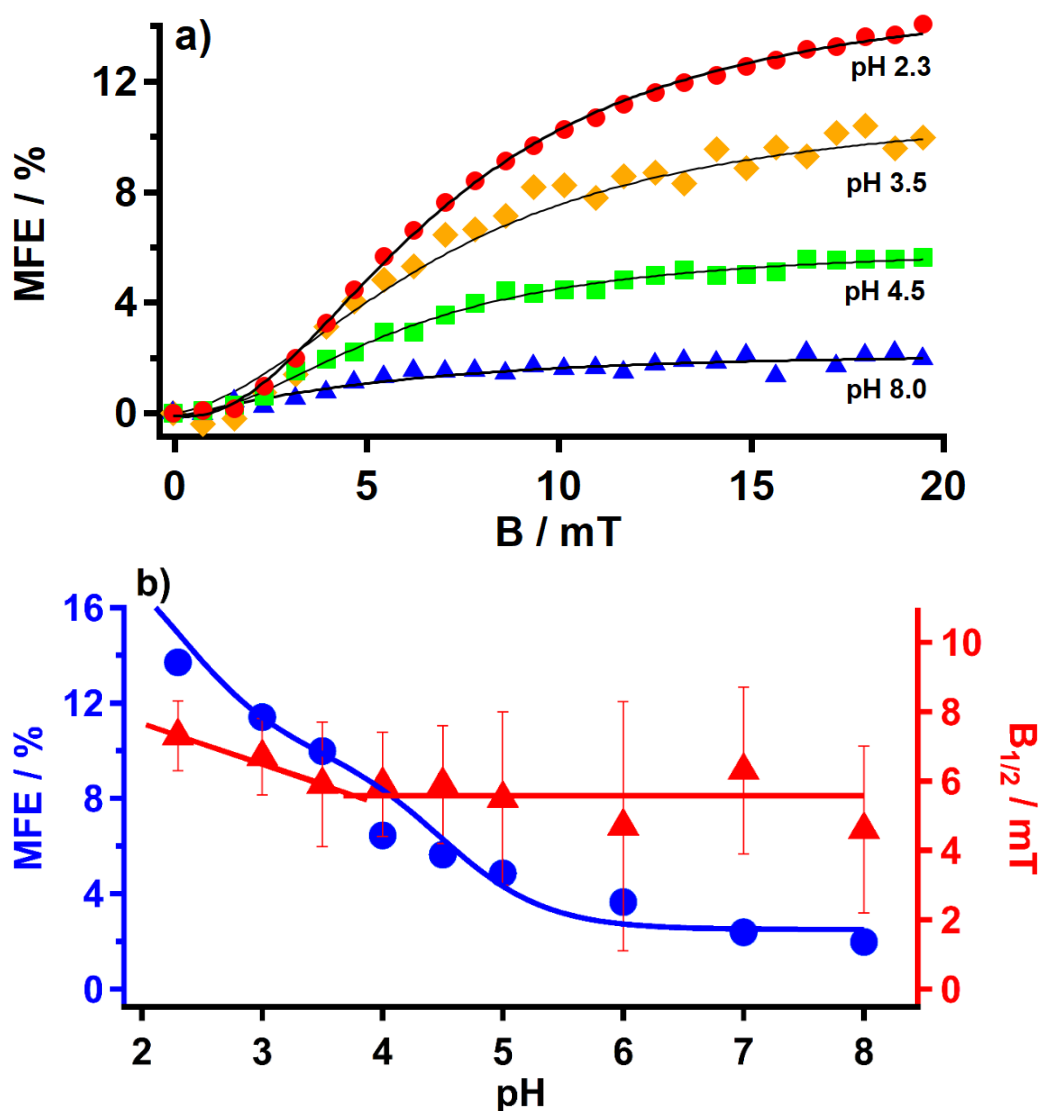
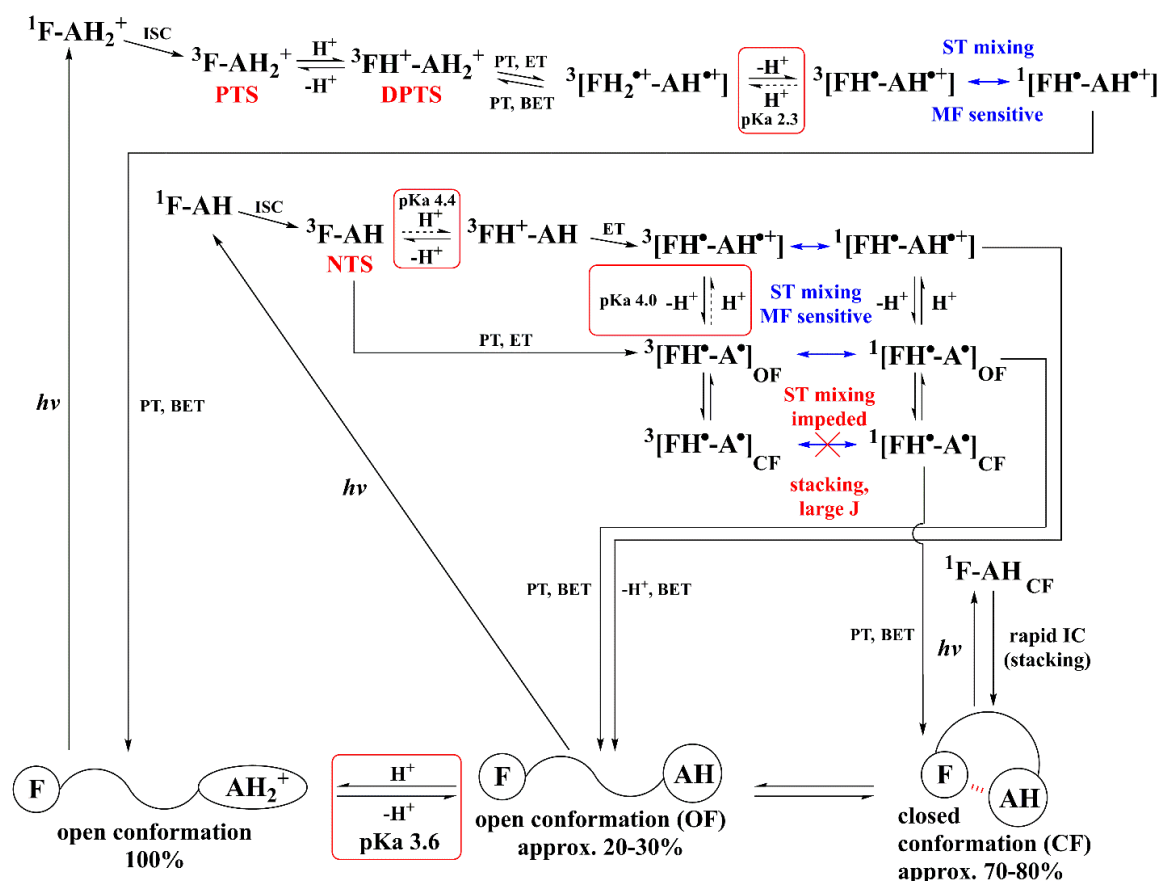


Figure 3.3. FAD MARY spectra and $B_{1/2}$ values. a) MARY spectra for FAD at 532 nm at various pH. Black curves represent a Lorentzian fit. b) pH dependence of the MFE (blue circles) and $B_{1/2}$ values (red triangles, calculated from Lorentzian fits) for FAD at each pH value are shown. MFEs were measured in a 20 mT field. The blue line is based on the simulation described in the main text.



Scheme 3.2. Proposed scheme for the pH dependence of FAD photochemistry in the range pH 2 to pH 8. F = flavin, A = adenine, PTS = protonated triplet state, DPTS = doubly protonated triplet state, NTS = neutral triplet state, $h\nu$ = light, PT = proton transfer, ET = electron transfer, BET = back electron transfer, IC = internal conversion, ISC = intersystem crossing, J = exchange interaction.

We have demonstrated that FAD photochemistry in solution is magnetic field sensitive even at physiological pH and higher. Scheme 3.2 incorporates the new findings in this work to present an overall reaction scheme of FAD photochemistry between pH 2 and 8. The TROA detection method (which also detects the FAD triplet state, the concentration of which is magnetic field sensitive at low pH due to back reaction from the RP) to some extent disguises the fact that FAD RPs at pH 8 are inherently only about 75% less field sensitive than FAD RPs low pH. As FAD is such a ubiquitous biological molecule and is present unbound in many cells, FAD RPs constitute a potential source of magnetic sensitivity at the cellular level. We are currently investigating the influence of magnetic fields on endogenous cellular FAD.

References

- [1] S. Weber, E. Schleicher, *Flavins and Flavoproteins: Methods and Protocols*, Methods in Molecular Biology, Springer, New York, **2014**.
- [2] J. Hühner, Á. Ingles-Prieto, C. Neusüß, M. Lämmerhofer, H. Janovjak, *Electrophoresis* **2015**, 36, 518.
- [3] A. Sancar, *Angew. Chem. Int. Ed.* **2016**, 55, 8502.
- [4] I. Chaves, R. Pokorny, M. Byrdin, N. Hoang, T. Ritz, K. Brettel, L. O. Essen, G. T. van der Horst, A. Batschauer, M. Ahmad, *Annu. Rev. Plant Biol.* **2011**, 62:1, 335.
- [5] K. Maeda, A. J. Robinson, K. B. Henbest, H. J. Hogben, T. Biskup, M. Ahmad, E. Schleicher, S. Weber, C. R. Timmel, and P. J. Hore, *Proc. Natl. Acad. Sci. U. S. A.* **2012**, 109, 4774.
- [6] D. M. W. Sheppard, J. Li, K. B. Henbest, S. R. T. Neil, K. Maeda, J. Storey, E. Schleicher, T. Biskup, R. Rodriguez, S. Weber, P. J. Hore, C. R. Timmel, and S. R. Mackenzie, *Sci. Rep.* **2017**, 7, 42228.
- [7] H. Mouritsen, and P. J. Hore, *Annu. Rev. Biophys.* **2016**, 45, 299.
- [8] S. Greenland, A. R. Sheppard, W. T. Kaune, C. Poole, M. A. Kelsh, *Epidemiology* **2000**, 11, 624.
- [9] S. Ahlbom, N. Day, M. Feychting, E. Roman, J. Skinner, J. Dockerty, M. Linet, M. McBride, J. Michaelis, J. H. Olsen, T. Tynes, and P. K. Verkasalof, *Brit. J. Cancer* **2000**, 85, 692.
- [10] Advisory Group on Non-Ionising Radiation (AGNIR) ELF Electromagnetic Fields and the Risk of Cancer. *Report of an Advisory Group on Non-Ionising Radiation. Documents of the NRPB*, Vol. 12, National Radiology Protection Board, Chilton, Oxon, UK, **2001**.
- [11] International Agency for Research on Cancer, *Static and Extremely Low-Frequency (ELF) Electric and Magnetic Fields. IARC Monographs on the Evaluation of Carcinogenic Risks to Humans*, vol. 80, IARC, Lyon, **2002**.
- [12] P. L. Bounds and N. Kuster, *Biophys J.* **2015**, 108, 562a.
- [13] I. Lagroye, Y. Percherancier, J. Juutilainen, F. Poullietier De Gannes, and B. Veyret, *Prog. Biophys. Molec. Biol.* **2011**, 107, 369.
- [14] S. Stob, J. Kemmink, and R. Kaptein, *J. Am. Chem. Soc.* **1989**, 111, 7036.

- [15] M. Murakami, K. Maeda, and T. Arai, *J. Phys. Chem. A* **2005**, 109, 5793.
- [16] M. Murakami, K. Maeda, and T. Arai, *Chem. Phys. Lett.* **2002**, 362, 123.
- [17] A. Sengupta, R. V. Khade, P. Hazra, *J. Photochem. Photobiol A: Chem.* **2011**, 221, 1, 105.
- [18] P. A. W. van den Berg, K. A. Feenstra, A. E. Mark, H. J. C. Berendsen, and A. Visser, *J. Phys. Chem. B* **2002**, 106, 8858.
- [19] H. Chosrowjan, S. Taniguchi, N. Mataga, F. Tanaka, A. Visser, *Chem. Phys. Lett.* **2003**, 378, 354.
- [20] R. A. Copeland, T. G. Spiro, *J. Phys. Chem.* **1986**, 90, 6648.
- [21] R. J. Stanley, A. W. MacFarlane, *J. Phys. Chem. A* **2000**, 104, 6899.
- [22] M. Raszka, N. O. Kaplan, *Proc. Natl. Acad. Sci.* **1974**, 71, 4546.
- [23] J. P. Beardmore, L. M. Antill, and J. R. Woodward, *Angew. Chem. Int. Ed.* **2015**, 54, 8494.
- [24] L. M. Antill, J. P. Beardmore, and J. R. Woodward, *Rev. Sci. Instrum.* **2018**, 89, 023707.
- [25] M. S. Grodowski, B. Veyret, and K. Weiss, *Photochem. Photobiol.* **1977**, 26, 341.
- [26] M. Sakai, H. Takahashi, *J. Mol. Struct.* **1996**, 379, 9.
- [27] A. Weller, F. Nolting, and H. Staerk, *Chem. Phys. Lett.* **1983**, 96, 24.
- [28] S. D. Wetmore, L. A. Eriksson, and R. J. Boyd, *J. Phys. Chem. B* **1998**, 102, 10602.

CHAPTER 4

Immobilised Flavins

This chapter discusses the immobilisation of flavin-based systems in small and giant unilamellar vesicles, with the aim of mimicking a biological environment, in a controlled manner, for studying chemical magnetoreception relevant magnetosensitive photochemistry.

Chapter 4.1: Prof. Shin-ya Takizawa synthesised all small unilamellar vesicle systems. The author conducted all TROA and MARY experiments. A thank you is provided for Mr. Yuta Sato for preliminary experiments regarding the vesicle preparation.

Chapter 4.2: Prof. Toyota schooled the author in giant unilamellar vesicle synthesis. All sample preparation, experiments, and analysis were conducted by the author.

The work in this chapter has been submitted to the following peer-review journal:

L. M. Antill, S. Takizawa, S. Murata and J. R. Woodward, Photoinduced flavin-tryptophan electron transfer across vesicle membranes generates magnetic field sensitive radical pairs, *Molecular Physics*, accepted for publication **2018**

Chapter 4.1 is a reformatted version of the above publication.

The work presented in Chapter 4.2 was published as a cover article titled Magnetic field sensitive microspectroscopy in *Electron Spin Science* (電子スピンサイエンス), Vol. 15, **2017**, by Prof. J. R. Woodward.

4.1 SMALL UNILAMELLAR VESICLES

Abstract

Due to the photobiology of the flavoproteins DNA photolyase and cryptochrome, electron transfer reactions between flavins and tryptophan are of significant biological relevance. In addition, electron transfer across vesicle membranes has also seen much attention. In this work, we study the electron transfer reaction between flavins and tryptophan across lipid bilayer membranes in 1,2-dipalmitoyl-*sn*-glycero-3-phosphocholine small unilamellar vesicles using time-resolved optical absorption microspectroscopy and magnetically affected reaction yield spectroscopy. We demonstrate that riboflavin tetrabutryate is embedded in the vesicle bilayer and can undergo electron transfer with tryptophan molecules in either the inner water pool or the bulk solution. Remarkably, flavin mononucleotide encapsulated in the inner water pool can undergo electron transfer across the vesicle bilayer to generate a magnetically sensitive radical pair with tryptophan molecules located in the bulk solution. The observed kinetics suggest that back electron transfer occurs between radical pairs generated by diffusive reencounter, either in the vesicle surface water or via electron hopping through degenerate electron exchange.

Introduction

The magnetic field sensitivity of photochemical reactions is of relevance across diverse disciplines from solid-state photonic devices to animal navigation. In the case of the latter, many different animal species are known to be able to use the geomagnetic field for orientation and navigation, an ability referred to as magnetoreception. The mechanism by which this process operates is still under debate. One hypothesis, chemical magnetoreception, involves the radical pair mechanism (RPM), in which magnetic fields can influence the rate and yield of chemical reactions.¹ The proposed receptor molecule in this hypothesis is the blue-light receptor protein, cryptochrome.² Cryptochrome photochemistry involves photoinduced intermolecular electron transfer reactions, which produce radical pairs (RPs) comprised of a reduced flavin cofactor and an oxidised tryptophan (Trp) residue inside the protein.³ Immobilisation of flavins is desirable to simulate the orientationally structured protein environment of cryptochrome. Vesicles (liposomes) are mimetic systems for cell membranes, which are self-assemblies formed by phospholipid or synthetic surfactants that form bilayers. They can be defined by three distinct regions: the inner water pool, the hydrophobic bilayer, and the homogeneous aqueous solution. Vesicles are more ordered and have longer lifetimes than other aggregates such as micelles.^{4,5} In this work, we study the photochemistry and magnetosensitivity of flavins (electron acceptors) and tryptophan (electron donor) in DPPC small unilamellar

vesicles (SUV, diameter ~60 nm), reporting transmembrane electron transfer (ET) reactions across both single and double membrane layers.

Materials and Methods

Vesicle preparation

A CHCl_3 solution of riboflavin tetrabutrate (RFTB) (1.00 μmol , Tokyo Chemical Industry (TCI) Co., Ltd.) and 1,2-dipalmitoyl-*sn*-glycero-3-phosphocholine (DPPC, 12.1 μmol , Wako) was evaporated under reduced pressure to form a thin film in a flask. The film was dried under vacuum overnight and dispersed in a 4 mL solution of 1.0 M NaCl/Tris-HCl buffer (pH 7.5) (for RFTB experiments) or 1.5 mM tryptophan (for tryptophan in the inner water pool and solution experiments, Sigma-Aldrich) by vortex mixing (TTM-1, Shibata). For preparation of vesicles containing FMN-Na (flavin mononucleotide) in the inner water pool, the DPPC film prepared without flavins was dispersed in a 4 mL 0.1 M FMN-Na aqueous solution. Each suspension was treated with an ultrasonic process (UT-206H, Sharp) for 2 h at 55 °C. The resulting solution was developed on a column with Sephadex G-50 (Amersham Biosciences) equilibrated with the 1.0 M NaCl/Tris-HCl buffer solution to remove flavins or tryptophan outside the vesicles, and the fraction containing the lipids was collected to give a vesicle solution (See Figure 4.1). The retention time of the samples ranged from approximately 10 to 26 min when using the Sephadex G-50 column (2 x 23 cm) equipped with a peristaltic pump (Perista, Bio-minipump, ATTO) at a flow rate of 35 mL h^{-1} . As vesicles generally show slight light scattering in the UV region, DPPC vesicles can be identified using a UV-absorption monitor ($\lambda_{\text{abs}} = 340 \text{ nm}$, ADVANTEC, CHU600AA) during gel filtration, even when the desired flavin was not incorporated into the vesicles. The relevant fractions were collected on a fraction collector (ADVANTEC, CHF100AA).

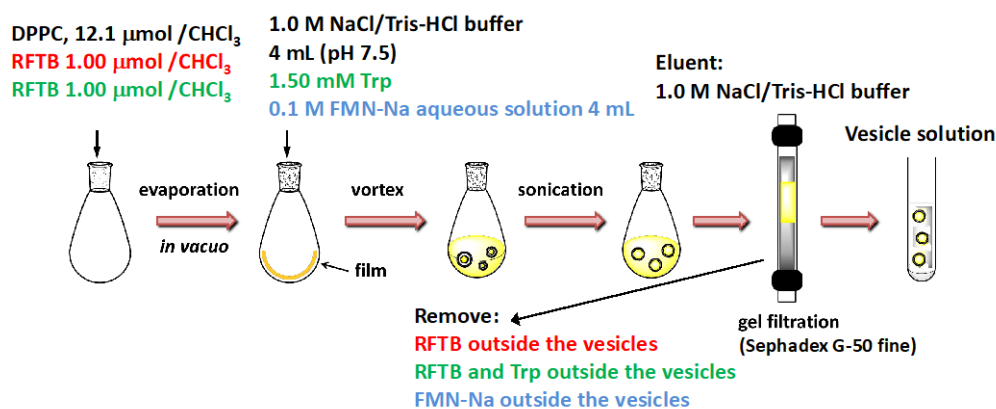


Figure 4.1. Procedure for vesicle preparation.

UV-Vis absorption spectroscopy

The concentration of RFTB in typical vesicle solutions was determined to be $\sim 60\ \mu\text{M}$ by the absorbance at 449 nm and its molar extinction coefficient determined in CHCl_3 ($\epsilon = 13,200\ \text{M}^{-1}\ \text{cm}^{-1}$, determined in our lab). The total FMN concentration in solution was determined to be $\sim 25\ \mu\text{M}$ by the absorbance at 449 nm and its molar extinction coefficient in water ($\epsilon = 12,600\ \text{M}^{-1}\ \text{cm}^{-1}$, ref. 6). All spectra were recorded with a Jasco V-560 UV-Vis spectrophotometer.

Dynamic light scattering

Our preparation method using DPPC generally produces a solution containing particles with the size distribution as shown in ref. 7, which indicates the formation of the vesicles with a unilamellar structure. Dynamic light scattering studies of vesicle solutions were made using a Honeywell Microtac UPA-150 at room temperature.

TOAD microspectroscopy

All data were recorded with our TOAD microspectroscope, which has been described in detail elsewhere.^{8,9} Samples were photoexcited with a 449 nm pump beam (power density $\sim 6\ \text{kW cm}^{-2}$, CUBE laser, Coherent) with a 700 ns pulse width and a 10 kHz repetition rate. A 532 nm probe beam (power density $\sim 10\ \text{kW cm}^{-2}$, Sapphire laser, Coherent) monitored the transient species. In comparison to power densities used in confocal microscopy-based biological studies, our excitation power is relatively weak.¹⁰ The confocal arrangement consists of two super apochromatic objective lenses (UPlanSApo 20 \times / NA 0.75, Olympus). Samples were produced by adding polymer 100 μm glass beads (acting as spacers between cover slips to fix the sample thickness at 100 μm) (Toshin Riko) to the sample solution and sandwiching 5 μL of sample between glass cover slips (0.13–0.16 mm, Marienfeld).

Results and Discussion

Previous work on intermolecular electron transfer reactions between different flavins and indole rings confined in micelles found that the MFEs were affected by the hydrophobic properties of the flavin moieties.^{11,12} The work found that MFEs were higher for more hydrophobic flavins and indole derivatives, which were rationalised by their confinement within the hydrophobic environment of the micelle leading to an extended RP lifetime and increased MFE. Flavins for our vesicle systems were chosen based on their hydrophilicity, which increases from RFTB to FMN. Unlike flavin adenine dinucleotide, both of these flavin derivatives cannot undergo intramolecular RP formation, making them ideal for studying intermolecular ET reactions. These characteristics

were key in designing the biomimetic vesicle systems. Experiments were conducted using 1) hydrophobic RFTB which we anticipated to be encapsulated in the hydrophobic bilayer (~6 nm diameter, Fig. 4.2) of the DPPC vesicles (See Materials and Methods) and 2) Hydrophilic FMN which was prepared inside the inner water pool of the vesicles and where we anticipate it should remain encapsulated. These two reaction systems are considered in turn.

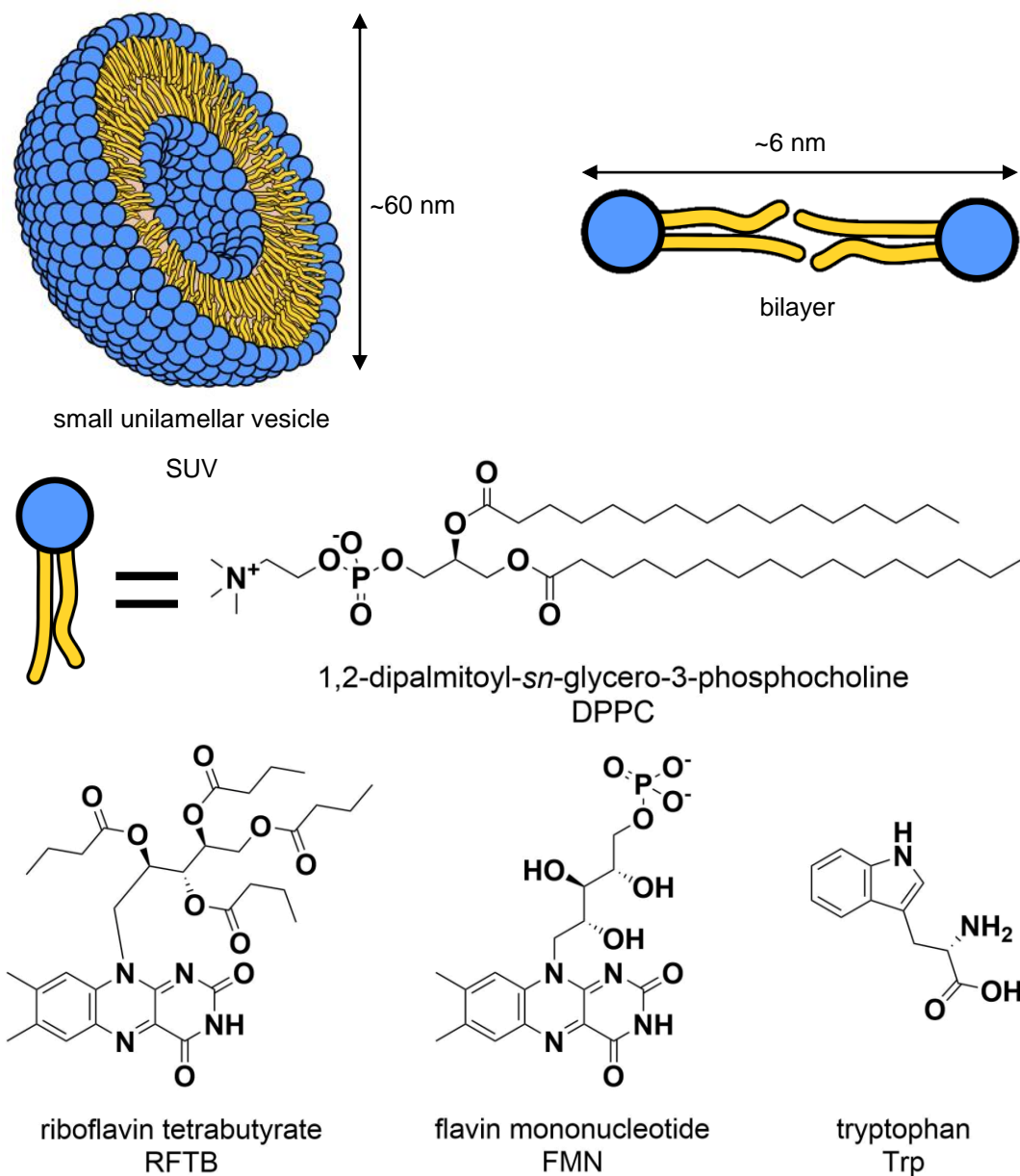


Figure 4.2. Schematic representation of small unilamellar vesicles (SUVs), providing dimensions for key features of DPPC SUVs, with chemical structures of DPPC, riboflavin tetrabutyrate (RFTB), flavin mononucleotide (FMN), and tryptophan (Trp).

RFTB encapsulated in the bilayer of DPPC vesicles

The UV/Vis absorption spectrum for the synthesised vesicle solution containing RFTB in the bilayer is shown in Fig. 4.3. The spectrum is characteristic of a flavin ground state absorption spectrum, showing two broad bands centred at 445 nm ($S_0 \rightarrow S_1$, $\pi \rightarrow \pi^*$) and 360 nm ($S_0 \rightarrow S_2$, $\pi \rightarrow \pi^*$) displaying three partial vibronic structures ($S_1(\nu=0)$; ($\nu=1$); ($\nu=2$)) at 475, 445, and 430 nm, suggesting that the flavin is somewhat bound (much like a flavoprotein environment) in the vesicle bilayer.¹³ The structural organisation and molecular dynamics of the vesicle membrane is temperature dependent. Above the phase transition temperature (T_m), vesicle membranes are in a liquid-crystalline phase (where lipid molecules can diffuse laterally), below the T_m , a phase change to a gel occurs, where any lateral diffusion of molecules in the vesicle bilayer is totally restricted.^{14,15} DPPC vesicles are in the gel phase at room temperature ($T_m = 42^\circ\text{C}$), therefore we propose that all RFTB molecules are bound inside the vesicle bilayer⁷ and have limited mobility. Furthermore, work conducted on RFTB in solvents of varying polarity (a series of mixtures with water and 1, 4-dioxane) found that as polarity increased a three banded structure appeared (with an associated blue shift) in the absorption spectrum at ~ 445 nm.¹⁶ This further supports our hypothesis that RFTB is encapsulated in the polar environment of the vesicle bilayer. Given that our laser powers are relatively low (see Materials and Methods) we expect the DPPC vesicle bilayer to be in the gel phase, however, there is a possibility of localised heating of the sample at the focal point of our lasers.

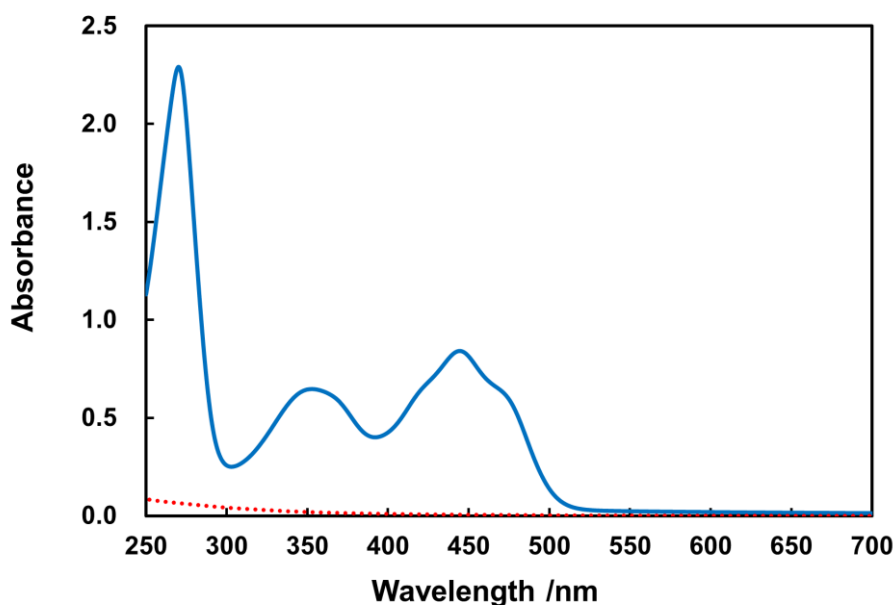


Figure 4.3. Typical UV-Vis absorption spectra for a RFTB vesicle solution (solid blue line) and a vesicle solution without RFTB (dotted red line). A bulk (whole solution) concentration of $\sim 60\ \mu\text{M}$ was obtained for all vesicle solutions. A bulk (whole solution) concentration of $\sim 60\ \mu\text{M}$ was obtained for all vesicle solutions.

There are an estimated number of $\sim 1.5 \times 10^{15}$ vesicles in the bulk solution, with a RFTB concentration of ~ 8.6 mM in one vesicle bilayer (see Appendix). The local concentration of RFTB per vesicle is relatively high. Figure 4.4 shows the time-resolved optical absorption (TROA) signal obtained after the 449 nm photoexcitation of RFTB inside the vesicle bilayer. The TROA signal at 532nm consists of absorption from both the flavin semiquinone radical and the flavin triplet state, which have roughly equal extinction coefficients at this wavelength.¹⁷ In addition, the Trp radical also absorbs with a much smaller extinction coefficient ($\sim 20\%$). The decay curve is well fit using a second order function (see Fig. 4.4), strongly suggesting that the decay of the observed transient species takes place with second order reaction kinetics. In addition, it should be noted that even in the case of no added electron donor, the TROA signal may correspond to the photoexcited triplet state of RFTB, however, the lifetime is rather long, well fit by a second order decay, and shows a magnetic field dependence (see later) so is assigned to a transient radical (see later for discussion of its possible identity). The rate coefficients are for a back electron transfer process which can occur at distances beyond the encounter distance. In addition, for the RFTB alone vesicle system the rate coefficient could be explained by degenerate electron exchange (DEE) between RFTBH[•] and RFTBH[•] (given the pH of the solution). This is reasonable given the relatively high concentration (~ 8.6 mM) and that the RFTB molecules are constrained in the gel phase of the bilayer. Addition of Trp to the bulk solution results in a doubling of the TROA signal size and a substantial decrease in the rate of decay of the signal, while the decay is still characteristic of a second order reaction. This suggests that a reaction takes place between the photoexcited flavin and Trp, which can be reasonably assigned as electron transfer from the Trp to the flavin, generating a RP. If instead the Trp is added to the inner water pool, the signal becomes still stronger but the second order decay rate coefficient is only slightly reduced relative to the bulk solution case.

It is important to note that our relatively long laser pulse (700 ns) and the presence of an intense fluorescence signal during this period obscure the TROA signal at early times, so that the TROA signal only informs on the species present after 700 ns of irradiation. If short lived species are replaced with long lived species during this period, the observed TROA signal will increase.

We first consider the magnitude of the TROA signals. If the RFTB is embedded and largely immobile inside the vesicle bilayer, then RP formation can occur only if the Trp is initially located close enough to the RFTB for electron transfer to occur, or if it can move to become close enough during the RFTB triplet state lifetime. From this we can conclude that 1) as electron transfer appears to be taking place, the Trp is either partially embedded into the vesicle bilayer, or is capable of moving between the aqueous phase and such a location; 2) Given that the TROA magnitudes differ depending on whether the Trp is located in the outer bulk aqueous solution or the inner

water pool, it seems unlikely that the Trp is permanently embedded into the vesicle bilayer, as if it were, one would anticipate similar TROA magnitudes and kinetics in the two cases. Therefore, the TROA data suggests that the Trp is mobile and can move between the aqueous and lipid bilayer regions, and the chances of RFTB encountering a Trp at a suitable distance are enhanced if the Trp is constrained in the inner water pool. The dwell time of the vesicles in the confocal volume of our microscope was estimated to be ~ 6 ms (see Appendix) and therefore diffusion out of the confocal volume should not contribute to the observed decays.

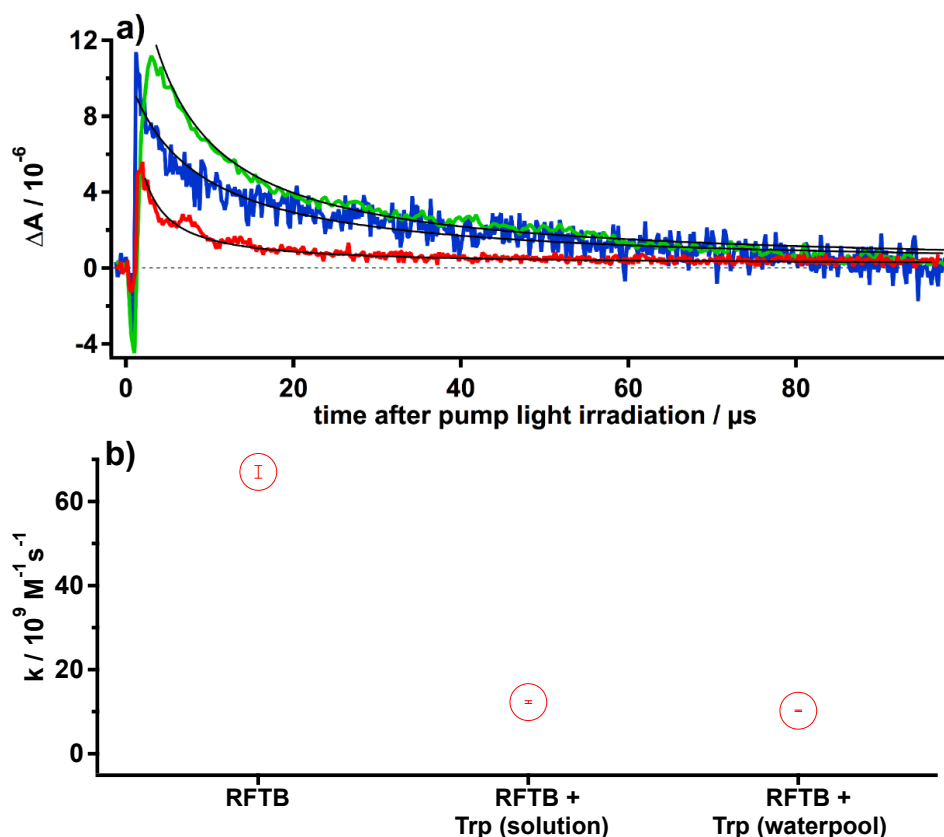


Figure 4.4. RFTB encapsulated in the bilayer membrane of DPPC vesicles in the presence and absence of tryptophan. a) Time-resolved optical absorption signals recorded at 532 nm following 449 nm laser excitation for the three different vesicle systems. Black lines represent a second order fit $[A]_t = \frac{[A]_0}{kt[A]_0 + 1}$ corresponding to bimolecular reaction kinetics for each vesicle system. Red = RFTB only, blue = RFTB with Trp in the outer aqueous solution, green = RFTB with Trp in the inner water pool. b) Rate coefficients obtained from the fits in a). Error bars represent one standard deviation (1σ).

The second order kinetic decays strongly suggest that the members of the RPs produced on electron transfer are able to escape from one another and undergo some kind of diffusive reencounter (f-pair) process followed by back electron transfer. To provide further insight, the influence of an applied external magnetic field on the decay kinetics was investigated. Figure 4.5 shows the MARY (Magnetically Affected Reaction Yield) spectra obtained

for each of the cases just described. These spectra were recorded using a lock-in amplifier referenced to the laser flash repetition frequency, observing directly the signal from the balanced photodetector. The MARY curve indicates the percentage change in the observed signal as the magnitude of an applied field is increased (in practice the field is swept through zero from negative to positive field values and the values at equivalent positive and negative fields are averaged).

Even in the absence of an added electron donor, a magnetic field effect (MFE) is observed on the RFTB photochemistry. This means that RPs are generated even in this case, for which there are two possible explanations. First is that the RFTB is able to undergo photochemical reaction with the DPPC molecule itself, generating a magnetic field sensitive RP. Second, it is known^{18,19} that reaction between two flavin triplet states can lead to the generation of a semiquinone radical by electron transfer. Electron transfer in the singlet state of a pair of such semiquinone radical can yield the fully oxidised and fully reduced flavins and thus this spin-selective RP reaction can give rise to the observed MFE. We have previously observed weak MFEs from such a reaction between riboflavin molecules⁹ and given the relatively high light intensity in the microscope and the high local concentration of RFTB inside the vesicle bilayer membrane, this explanation seems more likely. Given that the signal changes substantially with the addition of Trp, it seems reasonable to suggest electron transfer takes place more rapidly and effectively than the triplet-triplet reaction.

Addition of Trp into the bulk solution leads to a decrease in the observed MFE. This is consistent with the TROA data and discussion above, suggesting a reaction between the photoexcited RFTB and the Trp to generate a magnetic field sensitive RP by electron transfer from the Trp to the RFTB. Addition of Trp into the inner water pool results in a substantial increase in the magnitude of the MFE. Thus, the MFE data first suggest the formation of a RP composed of an RFTB semiquinone radical and a neutral tryptophan radical (based on the pH of the solution) by intermolecular electron transfer.

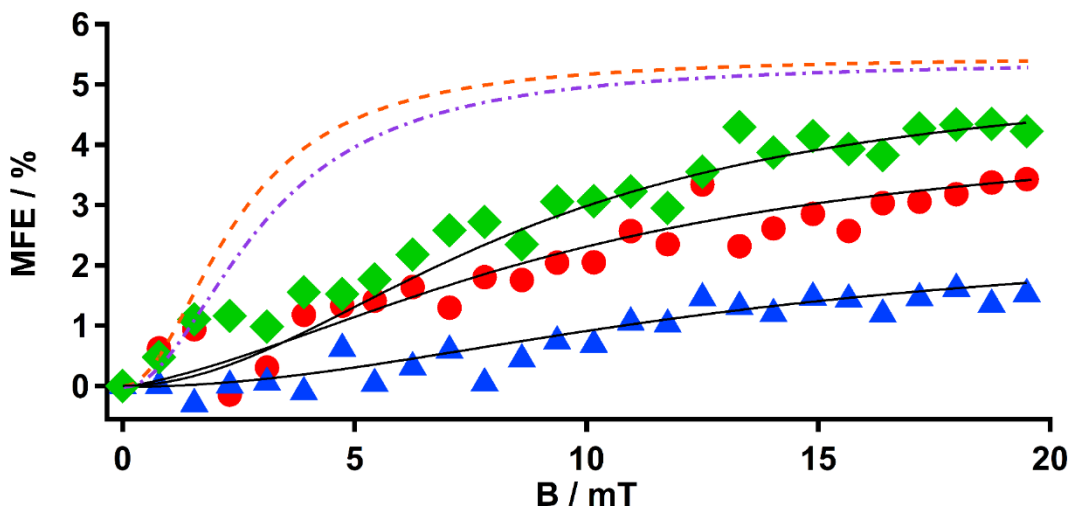


Figure 4.5. MARY spectra for the three different vesicle systems. Red = RFTB only, blue = RFTB with Trp in the outer aqueous solution, green = RFTB with Trp in the inner water pool. Black curves represent Lorentzian fits. $B_{1/2}$ values of 9.6 ± 5.4 mT, 13 ± 8.2 mT, and 8.6 ± 3.8 mT, for the red, blue, and green curves, respectively. The dashed orange curve represents a MARY curve for a RP composed of two flavin semiquinone radicals, with a $B_{1/2}$ of 2.4 mT, and the purple dash-dot curve represents a MARY curve for a flavin – Trp RP with a $B_{1/2}$ of 3 mT (based on ref. 20, see Appendix). The saturation field of these calculated curves was chosen arbitrarily for clarity of the figure.

There are two possible reasons for the difference in the MFE magnitude for Trp in the bulk solution and in the inner water pool. First, if the rate of electron transfer from triplet state to Trp is greater when the Trp is in the inner water pool, this could lead to a greater ratio of RP : triplet state and thus an increase in the fractional effect of a magnetic field on the total signal. In other words, the MFE reflects the efficiency of the initial electron transfer process from Trp to RFTB. This would imply that the concentration of Trp molecules embedded into the surface of the bilayer is greater at the inner surface than the outer surface. This explanation also explains the difference in the size of the TROA signals. However, such an explanation alone cannot account for the difference in the TROA signal decay rates. Alternatively, the RPs produced at the two different vesicle surfaces may exhibit different MFE magnitudes based on the spin dynamics and diffusional kinetics of the RPs produced. If the Trp is strongly embedded in the surface layer and relatively immobile, then once the RP is formed, it should behave similarly regardless of which surface it is formed at (outer or inner) and one would expect similar MFEs at both surfaces. Only if Trp radical diffusion in the inner water pool and reencounter with the original RFTB radical could take place during the lifetime of the geminate pair, could this influence the observed MFE. Given that the second order decay rate constant of the TROA signal is very similar regardless of whether the Trp is in the inner water pool or

the bulk solution, it is reasonable to assume that after formation, the RPs behave similarly in each case. Therefore, we propose that the difference in RP magnitudes comes from the efficiency of the initial electron transfer process.

It is necessary to discuss why the kinetics are second order, rather than the first order process expected by the back electron transfer of a geminate RP. For FMN and Trp in aqueous solution, second order reaction is also observed. However, in this case, we might imagine that if the Trp were strongly bound into the vesicle membrane surface, that the RP members would be likely to undergo reasonably efficient geminate recombination from the singlet RP state. This implies, then, that the RP members can escape from the initial RP in some way. The first possibility is that the Trp radical is not tightly held at the surface but can move to the bilayer exterior and diffuse along the surface of the vesicle membrane. Such a process would be similar at both inner and outer membrane surfaces. However, it is also possible that another Trp molecule nearby can undergo degenerate electron exchange (DEE) with the Trp semiquinone radical generating a new RP with a different separation between members (DEE between Trp and Trp semiquinone radicals is well known in flavoproteins^{21,22}). This electron hopping can take place even if the Trp is tightly bound in the vesicle membrane and may lead to the formation of the new Trp radical that is more or less tightly bound. A recent theoretical study²³ suggests that Trp resides both inside the vesicle membrane and in the surface water which is in good agreement with our observations and proposal.

If Trp radicals can escape from the vesicle surface, then it is possible that some back electron transfer occurs after diffusion of the Trp radical to a different vesicle. Given the concentration of vesicles in the solution (approximately 700 nM) the observed TROA decay is too rapid to be explained in terms of movement of Trp semiquinone radicals between vesicles. Also, this should only be possible in the case of bulk aqueous Trp but would lead to a very large change in the observed kinetics, which is also inconsistent with the TROA data. Therefore, it seems that the decay kinetics are primarily explained in terms of either Trp diffusion along the vesicle surface or DEE between the Trp semiquinone radical in the RP and nearby ground state tryptophan molecules, or some combination of the two.

The calculated $B_{1/2}$ value for the RP generated by electron transfer from tryptophan to flavin is around 3 mT.²⁰ It is clear from the MARY curves recorded with Trp in the inner water pool and in the bulk solution that in both cases, the $B_{1/2}$ value is much larger. For FMN and Trp in aqueous solution, we measured the MFE to be around 3.6 mT which is close to the theoretical estimate (which is based on hyperfine couplings generated by DFT calculations, rather than experimental observations). This tells us that the RP dynamics thus differ substantially from the situation in aqueous solution. Increases in observed $B_{1/2}$ values are commonly encountered in RPs where

incoherent electron spin relaxation processes can occur. As these processes typically take place on timescales of microseconds, this might suggest that the RP generated is sufficiently long lived for such relaxation to take place. If the Trp is quite well bound inside the surface of the vesicle, an extended RP lifetime is likely. During this geminate period, back electron transfer may be relatively slow due to the separation between RFTB and Trp, meaning that even though the pair lives long enough for relaxation to be observed, escape of the Trp into the surface water is possible and diffusion on the surface and f-pair reencounter gives rise to the observed TROA kinetics. Another possibility is that the increase in $B_{1/2}$ is explained by DEE, which has been previously characterised as giving rise to an increase in the observed $B_{1/2}$ value of MARY spectra^{24,25} in many different electron transfer reactions. DEE could reasonably be responsible not only for the increase in the $B_{1/2}$ value of the geminate pair, but also for separating the electron centres in the RP, leading to 2nd order reencounter.

Therefore, based on the observed TROA magnitudes and kinetics, the MFE magnitudes and the observed $B_{1/2}$ values, the most plausible mechanism consistent with all features involves electron transfer between RFTB well embedded in the bilayer interior and a Trp embedded into the vesicle surface. Direct electron transfer to RFTB from a Trp in the water layer is unlikely as the separation is too great. After RP generation, the geminate RP itself exhibits spin selective recombination. The RP is either long lived (implying that the Trp is quite well embedded) and subject to incoherent spin relaxation or degenerate electron exchange between the Trp semiquinone radical and a nearby neutral ground state Trp. The latter process can give rise to an increase in the observed $B_{1/2}$ value, even if the RP is not particularly long lived.^{24,25} Removal of RPs occurs via a second order ‘diffusive’ reaction between RFTB and Trp radical, where the “diffusion” may involve Trp diffusing in the water layer at the outer vesicle surface or hopping of the electron via DEE. It is also possible that DEE can take place between RFTB semiquinone radicals and RFTB ground state molecules, although this process cannot be resolved in these measurements.

This conclusion caused us to question whether it may be possible to observe electron transfer between a flavin molecule located in the inner water pool of the vesicle and a tryptophan molecule located in the bulk solution. To attempt such a measurement, we made measurements using hydrophilic FMN, which we initially loaded into the inner water pool of DPPC vesicles.

FMN encapsulated in the inner water pool of DPPC vesicles

The UV/Vis absorption spectrum for the synthesised vesicle solution containing FMN in the inner water pool is shown in Fig. 4.6. While there is still some evidence of the vibronic coupling observed in the RFTB sample, it is less pronounced in this case, suggesting that the flavin is partially constrained, but much more mobile than RFTB. This is reasonable if the FMN is located at the interface between the bilayer and the inner water pool. Were the FMN diffusing freely in the bulk solution, there should be no vibronic structure, as shown in Fig 4.6. It seems likely that the organic part of the FMN molecule becomes partially embedded into the vesicle bilayer with the phosphate group residing in the aqueous interface in the same region as the DPPC charged head groups. The concentration of FMN inside the inner water pool was calculated to be ~3.4 mM (see Appendix).

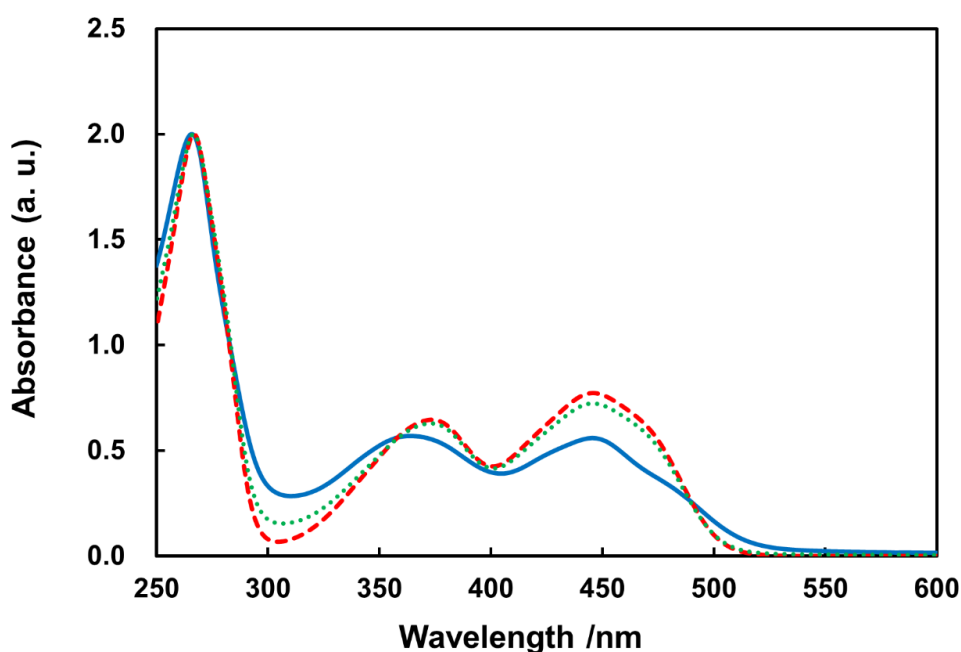


Figure 4.6. UV-Vis absorption spectrum of the solution containing FMN inside the vesicle water pool (solid blue line), solution containing FMN (25 μ M) in the outer aqueous solution surrounding DPPC vesicles (dotted green line), and FMN in water (dashed red line). All spectra were normalised at ~270 nm. Vibronic structure is clearly shown in the solid blue line, however, not observed for the other two spectra. This suggests that FMN is encapsulated in the inner water pool of the DPPC vesicle.

Figure 4.7a shows the TROA and MARY signals obtained for this vesicle solution in the absence and presence of Trp added to the outer bulk water. With FMN alone, the transient signal decays rapidly in a manner completely consistent with the formation and subsequent decay of the excited FMN triplet state. No effect of a magnetic field is observed on the photochemistry. These two facts provide good evidence that no electron transfer takes place and therefore no magnetic field sensitive RP is generated. However, addition of Trp to the bulk solution results in

a dramatically different TROA response. There is clearly a substantial interaction taking place, most simply explained by electron transfer from the Trp to FMN. Due to the technical difficulty of making these measurements, the signal to noise level is poor in the MARY spectrum, but a MFE is clearly distinguishable and the magnitude is similar to that for FMN and Trp in bulk aqueous solution. In addition, the $B_{1/2}$ value is clearly less than for the RFTB case and appears to be close to the theoretical value in the absence of relaxation. (Figure 4.7 shows a simulated MARY curve corresponding to the calculated $B_{1/2}$ value of 3 mT for comparison (based on ref. 20)). In this experiment, the Trp can still undergo degenerate electron exchange. Therefore, to explain the reduced $B_{1/2}$ value, the RP lifetime must be reduced. This suggests that the FMN's association with the bilayer interior is weaker than for Trp and that FMN semiquinone radicals can escape relatively rapidly into the inner water pool, destroying the spin coherence. This would also lead to slower RP recombination and a weaker MFE, both of which are observed. In addition, in this system, the distance between pair members will be larger than in the RFTB case, which may reduce the electron transfer rates substantially. Indeed, the TROA kinetics show a clear time component that matches the triplet FMN decay in the absence of Trp. This suggests that the initial electron transfer is slow and implies that the back electron transfer is also slow. It is likely then, that the electron needs to jump back relatively early in the RP lifetime before the pair members separate either by diffusion or degenerate electron exchange.

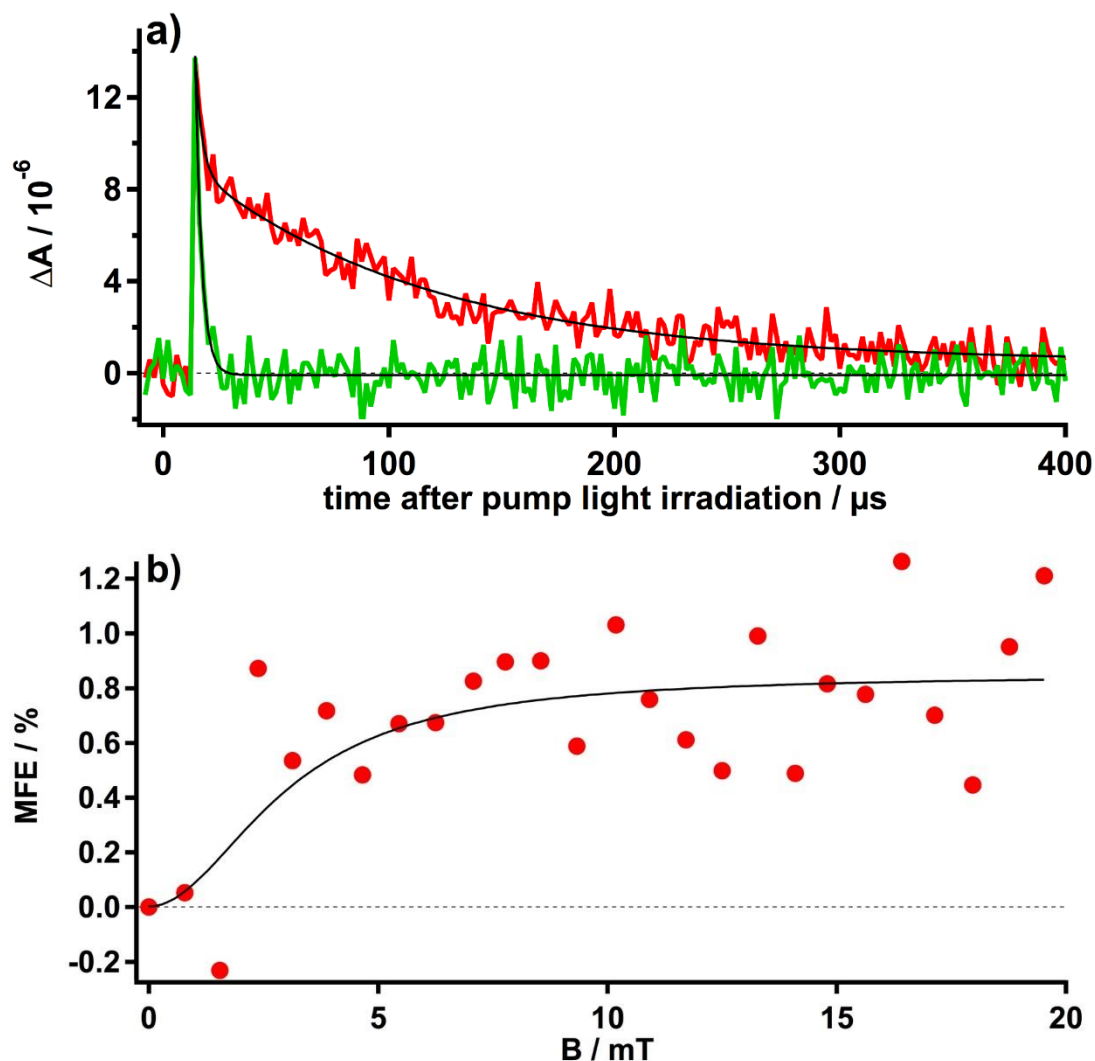


Figure 4.7. FMN encapsulated in the inner water pool of DPPC vesicles with / without Trp in the outer aqueous solution. a) Decay curves for FMN:DPPC vesicles without Trp (green curve) and with Trp (red curve) in the outer aqueous solution. The black line overlaying the kinetic trace for the FMN and Trp system was calculated using a biexponential decay using the fast decay component of $k = 3.7 \pm 0.4 \times 10^5 \text{ s}^{-1}$ obtained from the FMN only system, giving a decay rate of $k = 9.5 \pm 0.6 \times 10^3 \text{ s}^{-1}$ for the slow component. b) MARY curve for FMN:DPPC vesicles with Trp in the outer aqueous solution, A MARY curve with a $B_{1/2}$ of 3.0 mT (based on ref. 20) is represented by the black line. No MARY spectrum was observed for FMN:DPPC vesicles.

Figure 4.8 summarises our proposed model for the electron transfer reactions taking place in these experiments.

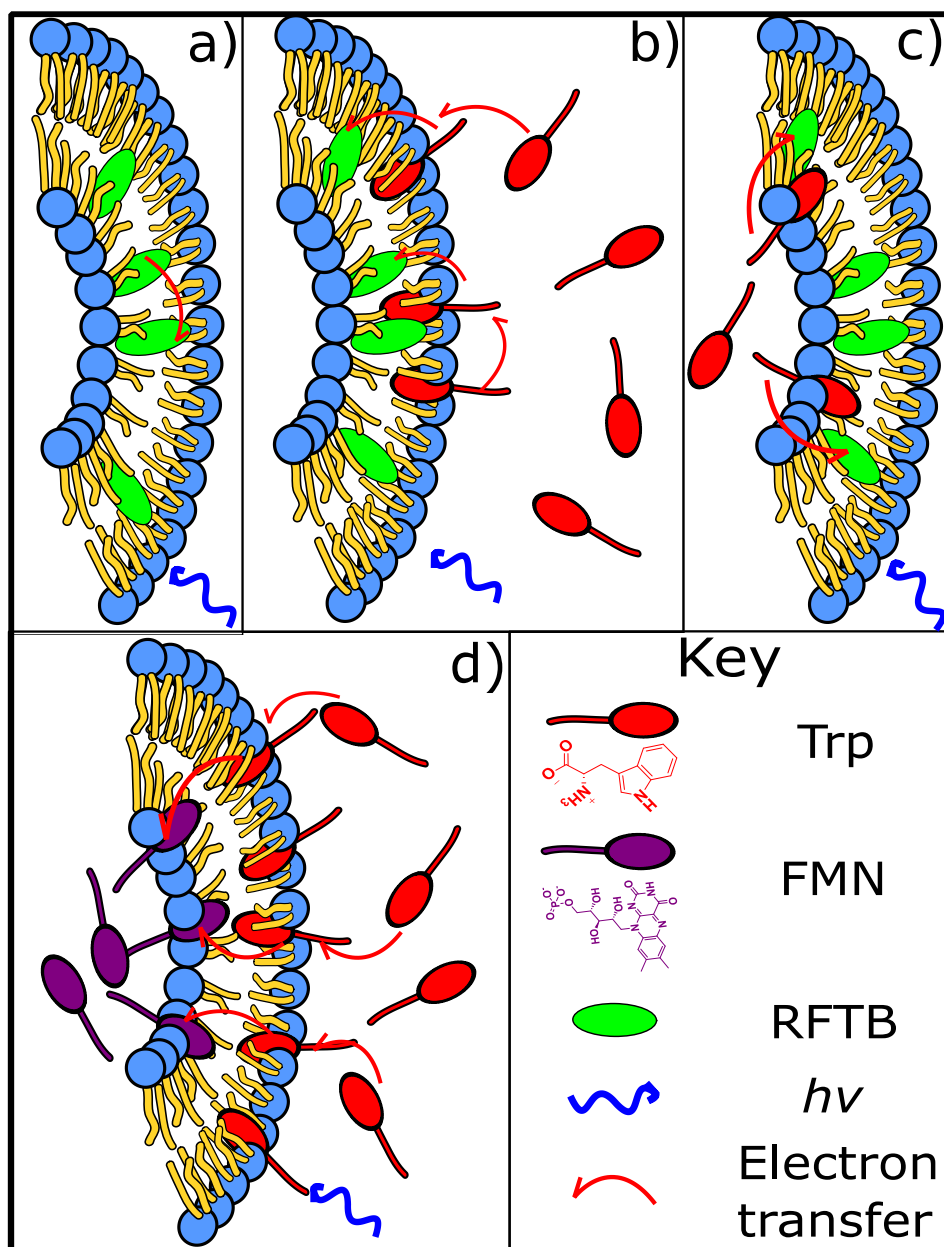


Figure 4.8. A cartoon of the proposed model for the electron transfer reactions (after 449 nm irradiation, not to scale) taking place in each vesicle experiment. a) RFTB only, b) RFTB with Trp in the outer aqueous solution, c) RFTB with Trp inside the inner water pool, and d) FMN inside the inner water pool with Trp in the outer aqueous solution.

Summary and conclusions

In this work, we studied the electron transfer reactions from Trp to flavins in DPPC vesicles using TROA spectroscopy and MFES. By tuning the hydrophilicity of the flavin we were able to selectively locate it within the vesicle bilayer (RFTB) or in the inner water pool (FMN). Similarly, the Trp could be located in either the bulk

aqueous solution or the inner water pool based on the vesicle preparation methodology. For RFTB located in the vesicle bilayer, the TROA and MARY data are consistent with a model in which tryptophan added to either the inner water pool or outer bulk solution can become substantially embedded in the lipid bilayer and undergo photoinduced electron transfer to the flavin, generating a magnetically sensitive RP. RP formation appears to be more effective from the inner surface than the outer surface and the MARY data suggests that degenerate electron exchange between the flavin and Trp radicals and their parent molecules contributes to the spin dynamics of the RP. For Trp located in the inner water pool the magnetic field response is a factor of 3 greater than observed for electron transfer in aqueous solution, suggesting that careful tuning of the concentrations and optimisation of the vesicle environment might allow tuned RP dynamics with increased magnetic field responses. Remarkably, for FMN located in the inner water pool, the kinetics and magnetic field dependence provide evidence for electron transfer across the vesicle bilayer from Trp molecules added to the bulk aqueous solution. In this case, the RP appears to be much shorter lived, which stops the effects of DEE appearing in the magnetic field dependence. This work is a first step in the study of flavin - Trp electron transfer in biomimetic systems and it is anticipated that further experiments can provide more detailed information on the complex molecular and spin dynamics taking place.

4.2 GIANT UNILAMELLAR VESICLES

Introduction

In Chapter 4.1, we studied the photochemistry and magnetosensitivity of flavins (electron acceptors) and tryptophan (electron donor) in DPPC small unilamellar vesicles (SUVs), reporting transmembrane electron transfer (ET) reactions across both single and double membrane layers and MFEs thereon. SUVs have a diameter of ~60 nm, and are thus not resolvable with our microspectroscope. Therefore, one would like to visualise the reactions inside the vesicle systems on the micron scale. DOPC (1,2-Dioleoyl-*sn*-glycero-3-phosphocholine) giant unilamellar vesicles (GUVs) possess diameters typically ranging between 10-30 μm , which is ideal for our microspectroscope. DOPC GUVs were synthesised, using the water-in-oil (W/O) emulsion centrifugation method,²⁶ with various flavin-based systems. Here we present images of flavin transient radical species encapsulated within liposomes, which were resolved with our TOAD (transient optical absorption detection) microspectroscope. These initial results display that TOAD imaging has the potential to observe flavin radicals inside living cells.

Experimental

GUV Preparation

Vesicle preparation was based on an existing methodology.²⁶ A stock solution of DOPC (50mM, Wako) and cholesterol (5 mM, Wako) in chloroform was prepared and stored at -20 °C. The stock solution was evaporated under flowing nitrogen gas and liquid paraffin (0.86-0.89 g cm⁻³ at 20 °C) was added. The mixture was incubated overnight at 65 °C (final DOPC concentration of 1.25 mM). The desired flavin (2 mM, see main text for details, Wako) or hen egg-white lysozyme (HEWL) (1 mM, see main text, Sigma-Aldrich) were added to a Tris-buffered solution (100 mM, Tris-HCl (pH 7.5), 0.5 M *D*-glucose, 0.5 M sucrose, total density: 1.27 g cm⁻³, Wako). 0.3 mL of the Tris-buffered solution was added to 1 mL of the liquid paraffin solution and emulsified mechanically. 1 mL of another Tris-buffered solution (100 mM, Tris-HCl (pH 7.5), 1 M *D*-glucose, total density: 1.19 g cm⁻³) was poured into an Eppendorf centrifuge tube (1.5 mL, Sigma-Aldrich) and layered with 0.3 mL of the W/O emulsion containing the flavin-based system. The biphasic system was incubated for 10 min at 4 °C, and centrifuged at 18,800×*g* for 30 min at 20 °C. The GUV dispersion was separated from the biphasic system by inserting a hole in the bottom of the centrifuge tube, then centrifuged again at 18,800×*g* for 5 min at 20 °C and removal of

supernatant. Subsequent washes were performed as needed. Finally, a Tris-buffer solution (100 mM, Tris-HCl (pH 7.5), 0.5 M *D*-glucose, 0.5 M sucrose) was added to the GUV dispersion (see Fig. 4.9).

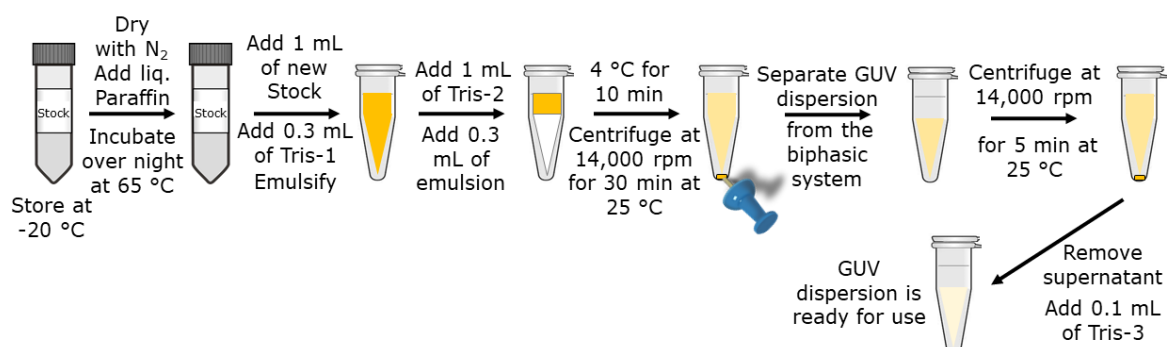


Figure 4.9. Procedure for giant unilamellar vesicle preparation. Stock = DOPC (1,2-Dioleoyl-*sn*-glycero-3-phosphocholine, 50 mM) and cholesterol (5 mM) in chloroform. Tris-1 = Tris-buffered solution (100 mM Tris-HCl (pH 7.5), 0.5 M *D*-glucose, 0.5 M sucrose, 2 mM flavin (or 1 mM HEWL)). Tris-2 = Tris-buffered solution (100 mM Tris-HCl (pH 7.5), 1 M *D*-glucose). Tris-3 = Tris-buffered solution (100 mM Tris-HCl (pH 7.5), 0.5 M *D*-glucose, 0.5 M sucrose).

Optical Microscopy

The W/O emulsion and GUV dispersion were observed with coverslips (0.12-0.17 mm) and spacer (36 μ L frame-seal-chamber, 280 μ m thickness, Bio-Rad) with a phase contrast/fluorescence microscope (IX-71 Inverted Microscope, Olympus), equipped with a mercury-vapour lamp light source and objective lens (SLCPlanFL 40 \times / NA 0.55, LUCPlanFLN 20 \times / NA 0.45, Olympus). For fluorescence microscopy measurements, the filter unit NIBA (λ_{ex} : 470-495 nm, λ_{em} 515-550 nm, Olympus) was used.

TOAD Microspectroscopy

The GUVs were housed between coverslips (0.13-0.16 mm, Marienfeld) and spacer (36 μ L frame-seal-chamber, 280 μ m thickness, Bio-Rad). Samples were photoexcited at 449 nm (Coherent CUBE laser) and monitored at 532 nm (Coherent Sapphire laser). The confocal arrangement consists of two super apochromatic objective lenses (UPlanSApo 20 \times / NA 0.75, Olympus). Full technical details are explained in Chapter 2.

Results and Discussion

Flavin-Based Systems

Flavins were chosen based on their hydrophilicity, which increases from RFTB to FMN to FAD. RFTB and FMN cannot undergo intramolecular RP formation, making them ideal for studying intermolecular ET reactions. Conversely, FAD can undergo intramolecular RP formation, with ET from the adenine to flavin moiety. These characteristics were key in designing the biomimetic vesicle systems. Experiments were conducted using 1) hydrophobic RFTB which we anticipate to be encapsulated in the hydrophobic bilayer (~10 nm diameter) of the DOPC vesicles, and 2) hydrophilic FMN or FAD which were prepared inside the inner water pool of the vesicles and where we anticipate it should remain encapsulated. Three systems were developed for investigation, 1) FAD encapsulated in the inner water pool of the GUV, 2) flavin mononucleotide (FMN) and HEWL (hen egg-white lysozyme) encapsulated in the inner water pool of the GUV, and 3) riboflavin tetrabutryate (RFTB) encapsulated inside the hydrophobic lipid bilayer of the liposome. System 1 was developed with the aim of studying FAD photo-generated radical pairs in a spatially localised environment. The motivation behind system 2 was to mimic the flavin-tryptophan RP found in cryptochrome, by using the protein surface of HEWL as an electron donor. According to photo-CIDNP studies (as discussed in Chapter 1.4) flavin excited triplet and semiquinone radicals are generated by electron-transfer reaction from the exposed aromatic tryptophan residues (Trp-62 and Trp-123) in the native state of HEWL. Finally, system 3, by encapsulating the hydrophobic RFTB in the bilayer (diameter ~10 nm, Figure 4.10), by adding an electron donor inside the GUV water pool or in the surrounding buffer solution to initiate an electron transfer reaction across the lipid bilayer. Unlike the phase transition temperature (T_m) of DPPC vesicles (Chapter 4.1), where the bilayer is in a gel phase at room temperature ($T_m = 42\text{ }^{\circ}\text{C}$), DOPC vesicles are in a liquid-crystalline phase (where lipid molecules can diffuse laterally). A T_m of $-16.5\text{ }^{\circ}\text{C}^{27}$ means that the RFTB molecules can move laterally in the bilayer and possess some mobility at room temperature. The initial results for these three reaction systems are shown in turn.

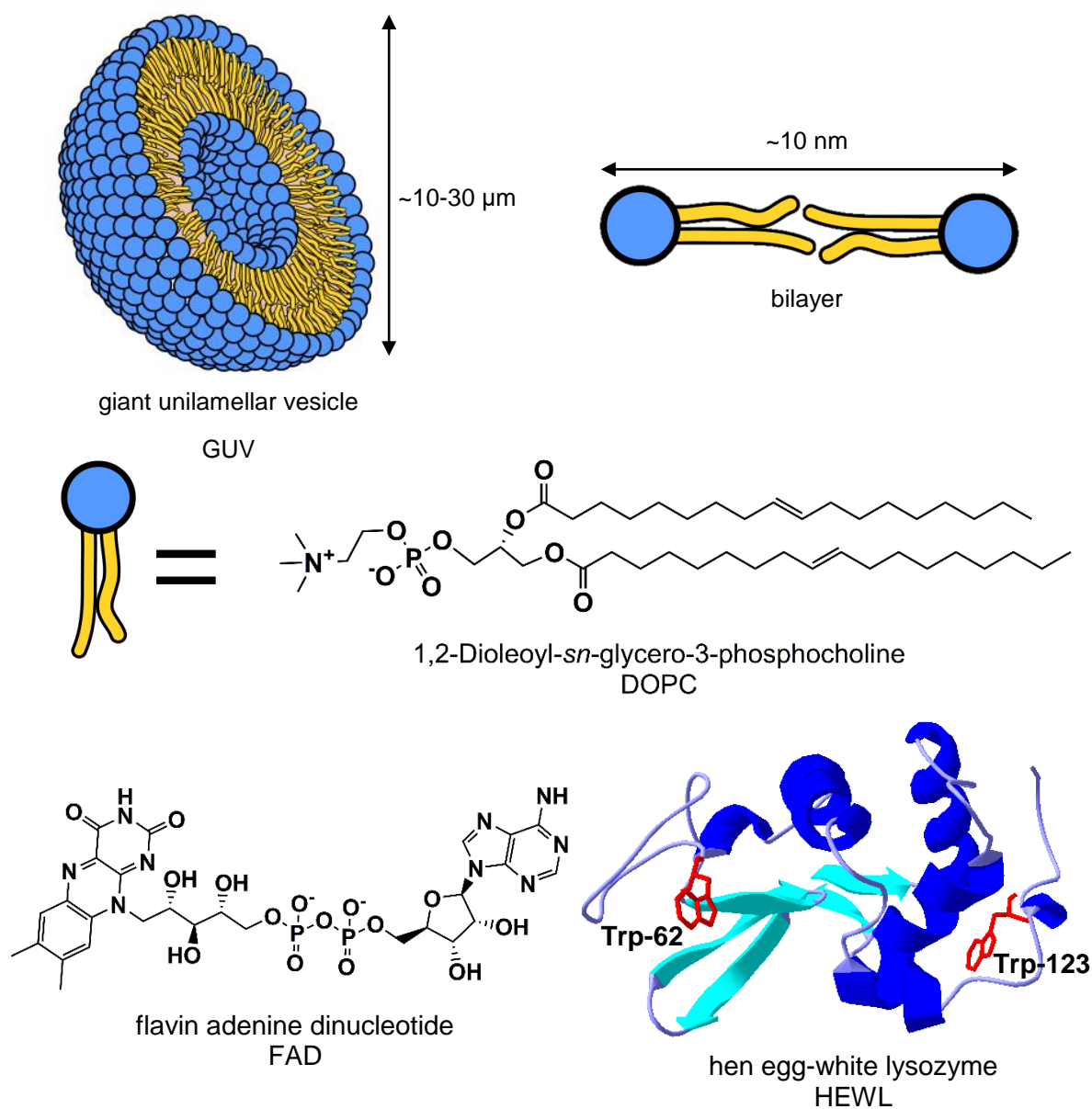


Figure 4.10. Schematic representation of giant unilamellar vesicles (GUVs), providing dimensions for key features of DOPC GUVs, with chemical structures of DOPC, flavin adenine dinucleotide (FAD) and hen egg-white lysozyme (HEWL) (PDB no. 3ZEK, tryptophan residues involved in electron transfer reactions with free flavins are marked).

FAD encapsulated in the inner water pool of DOPC vesicles

The photochemistry of FAD has been discussed extensively in previous chapters. A phase contrast microscopy image of a typical GUV can be seen in Figure 4.11a, this image displays the difference in sugar densities between the solution and inner water pool of the liposome. The fluorescence microscopy image and intensity profiles (processed with ImageJ) (Fig. 4.11b) confirms successful encapsulation of FAD. Finally, to observe the flavin

radicals created by the intramolecular electron transfer reaction from the adenine moiety to the flavin, we utilised TOAD microscopy (Fig. 4.11c).

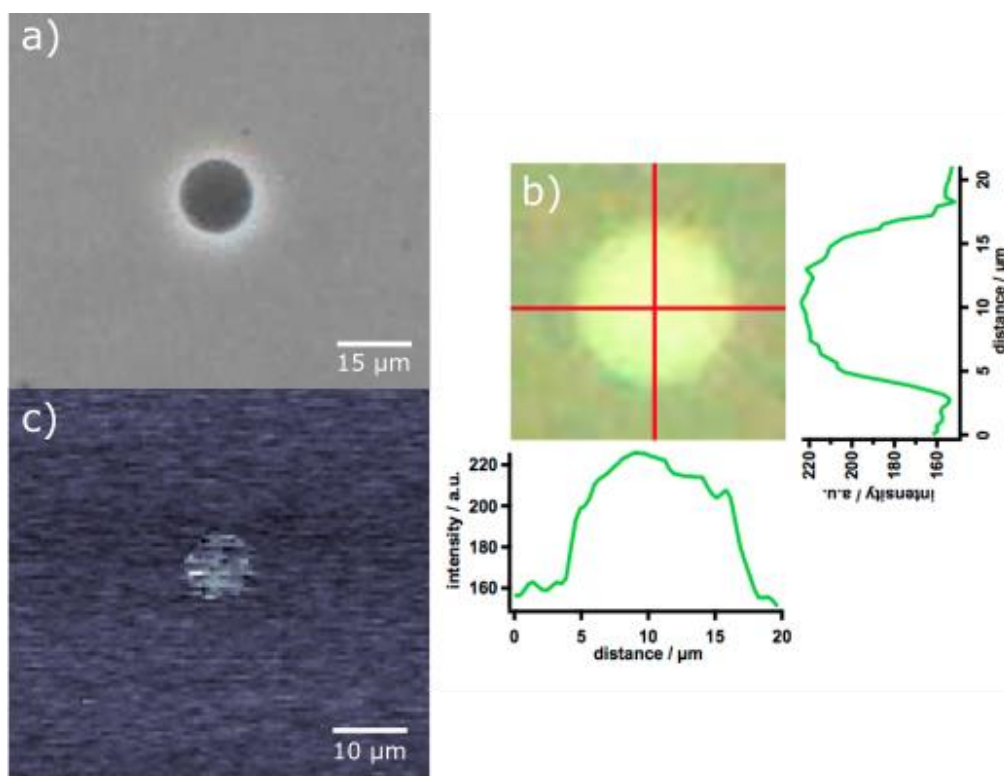


Figure 4.11. a) Phase contrast microscopy image of a typical GUV. b) Fluorescence microscopy image displaying the presence of FAD, with cross-sectional intensity plots. c) TOAD image revealing the flavin excited triplet state and semiquinone radicals encapsulated in the water pool of the GUV.

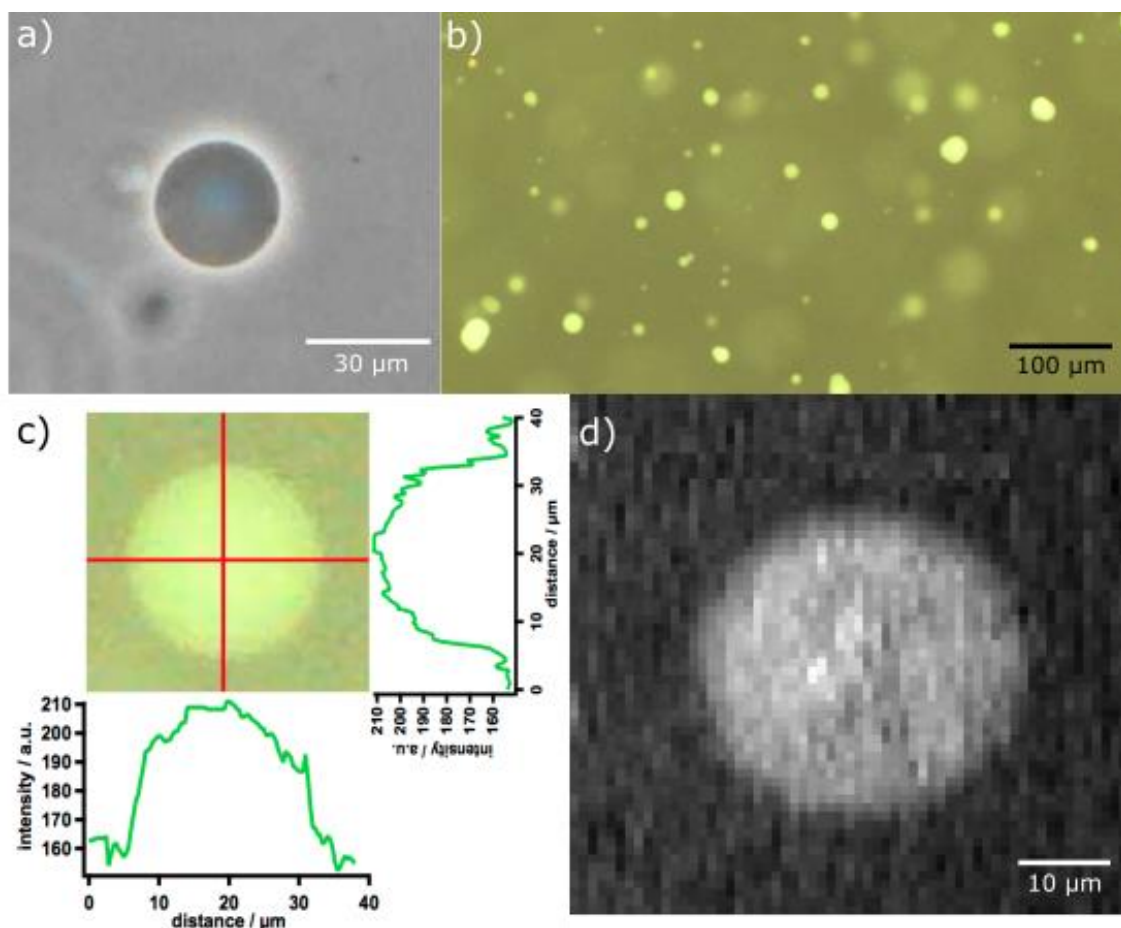


Figure 4.12. a) A typical phase contrast microscopy image of a GUV. b) Fluorescence microscopy image displaying the presence of numerous encapsulated FMN and HEWL GUVs. c) Fluorescence microscopy image of an individual FMN and HEWL liposome, with cross-sectional intensity plots. d) TOAD image revealing the flavin semiquinone radicals created by the intermolecular electron transfer reactions between FMN and the HEWL protein, whilst encapsulated in the water pool of the GUV.

RFTB encapsulated in the bilayer of DOPC vesicles

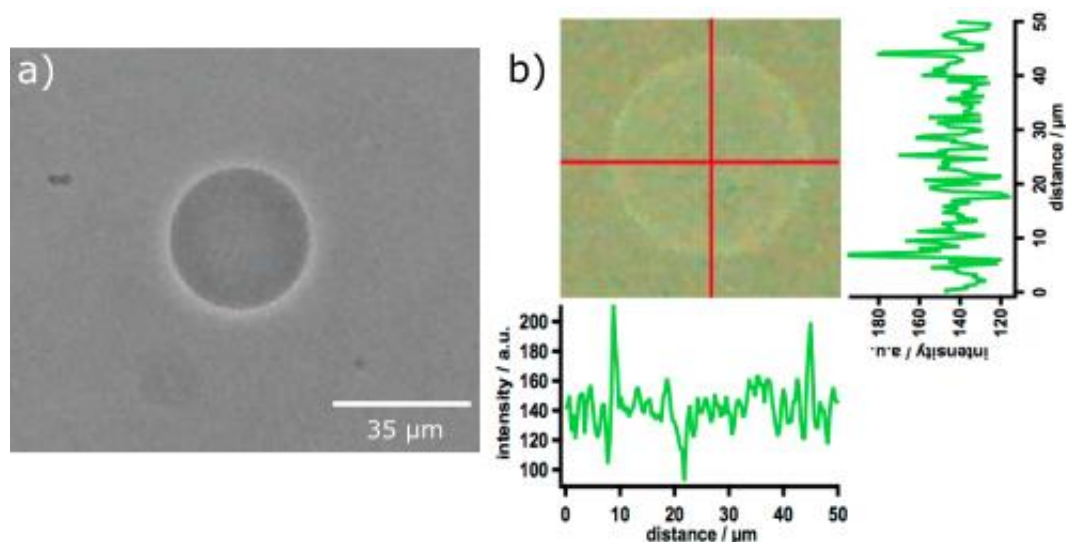


Figure 4.13. a) Phase contrast microscopy image of a typical GUV. b) Fluorescence microscopy image displaying RFTB in the GUV bilayer, with cross-sectional intensity plots confirming its presence.

Conclusion

Preliminary work on GUVs studied electron transfer reactions between FAD and FMN + HEWL in DOPC vesicles using TOAD and fluorescence imaging. TOAD images both FAD and FMN + HEWL encapsulated in GUVs display the potential to observe flavins radicals inside living cells. Furthermore, fluorescence imaging of RFTB confirmed successful encapsulation in the hydrophobic GUV bilayer. The results provide a basis for studying transmembrane electron transfer reactions with hydrophilic electron donors. Due to rapid photobleaching in all GUV systems, no kinetics or MFEs were resolved. Future work will focus on resolving this issue, with the aim of measuring MFEs in the biomimetic systems.

The preliminary results of the work presented in this chapter provide a new method for encapsulating flavin-based systems in a micron-scale biomimetic environment. Being able to spatially resolve the transient radical species inside environments similar to that of a cell, shows great promise for the TOAD microspectroscopy. In all three systems photobleaching was observed, meaning upon irradiation of the pump and probe beams the transient signal

faded over time. This result was surprising as flavin photochemistry is cyclic in solution and no photobleaching was observed for the SUV experiments. Reasons for photobleaching could be due to the laser intensity and repetition rate being too high, or upon photoexcitation the transition to the excited triplet state, the flavin molecules may be interacting with other molecules in the GUV water pool, for example, sucrose or glucose, leading to unwanted chemical reactions and irreversible covalent modifications. Methods of overcoming this photobleaching could be to increase the flavin concentration, reduce laser intensity and repetition rates, or to change the other molecules involved in the GUV preparation or reduce their respective concentrations. Another possibility is that the flavin molecules are degrading over time, which is observed in numerous studies, as it is trapped inside the vesicle. This is not observed when we observe flavins in solution as the sample is constantly being refreshed.

To conclude, preliminary work on GUVs studied electron transfer reactions between FAD and FMN + HEWL in DOPC vesicles using TOAD and fluorescence imaging. TOAD images both FAD and FMN + HEWL encapsulated in GUVs display the potential to observe flavins radicals inside living cells. Furthermore, fluorescence imaging of RFTB confirmed successful encapsulation in the hydrophobic GUV bilayer. The results provide a basis for studying transmembrane electron transfer reactions with hydrophilic electron donors. Due to rapid photobleaching in all GUV systems, no kinetics or MFEs were resolved. Future work will focus on resolving this issue, with the aim of measuring MFEs in the biomimetic systems.

References

- [1] U. E. Steiner and T. Ulrich, *Chem.Rev.* **1989**, 89, 1, 51-147.
- [2] T. Ritz, S. Adem, and K. Schulten, *Biophys. J.* **2000**, 78(2), 707-718.
- [3] H. Mouritsen, and P. J. Hore, *Annu. Rev. Biophys.* **2016**, 45, 299.
- [4] M. H. Kleinman, T. Shevchenko and C. Bohné, *Photochem. Photobiol.* **1998**, 68(5), 710-718.
- [5] J.H. Fendler, *Acc. Chem. Res.* **1980**, 13, 7-13.
- [6] J. Koziol, *Methods in Enzymology*, **1971**, 18, part B, 253-285.
- [7] K. Watanabe, K. Moriya, T. Kouyama, A. Onoda, T. Minatani, S. Takizawa and S. Murata, J. *Photochem. Photobiol. A: Chemistry*, **2011**, 221, 113-122.
- [8] J. P. Beardmore, L. M. Antill and J. R. Woodward, *Angew. Chem. Int. Ed.* **2015**, 54, 8494–8497.
- [9] L. M. Antill, J. P. Beardmore and J. R. Woodward, *Rev. Sci. Instrum.* **2018**, 89, 023707.
- [10] Y.-C. Tseng and S.-W. Chu, *Plant Methods*, **2017**, 13, 43.
- [11] M. Horiuchi, K. Maeda, and T. Arai, *Appl. Magn. Reson.* **2003**, 23, 309.
- [12] E. W. Evans, C. A. Dodson, K. Maeda, T. Biskup, C. J. Wedge, and C. R. Timmel, *Interface Focus* **2013**, 3: 20130037.
- [13] K. Yagi, N. Ohishi, M. Naoi, and A. Kotaki, *Archives of biochemistry and Biophysics*, **1969**, 134, 500.
- [14] S. Weber and E. Schleicher, editors, *Flavins and Flavoproteins: Methods and Protocols, Methods in Molecular Biology*, Springer, New York, **2014**.
- [15] P.F. Devaux and H.M. McConnell, *J. Am. Chem. Soc.* **1972**, 94, 4475.
- [16] E.-S. Wu, K. Jacobson and D. Papahadjopoulos, *Biochemistry* **1977**, 16, 3936.
- [17] M. Murakami, K. Maeda, and T. Arai, *Chem. Phys. Lett.* **2002**, 362, 123.
- [18] T. B. Melø, M. A. Ionescu, G. W. Haggquist, and K. Razi Naqvi, *Spectrochim. Acta, Part A* **1999**, 55, 2299.
- [19] V. Massey and G. Palmer, *Biochemistry* **1966**, 5, 3181.
- [20] K. Maeda, A. J. Robinson, K. B. Henbest, H. J. Hogben, T. Biskup, M. Ahmad, E. Schleicher, S. Weber, C. R. Timmel, and P. J. Hore, *Proc. Natl. Acad. Sci. U. S. A.* **2012**, 109, 4774.
- [21] B. Giovani, M. Byrdin, M. Ahmad, and K. Brettel, *Nat. Struct. Biol.* **2003**, 10, 489.

- [22] M. Byrdin, V. Sartor, A. P. M. Eker, M. H. Vos, C. Aubert, K. Brettel, and P. Mathis, *Biochim. Biophys. Acta*, **2004**, 1655, 64.
- [23] J. Marti and H. Lu, *Procedia Computer Science*, **2017**, 108C, 1242.
- [24] S. N. Batchelor, C. W. M. Kay, K. A. McLauchlan, and I. A. Shkrob, *J. Phys. Chem.* **1993**, 97, 13250.
- [25] S. Richert, A. Rosspeintner, S. Landgraf, G. Grampp, E. Vauthey, and D. R. Kattnig, *J. Am. Chem. Soc.* **2013**, 135, 15144.
- [26] Y. Natsume and T. Toyota, *Chemistry Letters*, **2013**, 42 (3), 295.
- [27] A. Ulrich, M. Sami, A. Watts, *Biochim. Biophys. Acta-Biomembr.*, **1994**, 1191, 225.

Flavins in Biological Environments

This chapter discusses the current progress on our long-term goal of studying spectroscopic measurements of radical pairs in biological systems both ‘*in vitro*’ purified cryptochrome proteins, and ‘*in vivo*’ by imaging photoinduced RP reactions localised in living cells. Chapter 5.1 discusses the work conducted on purified *D. melanogaster* cryptochrome (*DmCry*). All studies on Crys are typically studied under short nanosecond pulsed flash photolysis measurements. Our experiments were performed under pseudo-continuous irradiation, much like the continuous exposure to light that animals navigating experience. Chapter 5.2 discusses the initial cellular experiments on cheek cells, which showed promising results. This led to establishing cell culturing facilities and developing a model system (HeLa cells) for investigating the magnetosensitive photochemistry of FAD at the cellular level.

5.1 D. MELANOGASTER CRYPTOCHROME

The current understanding of *DmCry* photochemistry and MFEs thereon are described in Chapter 1.3. To summarise, blue light irradiation and subsequent electron transfer produces a singlet born ($[FAD\cdot^- + Trp_cH\cdot^+]$) radical pair, which is magnetic field sensitive. Back electron transfer from the fourth Trp residue, of the Trp tetrad, is relatively slow and accounts for the small MFE ($\sim 2\%$). These experiments were conducted with a purified *DmCry* protein concentration of $\sim 50\ \mu\text{M}$, at temperatures between 267-278 K, and with the addition of glycerol (50% and 20% for transient absorption (TA) spectroscopy and cavity-enhanced absorption spectroscopy (CEAS) experiments, respectively). These parameters were chosen to optimise the magnetic field responses, where lowering the temperature and high viscosity of glycerol slow diffusion processes. No MFE was observed at 282 K. For TA experiments the sample was photoexcited at 450 nm with a 10 ns pulse width at a 1/120 Hz repetition rate. CEAS experiments were conducted under pulsed (10 Hz) or continuous-wave (CW) 450 nm (50 ms intergration) irradiation.¹ Low repetition rates were chosen to minimise sample degradation and, for TA experiments, to allow the protein to completely return to the ground state ($\sim 2\ \text{min}$) between laser flashes.

The TOAD microscope can operate in a pulsed mode ($\sim 300\ \text{ns}$ pulse width, up to 100 kHz) and a square wave mode (50% duty cycle, variable oscillation frequencies $< 1\ \text{kHz}$). It was expected that after applying either of these microscope modes to a static sample, the FAD ground state should be rapidly removed, and the transient absorption signal should disappear shortly after turning on the lasers. The strategy to counter this issue was to use the spiral stage scanning algorithm (Chapter 2) to scan the protein in the xy plane, meaning that fresh sample will be constantly introduced (like a flow cell). To our surprise, we were able to measure a stable transient absorption signal without scanning the sample, which seems to suggest that the sample returns to the FAD ground state rapidly. One possible explanation might involve the 532 nm probe beam returning the anionic semiquinone radical to the ground state. The experiments were conducted at room temperature (298 K), without glycerol, sealed, and with a *DmCry* concentration of $\sim 40\ \mu\text{M}$.

Figure 5.1 shows a reproducible kinetic decay on the timescale of hundreds of microseconds initiated with pulsed mode (300 ns pulse width) irradiation. The signal intensity changes slightly with repetition rate until the rate is sufficiently high that the next pulse arrives before the absorption signal has decayed (typically at frequencies greater than 5 kHz).

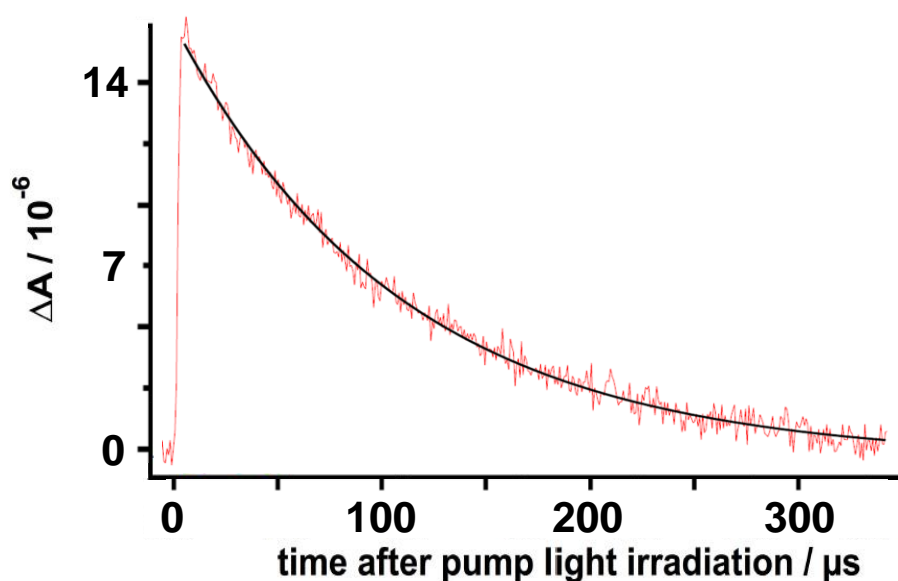


Figure 5.1. Short pulse irradiation of *DmCry* at 449 nm. Change in absorption at 532 nm. Single exponential fit, $k = 8.8 \times 10^{-3} \text{ s}^{-1}$.

For square wave mode experiments (368.9 Hz repetition rate) the effect of varying 449 nm laser power at fixed 532 nm laser power (Fig. 5.2) and the 532 nm laser power at fixed 449 nm (Fig. 5.3) on the dependence of the absorption at 532 nm was observed. For most laser powers there is little or no laser power dependence on the shape of the kinetic traces, indicating that the rate determining step of the reaction cycle is not (strongly) light dependent. At high powers, small effects on the kinetics are observed. Under pseudo-continuous irradiation an equilibrium is established between the ground state and radical pair, the observed kinetics display a rise to the RP and a decay to the ground state under steady state conditions.

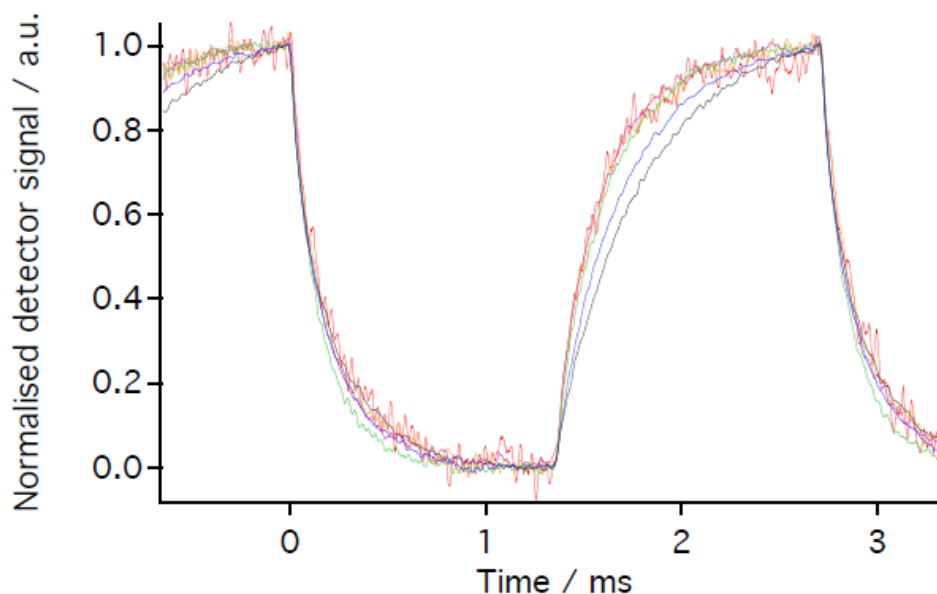


Figure 5.2. Effect of 449 nm laser power (32 μW to 1 mW) on *DmCry* kinetics (532 nm laser power at 2 mW).

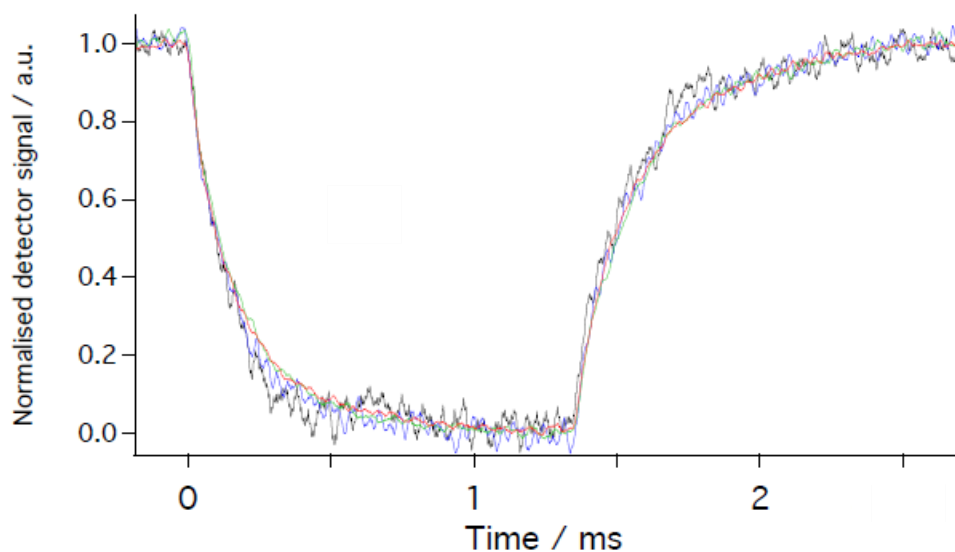


Figure 5.3. Effect on 532 nm laser power (0.25 to 2 mW) on *DmCry* kinetics (449 nm laser power at 0.13 mW).

These observations agree with some of the literature. Even though *DmCry* is a Type I Cry, its signaling state is still unclear.² The current understanding is that the anionic semiquinone radical is the intermediate in the photoreduction process. Nonetheless, a green light inhibition effect was found on biological activity, displaying a considerably slower degradation of *DmCry* in blue + green light than observed in blue light alone. *DmCry* photoreduction is faster by blue + green light irradiation than by blue light irradiation alone *in vivo*.³ These observations are consistent with the effects of green light on the biological activity of living fruit flies.³ This can be explained by green light-induced radical interconversion, but contradicts the current understanding that the photoreaction intermediate is $\text{FAD}^{\bullet-}$, which has little or no absorption of green light (however in Fig. 1.14, a small amount of absorption at our probe wavelength of 532 nm is observed).⁴

For all square wave experiments run at 368.9 Hz, a triplet born MFE on the photochemistry of *DmCry* was observed. The effect of changing both blue and green laser power on the field effect was investigated. For fixed blue power, the field effect was reduced at high green powers (Fig. 5.4) and at fixed green power, the field effect was reduced at high blue powers (Fig. 5.5). These results suggest that green light might be responsible for maintaining reaction cycling by reduction of the anionic semiquinone (either directly or possibly via the hydroquinone form). This result contradicts the results observed in previous work on *in vitro* Crys, which observe singlet born MFEs in all cases.^{1,5} However, in neuronal firing and behavioural experiments in fruit flies, triplet born MFEs were observed (using the RPM), if the assumption is made that the effects reflect the concentration of the flavin radicals.⁶⁻⁹

A recently proposed radical scavenging model¹⁰ amplifies the performance of the quantum magnetic compass. This model is resilient to decoherence and spin relaxation (found in the current chemical magnetoreception model) caused by noisy biological environments. The presence of radical scavenging increases the rate of spin relaxation to achieve the necessary anisotropy required for the compass to operate compared to that in the current RP model for magnetoreception. We consider a possible reaction scheme invoking such a radical scavenging, generated by photoexcitation of the anionic semiquinone form of the flavin radical.

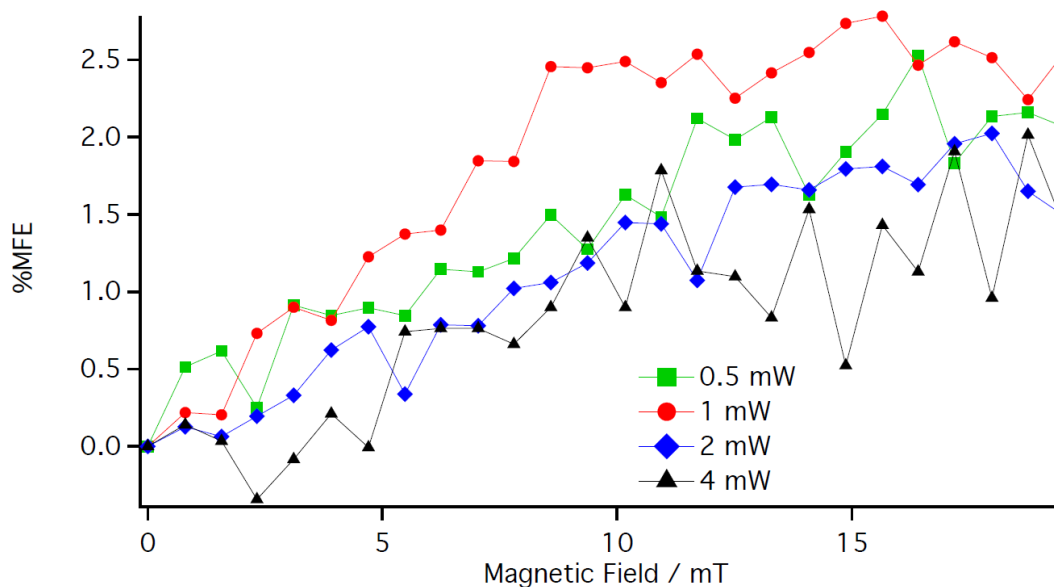


Figure 5.4. Effect on 532 nm laser power on *DmCry* MARY curve (449 nm laser power at 0.13 mW).

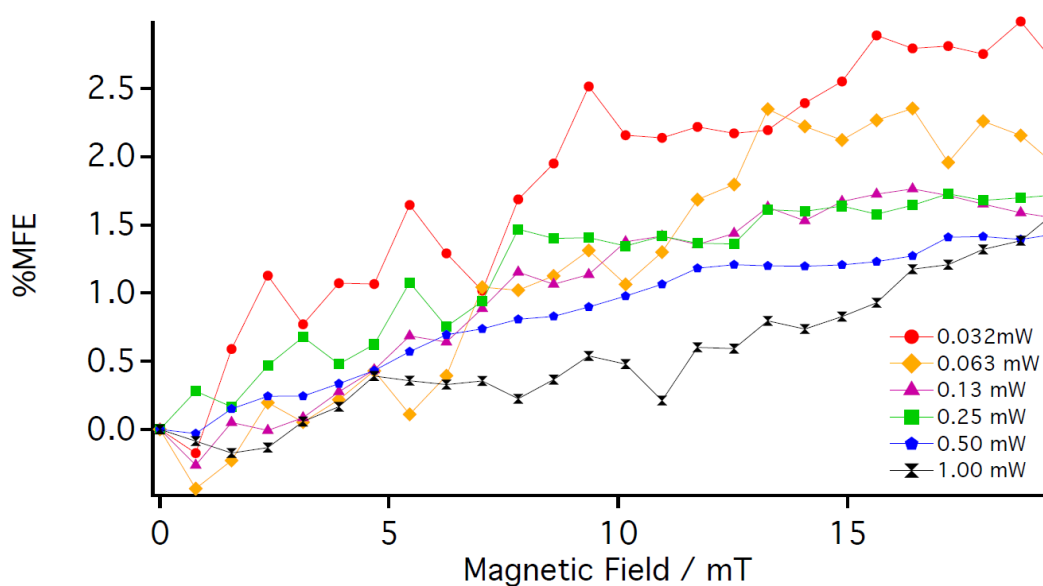


Figure 5.5. Effect on 449 nm laser power on *DmCry* MARY curve (532 nm laser power at 2 mW).

The reaction scheme is given in Fig. 5.6. The reaction scheme proceeds from the light exposed state of *DmCry* of $\text{FAD}^{\cdot-}$, as no pre-treatment with potassium ferricyanide to ensure the FAD cofactor was in the fully oxidised state, was undertaken.^{1,11} After blue light irradiation, the photoexcited flavin radical, $^2\text{FAD}^{\cdot-}$, undergoes electron transfer, again from the chain of tryptophan residues resulting in the fully reduced form of the flavin, and a protonated tryptophan radical, $^2\text{TrpH}^{\cdot+}$. Subsequent reaction of FADH^- with oxygen present in the binding pocket generates both doublet and quartet states of the $\text{FAD}^{\cdot-} + \text{TrpH}^{\cdot+} + \text{O}_2^{\cdot-}$ triad, which can undergo coherent hyperfine driven spin state interconversion (which is magnetic field dependent). Spin selective electron transfer between the superoxide ion and the tryptophan radical returns the initial species. $\text{FAD}^{\cdot-}$ does not absorb at our probe wavelength (532 nm), meaning that the blue laser is required to photoexcite the flavin and radical and also that the observed transient signal comes not from the flavin but from $\text{TrpH}^{\cdot+}$, which absorbs at 532 nm and leads to an increase in probe light absorption after photoexcitation. In other words, the observed kinetics and MFEs are for changes in the concentration of $\text{TrpH}^{\cdot+}$.

To further test the hypothesis that light and oxygen are involved in the observed reaction cycling an additional experimental strategy was undertaken. A test sample, stored in the dark was prepared by irradiating the *DmCry* protein for 10 min in the presence of oxygen (air), which was subsequently sealed. A control sample was prepared from the same stock of *DmCry* and sealed without prior exposure to light or oxygen. The MARY spectrum for *DmCry* that was pre-irradiated (532 nm) in oxygen displayed a MFE ~1% (Fig. 5.7), however, for the non-irradiated sample no MFE was observed (Fig. 5.8).

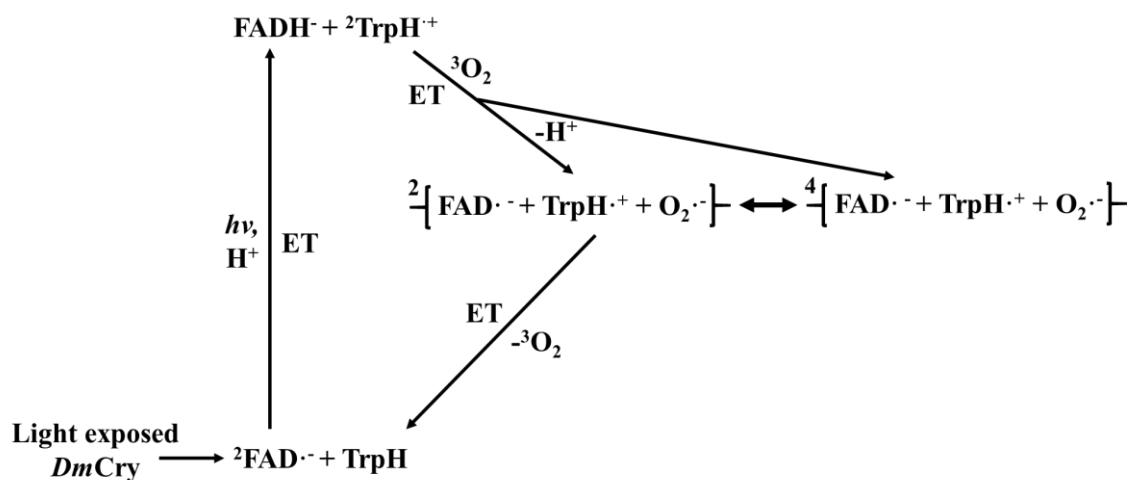


Figure 5.6. Proposed reaction scheme for *DmCry* using the radical scavenging model.

These observations further support our hypothesis. It is also noteworthy to mention the difference in LIA (lock-in amplifier) signal between samples. The LIA signal (as discussed in Chapter 2) represents the Trp radical concentration, which is higher for the pre-exposed sample, suggesting more $\text{TrpH}^{\cdot+}$ species are being made.

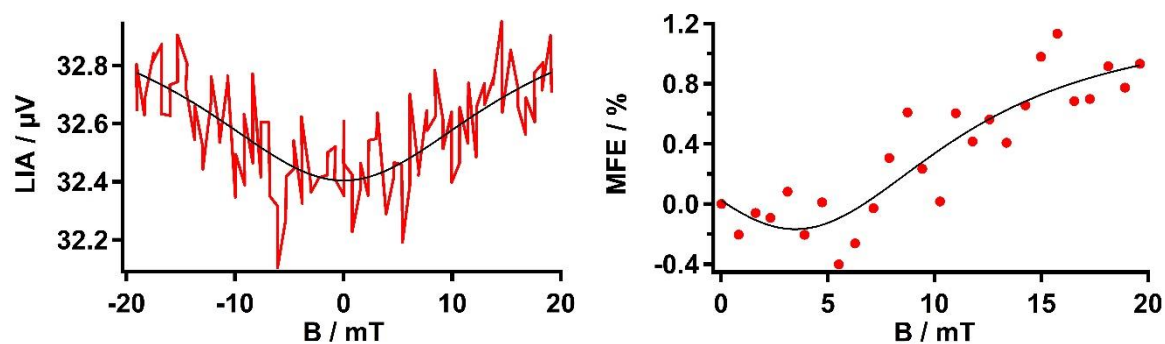


Figure 5.7. MARY spectra for *DmCry* which was pre-exposed to green light and oxygen.

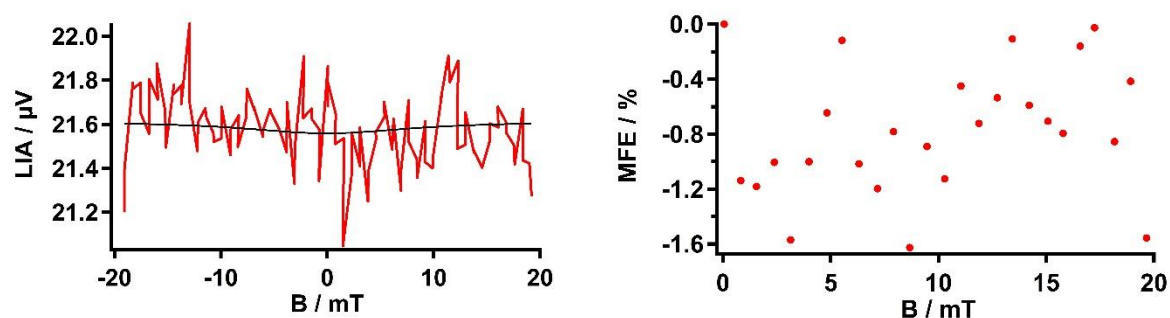


Figure 5.8. MARY spectra for *DmCry* without prior exposure to green light or oxygen.

Furthermore, comparable reaction cycling and MFEs were observed under 632 nm irradiation (0.46 mW, replacing the 532 nm probe, 449 nm at 0.13 mW, 368.9 Hz repetition rate) (Fig. 5.9), which further supports that the observed species is $\text{TrpH}^{\cdot+}$ as it also absorbs at this wavelength (Fig. 5.10).

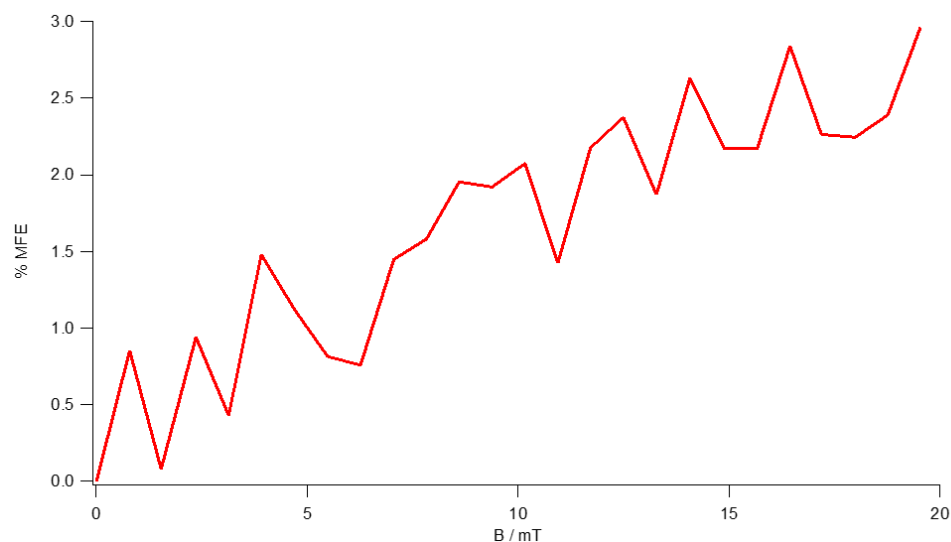


Figure 5.9. Effect of red laser (632 nm) power at 0.46 mW on MARY curve. Blue laser (450 nm) power was 0.13 mW, square wave mode irradiation at 368.9 Hz.

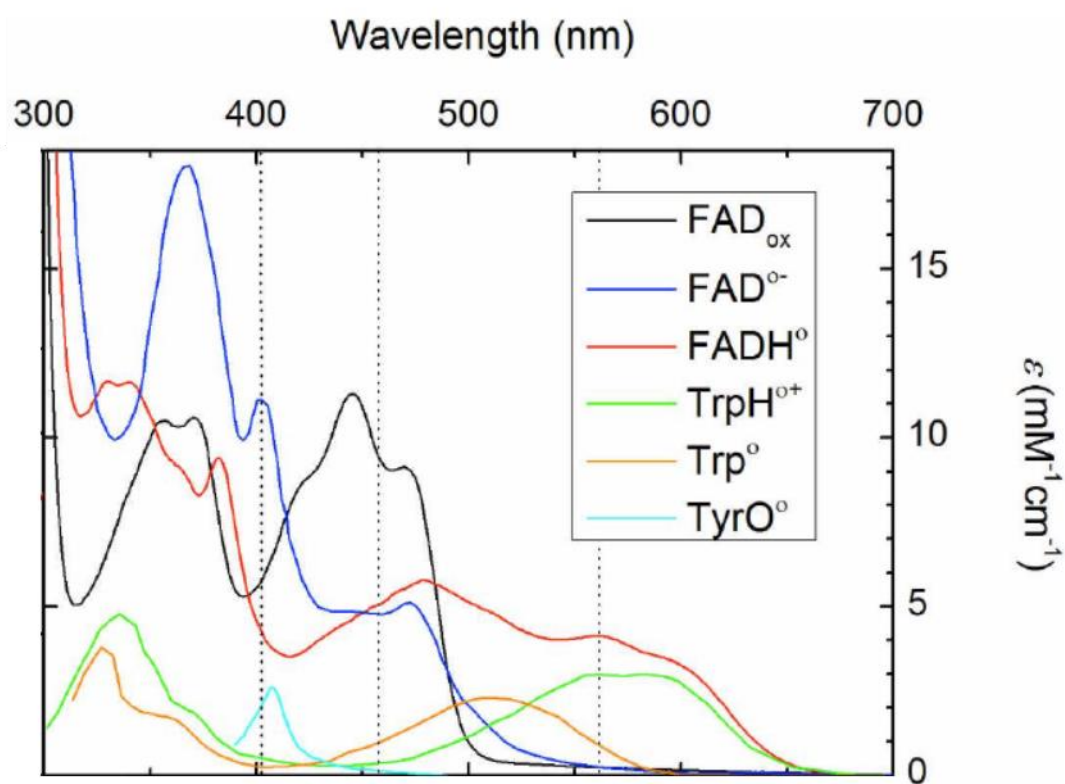


Figure 5.10. Absorption spectra of FAD in three of its redox forms (FAD_{ox} , $\text{FAD}^{\cdot-}$ and FADH^{\cdot}) and the two tryptophan radical species ($\text{TrpH}^{\cdot+}$ and Trp^{\cdot}). Adapted from ref. 12 and references therein.

Finally, MFE measurements on square wave modulation suggested the presence of a LFE and so experiments were performed over a shorter field range with additional signal averaging to confirm whether the LFE was genuine. The LFE was clearly resolved and is presented in Fig. 5.11.

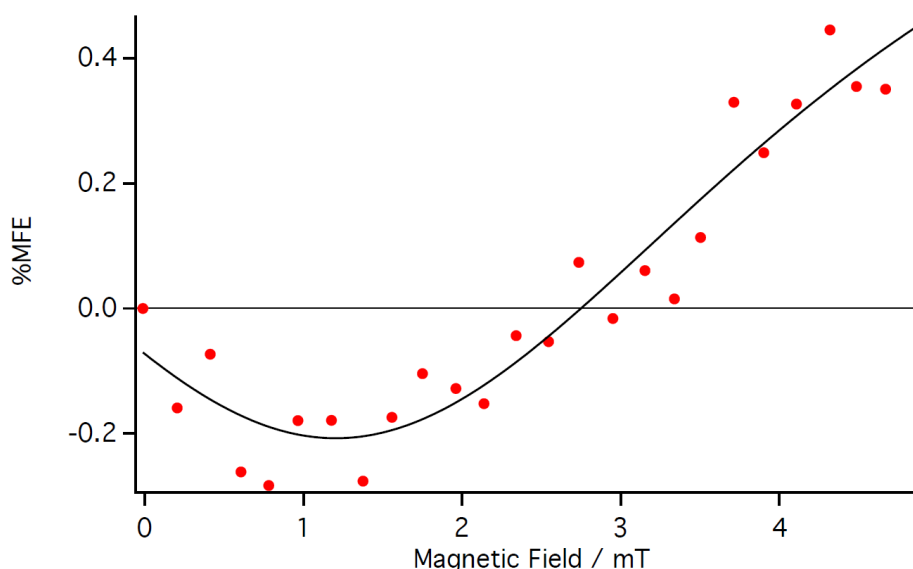


Figure 5.11. Low field effect on the 50% modulated 449 nm irradiation signal observed at 532 nm. 449 nm laser power was 0.13 mW, and 532 nm laser power was 2 mW.

Although the results are promising, we cannot rule out the possibility of sample degradation (protein denaturing), which might allow the FAD molecule to escape the binding pocket into solution. Photoexcitation might then generate RPs either by intramolecular electron transfer in DNA or directly to surface exposed tryptophan residues. Both of these processes would generate triplet born RPs, which would explain both the sense of the observed MFEs and the signal observed with a 632 nm probe light (the neutral form of the flavin semiquinone radical which absorbs at this wavelength). Possible denaturing routes could arise from high laser intensity (although our 532 nm laser intensity (at the sample) was typically $\sim 350 \mu\text{W}$), or from damage during sample unfreezing.

To gain further insight into the observed relatively short, reproducible photocycle and MFEs, the author has begun constructing a UV-Vis microspectrophotometer to enable the absorption spectrum of *DmCry* to be measured in the microscope sample, i.e. 5 μL of *DmCry* in a 100 μm thick sample. This is required due to the very small sample volume that is produced from the protein purification technique. Measurements should provide insight whether the FAD molecule is bound or not (see Chapter 4), although not the condition of the protein. Furthermore, it will be difficult to discern which species we are observing $\text{FADH}\cdot$ or $\text{Trp}\cdot^+$ and their absorption wavelengths (and other flavin and Trp species) overlap. We are unable to do this in the TOAD/MIM microspectroscope due to restricted access to the sample. The new setup has incorporated a similar confocal arrangement with two objective

lenses with longer working distances, which allows greater access to the sample (Fig. 5.12). This system does not have the spatial resolution of the original microscope, but is sufficient for measurements of photochemistry in isotropic solution.



Figure 5.12. A picture of the new microspectrophotometer confocal arrangement, exemplifying a more spacious sample environment.

5.2 FLAVINS IN CELLULAR ENVIRONMENTS

This chapter describes initial cellular experiments on buccal mucosa squamous epithelial ('cheek') cells, and a discussion of the preliminary work on human cervical carcinoma (HeLa) cells. HeLa cells were chosen as they are known to exhibit auto-fluorescence due to the presence of FAD, which was developed as model system to investigate magnetosensitive FAD photochemistry at the cellular level.

5.2.1 Buccal Mucosa Squamous Epithelial Cells

At the beginning of this thesis, the author did not have access to cellular samples or cell culturing facilities. Under the tutelage of Prof. Omi (The University of Tokyo) the author was able to conduct preliminary experiments on his own cheek cells. His cells were examined as both wild-type (WT) and modified (Mod, in the presence of externally added FAD).

The procedure for *WT cheek cell* preparation is as follows:

PBS (phosphate buffered saline, 1 mL) was added to an Eppendorf tube (1.5 mL) and kept on ice. Cheek cells were harvested by gently scraping the inside of the author's cheek with a cotton bud and dipped into the Eppendorf tube kept on ice. The tube was then centrifuged (5 min, 1500 rpm), supernatant removed and PBS (100 μ L) solution added. The viability of the cells was assessed with a dye exclusion method, with the vital stain Trypan Blue (TB) which selectively colours dead tissues and cells. Viable (live) cells possess intact cell membranes which do not allow TB to be absorbed, conversely, in non-viable (dead) cells TB can freely traverse the cell membrane and is absorbed. The azo dye (TB) appears as a distinctive blue colour under a microscope and therefore it is possible to distinguish between live and dead cells. The cell/PBS solution (20 μ L) and TB (20 μ L) were added to a microscope slide and viability of the cells was confirmed. If cells were viable, they were examined under the TOAD microscope.

The procedure for *Mod cheek cell* preparation is as follows:

PBS (phosphate buffered saline, 1 mL) was added to an Eppendorf tube (1.5 mL) and kept on ice. Cheek cells were harvested by gently scraping the inside of the author's cheek with a cotton bud and dipped into the Eppendorf tube kept on ice. The tube was then centrifuged (5 min, 1500 rpm), supernatant removed and a 2:1 mixture of cell/PBS (50 μ L) and FAD (25 μ L, 2 mM) was added and incubated for 30 min on ice. After 30 min, the solution was centrifuged (5 min, 1500 rpm), supernatant removed, PBS (1 mL) added, and centrifuged again (5 min, 1500

rpm). The supernatant was removed and PBS (100 μ L) solution was added. The 1:1 mixture of cell/PBS solution (20 μ L) and TB (20 μ L) were added to a microscope slide and viability of the cells was confirmed. If cells were viable, they were examined under the TOAD microscope.

Figure 5.13 displays transmission and TOAD images of both WT and Mod cheek cells. In the case of the WT cheek cell, a transmission image is clearly resolved exhibiting the typical size ($\sim 60 \mu\text{m}$) and shape of human cheek cells. However, in the TOAD image no image was resolved as the TOAD microspectroscope selectively images transient species which absorb at 532 nm, in this case flavin excited triplet states and semiquinone radicals, the result suggests that there are no flavin molecules present. For the modified cheeks cells, with FAD embedded inside the cheek cells, the results were quite different. Both transmission and TOAD images were resolved for the modified cheek cells (Fig. 5.13b), the TOAD images confirm the presence of FAD by displaying the 532 nm absorption signal of the excited triplet states and semiquinone radicals.

This preliminary result showed great promise for the TOAD microspectroscope in observing flavins in cellular locales. The technical difficulty of working with non-cultured cells, the main issue being the short lifetime of the cells, made experimental procedures both difficult and non-productive. The promising result led us to establish cell culturing facilities in the laboratory, which will be described in the following chapter.

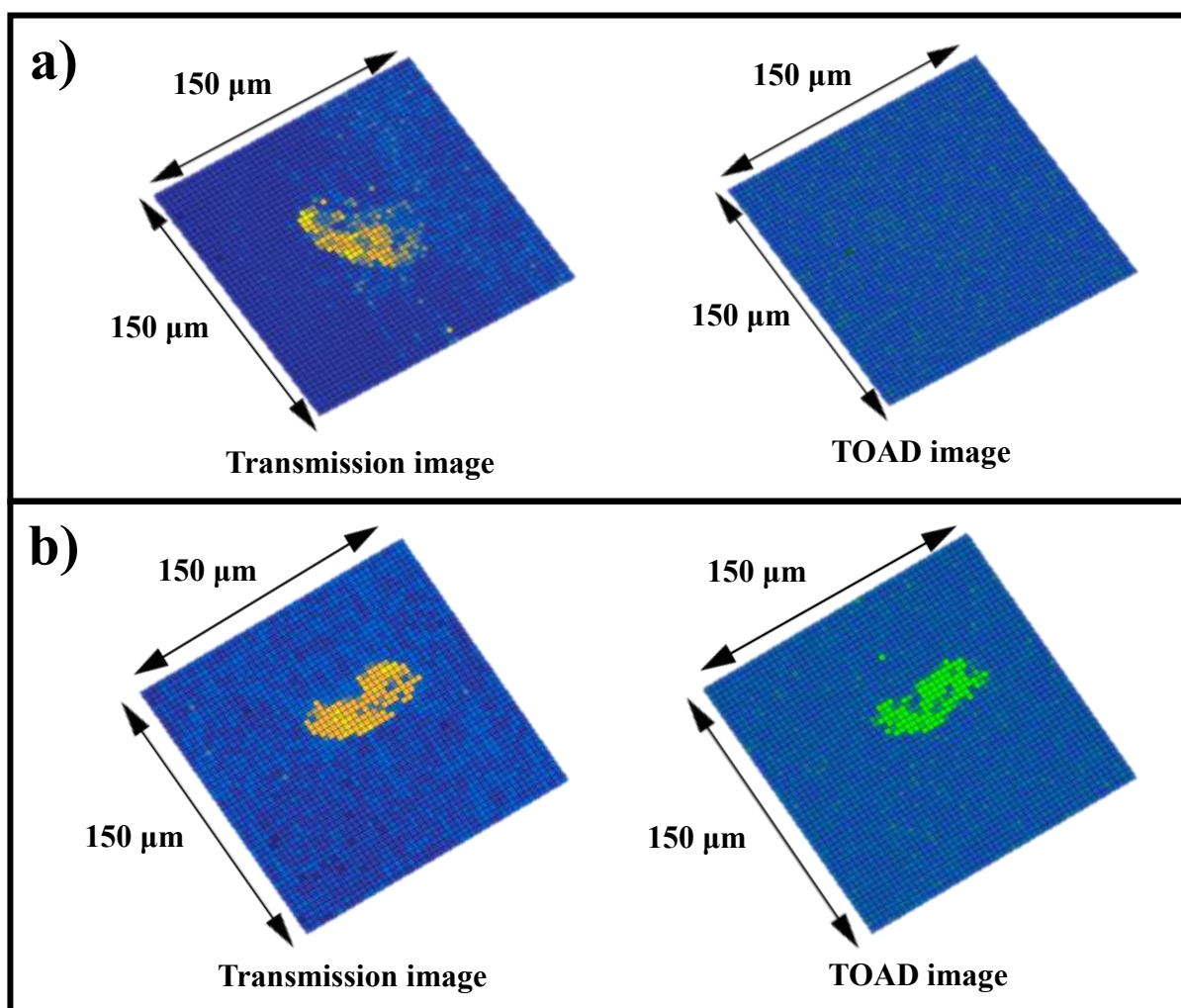


Figure 5.13. Initial transmission and TOAD images of cheek cells. a) Wild-type cheek cell, and b) Modified cheek cell, which was incubated with FAD.

5.2.2 Human Cervical Carcinoma Cells

HeLa cells are an immortal (they do not undergo cellular senescence) cell line that is widely used in scientific research, they are human cervical carcinoma cells which were taken from Henrietta Lacks on the 8th February, 1951. The cell line name HeLa is derived from the first two letters from the patients given name and surname, respectively.¹³ Due to their inherent durability they have been extremely valuable in scientific studies, and since their introduction to the scientific community an estimated 20 tons of HeLa cells have been grown in laboratories worldwide.¹⁴ HeLa cells are known to contain endogenous chromophores which exhibit auto-fluorescence,¹⁵ one of which, FAD, is of interest to this work. FAD exists as many forms inside living systems, mainly bound in flavoproteins (which have extremely weak fluorescence due to efficient quenching by the neighbouring protein

environment^{16,17}) and as free FAD, which can exist in an open or stacked conformation at physiological pH (Chapter 1.4). The stacked conformation has a relatively short lifetime of several picoseconds, with the open conformation exhibiting relatively long-lived fluorescence with a lifetime of 2-3 ns.¹⁸⁻²⁴ In cultured cells, only a few FAD bound flavoproteins have been reported to exhibit autofluorescence, such flavoproteins include lipoamide dehydrogenase (LipDH).²⁵⁻²⁹ A study by Islam *et al.*,²³ which investigated the autofluorescence of endogenous FAD in HeLa cells, were able to distinguish between bound and free FAD species present in HeLa cells by measuring their respective lifetimes. These factors led us to develop HeLa cells as a model system to investigate FAD photochemistry and MFEs thereon at the cellular level.

Culturing cells requires specific equipment, with the guidance of Prof. Omi (The University of Tokyo), the author established cell culturing facilities in the Woodward group laboratory. Due to the time required to gather equipment, install, evaluate, and finally culture cells, work is still at the preliminary stage. The HeLa cell line (RCB0007) was purchased from the Riken BRC Cell Bank, Japan. The cell culturing procedure is summarised in Figure 5.14. The initial experiments on HeLa cells under the TOAD microscope did not produced a visible transient flavin signal. This requires further examination. A long-term goal is to transfect HeLa cells with an *ArCry* plasmid to overexpress the cryptochrome protein within the cell.³⁰ A common method of transfection is to use Lipofectamine LTX (Invitrogen) by following the manufacturer's instructions.³¹ Allowing the study of cryptochrome magnetosensitive photochemistry at the cellular level.

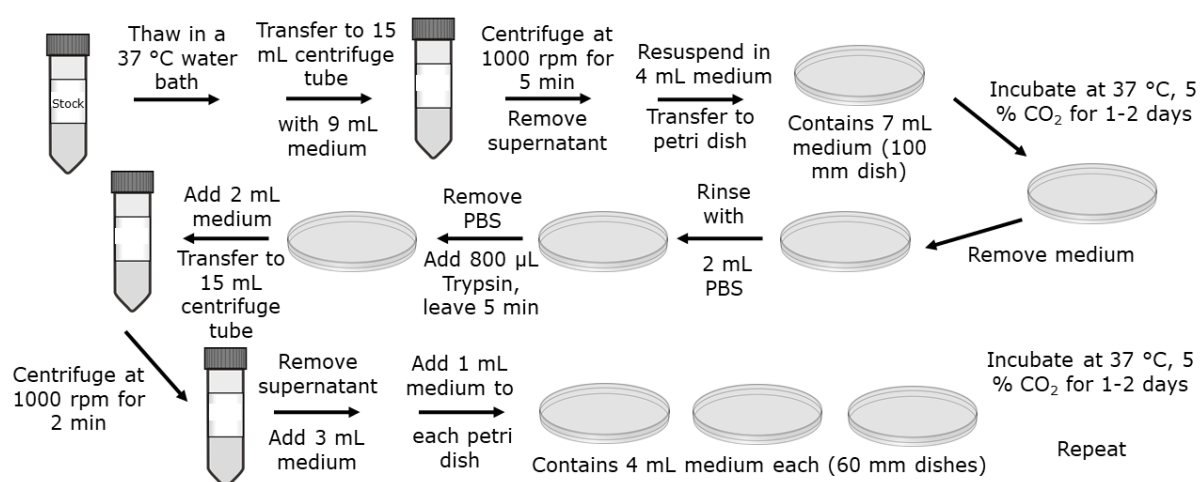


Figure 5.14. Cell culture procedure for HeLa cells. Stock = HeLa cell line, medium = Minimum Essential Medium (MEM), 10 % Calf Serum, 1% Penicillin-Streptomycin. Trypsin is added to break down the proteins which enable the cells to adhere to the dish, through the process of trypsinisation.

References

- [1] D. M. W. Sheppard, J. Li, K. B. Henbest, S. R. T. Neil, K. Maeda, J. Storey, E. Schleicher, T. Biskup, R. Rodriguez, S. Weber, P. J. Hore, C. R. Timmel, and S. R. Mackenzie, *Scientific Reports*, **2017**, 7, 42228.
- [2] I.A. Solov'yov, and K. Schulten, *J. Phys. Chem. B*, **2012**, 116, 1089.
- [3] N. Hoang, E. Schleicher, S. Kacprzak, J.-P. Bouly, M. Picot, W. Wu, A. Berndt, E. Wolf, R. Bittl, and M. Ahmad, *PLoS Biol.*, **2008**, 6, 1559.
- [4] J. Wang, X. Du, W. Pan, X. Wang, and W. Wu, *J. Photochem. Photobiol. C*, **2015**, 22, 84.
- [5] K. Maeda, A. J. Robinson, K. B. Henbest, H. J. Hogben, T. Biskup, M. Ahmad, E. Schleicher, S. Weber, C. R. Timmel, and P. J. Hore, *Proc. Natl. Acad. Sci. U. S. A.* **2012**, 109, 4774.
- [6] C. N. G. Giachello, N. S. Scrutton, A. R. Jones, and R. A. Baines, *J. Neurosci.*, **2016**, 36, 10742.
- [7] R. Marley, C. N. G. Giachello, N. S. Scrutton, R. A. Baines, and A. R. Jones, *Sci. Rep.*, **2015**, 4, 5799.
- [8] G. Fedele, M. D. Edwards, S. Bhutani, J. M. Hares, M. Murbach, E. W. Green, S. Dissel, M. H. Hastings, E. Rosato, C. P. Kyriacou, *PLoS Genet.*, **2014**, 10, e1004804.
- [9] G. Fedele, E. W. Green, E. Rosato, C. P. Kyriacou, *Nat. Commun.*, **2014**, 5, 4391.
- [10] D. R. Kattnig, *J. Phys. Chem. B*, **2017**, 121, 10215.
- [11] J.-P. Bouly, E. Schleicher, M. Dionisio-Ses, F. Vandenbussche, D. Van Der Straeten, N. Bakrim, S. Meier, A. Batschauer, P. Galland, R. Bittl, and M. Ahmad, *J. Biol. Chem.*, **2007**, 282, 9383.
- [12] P. Müller, J.-P. Bouly, K. Hitomi, V. Balland, E. D. Getzoff, T. Ritz, and K. Brettel, *Sci. Rep.*, **2014**, 4, 5175.
- [13] W. F. Scherer, J. T. Syverton, and G. O. Gey, *J. Exp. Med.*, **1953**, 97(5), 695.
- [14] D. M. Watson, Cancer killed Henrietta Lacks – then made her immortal. *The Virginian-Pilot*. May 10th, **2010**.
- [15] Md. S. Islam, M. Honma, T. Nakabayashi, M. Kinjo, and N. Ohta, *Int. J. Mol. Sci.*, **2013**, 14, 1952.
- [16] N. Mataga, H. Chosrowjan, Y. Shibata, F. Tanaka, Y. Nishima, K. Shiga, *J. Phys. Chem. B*, **2000**, 104, 10667.

- [17] H. Chosrowjan, S. Taniguchi, N. Mataga, T. Nakanishi, Y. Haruyama, S. Sato, M. Kitamura, F. Tanaka, *J. Phys. Chem. B*, **2010**, 114, 6175.
- [18] R. Y. Stanley and A. W. MacPharlane IV, *J. Phys. Chem. A*, **2000**, 104, 6899.
- [19] P. A. W. Van den Berg, K. A. Feenstra, A. E. Mark, H. J. C. Berendsen, A. J. W. G. Visser, *J. Phys. Chem. B*, **2002**, 106, 8858.
- [20] Y. Kao, C. Saxena, T. He, L. Guo, L. Wang, A. Zhu, and D. Zhong, *J. Am. Chem. Soc.*, **2008**, 130, 13132.
- [21] G. Li and K. D. Glusac, *J. Phys. Chem. A*, **2008**, 112, 4573.
- [22] A. Sengupta, R. V. Khade, and P. Hazra, *J. Photochem. Photobiol. A*, **2011**, 221, 105.
- [23] S. D. M. Islam, T. Susdorf, A. Penzkofer, and P. Hegemann, *Chem. Phys.*, **2003**, 295, 137.
- [24] T. Nakabayashi, M. S. Islam, and N. Ohta, *J. Phys. Chem. B*, **2010**, 114, 15254.
- [25] W. S. Kunz, *FEBS Lett.*, **1986**, 195, 92.
- [26] C. L. Hall and H. Kamin, *J. Biol. Chem.*, **1975**, 250, 3476.
- [27] W. S. Kunz and W. Kunz, *Biochim. Biophys. Acta*, **1985**, 841, 237.
- [28] D. N. Romashko, E. Marban, and B. O'Rourke, *Proc. Natl. Acad. Sci. USA*, **1998**, 95, 1618.
- [29] D. Chorvat Jr. and A. Chorvatova, *Eur. Biophys. J.*, **2006**, 36, 73.
- [30] H. Park, N. Y. Kim, S. Lee, N. Kim, J. Kim and W. D. Heo, *Nat. Commun.*, **2017**, 8, 30.
- [31] https://tools.thermofisher.com/content/sfs/manuals/LipofectamineLTX_PLUS_Reag_protocol.pdf

Conclusion

The aim of this work was to develop a spatially resolved microspectroscope to allow the study of magnetosensitive photochemistry of flavins not only in solution, but biomimetic and cellular environments. In Chapter 2, two key experimental challenges in studying the magnetic field sensitivity of cryptochrome photochemistry were addressed, which produced the following results,

- 1) **Measurement sensitivity:** The excellent sensitivity of the instrument was displayed by observing, for the first time, MFEs on the photochemistry of FAD at physiological pH ($\Delta\Delta A \sim 2 \times 10^{-7}$) and on the photochemistry of riboflavin (vitamin B2) in water ($\Delta\Delta A \sim 6 \times 10^{-7}$). The ability to work with non-cyclic reactions in both solution and the solid-state, using a spiral scanning approach, was confirmed through the observation of a MFE on the non-cyclic reaction between riboflavin and a thin film starch matrix at neutral pH. Finally, the possibility of recording two probe wavelengths simultaneously was demonstrated in acidic FAD solution, and this arrangement is freely extendable to a much larger number of wavelengths, where sources, detectors, and bench space allow.
- 2) **Spatially resolved measurements:** We demonstrated for the first time the techniques of TOAD microscopy, which allows direct imaging of photochemically generated radicals, and MIM microscopy, which can selectively image regions containing magnetically sensitive radical pairs. The techniques have both submicron spatial resolution and high sensitivity, as demonstrated by the ability to rapidly record images and MARY curves by irradiating a 200 μM FAD sample of less than 4 fL. In addition, a low field effect on FAD photochemistry was resolved for the first time, and the shift of MFE from radical pair to FAD ground state under cycling conditions was also clearly observed. These features are both important for the understanding of magnetoreception in cryptochromes.

The ability to make magnetic field measurements on photochemistry both in a spatially resolved manner and with high sensitivity in small volume, low concentration samples makes this a powerful tool in the arsenal of a spin chemist.

In Chapter 3, we exploited the high sensitivity of our instrument and demonstrated, for the first time, that FAD photochemistry in solution is magnetic field sensitive above pH 3.6 and even at physiological pH and higher. This result is important as FAD is such a ubiquitous biological molecule and is present unbound in many cells. FAD radical pairs constitute a potential source of magnetic field sensitivity at the cellular level.

Chapter 4 focussed on studying magnetosensitive photochemistry of flavins in biomimetic environments in the form of small and giant unilamellar vesicles (SUVs and GUVs, respectively). The work conducted on SUVs studied the electron transfer reactions from Trp to flavins in DPPC vesicles using TROA spectroscopy and MFEs. By tuning the hydrophilicity of the flavin we were able to selectively locate it within the vesicle bilayer (RFTB) or in the inner water pool (FMN). Similarly, the Trp could be located in either the bulk aqueous solution or the inner water pool based on the vesicle preparation methodology. This work is a first step in the study of flavin - Trp electron transfer in biomimetic systems and it is anticipated that further experiments can provide more detailed information on the complex molecular and spin dynamics taking place.

Preliminary work on GUVs studied electron transfer reactions in FAD and between FMN + HEWL in DOPC vesicles using TOAD and fluorescence imaging. TOAD images both FAD and FMN + HEWL encapsulated in GUVs display the potential to observe flavins radicals inside living cells. Furthermore, fluorescence imaging of RFTB confirmed successful encapsulation in the hydrophobic GUV bilayer. The results provide a basis for studying transmembrane electron transfer reactions with hydrophilic electron donors on length scales comparable to that of a cell.

In all three systems photobleaching was observed, meaning upon irradiation of the pump and probe beams the transient signal faded over time. This result was surprising as flavin photochemistry is cyclic in solution and no photobleaching was observed for the SUV experiments. Reasons for photobleaching could be due to the laser intensity and repetition rate being too high, or upon photoexcitation the transition to the excited triplet state, the flavin molecules may be interacting with other molecules in the GUV water pool, for example, sucrose or glucose, leading to unwanted chemical reactions and irreversible covalent modifications. Methods of overcoming this photobleaching could be to increase the flavin concentration, reduce laser intensity and repetition rates, or to change the other molecules involved in the GUV preparation or reduce their respective concentrations. Another possibility is that the flavin molecules are degrading over time, which is observed in numerous studies, as it is trapped inside the vesicle. This is not observed when we observe flavins in solution as the sample is constantly being refreshed.

Chapter 5 described one of the longer-term goals of making direct spectroscopic measurements of RPs in biological systems, both purified proteins and living cells. Experiments on *DmCry* were conducted under pseudo-continuous illumination, much like the continuous exposure to light that animals navigating experience. A clear reproducible light induced reaction cycle was observed where previous studies have suggested that substantial time must pass after photoexcitation before the sample returns to the ground state. We observed triplet born MFEs on the photochemistry of the isolated protein, which contradicts all previous work on purified cryptochrome proteins. We proposed a new reaction scheme to account for our observations based on a recent oxygen scavenger model. Work has already started on constructing a microspectrophotometer to identify the species with UV/Vis spectrometry using microlitre sample volumes. This system does not have the spatial resolution of the original microscope; however, it is sufficient for measurements of photochemistry in isotropic solution.

Initial cellular experiments on cheek cells incubated with FAD displayed a TOAD image, where unaltered cheek cells did not. This led to the development of cell culturing facilities and develop HeLa cells as a model system for investigating the magnetosensitivity of FAD photochemistry at the cellular level. Future work will focus on transfecting HeLa cells with cryptochrome proteins, with aim of studying cryptochrome photochemistry at the cellular level.

Although this work focused on molecules and systems related to animal magnetoreception, the potential uses of the developed instrumentation are far broader and allow for a new arena of spin dependent reactivity to be explored. By allowing spatially localised observations of magnetic field sensitivity, investigations into hitherto unstudied locales, including interfaces, localised microstructures and thin films, become tractable. This includes areas of current frenzied research activity in solid-state devices like solar cells and organic light emitting diodes where electron-hole recombination, which is essentially a radical ion pair recombination reaction, is critical to performance. The work also demonstrates the broad scope of potential further studies that can be undertaken using the new methodologies developed.

Publications and Related Information

The following lists all publications, awards, and conferences relevant to the work described in this dissertation.

Journal Publications

- (1) L. M. Antill, S. Takizawa, S. Murata, and J. R. Woodward, Photoinduced Flavin-Tryptophan Electron Transfer Across Vesicle Membranes Generates Magnetic Field Sensitive Radical Pairs, *Molecular Physics*, accepted for publication, **2018**.
- (2) L. M. Antill and J. R. Woodward, Flavin adenine dinucleotide photochemistry is magnetic field sensitive at physiological pH, *The Journal of Physical Chemistry Letters*, 9, 2691-2696, **2018**.
- (3) L. M. Antill, J. P. Beardmore, and J. R. Woodward, Time-resolved optical absorption microspectroscopy of magnetic field sensitive flavin photochemistry, *Review of Scientific Instruments*, 89, 023707, **2018**.
- (4) J. P. Beardmore, L. M. Antill, and J. R. Woodward, Optical Absorption and Magnetic Field Effect Based Imaging of Transient Radicals, *Angewandte Chemie International Edition*, 54, 8494-8497, **2015**.
- (5) J. P. Beardmore, L. M. Antill, and J. R. Woodward, Optical Absorption and Magnetic Field Effect Based Imaging of Transient Radicals, *Angewandte Chemie*, 127, 8614-8617, **2015**.

Magazine and News Articles

- (1) Magnetic field sensitive microspectroscopy – cover article in *Electron Spin Science* (電子スピンサイエンス), Vol. 15, **2017**, by Prof. J. R. Woodward.

- (2) An intracellular search for a magnetic sense – review in *Oyo Buturi* (応用物理), Vol. 85, No. 5, **2016**,
by Prof. J. R. Woodward.
- (3) *UTokyo Research News*
English: <http://www.u-tokyo.ac.jp/en/utokyo-research/research-news/a-microscopic-approach-to-the-magnetic-sensitivity-of-animals.html>
Japanese: <http://www.u-tokyo.ac.jp/ja/utokyo-research/research-news/a-microscopic-approach-to-the-magnetic-sensitivity-of-animals.html>
- (4) *American Association for the Advancement of Science (AAAS) EurekAlert!*
English: https://www.eurekalert.org/pub_releases/2015-06/uot-ama060415.php
Japanese: https://www.eurekalert.org/pub_releases_ml/2015-06/aaft-060515.php
- (5) *Phys.org*
<https://phys.org/news/2015-06-microscopic-approach-magnetic-sensitivity-animals.html>
- (6) *Nanowerk*
<https://www.nanowerk.com/nanotechnology-news/newsid=40317.php>
- (7) *Science Daily*
<https://www.sciencedaily.com/releases/2015/06/150604104145.htm>
- (8) *Science Newsline Biology*
<http://www.sciencenewsline.com/news/2015060421380078.html>

Awards

- (1) Taylor & Francis Spin Chemistry Meeting 2017 Poster Prize – *The 15th International Symposium on Spin and Magnetic Field Effects in Chemistry and Related Phenomena*, Schluchsee, Germany, **2017**.
- (2) PhD Scholarship – *Ministry of Education, Culture, Sports, Science and Technology: MEXT-Japan*, **2014**.

Conferences

- (1) Magnetosensitive flavin photochemistry in micron-scale reaction environments – *The 56th Annual Meeting of the Society of Electron Spin Science and Technology (SEST)* (**2017/11/02 - 04** Tokyo, Japan)

- (2) Magnetosensitive flavin photochemistry in micron-scale reaction environments – *Spin Chemistry Meeting 2017 - 15th International Symposium on Spin and Magnetic Field Effects in Chemistry and Related Phenomena* (2017/09/17 - 21 Schluchsee, Germany)
- (3) Magnetosensitive flavin photochemistry in micron-scale reaction environments – *Annual Meeting on Photochemistry 2017* (2017/09/04 - 06 Sendai, Japan)
- (4) Spatially resolved spectroscopy of flavin magnetosensitive photochemistry – *The 55th Annual Meeting of the Society of Electron Spin Science and Technology (SEST)* (2016/11/10 - 12 Osaka, Japan)
- (5) Microscopic studies of magnetosensitive photochemistry – *The 2nd Kanto Area Spin Chemistry (KASC) Mini Symposium* (2016/06/24 Saitama, Japan)
- (6) Microscopic studies of magnetosensitive photochemistry – *32nd Symposium on Chemical Kinetics and Dynamics* (2016/06/01 - 03 Saitama, Japan)
- (7) A sub-micron step closer to spatially resolving the magnetosensitivity of photochemically induced electron transfer reactions of flavins – *16th Todai Life Science Symposium* (2016/04/23 Tokyo, Japan)
- (8) A microscopic approach to observing the magnetosensitivity of photochemical intermediates – *Molecular Integrated System and Reaction: Analytical and Constructive Approaches* (2016/03/02 Tokyo, Japan)
- (9) A sub-micron step closer to spatially resolving the magnetosensitivity of photochemically induced electron transfer reactions of flavins – *The 54th Annual Meeting of the Society of Electron Spin Science and Technology (SEST)* (2015/11/02 - 04 Nigata, Japan)
- (10) A sub-micron step closer to spatially resolving the magnetosensitivity of photochemically induced electron transfer reactions of flavins – *The 9th Annual Meeting of Japan Society for Molecular Science* (2015/09/16 - 19 Tokyo, Japan)
- (11) A sub-micron step closer to spatially resolving the magnetosensitivity of photochemically induced electron transfer reactions of flavins – *Annual Meeting on Photochemistry 2015* (2015/09/08 - 11 Osaka, Japan)
- (12) A sub-micron step closer to spatially resolving the magnetosensitivity of photochemically induced electron transfer reactions of flavins – *The 1st Kanto Area Spin Chemistry (KASC) Mini Symposium* (2015/07/11 Tokyo, Japan)

Supporting Information

B. 1 CHAPTER 3.1

Experimental Methods

All data were recorded with our TOAD/MIM microspectroscope, which has been described in detail elsewhere (Chapter 2).^{1,2} Samples were photoexcited with a 449 nm pump beam (~2 mW, CUBE laser, Coherent) with a 700 ns pulse width and a 10 kHz repetition rate. A 532 nm probe beam (~1.5 mW, Sapphire laser, Coherent) monitored the transient species. The confocal arrangement consists of two super apochromatic objective lenses (UPlanSApo 20 \times / NA 0.75, Olympus). FAD was purchased from Wako and used as received. The concentration of FAD was adjusted to 200 μ M. pH 2.3-8.0 buffer solutions were made with combinations of citric acid and disodium hydrogen phosphate solutions (Wako) in distilled water (Wako).³ All pH values were verified with a pH meter (HI 991002, Hanna). Thin samples were produced by adding polymer 100 μ m glass beads (Toshin Riko) to the sample solution, thicker samples utilized 280 μ m frame-seal chambers (Bio-rad), and sandwiching 5 μ L of sample between glass cover slips (0.13–0.16 mm, Marienfeld).

pH Dependence of Time-Resolved Optical Absorption Signal Magnitude

Based on the proposed mechanism, the overall size of the time-resolved optical absorption (TROA) signal falls rapidly with pH as the pK_a of protonation of the adenine group in ground state FAD is 3.6 and thus at higher pH the ground state FAD is not protonated and can exist in a stacked conformation that undergoes rapid internal conversion (IC) back to the ground state on photoexcitation. Furthermore, other non-stacked conformers of FAD can become stacked during the excited singlet state lifetime and can similarly undergo rapid IC more rapidly than intersystem crossing to form the excited triplet state. The overall concentration of excited state triplets is diminished through these two routes and Figure B.1 shows the observed maximum TROA signal sizes plotted

against pH and fit to match a single pH curve for pKa 3.6. As the observation of the TROA signal is a little delayed in our measurements due to the long (700 ns) laser pulse, values extracted from the published TROA signals for low pH values in Murakami *et al.*,⁴ are plotted alongside for comparison. These are less influenced by RP reaction during the initial observation period due to the much more rapid laser flash from a Nd:YAG laser.

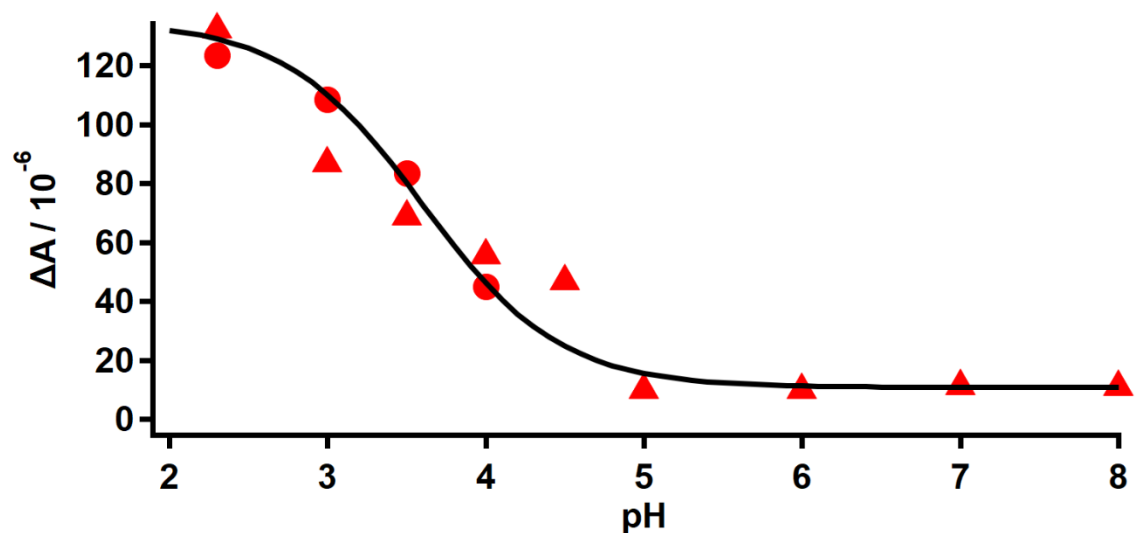


Figure B.1. pH dependence of time-resolved transient absorption signal magnitude for FAD. Red circles represent scaled TROA signals from Murakami *et al.*,⁴ and red triangles are the observed maximum TROA signals from this study. The black line is based on the simulation described in the text.

B. 2 CHAPTER 4.1

Concentration Calculations

Number of vesicles

One vesicle is composed of 4000-6000 DPPC molecules. Assuming that all DPPC molecules form vesicles:

$$11.4 \text{ mL solution contains } 12 \text{ } \mu\text{mol DPPC} = 72 \times 10^{17} \text{ molecules}$$

$$72 \times 10^{17} \text{ molecules} / 4000\text{-}6000 \text{ DPPC molecules} = 1.2\text{-}1.8 \times 10^{15} \text{ vesicles in the bulk solution.}$$

Number of RFTB molecules in one vesicle

$$\sim 60 \text{ } \mu\text{M} \times 11.4 \text{ mL} \times 6.022 \times 10^{23} \text{ mol}^{-1} = 4.1 \times 10^{17} \text{ molecules of RFTB in the bulk solution.}$$

Therefore, in one vesicle:

$$4.1 \times 10^{17} \text{ molecules} / 1.2\text{-}1.8 \times 10^{15} \text{ vesicles} = 228\text{-}342 \text{ RFTB molecules in one vesicle.}$$

Therefore, RFTB:DPPC ratio for one vesicle = 1:17-1:18

Concentration of RFTB in one vesicle bilayer

$$\text{Volume of a vesicle} = V = \frac{1}{6} \pi d^3$$

$$d_{total} = \sim 60 \text{ nm, therefore } V_{total} = 113,097 \text{ nm}^3$$

$$d_{waterpool} = 60 \text{ nm} - 12 \text{ nm} (6 \text{ nm} \times 2) = 48 \text{ nm}$$

$$\text{Therefore, } V_{waterpool} = 57,906 \text{ nm}^3$$

$$V_{bilayer} = V_{total} - V_{waterpool} = 55,191 \text{ nm}^3$$

$$\text{Number of molecules of RFTB in one vesicle} = \sim 285 / 6.022 \times 10^{23} \text{ mol}^{-1} = 4.73 \times 10^{-22} \text{ mol}$$

$$\text{Concentration of RFTB in one vesicle bilayer} = 4.73 \times 10^{-22} \text{ mol} / 55,191 \text{ nm}^3 = \sim 8.6 \text{ mM}$$

Number of FMN molecules in one vesicle

$$\sim 25 \text{ } \mu\text{M} \times 11.4 \text{ mL} \times 6.022 \times 10^{23} \text{ mol}^{-1} = 1.7 \times 10^{17} \text{ molecules of FMN in the bulk solution.}$$

Therefore, in one vesicle:

$$1.7 \times 10^{17} \text{ molecules} / 1.2\text{-}1.8 \times 10^{15} \text{ vesicles} = 93\text{-}140 \text{ FMN molecules in one vesicle.}$$

Therefore, FMN:DPPC ratio for one vesicle = 1:43

Concentration of FMN in one vesicle water pool

$$\text{Volume of a vesicle} = V = \frac{1}{6} \pi d^3$$

$$d_{\text{total}} = \sim 60 \text{ nm, therefore } V_{\text{total}} = 113,097 \text{ nm}^3$$

$$d_{\text{waterpool}} = 60 \text{ nm} - 12 \text{ nm} (6 \text{ nm} \times 2) = 48 \text{ nm}$$

$$\text{Therefore, } V_{\text{waterpool}} = 57,906 \text{ nm}^3$$

$$\text{Number of molecules of RFTB in one vesicle} = \sim 117 / 6.022 \times 10^{23} \text{ mol}^{-1} = 1.94 \times 10^{-22} \text{ mol}$$

$$\text{Concentration of FMN in one vesicle water pool} = 1.94 \times 10^{-22} \text{ mol} / 57,906 \text{ nm}^3 = \sim 3.4 \text{ mM}$$

B_{1/2} Calculation for RFTB Radical Pair

The B_{1/2} was calculated using the Weller equation:⁵

$$B_{1/2} = \sqrt{3} \frac{\tilde{a}_A^2 + \tilde{a}_B^2}{\tilde{a}_A + \tilde{a}_B} \quad (1)$$

Where A and B are the different radicals, and \tilde{a} is the effective hyperfine coupling of the radical. As both radicals are the same, the formula can simplify to:

$$B_{1/2} = \sqrt{3} \tilde{a}_A \quad (2)$$

Using the calculated \tilde{a}_{RFTB} value of 1.4 mT,⁶ the B_{1/2} value for a two flavin semiquinone RP is 2.4 mT.

Dwell Time in the Confocal Volume

The diffusion rate was estimated using the Stokes-Einstein equation,

$$D = \frac{k_B T}{6\pi\eta a} \quad (3)$$

where $a = 30 \text{ nm}$ (radius of SUV), k_B is the Boltzmann constant, $T = 298 \text{ K}$, η is the viscosity of water, therefore $D = 7.27 \times 10^{-12} \text{ m}^2 \text{ s}^{-1}$.

Setting the RMS distance travelled as the beam waist ($\sim 300 \text{ nm}$) and employing,

$$t = \frac{\bar{x}^2}{2D} \quad (4)$$

the dwell time at our focal point was estimated to be $t = \sim 6$ ms.

References

- [1] J. P. Beardmore, L. M. Antill, and J. R. Woodward, *Angew. Chem. Int. Ed.* **2015**, 54, 8494.
- [2] L. M. Antill, J. P. Beardmore, and J. R. Woodward, *Rev. Sci. Instrum.* **2018**, 89, 023707.
- [3] T. C. McIlvaine, *J. Biol. Chem.* **1921**, 49, 183-186.
- [4] M. Murakami, K. Maeda, and T. Arai, *J. Phys. Chem. A* **2005**, 109, 5793.
- [5] A. Weller, F. Nolting and H. Staerk, *Chem. Phys. Lett.* **1983**, 96, 24-27.
- [6] K. Maeda, A. J. Robinson, K. B. Henbest, H. J. Hogben, T. Biskup, M. Ahmad, E. Schleicher, S. Weber, C. R. Timmel, and P. J. Hore, *Proc. Natl. Acad. Sci. U. S. A.* **2012**, 109, 4774.